The Dissertation Committee for Shiv Shanker Ravichandran certifies that this is the approved version of the following dissertation:

DESIGN PROVISIONS FOR AUTOCLAVED AERATED CONCRETE (AAC) INFILLED STEEL MOMENT FRAMES

Committee:

Richard E. Klingner, Supervisor

Michael D. Engelhardt

James O. Jirsa

Sharon L. Wood

Eric B. Becker

DESIGN PROVISIONS FOR AUTOCLAVED AERATED CONCRETE (AAC) INFILLED STEEL MOMENT FRAMES

by

Shiv Shanker Ravichandran, B.Tech., M.S.

Dissertation

Presented to the Faculty of the Graduate School of

The University of Texas at Austin

in Partial Fulfillment

of the Requirements

for the Degree of

Doctor of Philosophy

The University of Texas at Austin

December 2009

Dedication

To my family

Acknowledgements

I am grateful to AACPA and Xella AAC for providing financial assistance for this research project. I am also grateful to Trustone AAC for initiating the project.

My deepest gratitude to Dr. Richard Klingner. It has been a privilege to work with him and follow his systematic approach. The personal lessons I have learnt from him will be just as important in my life as the technical knowledge he has shared with me.

I express my thanks to Dr. Engelhardt for the discussions I have had with him on many occasions. I also express my thanks to my committee members for being willing to supervise this dissertation. I am grateful to Dr. Curt Haselton and Dr. Abbie Liel for their prompt advice and help on the ATC-63 methodology.

I really appreciate the support provided by technical staff of the Ferguson lab Dennis, Blake, Greg, David and Andrew. I thank Mr. Salvador Ochoa and his team for constructing the AAC infill. Working in the lab has been a very challenging and satisfying experience and has taught me many lessons. I also appreciate help provided by Barbara, Ella and Jessica.

My friends at the Ferguson lab have been very kind and I cherish the time they spent with me, particularly Ali, Quan, Jo, Rangsan, Ali Youssef, Hossein, Guanyu, Andrew, Gunup, Seong, Catherine, Kim and others. My room-mates and friends have been an integral part of my life during these years – Shrawan, GG, Gaga, Ankit, Nitesh, Tanuj, Singhal and others. I am thankful for their wonderful company.

My gratitude to UT Austin and its community for giving me the space to be within it. It has been a memorable experience.

I express my deep appreciation to my parents and brother for their love and support. Without their insistence I may not have come to UT Austin.

Many thanks to everyone who has been part of this journey.

DESIGN PROVISIONS FOR AUTOCLAVED AERATED CONCRETE (AAC) INFILLED STEEL MOMENT FRAMES

Publication No._____

Shiv Shanker Ravichandran, Ph.D.

The University of Texas at Austin, 2009

Supervisor: Richard E. Klingner

In this dissertation, the seismic behavior and design of AAC-infilled steel moment frames are investigated systematically. The fundamental vehicle for this investigation is the ATC-63 methodology, which is intended for the establishment of seismic design factors for structural systems. The ATC-63 methodology is briefly reviewed, including the concepts of archetypical structures, design rules and mathematical models simulating the behavior of those archetypes.

A limited experimental investigation on the hysteretic behavior of an AAC-infilled steel moment frame is developed, conducted, and discussed. Using the experimental results of that investigation, the draft infill design provisions of the Masonry Standards Joint Committee (MSJC) are extended to AAC infills, and a mathematical model is developed and calibrated to simulate the behavior of AAC infills under reversed cyclic loads.

Prior to application of ATC-63 methodology to AAC-infilled steel moment frames, the methodology is applied to an example steel moment frame to demonstrate the methodology and verify understanding of it. Then, archetypical infilled frames to be evaluated by the ATC-63 methodology are developed using a series of pushover analyses. Infill configurations whose total lateral strength in a particular story exceeds about 35% of the lateral strength of the bare frame in that story are observed to provoke story mechanisms in the frame. Based on this observation, archetypical infilled frames are selected conforming to two infill configurations: uniformly infilled frames, and open ground story frames. Each infill configuration includes archetypes whose ratio of infill strength to bare-frame strength at each story is less than 35%, and archetypes whose ratio is greater than 35%. The former archetype is typical of steel moment frames infilled with AAC; the latter archetype is typical of steel moment frames infilled with conventional (clay or concrete) masonry. The ATC-63 methodology, specialized for application to infilled frames, is applied to the archetypical infilled frames developed above. The performance of those archetypical infilled frames is evaluated, and seismic design factors are proposed for AAC-infilled steel moment frames. The extension of this work to other types of infilled frames is discussed.

Table of Contents

List of Tables

List of Figures

CHAPTER 1
Introduction

1.1 GENERAL

Infilled frames are used as a structural system in many parts of the world. An infill is a panel of masonry or concrete, placed within the beams and columns of a frame, usually for non-structural reasons. Infills are primarily intended to serve as interior partitions between adjoining rooms or as external envelope between the building and its surroundings. They define space, and serve as thermal and acoustical barriers.

Although infills are placed for largely non-structural reasons, they nonetheless participate in the structural action of frames, particularly under lateral loads. Some modern building codes have limited provisions to include infills in the design process, but these provisions are not comprehensive or adequate (Kaushik 2006). In the US, infill panels are generally ignored in the structural design process. Although undoubtedly simple, it is also incorrect. In the elastic range, infills increase the stiffness of a structure. While this increase in stiffness can be beneficial in reducing drift, it also decreases the natural periods of vibration, thereby usually attracting greater inertial forces and changing the global seismic response of the frame. Infills also change the internal distribution of actions in frame elements. In the inelastic range, the strength of infills can change the global collapse behavior of a structure, and can cause local failures of bounding frame elements.

These theoretical concerns are supported by empirical evidence. During earthquakes, infills have been observed at some times to improve the seismic performance of frames (Hamburger 2006, Murty 2002), and at other times, to degrade that performance (Dolsek 2000, Scawthorn 2000, Humar 2001). Of particular concern are open ground story frames, where infills are placed in all stories except the ground story. Such frames tend to develop a weak ground story mechanism (Humar 2001).

Autoclaved aerated concrete (AAC) is a lightweight cementitious material with a closed-cell void system. Though it has been widely used in Europe and other countries outside the US since the late 1920s, it has not been widely used in the US. The last 10 years have witnessed increasing use of AAC in the US. Previous research at the University of Texas at Austin (Tanner 2005a, Tanner 2005b, Varela 2006) led to the development of design provisions for AAC shear wall systems. AAC is potentially attractive as an infill material due to its light weight, thermal and acoustic insulation properties and fire resistance. Also, because of its lower stiffness and strength than conventional infill materials, AAC infills could affect the behavior of frames in a different manner than has been previously observed for other infill materials.

The overall objective of the research described in this dissertation is to develop general and seismic design provisions for steel moment frames infilled with AAC. The results are applicable to steel moment frames with other types of infills, and applicable in principle to reinforced concrete infilled frames.

1.2 SCOPE OF DISSERTATION

In this dissertation, the seismic behavior and design of infilled frames is investigated systematically. The fundamental vehicle for this investigation is the methodology proposed by the ATC-63 report (ATC-63 2008), intended for the establishment of seismic design factors for structural systems. That procedure is not discussed further in detail in this chapter. Its essential elements are discussed, however, because they are the motivating factors behind each facet of the work described here.

The ATC-63 methodology requires the following basic elements:

a. Archetypical structures

b. Design rules for archetypical structures and their elements

c. Mathematical models based on test results

While the precise definition of “archetypical structure” will be given later, it can be understood as the general class of infilled-frame structures addressed by this dissertation: frames up to about 5 stories high, with masonry infills. This definition

might be expanded later, but suffices for now. "Design rules" are required to determine proportions and details of the structural components comprising those archetypical structures based on code-prescribed loads. "Mathematical models" are required to simulate the response of those archetypical structures to imposed loads, particularly seismic loads. At this point in this dissertation, "design rules" and "mathematical models" for infilled frames are undefined. Their definition, particularly for AAC-infilled steel moment frames, makes up a significant part of this dissertation.

The scope and organization of this dissertation are shown in Figure 1.1 and summarized below:

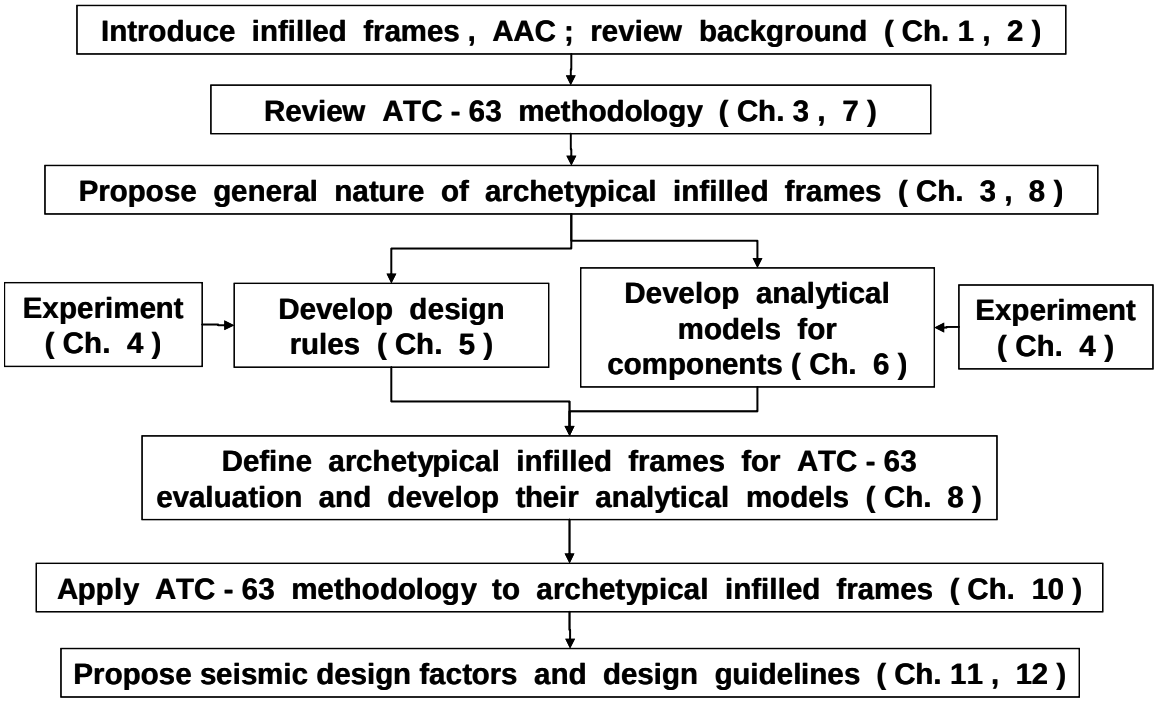

Figure 1.1: Scope and organization of dissertation

o In Chapter 2, the structural behavior of infilled frames is reviewed, and their use around the world and in the US is discussed. Their structural action, their effect on the behavior of frames, and the observed seismic performance of infilled

frames are summarized. A brief background on AAC is presented, including its possible usefulness as an infill material. Previous investigations on the behavior of infilled frames, their analytical modeling, and assessments of their seismic performance are reviewed.

- In Chapter 3, the research plan is presented in more detail. The ATC-63 methodology is briefly reviewed, including the concepts of archetypical structures, design rules and mathematical models simulating the behavior of those archetypes.
- In Chapter 4, a limited experimental investigation on behavior of an AAC infilled steel moment frame is developed and discussed.
- Chapter 5 addresses design rules for infilled frames. Design rules for bare frames will be based on AISC (2005) and ACI (2008). Design rules for infills will be based on MSJC draft infill provisions. Applicability of draft MSJC infill provisions to AAC infills is assessed based on experimental results.
- Chapter 6 deals with mathematical models to simulate behavior of infilled steel moment frames. A mathematical model for AAC infills is calibrated based on the experimental results obtained earlier.
- In Chapter 7, the ATC-63 methodology is applied to an example steel moment frame to demonstrate the ATC-63 methodology and verify understanding of it.
- In Chapter 8, the archetypical infilled frames that will be analyzed using the methodology are developed. The archetypes include both uniformly infilled and open ground story systems.
- In Chapter 9, the ATC-63 methodology is specialized for application to infilled frames in particular.
- In Chapter 10, applies that specialized ATC-63 methodology to the proposed archetypical infilled steel moment frames.
- In Chapter 11, the performance of those archetypical infilled steel moment frames is evaluated, and seismic design factors are proposed.

- In Chapter 12, this dissertation is summarized; its conclusions are presented; and implementation and future research are recommended.

1.3 OBJECTIVES OF DISSERTATION

The objectives of this dissertation are:

1. Determine whether draft MSJC infill provisions are applicable to AAC infills;
2. Using the ATC-63 methodology, establish seismic design factors and design guidelines for steel moment frames with AAC infills; and
3. Using the ATC-63 methodology, propose seismic design factors and design guidelines for steel moment frames with uniform infills, and with open ground story infills.

CHAPTER 2
Background on infilled frames

2.1 INTRODUCTION AND SCOPE OF CHAPTER

This chapter is a general introduction to the subject of infilled frames. How infills participate in the response of framed structures is explained, and the concept of idealizing an infill as an equivalent strut is introduced. General experience and anecdotal evidence are summarized regarding the performance of infilled frames, particularly during earthquakes. Previous investigations on infilled frame behavior, analytical modeling of infills and seismic performance assessment of infilled frames, are reviewed. An overview of design provisions for infilled frames in modern building codes is presented. Autoclaved aerated concrete (AAC) is introduced, its material properties are summarized, and its potential usefulness as an infill material is proposed.

2.1.1 Infilled frames

An infilled frame, shown in Figure 2.1, is a hybrid structural system in which a frame of steel or reinforced concrete is filled with a panel of another material, such as concrete, conventional masonry, or AAC masonry. The infill is generally a partition wall that also can serve as a thermal or acoustical barrier. When placed in bays defining elevator shafts or stairwells, infills also can act as fire barriers, and are a potential alternative to the steel studs and gypsum board commonly used for this purpose in the US. This use is more common in Europe and Asia than the US, and includes AAC infills.

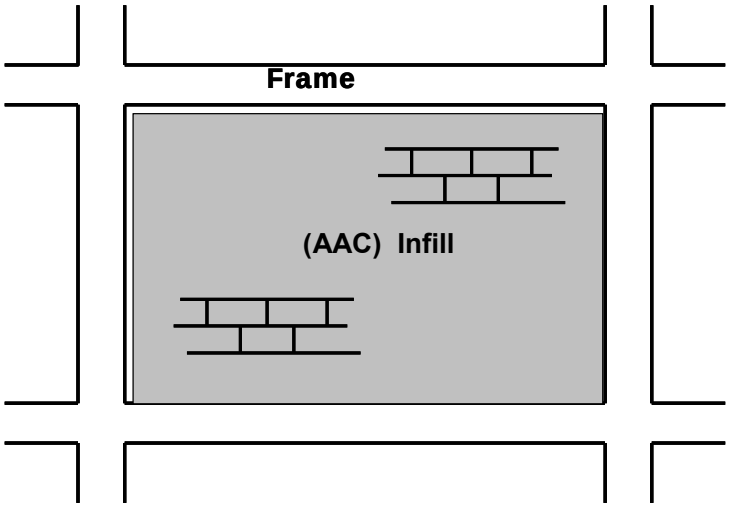

Figure 2.1: An infilled frame

Infills can be located in a frame in many ways, ranging from placement in all bays and stories of the frame (Figure 2.2 (a)), to random placement (Figure 2.2 (d)). The open ground story system of Figure 2.2 (b) is popular system in many parts of the world, as it leaves the ground story available for lobby or parking.

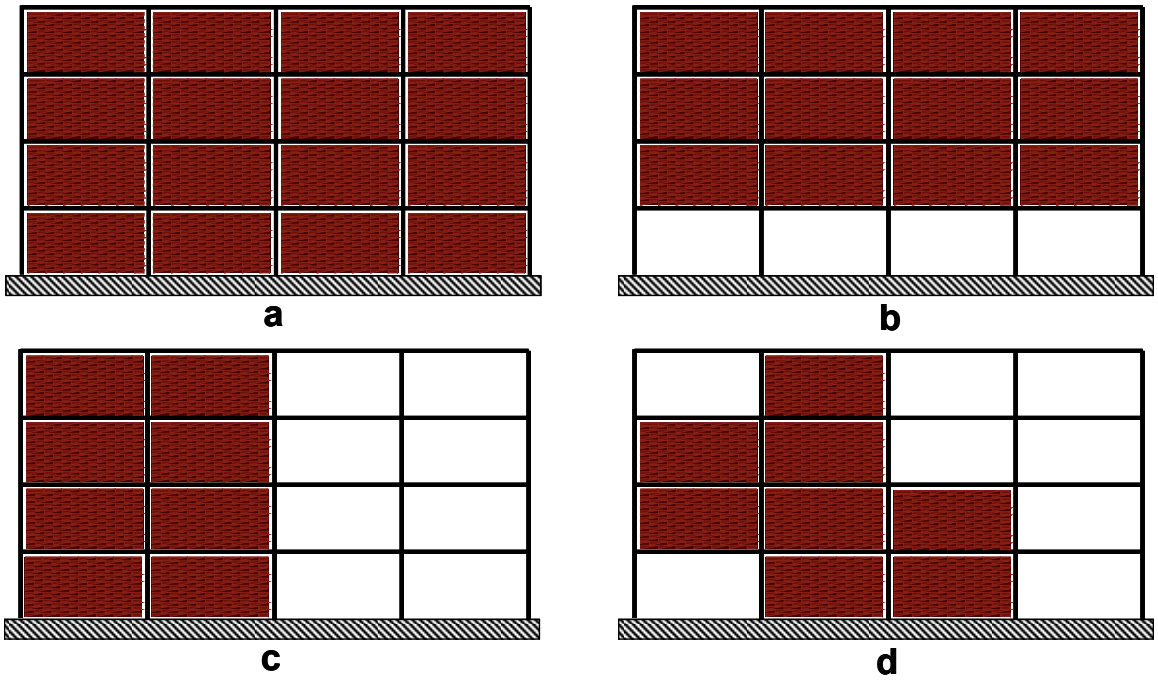

Figure 2.2: Example locations of infills in the panels of a frame

2.2 STRUCTURAL ACTION OF INFILLS

Under lateral loads, infills act as compression struts extending between diagonally opposite corners of the infilled bay, as shown in Figure 2.3. The infill stiffens the frame, significantly reducing drift under lateral loads from service level winds or earthquakes. The infill also strengthens the frame, and if properly designed may be able to reduce damage and probability of collapse under strong earthquakes. Unfortunately, no clear guidelines exist for designing infills to improve seismic response. Infills are generally either not considered in design, or are required to be isolated from the frame.

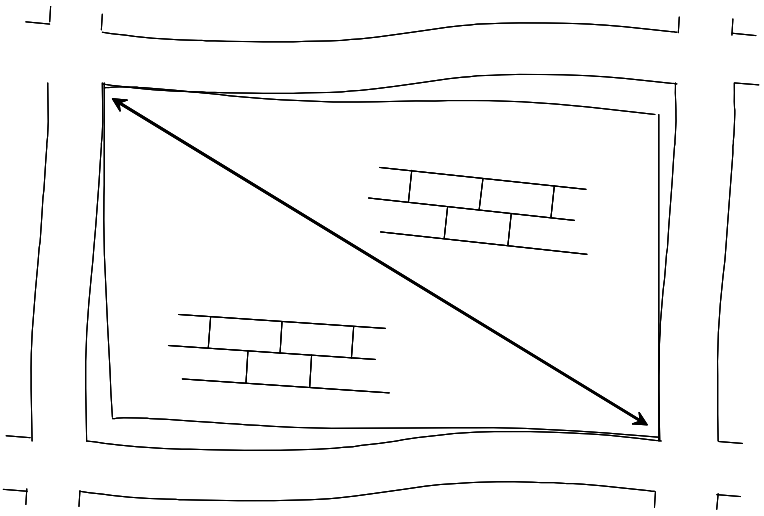

Figure 2.3: Structural action of infills

2.2.1 Observed behavior of infilled frames during earthquakes

Evidence abounds regarding the beneficial effect of infills on seismic behavior of frames. In numerous instances, infilled frames have withstood an earthquake that collapsed otherwise similar frames without infills. A fraction of that published evidence is noted here. However, this evidence generally refers to reinforced concrete frames only, and contains no references to observed performance of steel moment frames, except Hamburger (2006). This is probably because infills are commonly used in developing countries, where steel moment frames are rare.

Hamburger (2006) discusses the superior structural performance and fire resistance of steel-frame buildings with clay brick or hollow clay tile masonry infills, compared with that of other structural systems during the 1906 San Francisco earthquake. Infilled frame buildings were probably the only ones to survive the combined effect of earthquake and fire in the zone of burnout. While early investigators attributed this superior structural performance primarily to the steel frame, the infills could also have been beneficial. A specific instance of this was the better performance of steel frames in which partition walls were built as infills, compared with frames in which such walls were self-supported over the height of the building and independent of the steel frame. In

spite of deficiencies such as vertical and torsional irregularities, many of these buildings are still in use today.

Murty (2002) notes the excellent performance of reinforced concrete frames in India during moderate earthquakes. He attributes this to the presence of masonry infills, although such frames were not specifically designed to withstand seismic forces.

However, infilled frames are also known to adversely affect the behavior of frame during earthquakes. Saatcioglu (2001) notes the poor performance of reinforced concrete infilled frames, the primary structural system used in Turkey, during the Kocaeli earthquake of 1999. Being stiffer, the infills attracted higher seismic loads, which could only be withstood as long as the infills remained elastic. After the infills started to degrade, the remaining frames did not have enough lateral load resistance or inelastic deformation capacity, and often collapsed.

Of particular concern is the tendency of infilled frames to form adverse failure mechanisms, such as those shown in Figure 2.4, that result in premature structural collapse. Such failure mechanisms are generally a result of irregular placement of infills leading to a weak story that has many fewer infills than adjacent stories. This results in concentration of inelastic deformations at those stories. Irregular placement of infills in plan also leads to torsional effects which increase the inelastic deformation demand on some columns of the frame. Even when infills are placed in a regular manner over the height of the frame, Dolsek (2000) observes that weak story failure mechanism can still occur as shown in Figure 2.5.

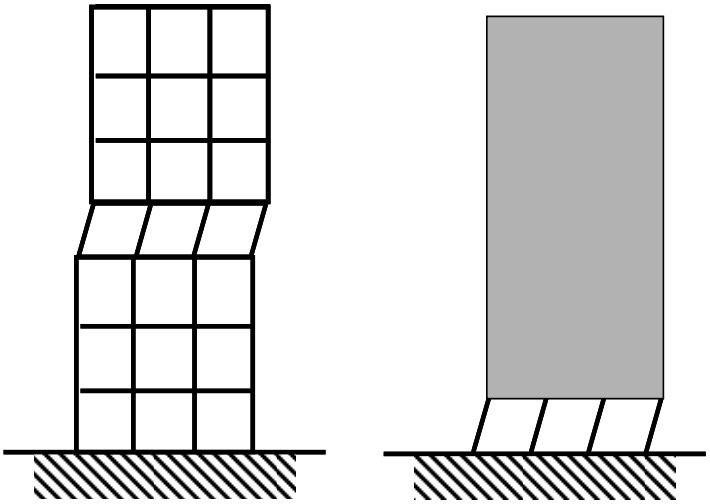

Figure 2.4: Story mechanisms due to irregular placement of infills

Figure 2.5: Collapse of an uniformly infilled frame in its bottom two stories during 1999 Kocaeli earthquake (Dolsek 2000)

Throughout the world, a particularly common irregularity in the placement of infills is the open ground story (Figure 2.2 (b)), which is left open for a variety of architectural reasons. As shown on the right side Figure 2.4, inelastic story drifts tend to be concentrated at the open ground story, leading to collapse there as shown in Figure 2.6. This is extensively presented in Humar (2001), Scawthorn (2000), Saatcioglu (2001), Christopoulus (2005) and elsewhere. Even a few infills at the ground story can prevent formation of a weak story mechanism at that level. This is exemplified by Figure 2.7,

which shows a frame damaged during the Bhuj earthquake (Humar 2001). As noted by Humar:

"The columns of this soft story were heavily damaged in the hinge regions as seen from the figure. However, it appears that a few infill walls at this level protected the building against total collapse. Interaction between the columns and the walls damaged the latter quite severely as evidenced by whose collapse was prevented due to the presence of infills. Although the infills were damaged, they stayed to provide lateral stability to the structure."

Figure 2.6: Collapse of open ground story systems during earthquakes (Humar 2001, Scawthorn 2000)

Figure 2.7: Example of frame saved during the Bhuj earthquake by the presence of a few infills at the ground floor (Humar 2001)

Apart from failure mechanisms resulting from weak stories, infills can also cause local shear failures in adjacent frame members. Development of strut action in the infill requires that the horizontal and vertical components of the compressive force be resisted by the bounding columns and beams, respectively (Figure 2.8). This can result in local shear failure in frame members as illustrated in Figure 2.9.

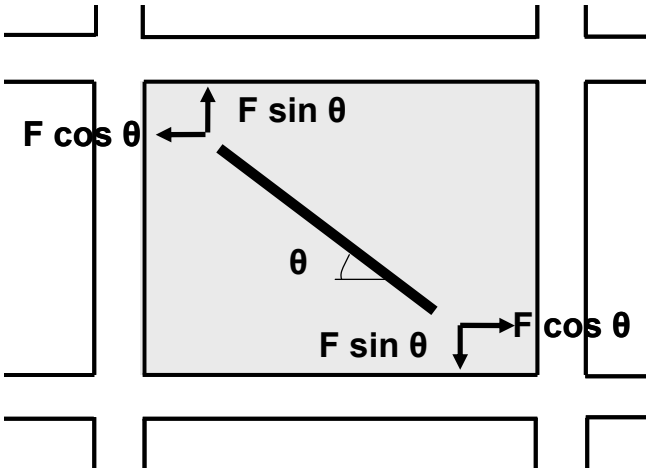

Figure 2.8: Shear forces on frame members due to infill strut action

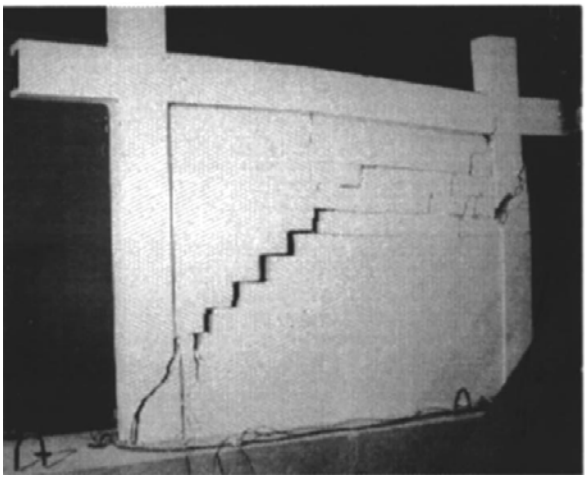

Figure 2.9: Shear failure in columns of bounding frame due to forces from the infill (Al-Chaar 2002)

The evidence presented here shows that while infills are sometimes structurally useful, they can also be detrimental.

2.3 PAST INVESTIGATIONS ON INFILLED FRAMES

Infilled frames have been investigated over many decades. These investigations primarily focused on infills made of clay or concrete masonry, with very few investigating AAC infills. Because experimental and analytical methodologies adopted for clay or concrete masonry infills masonry may be applicable to AAC infills as well, some pertinent investigations of infilled frames are reviewed here.

2.3.1 Investigations on infilled frame behavior

The stiffness and strength of infilled frames have been studied experimentally and analytically. Many investigations have characterized the behavior of infilled frames by idealizing the infill as an equivalent compression strut (Figure 2.10) that braces the frame, increasing its lateral stiffness and strength. Procedures have been proposed for computing the dimensions and properties of this equivalent strut.

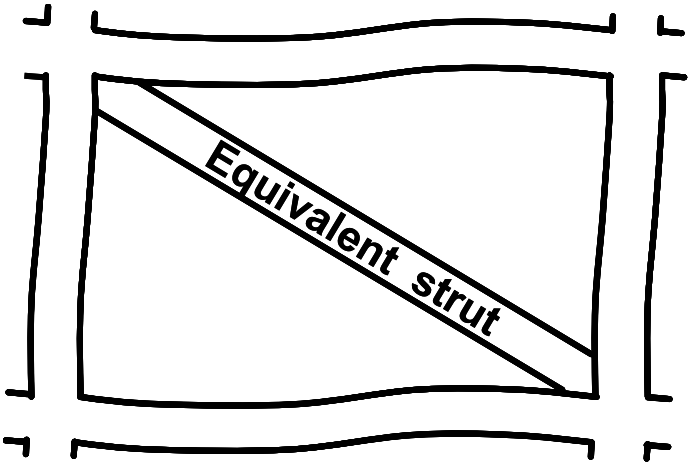

Figure 2.10: Idealization of structural action of infill as an equivalent strut

One of the earliest works was that of Holmes (1961), who proposed that the width of the equivalent strut be taken as one-third the length of the diagonal. Even at this early stage, investigators noted that complicated mathematical procedures to predict the behavior of infills were in "no way better or more reliable" than the simplest methods of structural analysis, due to inherent randomness associated with the system. After a series of experimental investigations on small-scale moment frames with mortar infilling, Stafford Smith (1962, 1966, 1969), proposed that the width of the equivalent strut would depend on a relative stiffness parameter λL. This early proposal is still widely accepted. Stafford Smith also proposed equations to predict the strength of the infill.

Klingner (1978) conducted tests on one-third scale, three-story, single-bay infilled frames and concludes that the beneficial effects of increased stiffness, strength and energy dissipation due to the presence of the infills exceeded the detrimental effects of increased stiffness. Riddington (1984) concludes that gaps between the infill and the bounding frame significantly reduce the stiffness and strength of infilled frames. Dawe (1989) tested several concrete masonry infilled steel frames, and concludes that interface conditions significantly affected the initial stiffness and strength of the infill; that infill-to-frame connections did not increase significantly the stiffness and strength; and that the

gap between the frame and the infill significantly decreased the stiffness and strength of the infilled frame. Flanagan (1999) conducted tests on several structural clay tile infilled steel frames and concluded that strength was insensitive to framing characteristics or panel geometry, and that the infill did not significantly affect the bending moments in the frame members. All his specimens failed by corner crushing. He presents a simple expression for the strength of the infill panel based only its thickness and the compressive strength of the infill material. Flanagan (2001) extended the methods presented in Flanagan (1999) to calculate stiffness and strength of infills for other types of infills. He suggests that these simple expressions can be useful for design purposes. Al-Chaar (2002) conducted tests on infilled reinforced concrete frames designed for gravity load only, and concludes that "the infilled reinforced concrete frames exhibited significantly higher ultimate strength, residual strength, and initial stiffness than bare frames without compromising any ductility in the load–deflection response." Al Chaar's specimens did not have ductile detailing, however, and failed by shear in frame members. This highlights the need to account in design for interaction forces between the infill and the bounding frame.

Analytical investigations based on the finite element method have been conducted by Liauw (1982), Riddington (1984), Dhanasekhar (1986), Mehrabi (1997), Chiou (1999), Dawe (2001), and many others. All predict the initial elastic behavior of infilled frames with reasonable accuracy. Liauw (1983) proposes a plastic analysis method to predict the collapse mode and strength of infilled frames. Saneinejad (1995) proposes analytical expressions based on frame analysis to predict the stiffness and strength on infilled frames. Although most of Saneinejad's work is based on static equilibrium of the frame and the infill, empirical assumptions based on the results of an earlier finite element analysis are also necessary. Based on its derivations, it proposes properties of the equivalent strut to be used for structural analysis of infilled frames. Evidence regarding the accuracy of the proposed procedure is contradictory. While Saneinejad (1995) reports a low coefficient of variation in ratios of observed to predicted capacities, later work by Flanagan (1999) indicates otherwise.

Kodur (1995) proposes a design method that takes into account the effect of the infill in all stages of the design process: determining fundamental period of the frame; determining the seismic loads; determining design forces; and determining design methods for frame and infill components. It notes that the design process must address failure modes due to increased axial forces in columns and local shear on frame members (Smith 1969) due to the presence of the infill. If these failure modes in frame members can be precluded, then increasing loads eventually lead to failure of the infill.

Today, Stafford Smith's approach is the most widely accepted for predicting initial stiffness of infilled frames. The ultimate strength of infills is satisfactorily predicted by many proposed relations, notably that of Flanagan (2001). Methods have been proposed for analysis and design of infilled frames (Saneinejad 1995, Kodur 1995). In this regard, methods based on experimental research appear more suitable than those based on analytical research, probably because of the inherent material and geometric variability associated with infills.

2.3.2 Investigations on AAC-infilled frames

Liu (2005) tested one-bay, two-story steel moment frames with and without AAC infill. A gap of 20 mm, tightly filled with foam-type material, was provided between the infill and the surrounding frame to simulate a flexible interface, and the infill was connected to the columns using welded angle sections. Liu reports that because the mortar was stronger than the AAC, the infills behaved as a monolithic block without horizontal cracks at the mortar-infill interface, and experienced inclined cracking along the compression strut. He suggests a drift limit for this diagonal cracking of AAC infills as 1/350. He does not, however, report the subsequent behavior of the infill. Considering the infill to behave as a shear panel, he proposes an expression for the initial stiffness of the infilled frame that has an accuracy of about 50% compared to their test results. They also report finite-element analytical studies that give reasonably good predictions of the specimens' load-displacement behavior. In those studies, the flexible material at the

frame-infill interface was modeled using nonlinear springs, and the infill was presumably modeled as monolithic.

Memari (1999) describes dynamic testing during construction of a six-story braced steel frame building with Autoclaved Cellular Concrete (same as AAC) interior partition walls and clay-brick curtain walls. The clay-brick curtain walls were isolated from the frame, and thus were assumed not to participate structurally. Memari concludes that the increase in stiffness of the bare steel frame due to the presence of AAC infills is much smaller than if the infills were clay or brick masonry. He also concludes that neglecting the presence of ACC infills in structural analysis will not significantly underestimate the design seismic base shear.

As outlined here, there is insufficient experimental information on the structural behavior of AAC-infilled frames. Such data are needed for studies of the seismic performance and design of AAC-infilled frames.

2.3.3 Literature on nonlinear hysteretic modeling techniques for infills

To study the global behavior of infilled frames requires reasonably accurate and efficient models representing the force-deformation behavior of infills. Given the variable geometry and material properties of infilled frames, such models need not be precise. Generally, macro-models have been used rather than micro-models (finite element method), because they require significantly less computational effort while offering reasonable accuracy. These macro-models generally idealize infills as compression-only equivalent struts (Figure 2.11). Literature on such models is now reviewed.

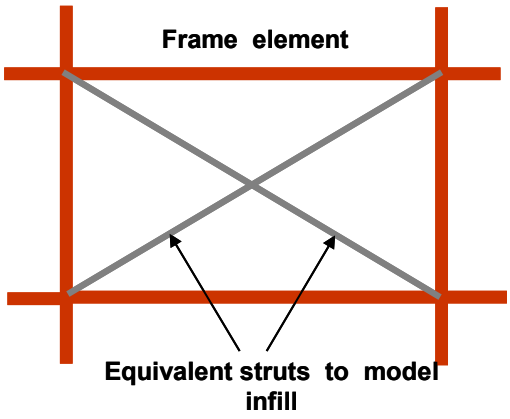

Figure 2.11: Modeling infill behavior using equivalent struts

One of the earliest works describing the use of macro-models to represent hysteretic behavior of infills is that of Klingner (1978), which idealizes the infill as two equivalent diagonal struts, each acting predominantly in compression. The strength envelope for the equivalent strut uses an initial elastic phase and an exponentially decreasing curve after attainment of peak strength. Although the model could have considered the tensile strength of the equivalent strut, this was ignored as insignificant. Hysteretic rules are proposed to capture the pinching behavior of the infill. The model is shown to adequately capture the response of an infilled frame that was experimentally tested earlier during the research. Even this early work attests to the computational efficiency of macro-models in simulating the global response of infilled frames.

FEMA (1998) quantifies the occurrence of limit states in infilled frames based on experimental results – corner crushing and diagonal cracking of infill at drift of 0.2% to 0.4%; and frame yielding and possible bed-joint sliding at drifts of 0.5% to 1.0%. At drifts beyond about 1%, cracking in the infill panel becomes more extensive, along with further frame damage. This information can be useful in developing the monotonic envelope of a hysteretic model representing infill behavior.

Panagiotakos (1993) used a bi-diagonal equivalent strut model (Figure 2.11) to study seismic behavior of a four-story reinforced concrete infilled frame that was also experimentally tested. Because this work forms the basis for the modeling approach used

later in this dissertation, it is discussed in more detail here. Based on experimental results, he calibrates a pinched hysteretic model that is used with the bi-diagonal equivalent struts. The values of the parameters α, β and γ of the hysteretic model depicted in Figure 2.12 that best represented the experimental results were found to be 0.15, 0.1 and 0.8 respectively. The shear strength and deformation at cracking for the infill are evaluated based on test results on masonry wallettes under diagonal compression and the ultimate strength (F_u) is estimated as 1.3 times the cracking strength. The resulting stiffness hardening ratio is about 1/7 to 1/10 of the initial stiffness. The descending branch of the monotonic curve beyond the ultimate strength is taken to have a slope of 0.5%. These values for the hysteretic models seemed to provide best agreement with experimental results.

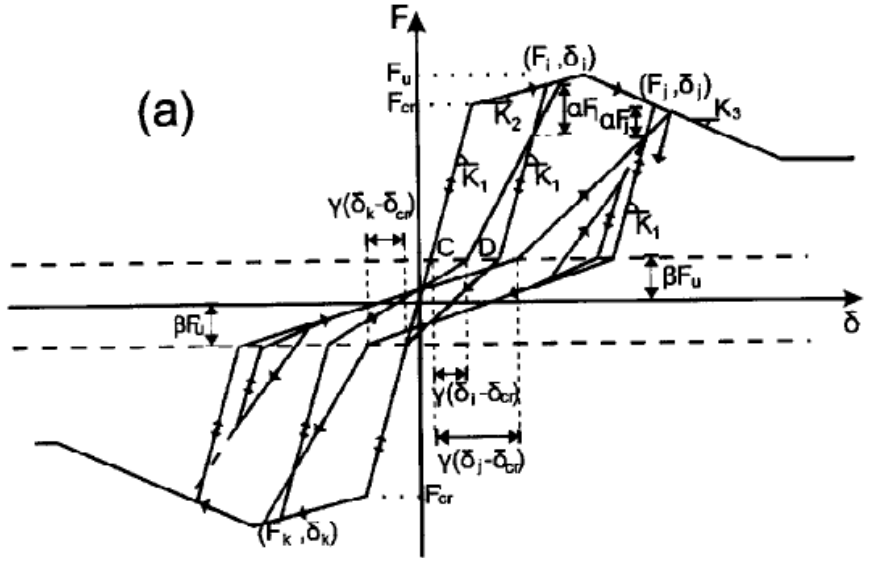

Figure 2.12: Hysteretic model used by Panagiotakos (1995) to simulate infill behavior

Madan (1997) used Saneinejad (1995) to obtain monotonic force-deformation properties of the equivalent strut and a modified version of Bouc-Wen model (Bouc 1967, Baber 1981) to represent the pinched hysteretic behavior of the equivalent strut. Majad demonstrated the performance of the model for a three-story reinforced concrete frame that was tested earlier. He concludes that macro-models (equivalent struts), such as

the one he presents, are better than micro-models for evaluating the seismic response of infilled frames, even though such models may not capture local interactions between the frame and the infill.

Flanagan (1999) observes that infills have significant post-peak strength and that the descending branch of the monotonic curve can be conservatively modeled as having 75% of peak strength at an in-plane drift of 1.5 times the displacement at peak. Based on experiments on steel frames infilled with structural clay tile infills, he proposes equations for strength and stiffness of infills, and suggests that the deflection corresponding to maximum strength of the infill be taken as 1 in. (25 mm). Flanagan (2001) performed a more detailed calibration of the equations for stiffness and strength proposed by Flanagan (1999) for many types of infills, and proposes deflections limits and properties of the diagonal strut for various limit states representing infill behavior. The information of Flanagan (1999) and Flanagan (2001) can be used to determine the properties of the backbone curve of the hysteretic model for infill response.

Combescure (2000) proposes the properties of the equivalent strut, specifically its width as a portion of the diagonal length, for various limit states representing the behavior of the infill. He suggests that the strain in the equivalent strut at the beginning of descending branch is 0.005, and strain at the end of the descending branch is 0.015.

Dolsek (2002) used pseudo-dynamic testing of a three-story reinforced concrete infilled frame to construct a hysteretic model for use with equivalent struts that simulate infill behavior. He provides valuable recommendations for the monotonic envelope of the hysteretic model, and uses a descending branch beyond attainment of maximum strength. He computed the initial stiffness of the equivalent strut using Mainstone (1971), the maximum strength of the infills according to Zarnic (1997), and took the cracking strength as about half the maximum strength. The lateral deflection at maximum strength was taken as about 0.5% to 0.6% of the story height. The stiffness of the descending branch of the backbone curve was taken as 5% of the initial stiffness. The final values for the backbone curve were computed based on comparison of analytical results with those from pseudo-dynamic testing of the RCC infilled frame. After trials with three different

hysteretic models to characterize infill behavior, Dolsek chose a shear-slip model as providing the best comparison with results from the pseudo-dynamic testing, while acknowledging that a pinched or a peak-oriented model might be equally effective. Dolsek (2005) adopted the same procedure as Dolsek (2002) to model behavior of infills, though with some differences. The displacement at the maximum strength was taken as 0.2% to 0.25% of the length of the diagonals, and the cracking strength as about 40% of the maximum strength.

Ibarra (2005) presents a family of hysteretic models, referred to as the Ibarra-Krawinkler hysteretic models, to capture the behavior of deteriorating systems. The salient features of the model are a backbone curve incorporating a residual branch with negative tangent stiffness. Three distinct hysteretic rules to be used with the model are proposed: bilinear, peak-oriented and pinched models. The pinched hysteretic model is particularly appropriate for infills, and the peak-oriented model may also be applicable. The pinched hysteretic model is further described later in this dissertation. Krawinkler (2007) illustrates the calibration of the Ibarra-Krawinkler hysteretic model with peak-oriented hysteretic rules using the experimental results of Mehrabi (1996).

Dolsek (2008) used equivalent struts to model the hysteretic behavior of infills, and assumed that the ratio between the cracking force and the maximum force is 0.6. Based on experimental observations, the drift at ultimate strength of the infills is generally assumed as about 0.15%. To establish the slope of the descending branch, the defection at zero residual strength is assumed as 5 times the deflection at the ultimate strength of the infill. Although the proposed parameters of the hysteretic model are arbitrary, they are calibrated against experimental results.

The investigations reviewed here are used later in this dissertation to develop and calibrate analytical models for hysteretic behavior of AAC and conventional masonry infills. These analytical models are then used to study the seismic performance of infilled frames, and to propose seismic design factors for such frames.

2.3.4 Investigations on seismic performance assessment of infilled frames

Many investigations have assessed the seismic performance of infilled frames. These investigations provide valuable insights into general seismic performance of infilled frames, specific parameters that significantly affect their behavior, and design guidelines that could lead to better performance. Because this dissertation has the same objective, the most relevant of those investigations are reviewed here.

Klingner (1978) notes that the increase in strength and ductility of frames due to infills may offset the increased seismic force demand due to increased stiffness.

Fardis (1995) idealized infilled frames as single-degree-of-freedom systems, and concludes that infills generally decrease the force and deformation demand on the frame, even though they shorten the fundamental period and consequently increase seismic forces. Because they are generally stiffer than the frame, infills attract more force than the frame, thereby reducing some actions in frame members and reducing lateral drifts. He observes that this is generally true regardless of the initial stiffness of the infill. The only exception is the case of a very stiff yet weak infill, which attracts high inertial forces but then fails shortly after transferring loads to the frame. He concludes that the most important parameter affecting the response of an infilled frame is the strength of the infill.

Madan (1997) analyzed a three-story, three-bay, reduced-scale model previously tested in the laboratory, and observes that infills reduce interstory drifts in frames. The shear demand in columns remained the same while the overall story shear demand increased, indicating that the stiffness of the infills led to increased seismic forces on the structure, and also indicating that that additional shear is resisted by the infills rather than the frame. Interstory drifts were also reduced, implying less damage in frame members.

To study the behavior of uniformly infilled and open ground story frames, Negro (1996, 1997) performed pseudo-dynamic testing and subsequent analytical investigation of a two-bay, four-story, reinforced-concrete frame. The frame was first tested as a bare frame, then as a uniformly infilled frame and finally as an open ground story frame. He

developed an analytical model and calibrated it against the test data. He concludes that masonry infills can significantly change the response of a frame, and that their effects should not be neglected during design. He points out that weak story mechanisms are possible even in uniformly infilled frames, and confirms that open ground story frames tend to concentrate failure mechanisms in the ground story. Failure in the open ground story frame spread to the infill panels in the second story and the overall failure mechanism resembled that of the uniformly infilled frame. Based on a vulnerability analysis, the open ground story frame had much higher damage indicators for only a small change in intensity, indicating a vulnerable structural system.

Dolsek (2001) investigated the formation of weak story mechanism in uniformly infilled frames. His work was motivated by the observation of soft story mechanisms in uniformly infilled frames during the Kocaeli earthquake of 1999. Based on the results of the analysis of a four-story reinforced concrete frame using a record from the Kocaeli earthquake and another artificial record representing the design spectrum of Eurocode 8, he concludes that soft-story mechanisms are possible even in uniformly infilled frames, if the ground motion intensity exceeds a threshold value, or if the bare frame has low global ductility, or if the infills are weak and brittle. He observes that uniformly distributed strong infills generally reduce drift and damage of frames, and that the initiation of weak story mechanism did not cause frame collapse under the ground motions used for his study.

Dolsek (2004) performed parametric studies of infilled frames represented as single-degree-of-freedom systems, and proposes equations for the relationship between the seismic response reduction factor, ductility and the fundamental period of infilled frame systems (R-μ-T relationships). Parameters considered in his study are the stiffness of the combined system; the ratio of strength of the infilled frame to that of the bare frame; the slope of the strength envelope for the infill after attainment of peak strength; and the slope of the descending branch of the strength envelope for the infill before its point of zero strength. His study shows that increasing the strength of the infill increases the ductility demand on the system, and also shows that the slope of the descending

branch of the infill before it reaches zero strength does not significantly affect R-μ-T relationships.

Two companion papers (Dolsek 2008a, 2008b) address deterministic and probabilistic assessment of the seismic performance of a four-story infilled reinforced concrete frame. Two cases are considered, a fully infilled frame and a partially infilled frame with openings. The deterministic performance assessment used the N2 method (Fajfar 2000), which relies on pushover analysis. The probabilistic performance assessment used the incremental N2 method (Dolsek 2004, 2007), which is similar to but simpler than the Incremental Dynamic Analysis (IDA) proposed by Vamvatsikos (2002). They conclude that infills significantly change the distribution of damage in a frame and their effect cannot be ignored in the design process. Weak story mechanisms can occur even in uniformly infilled frames, as demonstrated by concentration of the failure mechanism in the bottom two stories of the reinforced concrete infilled frame. He also observes, however, that formation of weak story did not reduce the collapse capacity of the frame. The deterministic assessment indicates that if seismic demand does not exceed the deformation capacity of infills, then infills generally help in reducing the drift and damage, provided that their distribution is uniform and they do not lead to local shear failure in columns. The probabilistic assessment indicates that regularly distributed infills reduce the probability of collapse of the frame. The benefits of infills are more evident from the probabilistic assessment than from the deterministic one.

Lignos (2007) performed a probabilistic seismic risk assessment of low-rise constructions, represented as single-degree-of-freedom systems. It acknowledges that this representation ignored higher-mode and soft-story effects. The parameters considered are strength, ductility and residual strength. Based on results of Incremental Dynamic Analysis, it concludes that increasing the strength of the infills has the maximum beneficial effect on the reducing the probability of collapse of the system, while residual strength and ductility had only limited effect. It concludes that systems with low ductility and low residual strength are likely to collapse unless the infills are strong.

From the investigations reviewed here, infills appear to improve the seismic performance of frames in some circumstances. However, the detrimental effects observed in other circumstances are also reflected in these investigations. The most important parameter affecting the seismic performance of infilled frames seems to be strength of the infill, but quantitative recommendations are inconsistent and inconclusive. Less important parameters include infill ductility, residual strength, and the slope of the descending branch of their backbone curve.

2.4 DESIGN PROVISIONS FOR INFILLED FRAMES IN MODERN BUILDING CODES

Design provisions for infilled frames in modern building codes are comprehensively treated by Kaushik (2006), which reviews national building codes of 16 countries. The observations of this work are presented below:

1. *Inclusion of infills in structural design process:* Many national codes allow use of infills to improve performance, while prescribing guidelines to avoid their detrimental effects. However, the New Zealand code recommends isolating the infill from participating in structural action of the frames. The International Building Code (2003) prohibits uses of masonry infills.

2. *Method of analysis:* Most codes recommend equivalent static analysis for regular low-rise infilled structures. When vertical or torsional irregularity exists due to the presence of infills, dynamic analysis is recommended. However, methods for analytical modeling of infills are not prescribed by most codes.

3. *Fundamental period:* Most national codes require that fundamental periods of frames be computed using empirical formulas, some of which include the effect of infills.

4. *Distribution of loads between infills and frame:* National codes vary widely on this. Most require that frame to be designed for at least 25% of the lateral loads. Some national codes (Columbia, Ethiopia, Egypt) also require that the infills be designed to withstand 100% of the lateral loads without assistance from the frame. The Eurocode recommends that frames resist all the gravity loads and at least 50-65% of the lateral

loads. The Algerian code prescribes that masonry infills should carry at most 20% of the vertical loads.

5. *Treatment of plan irregularities:* Most codes address plan irregularities, but few do so in the context of masonry infills. The Eurocode permits slight plan irregularity, but requires three-dimensional dynamic analysis if the eccentricity is excessive. The Nepalese code limits eccentricity between center of mass and center of rigidity limited to 10%. The Costa Rican code limits eccentricity in each direction to 25%, while the Israeli code limits it to 10%.

6. *Treatment of vertical irregularities:* National codes differ in their treatment of vertical irregularities introduced by infills, with some penalizing beams and columns in irregular stories. The Indian code, while allowing soft stories (stories with stiffness less than 70% of that in story above or less than 80% of the average lateral stiffness of three stories above), requires frame members in soft stories to be designed for 2.5 times the seismic story shears and moments obtained without considering effect of infills. The Eurocode recommends a similar procedure, but increasing the required strength of only the columns (not the beams) of a soft story. The increase is based on an index that is calculated using the reduction in strength of infills compared to the story above. The Bulgarian code allows soft stories, but requires frame members in such stories to be designed for about three times the design forces in corresponding bare frames. The Costa Rican code requires that all structural-resisting systems be continuous from the foundation to the top of buildings, and that the stiffness of a story be not less than 50% of that of the story below. The Israeli code allows soft or weak stories. Depending on the ductility of the building, beams and columns of the soft story and the two adjacent stories are required to be designed for at least 2.1–3.0 times the computed design forces for the irregular story.

7. *Response reduction factor for seismic design:* Most codes prescribe a lower force reduction factor for infilled frames than for corresponding bare frames, in effect requiring infilled frames to be designed for greater lateral forces than the corresponding bare frame.

8. *Strength and stiffness of infills:* Most codes do not prescribe adequate procedures to calculate strength of infills, without which they cannot be adequately considered in the design process.

The general shortcomings in national building codes with respect to design provision for infilled frames are:

1. Fundamental period of infilled frames: Many national codes prescribe empirical formulas for predicting fundamental period of infilled frames. However, these formulae may not be applicable in the presence of vertical or horizontal irregularities which are likely in infilled frames.

2. Design of frame members in weak/soft-stories: National codes vary in their approach towards design of soft and weak stories. Existing provisions are empirical and may not have a rational basis.

3. Stiffness and strength of infills: Most national codes do not prescribe equations for the stiffness and strength of infills. These are needed for analysis and design.

4. Response reduction factor for seismic design and allowable story drift: There is no consensus in national codes regarding value of response reduction factor for infilled frames. More research is required in this area.

Kaushik (2006) rightly points out there is an urgent need to adequately address infilled frames as a structural system in national building codes.

2.4.1 U.S design provisions for masonry infills

US design provisions for masonry infills can be summarized quite simply, because they do not yet exist. The Infill Subcommittee of the Masonry Standards Joint Committee (the ANSI-accredited technical committee charged with developing masonry design provisions for the US) is currently developing such provisions. Those are not expected to be approved, however, until the 2011 version of the MSJC Code and Specification at the earliest.

Draft infill design provisions currently under consideration by the MSJC are based on the equivalent-strut approach noted above. They provide equations to compute the stiffness and strength of the equivalent strut.

Representing the infill as an equivalent strut, however, ignores local interactions between the frame members and the infill, which are actually distributed along the ends of the frame members rather than being concentrated at a point (Figure 2.3 and Figure 2.8). The draft MSJC provisions address these local interactions.

2.5 AUTOCLAVED AERATED CONCRETE

General background on AAC is comprehensively presented in Tanner (2003), which is cited verbatim here:

> Autoclaved Aerated Concrete (AAC) is a lightweight cellular material composed of portland cement, quicklime, water, and finely ground sand (using a ball mill). Some or all of the sand can be replaced by fly ash (Chusid 1999). In the most common method of production, the dry materials are mixed with water to form slurry. Aluminum power is added to the slurry as it is poured into one third to one-half of the height of the forms (Figure 2.13). As the aluminum powder reacts with the alkaline cement, hydrogen gas forms which causes the slurry to increase in volume by two to three times. As the quicklime reacts with the water, sufficient heat is created to produce an accelerated initial set in the portland cement within three to four hours. At this time the mass is self-supporting; the molds are stripped and cut into the desired shapes using steel wires subject to tension (Figure 2.14). The cut shapes are then cured in an autoclave, producing a final material with about one-fifth to one-third the density of structural concrete. The material can be easily cut and shaped with hand tools (RILEM 1993). The cellular structure of AAC is shown in Figure 2.15.

Figure 2.13: AAC slurry in molds during the rising process (Tanner 2003)

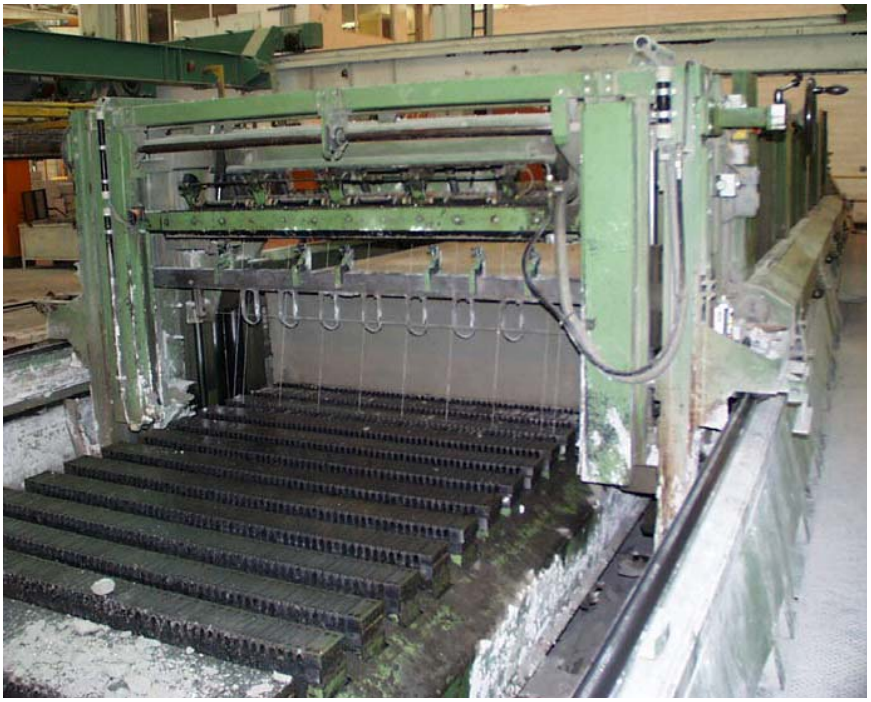

Figure 2.14: Cutting AAC mass after the forms are stripped (Tanner 2003)

Figure 2.15: Cellular structure of AAC (Tanner 2003)

2.5.1 Current uses of AAC

According to Tanner (2003),

AAC is a versatile material with typical products shown in Figure 2.16. Traditional elements include masonry-type units (blocks), floor panels, roof panels, wall panels, lintels, beams. Non-traditional elements include special shapes such as arches. These elements can be used in a variety of applications including residential, commercial and industrial construction. Reinforced wall panels can be used as cladding systems as well as load bearing and non-load bearing exterior and interior wall systems. Reinforced floor and roof panels can be efficiently used to provide the horizontal diaphragm system while supporting the necessary gravity loads.

The standard units in AAC structural systems are AAC shear walls and floor diaphragms. Shear walls may be constructed of modular blocks or panels oriented horizontally or vertically. Modular blocks are 8 in. (200 mm) in height and are 24 in. (610 mm) long. Wall panels are 24 inches (610 mm) in height and may have lengths up to 240 inches (6.10 m). The thickness of blocks and panels is variable, with a common thickness of 8 in. (200 mm) to 10 in. (250 mm). Floor panels have a width of 24 in. (610 mm) and are produced in lengths up to 240 in. (6.10 m). The height of floor and roof panels is variable, with a common

thickness of 8 in. (200 mm) to 10 in. (250 mm). Floor panels have a width of 24 in. (610 mm) and are produced in lengths up to 240 in. (6.10 m). The height of floor and roof panels is variable, with a common thickness of 8 in. (200 mm) to 10 in. (250 mm). Welded wire reinforcement in AAC panels consists of longitudinal wires, parallel to the axis of the panel and transverse, or cross-wires.

Individual AAC units are bonded together by thin-bed mortar. Joints are approximately 1/32 in. to 1/8 in. (1 mm to 3 mm) thick. Thin-bed mortar is a mix of portland cement, fine silica sand, polymers such as latex or vinylester, and admixtures such as water-retention admixtures. The compressive strength of the thin-bed mortar is greater than that of the AAC itself. A series of 2 in. (50 mm) by 2 in. (50 mm) thin-bed mortar cubes were tested at the Ferguson Structural Engineering Lab of UT Austin after curing in a laboratory environment for approximately 1 year. The average compressive strength of 12 cubes was 2100 psi (14.5 MPa), greater than the maximum compressive strength of the AAC.

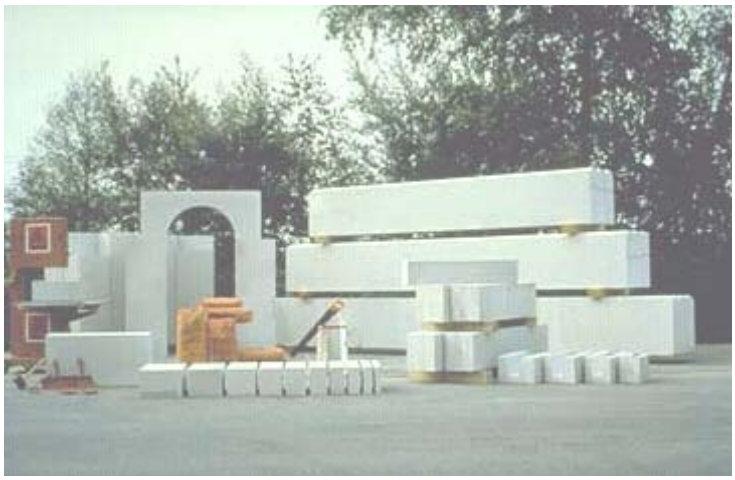

Figure 2.16: AAC blocks and panels (Tanner 2003)

2.6 AAC AS INFILL MATERIAL

AAC appears potentially useful as an infill material due to its light weight and its good thermal and acoustic insulation properties. Its excellent fire resistance can be important in bays and shafts accommodating elevators or staircase wells. Infills can be constructed of AAC modular blocks or panels oriented horizontally or vertically.

Structural characteristics of AAC that make it potentially useful as an infill material are its low stiffness and strength, which may modify the behavior of frames differently than what is normally observed of infilled frames. The low strength of AAC infills may also preclude adverse behaviors such as story mechanisms or local shear failure in frame members.

2.7 SUMMARY OF CHAPTER

A general introduction on infilled frames is presented. How infills participate in the structural response of frames is reviewed, and the concept of an equivalent strut is introduced. General experience regarding performance of infilled frames, particularly during earthquakes, is summarized. Past investigations on various aspects of infilled frame behavior are reviewed. An overview of design provisions for infilled frames in modern building codes around the world and in the US, is presented. This overview suggests the urgent need for development of comprehensive design provisions for infilled frames. The nature of AAC, its material properties, and its potential usefulness as an infill material are presented.

CHAPTER 3
Approach for determination of design provisions for AAC-infilled steel moment frames

3.1 INTRODUCTION AND SCOPE OF CHAPTER

In this chapter, the need for developing design provisions for infilled frames is pointed out, particularly with respect to seismic design. The goal of this dissertation is to fulfill that need by developing such design provisions, including seismic design factors, for AAC-infilled steel moment frames. This goal is broadly addressed by the systematic ATC-63 methodology for determination of seismic design factors of structural systems and is the current state of the art in the US for such determination. That methodology is used in this dissertation to determine seismic design factors for AAC-infilled steel moment frames. A general overview of the ATC-63 methodology is first presented. The concepts of "archetypical structures," "design rules," and "analytical models," introduced in Chapter 1, are further elaborated on, and specialized to the context of AAC-infilled steel moment frames. Steps in the methodology are discussed in more detail, and the criteria of the methodology for acceptance of a structural system and associated design rules, are presented.

3.2 NEED FOR DEVELOPING DESIGN PROVISIONS FOR INFILLED FRAMES

As noted in Chapter 2, infilled frames are a popular structural system throughout the world, including the US (Hamburger 2006). However, most building codes do not contain the design provisions that might ensure the safe and consistent performance of infilled frames, particularly during earthquakes. In fact, current US code provisions do not recognize infilled frames as a designated seismic force-resisting system (ASCE7-05).

In the past, infills have been found to be sometimes beneficial and other times detrimental to the seismic performance of frames. When they have been detrimental,

infills have caused collapse of many buildings during earthquakes, resulting in significant loss of life and property. Therefore, there is an urgent need to develop design provisions for infilled frames. While the immediate objective of this dissertation is to develop them for AAC-infilled steel moment frames, the approach and the results are in principle applicable to infilled frames in general.

3.3 ATC-63 METHODOLOGY FOR DETERMINATION OF DESIGN PROVISIONS FOR AAC-INFILLED STEEL MOMENT FRAMES

Determination of design provisions for a structural system involves establishing design rules for stiffness and strength of structural components, and also seismic design factors (R, C_d, Ω_o). This is broadly addressed by the ATC-63 methodology (ATC-63 2008). That methodology is used in this dissertation to validate design rules and establish corresponding seismic design factors for AAC-infilled steel moment frames. It is summarized in this dissertation, and described in detail in ATC-63 (2008). For convenience and clarity, some portions of ATC-63 (2008) are reproduced in the rest of this chapter, and are so identified.

According to ATC-63 (2008):

> This report describes a recommended methodology for reliably quantifying building system performance and response parameters for use in seismic design. The recommended methodology (referred to herein as the Methodology) provides a rational basis for establishing global seismic performance factors (SPFs), including the response modification coefficient (R factor), the system over-strength factor (Ω_o), and deflection amplification factor (C_d), of new seismic-force-resisting systems proposed for inclusion in model building codes…when properly implemented in the seismic design process, will result in equivalent safety against collapse in an earthquake, comparable to the inherent safety against collapse intended by current seismic codes, for buildings with different seismic-force-resisting systems.

3.4 BASIC REQUIREMENTS OF THE ATC-63 METHODOLOGY

In Chapter 1, the basic requirements of the ATC-63 methodology for its application to determine of seismic design factors of a structural system were outlined, as follows:

- archetypical structures;
- design rules to proportion and detail structural components comprising those archetypical structures for resisting code-prescribed loads; and
- mathematical models to simulate the response of those archetypical structures to imposed loads, particularly seismic loads.

These are further explained here, and are applied in the context of AAC-infilled steel moment frames. Additional information is also provided regarding application of the methodology to archetypical structures.

3.4.1 Archetypical structures

The first steps in the ATC-63 methodology involve proposing the general concept of the structural system under consideration, and identifying its seismic force-resisting system. "Archetypical structures," representing the type of structures that would probably be built using the proposed structural system, are envisaged. Typical parameters to be considered in establishing archetypical structures are: height; overall structural dimensions; smaller dimensions such as bay width and story height; seismic design categories to which the structures will probably be assigned; loading conditions; structural details; and other factors that may significantly affect structural performance. Once identified, archetypical structures can be further classified into performance groups based on their common characteristics. For example, performance groups can be identified based on height of the archetypical structures; the intensity of their gravity loading; or the type of structural component and lateral load-resisting system. The number of performance groups and the number of archetypical structures within a performance groups are not mandated. They should be selected so that the archetypical structures broadly represent the entire population of buildings that will probably be

constructed using the proposed structural system. ATC-63 (2008) recommends the identification of performance groups for the maximum and minimum spectral intensities in the highest seismic design category for which the structural system is intended to be assigned. When gravity loading significantly influences collapse behavior, performance groups of high and low gravity loading should be considered.

This dissertation primarily addresses AAC-infilled steel moment frames up to five stories high, with bay widths and story heights of 20 to 30 ft and 10 to 15 ft, respectively. The highest seismic design category in which they are intended to be located in the US is Seismic Design Category D (ASCE7-05). Two different infill configurations are considered: uniformly infilled frames; and uniformly infilled frames with an open ground story. These are depicted in Figure 3.1 and Figure 3.2, respectively. Uniformly infilled frames are infilled with identical infill panels in vertically continuous bays in all stories. Uniformly infilled frames with open ground story, referred to as open ground story frames, are the same except that they are not infilled in the ground story.

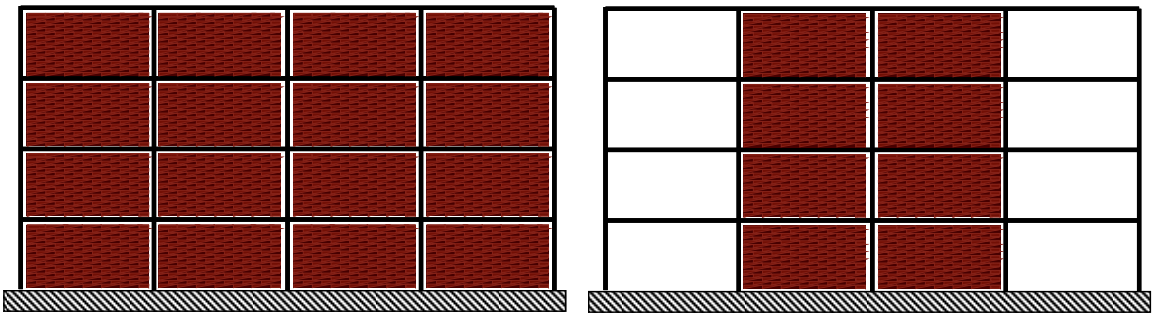

Figure 3.1: Examples of uniformly infilled frames

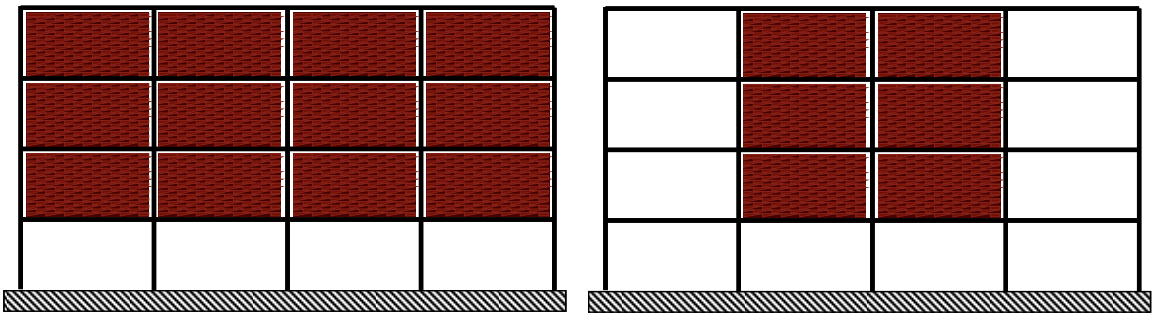

Figure 3.2: Examples of uniformly infilled frames with an open ground story

In this dissertation, archetypical AAC-infilled steel moment frames are selected for both infill configurations, and are categorized into performance groups later in this dissertation. The selected archetypical infilled frames are evaluated using the ATC-63 methodology, and seismic design factors and design guidelines are proposed for such infilled steel moment frames.

3.4.2 Design rules for AAC-infilled steel moment frames

The ATC-63 methodology requires that archetypical structures be designed for the loads prescribed by ASCE7-05, and hence requires basic design rules for determining the proportions and details of structural components of archetypical structures. For AAC-infilled steel moment frames, design rules must be established for the steel moment frame and for the AAC infill. Rules must also be provided for structural analysis and computation of internal force resultants in frame members and infills due to external loads, and also due to interaction between the infill and the bounding frame.

Design provisions for steel moment frames are adequately addressed by current building codes. In the US, the AISC Specification (2005) provides comprehensive requirements for analysis, design, detailing and fabrication of structural steel buildings. Those requirements are used in this dissertation. For AAC infills, the Masonry Standards Joint Committee (MSJC) is developing provisions for design of masonry infilled frames, including procedures for calculating the stiffness and strength of infills. Those procedures

are presented in Chapter 2. Because it would be desirable to extend them to AAC infills, their applicability to AAC infills is investigated in this dissertation.

3.4.3 Trial values for seismic design factors

The ATC-63 methodology requires that the archetypical structures be designed for the seismic loads prescribed by ASCE7-05 using trial values of seismic design factors, particularly the response reduction factor R. If, at the end of the evaluation process, the archetypical structures designed using that trial value of R do not meet the desired performance criteria, they are required to be re-designed and re-evaluated using a lower value of R, improved design methods, improved detailing, or other strategies. This process of re-designing and re-evaluation of archetypical structures must be repeated until all performance criteria prescribed by the methodology are met by each performance group of the archetypical structures.

In applying the ATC-63 methodology to AAC-infilled steel moment frames, the trial seismic design factors are assumed to be those prescribed by ASCE7-05 for the bare steel moment frame. In particular, for special steel moment frames, the factors R, Ω_o , and C_d , are assigned trial values of 8, 3 and 5.5, respectively.

3.4.4 Analytical modeling of archetypical structure and component behavior

To evaluate the seismic performance of the archetypical structures using the nonlinear analysis procedures of the ATC-63 methodology requires the development and calibration of nonlinear hysteretic models for structural components, especially those that contribute to inelastic behavior of the structure. This requires experimental data, including the monotonic and cyclic degradation of stiffness and strength, because non-deteriorating models can significantly over-predict collapse capacity of structures. An example of component behavior with stiffness and strength deterioration is shown in Figure 3.3, which illustrates (for the specific case of plywood panels) four numbered modes of deterioration: 1) basic strength deterioration; 2) post-capping strength

deterioration; 3) unloading stiffness deterioration; and 4) accelerated reloading stiffness deterioration (Gatto 2002, Ibarra 2005).

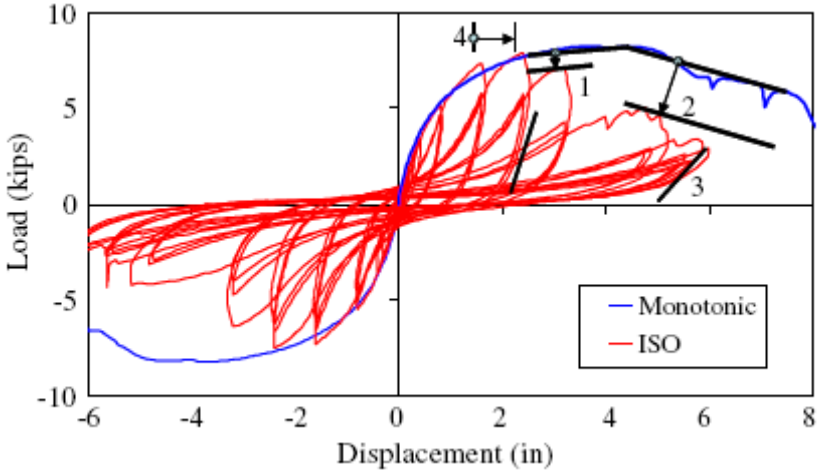

Figure 3.3: Cyclic degradation of stiffness and strength of structural components (Gatto 2002, Ibarra 2005)

For this ATC-63 investigation of infilled frames, a suitable force-deformation model is the Ibarra-Krawinkler hysteretic model (Ibarra 2005), which incorporates monotonic strength deterioration using a descending branch, and also considers residual strength of components. It uses an energy-based deterioration parameter to control basic strength deterioration, post-capping strength deterioration, unloading stiffness and accelerated reloading stiffness.

Once the force-deformation model is developed, it must be used in a structural analysis program capable of performing nonlinear static and dynamic analysis on analytical models of the archetypical structures, and also capable of handling large deformations. The model must then be calibrated based on experimental data for component behavior. This is illustrated in Figure 3.4 for the Ibarra-Krawinkler hysteretic model, calibrated against experimental data determined in this study for the lateral load-deflection response of an AAC infill, using the nonlinear structural analysis program OpenSees (OpenSees 2006). Using such verified component models, analytical models of entire archetypical structures are developed.

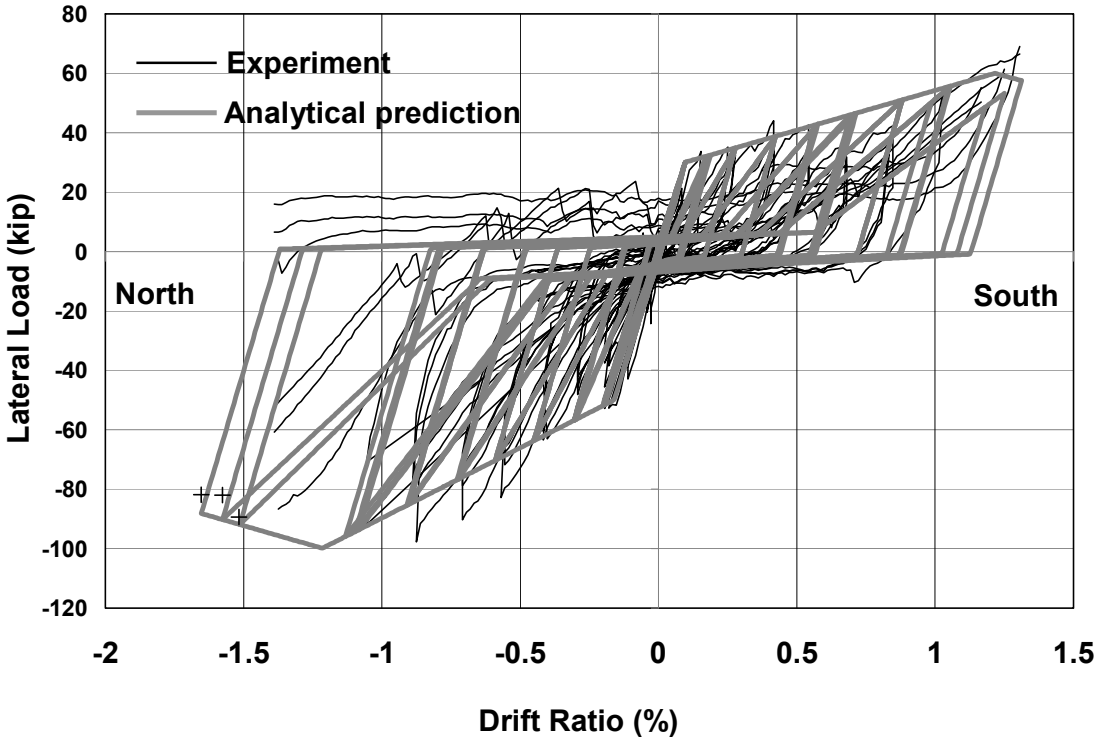

Figure 3.4: Calibration of Ibarra-Krawinkler model for AAC infills against experimental results using OpenSees

3.4.5 Seismic design category

The ATC-63 methodology requires that structural systems be evaluated for performance in different seismic design categories, using Site Class D (stiff soil) of ASCE7-05. These seismic design categories have short-period and 1-sec period spectral acceleration parameters, defined by the methodology in Table 6-1A and 6-1 of ATC-63 (2008), and presented here as Table 3-1 and Table 3-2. Definitions of parameters S_s, S_1, S_{MS}, S_{M1}, S_{DS}, S_{D1}, F_a and F_v in Table 3-1 and Table 3-2 are same as those in ASCE7-05. The definition of seismic design categories by the ATC-63 methodology closely follows Section 11.6, Table 11.6-1 and Table 11.6-2 of ASCE7-05. In Figure 3.5 are presented the MCE-level response spectra for the prescribed seismic design categories.

Table 3-1: Short- period spectral acceleration for seismic design categories (Table 6-1A of ATC-63, 2008)

Seismic Design Category		Maximum Considered Earthquake			Design
Maximum	**Minimum**	S_s **(g)**	F_a	S_{MS} **(g)**	S_{DS} **(g)**
D		1.5	1.0	1.5	1.0
C	D	0.55	1.36	0.75	0.5
B	C	0.33	1.53	0.50	0.33
	B	0.156	1.6	0.25	0.167

Table 3-2: 1-sec period spectral acceleration parameter for seismic design categories (Table 6-1B of ATC-63, 2008)

Seismic Design Category		Maximum Considered Earthquake			Design
Maximum	**Minimum**	S_1 **(g)**	F_v	S_{M1} **(g)**	S_{D1} **(g)**
D		0.60	1.50	0.90	0.60
C	D	0.132	2.28	0.30	0.20
B	C	0.083	2.4	0.20	0.133
	B	0.042	2.4	0.10	0.067

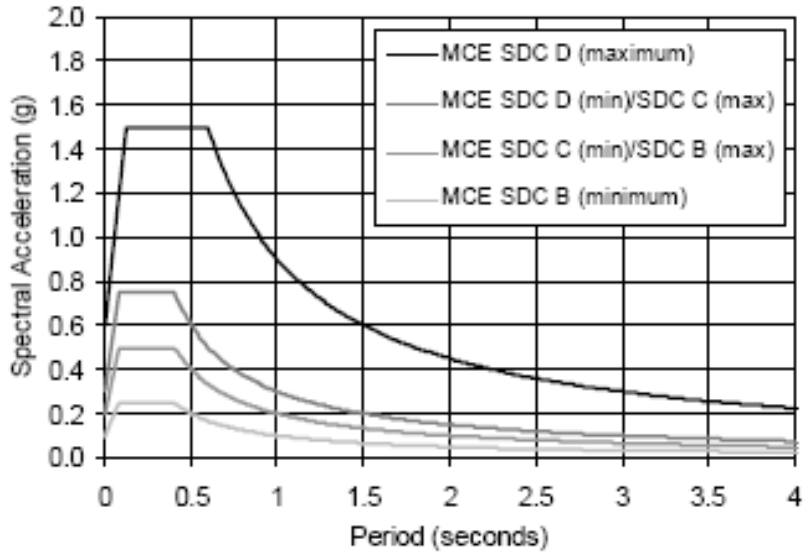

Figure 3.5: MCE-level response spectra defined by ATC-63 methodology for different seismic design categories (ATC-63 2008)

3.4.6 Ground-motion suite for ATC-63 methodology

The ATC-63 methodology provides for two suites of ground motions, far-field and near-field, for performing non-linear dynamic analysis of archetypical structures. The far-field suite corresponds to motions recorded at a distance greater than 10 km from the fault rupture, and near-field suite corresponds to those recorded at a distance of less than 10 km. Only the far-field suite is generally used, unless explicit modeling of near-field effects is required. The far-field ground-motion suite comprises 22 pairs of ground motions, and the near-field suite comprises 28 pairs of ground motions, taken from the PEER NGA database (PEER 2006). Those ground motions are not differentiated with respect to fault rupture mechanism or site conditions.

3.5 NEED FOR EXPERIMENTAL INVESTIGATION OF AAC-INFILLED STEEL MOMENT FRAMES

Verification of the applicability of draft MSJC infill provisions to AAC infills, and development of realistic hysteretic models for AAC infills, both require experimental

data on the behavior of AAC-infilled frames. Unfortunately, there is an almost total lack of published literature on this topic. Therefore, Chapter 4 of this dissertation includes a limited experimental investigation of the effects of AAC infills on the in-plane hysteretic behavior of steel moment frames. In Chapter 5, the applicability of the draft MSJC infill provisions to AAC infills is checked using those experimental results. In Chapter 6, an analytical model for AAC infills is developed and calibrated using those experimental results.

3.6 ANALYSIS OF ARCHETYPICAL STRUCTURES

Using the previously developed analytical models, archetypical structures are analyzed to assess their collapse capacity. In this section, the various steps prescribed by the ATC-63 methodology for these analyses are outlined.

3.6.1 Fundamental period

The ATC-63 methodology defines the fundamental period of archetypical structures as the limiting fundamental period determined by Section 12.8.2 of ASCE7-05.

3.6.2 Pushover analysis

Pushover analysis is performed on the analytical model developed for the archetypical structures, to validate the model and to determine over-strength and ductility factors for later use. The ATC-63 methodology requires that the lateral load pattern for the pushover analysis be computed as prescribed by Section 12.8 of ASCE7-05. Referring to Figure 3.6, and using the pushover curve, the ATC-63 methodology requires that the over-strength and ductility factors be computed as:

$$\Omega = \frac{V_{\max}}{V_{design}}$$

$$\mu_c = \frac{\Delta_u}{\Delta_y}$$

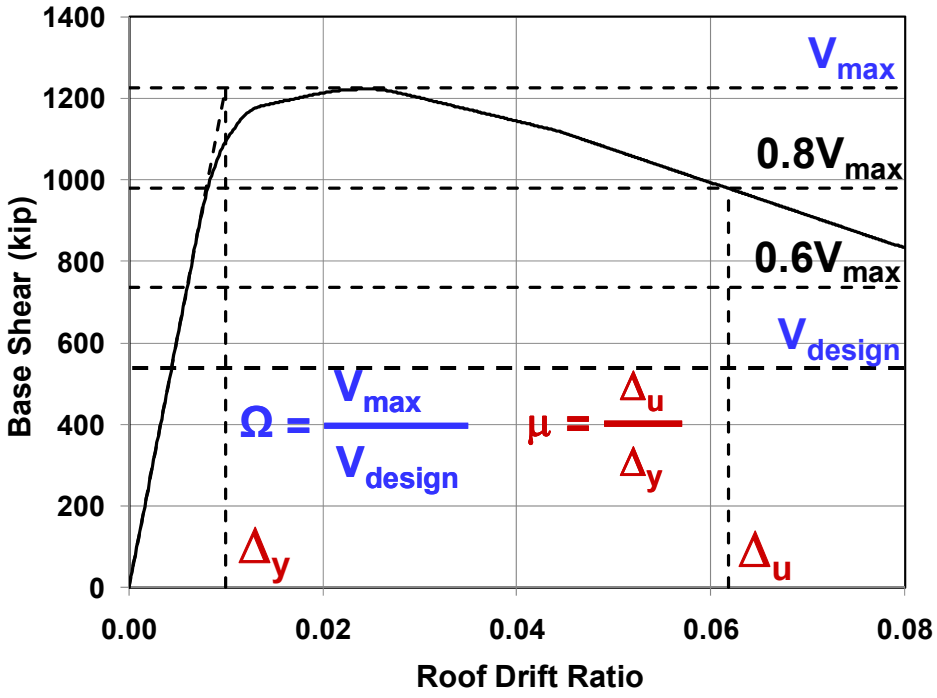

Figure 3.6: ATC-63 guidelines for determination of over-strength and ductility factors using pushover curve of archetypical structures

3.6.3 Incremental Dynamic Analysis

Incremental dynamic analysis, abbreviated as IDA and detailed in Vamvatsikos (2002, 2004), involves performing nonlinear dynamic analyses on archetypical structures for the selected suite of ground motions. In general and in this dissertation, those are the 44 ground motions of the far-field suite provided by the ATC-63 methodology. Each ground motion, scaled by increasing factors, is applied to the archetypical structure until collapse occurs. The intensity of each ground motion corresponding to collapse is defined as the scaled spectral acceleration of the ground motion at the defined fundamental period of the structure ($S_a[T]$). Collapse is considered to occur based on exceedance of a chosen damage indicator. Generally, maximum interstory drift is considered as the damage indicator, and an exceedance of 12 to 15% in maximum interstory drift is considered to denote collapse. For the AAC-infilled steel moment frames considered in this

dissertation, an interstory drift of 15% or more at any story of the frame is considered to denote collapse according to the recommendations of the ATC-63 methodology.

Figure 3.7 illustrates typical results obtained from IDA. Each point in the figure represents the maximum interstory drift obtained from nonlinear dynamic analysis of the archetypical structure for one of the ground motions scaled to a particular intensity. Each curve in the figure presents the maximum interstory drifts obtained from nonlinear dynamic analyses for increasing intensities of a particular ground motion until collapse is achieved under that ground motion. Using the far-field suite, there are 44 such curves in Figure 3.7. From this, the median collapse spectral intensity at the fundamental period of the structure, $S_{CT}[T]$, which produces collapse of the archetypical structure under half of the ground motions is determined. Basically, this is the mean of the 22nd and the 23rd largest collapse spectral intensities obtained for the 44 ground motions of the far-field ground motion suite. The MCE-level spectral intensity, $S_{MT}[T]$, is computed at the fundamental period of the archetypical structure using one of the response spectra given in Figure 3.5 depending on the seismic design category for which the archetypical structure is being evaluated. Thereafter, the collapse margin ratio (*CMR*), defined as the ratio of the $S_{CT}[T]$ and $S_{MT}[T]$, is computed as:

$$CMR = \frac{S_{CT}[T]}{S_{MT}[T]}$$

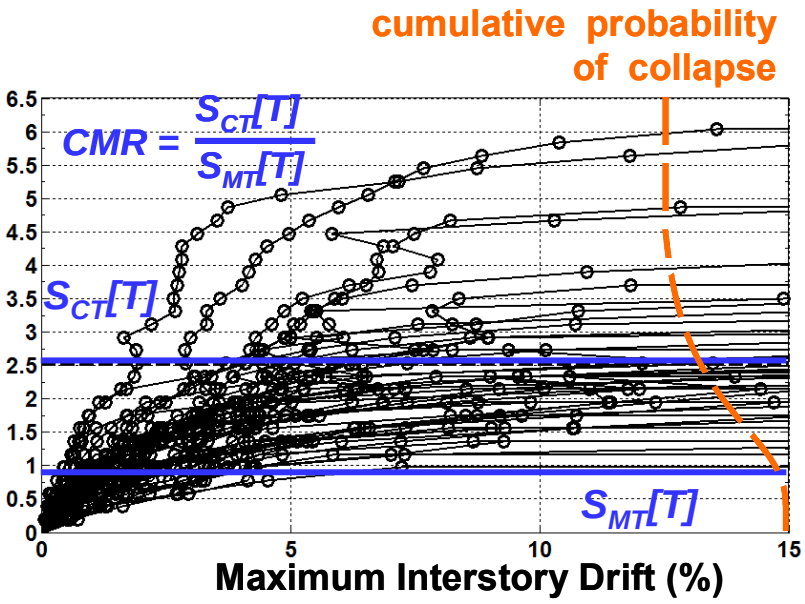

Figure 3.7: Typical results from incremental dynamic analysis (IDA)

3.6.4 Non-simulated collapse modes

Even state-of-the-art modeling techniques may not adequately address all possible failure mechanisms in archetypical structures, such as fracture in steel members or shear failure in reinforced concrete frame members. As shown in Figure 3.8, however, these failure mechanisms can be inferred from occurrence of associated component limit states. For example, fracture in plastic hinges of steel moment frame members may be expected to occur on exceedance of a threshold plastic rotation; and shear failure in reinforced concrete frame members may be expected to occur on exceedance of a threshold nominal shear stress. Such failure mechanisms are referred to in the ATC-63 methodology as "non-simulated" collapse modes, because their occurrence is inferred indirectly from the analytical results, rather than being simulated directly by the analytical models. The ATC-63 methodology explicitly addresses non-simulated collapse modes.

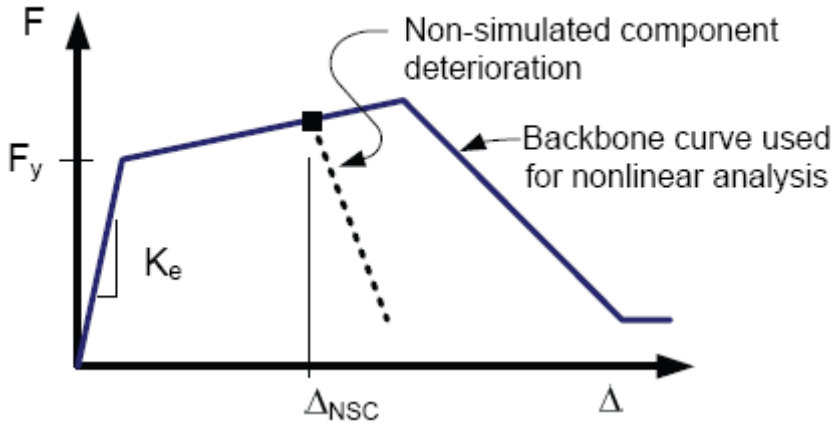

Figure 3.8: Non-simulated failure mode in a component (ATC-63 2008)

If component limit states associated with non-simulated collapse modes occur earlier than collapse by exceedance of maximum allowable interstory drift for a particular ground motion, then collapse is considered to have occurred. As a result, non-simulated collapse modes can decrease the collapse spectral intensity directly obtained from IDA for that ground motion. This is illustrated in Figure 3.9 for "Ground Motion 1," for which a succession of solid dots indicates consistent non-simulated collapse above a threshold spectral intensity. The main drawback in using non-simulated collapse modes to infer collapse spectral intensities lower than those given directly by IDA, is that the non-simulated collapse modes may represent only local component failures, and may not necessarily lead to collapse of the entire structure. Considering them as failure may result in under-prediction of the median collapse spectral intensity of the archetypical structure. In addition, if non-simulated collapse is detected at a particular spectral intensities, but does not occur at higher intensities, it is hard to justify interpreting the first such occurrence as collapse of the structure. This is illustrated in Figure 3.9 for "Ground Motion 2," for which the solid dots indicate that non-simulated collapse might occur at spectral intensities less than 1 g, but consistently does not occur at higher intensities. Therefore, careful judgment needs to be exercised in determining whether a non-simulated collapse mode should be interpreted as global collapse of the structure.

Consideration of non-simulated collapse modes is further explained in Section 5.6 of ATC-63 (2008), and is illustrated for an example steel moment frame in Section 10.2 of that document.

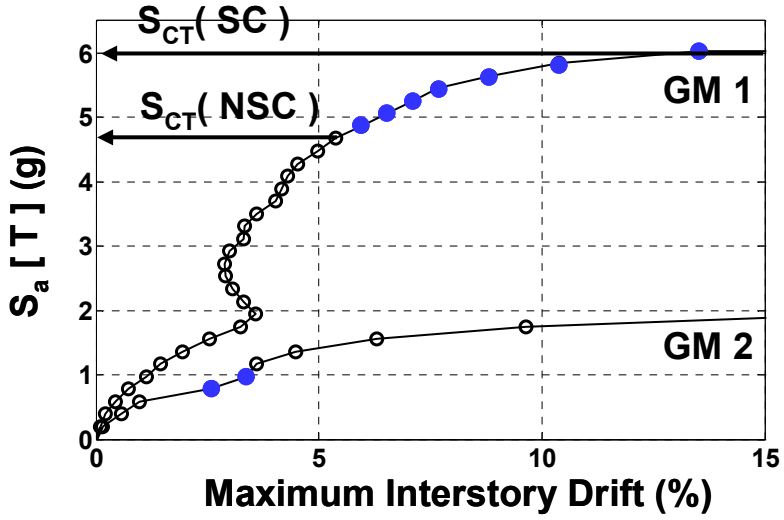

Figure 3.9: Non-simulated collapse modes lower collapse spectral intensity

3.7 EVALUATING PERFORMANCE OF ARCHETYPICAL STRUCTURES

The final step in performance evaluation is computation of the probability of collapse of archetypical structures under MCE-level ground motions. Based on results obtained from the pushover analysis and IDA, those computations are carried out using the steps described below.

3.7.1 Adjusting *CMR* for effects of spectral shape

Possible differences between the shape of the spectrum used for design (Figure 3.5) and the shapes of the spectra of the ground motions used for IDA, affect the estimation of collapse spectral intensity of archetypical structures using IDA. To account for these differences in spectral shape, the *CMR* determined from IDA is multiplied by a so-called "spectral shape factor" (*SSF*) to produce the Adjusted Collapse Margin Ratio

(*ACMR*). The values of *SSF* are provided in Table 7-1a and Table 7-1b of ATC-63 (2008), based on the fundamental period of the archetypical structure and the ductility (μ) obtained from pushover analysis for the archetypical structure.

The reason for adjusting *CMR* for effects of spectral shape is explained directly in ATC-63 (2008):

> Baker and Cornell (2006) have shown that rare ground motions in the Western United States, such as those corresponding to the MCE, have a distinctive spectral shape that differs from the shape of the design spectrum used for structural design in ASCE/SEI 7-05 (ASCE 2005). In essence, the shape of the spectrum of rare ground motions is peaked at the period of interest, and drops off more rapidly (and has less energy) at periods that are longer or shorter than the period of interest. Where ground motion intensities are defined based on the spectral acceleration at the first-mode period of a structure, and where structures have sufficient ductility to inelastically soften into longer periods of vibration, this peaked spectral shape, and more rapid drop at other periods, causes these rare records to be less damaging than would be expected based on the shape of the standard design spectrum.
>
> The most direct approach to account for spectral shape would be to select a unique set of ground motions that have the appropriate shape for each site, hazard level, and structural period of interest. This is not feasible, however, in a generalized procedure for assessing the collapse performance of a class of structures, with a range of possible configurations, located on a number of different sites. To remove this conservative bias, simplified spectral shape factors, SSF, which depend on fundamental period, T, and ductility capacity, μ, are used to adjust collapse margin ratios.

3.7.2 Uncertainties to be considered in evaluation

The collapse capacity of an archetypical structure is affected by various uncertainties that are difficult to consider explicitly during analyses. The ATC-63 methodology outlines important sources of these uncertainties and requires that their effects be considered post-analysis in performance evaluation. These sources of uncertainties are as follows:

1) Record-to-record (RTR) uncertainty: The response of archetypical structures varies depending on ground motion characteristics such as frequency content, and duration. Collapse of an archetypical structure may be indicated analytically at different scaling factors (and hence different spectral intensities $S_a[T]$) for different ground motions during the IDA. This variation in response is due to record-to-record uncertainty.

2) Design requirements-related (DR) uncertainty: This type of uncertainty accounts for possible variations in an archetypical structure due to the flexibility offered by the design and detailing rules. For example, in a structural steel member, for a given design moment, several W-sections may be suitable, all equally likely to be chosen. For another example, for a given design moment, for a reinforced concrete member, several diameters of reinforcing bars may be suitable, all equally likely to be chosen. This type of uncertainty also reflects the extent to which the archetypical structures represent real design and construction practice.

3) Test data-related (TD) uncertainty: Nonlinear models of structural components used for analysis of archetypical structures are calibrated based on available test data. These test data may not comprehensively represent all possible component designs, or may not give complete information regarding component behavior from initial elastic response through failure. Thus, test data-related uncertainty quantifies the quality and consistency of the test data against which component behavior is modeled and calibrated.

4) Modeling (MDL) uncertainty: The analytical model of an archetypical structure is constructed using component models, which must accurately simulate component behavior from initial elastic response through failure. Many component models exist, varying in their basic formulation and ability to accurately capture component behavior. Any one of those could equally likely to be chosen by the analyst. Thus, modeling uncertainty quantifies the uncertainty involved in the choice of component models and their relative accuracy. It also reflects errors made in analysis.

3.7.3 Collapse fragility curve

The next step in the evaluation process is determination of the collapse fragility curve for archetypical structures, which essentially presents the probability of collapse of the archetypical structure as a function of spectral intensity. The effects of the uncertainties described immediately above are included in this determination as explained below. The parameters associated with the uncertainties in expressions below use abbreviated subscripts whose context has been indicated in the previous section on uncertainties.

According to ATC-63 (2008):

> Formally, the collapse fragility of each index archetype is defined by the random variable, S_{CT} , assumed to be equal to the product of the median value of the collapse ground motion intensity, $S_{CT}[T]$, as calculated by nonlinear dynamic analysis, and the random lognormal variable, λ_{TOT}:
>
> $$S_{CT} = S_{CT}[T]\,\lambda_{TOT}$$
>
> where λ_{TOT} is a lognormal random variable with a median value of unity and a lognormal standard deviation of β_{TOT}. The lognormal random variable is assumed to be the product of four component random variables:

$$\lambda_{TOT} = \lambda_{RTR}\ \lambda_{DR}\ \lambda_{TD}\ \lambda_{MDL}$$

where λ_{RTR} , λ_{MDL} , λ_{DR} , and λ_{TD} are lognormal random variables with median values of unity, and lognormal standard deviation parameters, β_{RTR} , β_{DR} , β_{TD} and β_{MDL} respectively. Since these parameters are assumed to be statistically independent, the lognormal standard deviation parameter, β_{TOT} , describing total collapse uncertainty, is given by:

$$\beta_{TOT} = \sqrt{(\beta_{RTR}^2 + \beta_{DR}^2 + \beta_{TD}^2 + \beta_{MDL}^2)}$$

where,

β_{TOT} = total system collapse uncertainty

β_{RTR} = record-to-record collapse uncertainty (0.40)

β_{DR} = design requirements related collapse uncertainty

β_{TD} = test data related collapse uncertainty

β_{MDL} = modeling related collapse uncertainty

While record-to-record variability can be determined directly from the results of the IDA analysis, the ATC-63 methodology prescribes that the associated standard deviation parameter β_{RTR} be taken as 0.4 for this type of uncertainty (Haselton 2006; Ibarra 2005a, 2005b; and Zareian 2006).

Design requirements, test data and modeling related uncertainties are required to be rated as “superior,” “good,” “fair,” or “poor; “superior” indicates the least uncertainty, and “poor” indicates the greatest uncertainty. The value of the standard deviation parameter associated with each rating is given in Table 3-3.

Table 3-3: Lognormal distribution standard deviation parameters corresponding to qualitative uncertainty ratings

Uncertainty rating	Lognormal distribution standard deviation parameter
Superior	0.2
Good	0.3
Fair	0.45
Bad	0.65

The collapse fragility curve is then plotted as a lognormal cumulative distribution function with $S_{CT}[T]$ or *ACMR* as the median and β_{TOT} as the lognormal standard deviation parameter. An example of this is shown in Figure 3.10. The horizontal line is drawn from a probability of collapse of 50% (the median), and the corresponding vertical line indicates the *ACMR* (selected arbitrarily in this case). As shown in that same figure, for a constant $S_{CT}[T]$ or *ACMR*, greater uncertainties in collapse evaluation lead to a larger lognormal standard deviation parameter and a greater probability of collapse at MCE-level spectral intensity $S_{MT}[T]$.

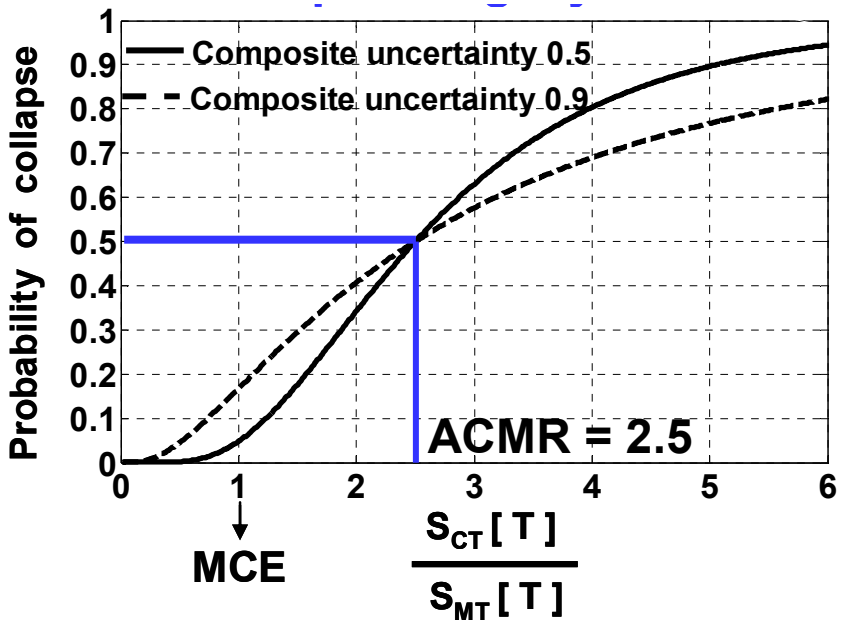

Figure 3.10: Collapse fragility curve and effect of greater system uncertainty

3.7.4 Probability of collapse at MCE

For each archetypical structure, the next step in the ATC-63 methodology is determination of the probability of collapse at MCE using the collapse fragility curve (Figure 3.10).

3.7.5 Acceptable performance and validation of structural system

According to the ATC-63 methodology, the performance of a structural system is acceptable if:

1. The probability of collapse at MCE of each archetypical structure is less than about 20%; and

2. The average probability of collapse at MCE of the archetypical structures in a performance group is less than about 10%.

If these conditions are met, the response modification factor (R) used in the original design of the archetypical structures is considered acceptable, and the ATC-63

performance evaluation ends with computation of the system over-strength and displacement amplification factors.

If these conditions are not met, the trial response modification factor must be increased, or the design and detailing rules must be refined, and the ATC-63 methodology must be repeated.

3.7.6 Determination of system over-strength factor

According to ATC-63 (2008), the system over-strength factor is to be determined as follows:

> The average value of archetype overstrength, Ω, is calculated for each performance group. The value of the system overstrength factor, Ω_0, for use in design, should not be taken as less than the largest average value of calculated archetype overstrength, Ω, from any performance group. The system overstrength factor, Ω_0, should be conservatively increased to account for variation in overstrength results of individual index archetypes, and judgmentally rounded to half-integer intervals (for example, 1.5, 2.0, 2.5, and 3.0). The system overstrength factor, Ω_0, need not exceed 1.5 times the response modification coefficient, *R*. A practical limit on the value of Ω_o is about 3.0, consistent with the largest value of this factor specified in Table 12.2-1 of ASCE 7-05 for all current approved seismic force-resisting systems.

3.7.7 Determination of displacement amplification factor

According to ATC-63 (2008), the displacement amplification factor is to be determined as follows:

> The deflection amplification factor, C_d, is based on the acceptable value of the response modification factor, R, reduced by the damping factor, B_{1E}, corresponding to the inherent and added viscous damping of the system of interest:

$$C_d = \frac{R}{B_{1E}}$$

where,

C_d = deflection amplification factor

R = system response modification factor

B_{1E} = numerical coefficient as set forth in Table 18.6-1 of ASCE7-05 for effective damping equal to $\beta_I + \beta_{VI}$ and period, T

β_I = component of effective damping of the structure due to the inherent dissipation of energy by elements of the structure, at or just below the effective yield displacement of the seismic-force-resisting system, Section 18.6.2.1 of ASCE7-05

β_{VI} = component of effective damping of the first mode of vibration of the structure in the direction of interest due to viscous dissipation of energy by damping devices (for systems with such devices), at or just below the effective yield displacement of the seismic force-resisting system, Section 18.6.2.3 of ASCE 7-05.

Most systems do not include damping devices (that is, $\beta_{VI} = 0$) and have only inherent damping, β_I. In general, inherent damping may be assumed to be 5% of critical, and a corresponding value of the damping coefficient, $B_{1E} = 1.0$ (Table 18.6-1, ASCE 7-05). Thus, for most systems the value of C_d will be equal to the value of R.

3.8 SUMMARY OF THIS CHAPTER

In this chapter, the motivation and need for development of design provisions, including seismic design factors, for AAC-infilled steel moment frames, are reiterated. The recently proposed ATC-63 methodology (ATC-63 2008), a systematic way of determining seismic design factors of structural systems, is selected for this purpose. The

ATC-63 methodology is first reviewed in general terms, and then discussed in more detail, including a presentation of its criteria for acceptance of a structural system, seismic design factors, and associated design rules.

The ATC-63 methodology is proposed for application to the specific case of AAC-infilled steel moment frames. Design rules for steel moment frames are given in AISC (2005). Design rules for AAC infills are proposed based on the draft MSJC infill provisions. The need for experimental investigation of AAC-infilled steel moment frames is stated, to obtain the results necessary to extend to the draft MSJC provision to AAC infills and to develop and calibrate nonlinear hysteretic models for AAC infills for use with the ATC-63 methodology.

CHAPTER 4
Experimental investigation of an AAC-infilled steel moment frame

4.1 INTRODUCTION AND SCOPE OF CHAPTER

In Chapter 3, it was pointed out that validation of the extension of draft MSJC infill design provisions to AAC infills, and the development of realistic hysteretic models for AAC infills, require experimental data on the behavior of AAC-infilled frames. Due to the lack of such data in published literature, this chapter contains the results of a limited experimental investigation to obtain such data. A typical steel moment frame is tested, first in the bare condition and then with an AAC infill. Differences in response are used to extract the lateral stiffness, strength, and hysteretic behavior of the AAC infill. In this chapter, the development and construction of the test setup and infilled frame specimen are reviewed, and the testing protocol is described. Test results for the bare frame and the infilled frame are presented, compared with each other, and discussed.

4.2 OBJECTIVES OF TEST AND TEST PROCEDURE

The objective of the test was to determine the in-plane lateral stiffness, strength, and hysteretic behavior of a typical AAC-infilled steel moment frame specimen. For this purpose, a bare steel frame was first tested under a history of reversed cyclic loading to monotonically increasing lateral displacements. The frame was then infilled with AAC, and was subjected to the same loading history. Comparison of the two resulting lateral load-deflection curves was used to extract the hysteretic behavior of the AAC infill.

4.3 DEVELOPMENT OF TEST SETUP

The test setup and the infilled frame specimen were constructed at the Ferguson Structural Engineering Laboratory of the University of Texas at Austin. The test setup,

shown in Figure 4.1, is a steel moment frame with a bay length of 20 ft and story height of 12 ft. The column sections are W14x82, and the beam sections W21x50.

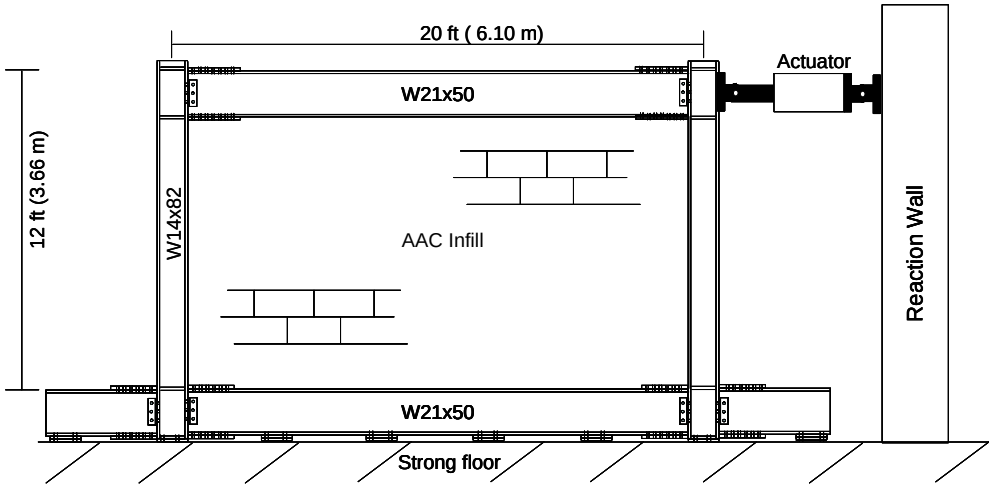

Figure 4.1: AAC-infilled steel moment frame specimen and test setup

Those W-sections were selected because they are fairly common in steel moment frames with heights up to five stories. The ratio of plastic moment capacity of this column section to that of this beam section is about 1.3, typical of steel moment frames designed using the "strong column-weak beam" concept. Although steel moment frames could use heavier W-shapes, the development of this setup required that the lateral collapse strength of this frame be only about as strong as the expected lateral strength of the infill, so that the behavior of the infill could be inferred from the differences in behavior between the infilled frame and the bare frame. The W-sections were chosen to meet this requirement. Also, the shear strengths of these W-sections were high enough so that local shear failure would not occur due to interaction forces between the AAC infill and the frame. In Table 4-1 are summarized the grade and mechanical properties obtained from mill tests for the W-sections used in the test setup.

Table 4-1: Grade of steel and mechanical properties from mill tests for W-sections of the test setup

Section	Specification (Grade)	Average yield strength (ksi)	Average tensile strength	Average % elongation
W14x82	A572 (50 ksi)	56	74.5	26
W21x50	A572 (50 ksi)	51	69.7	27.2

Moment connections were chosen for the test setup because the overall objective of the research project was to study the performance of AAC-infilled steel moment frames. The flange cover plate connection was chosen to study construction and detailing issues near bolted joints. In Figure 4.2 and Figure 4.3 are shown details of the flange cover plate connections used in the test setup. All welding on the test setup was performed by a certified welder.

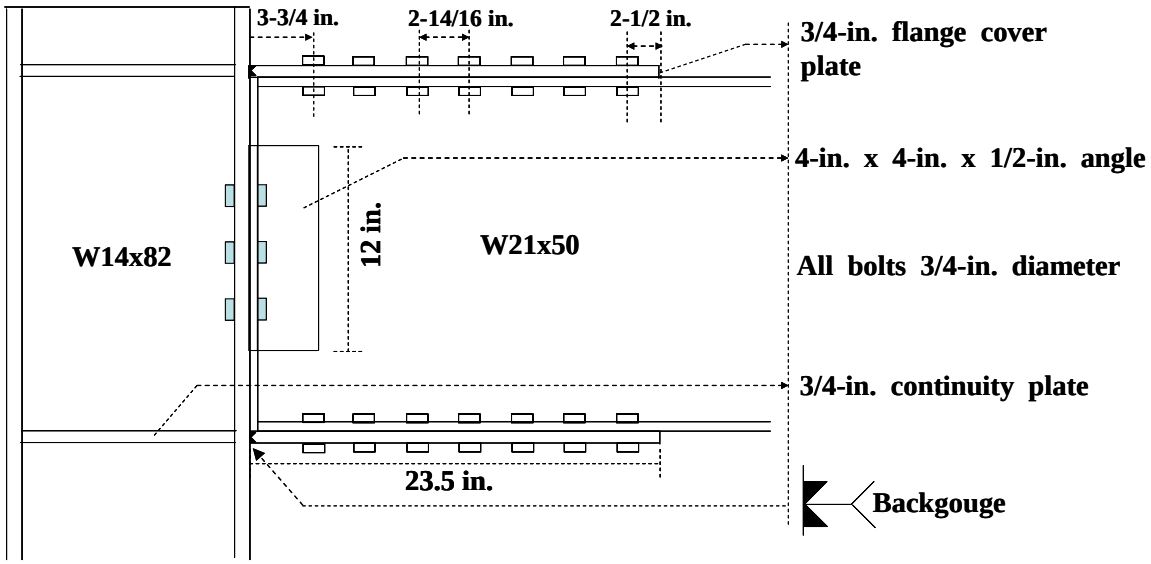

Figure 4.2: Flange cover plate connection for the steel moment frame test setup

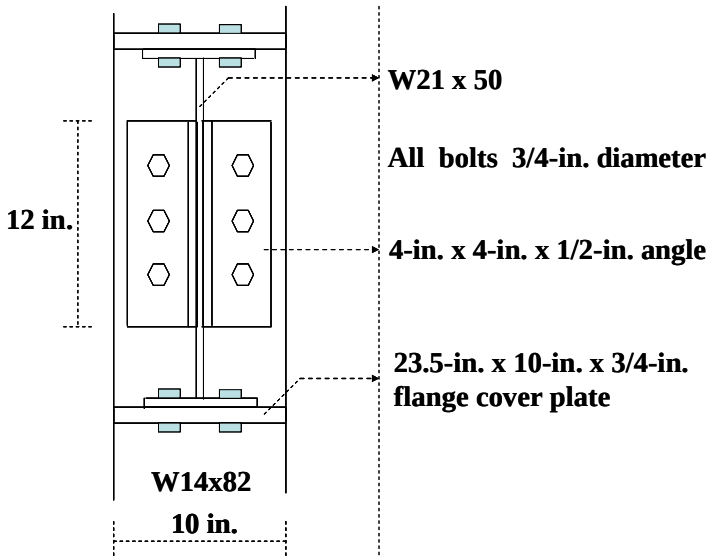

Figure 4.3: View of flange cover plate connection looking into the beam

The bottom beam of the test setup was anchored to the strong floor of the laboratory at intervals of 4 ft, simulating a stiff base. This was done for the following reasons:

1) Initially, an investigation was conducted to determine the ideal boundary condition for the test setup. Because the boundary conditions for the panels of a frame vary from the ground story to the top story, and also depend on the aspect ratio of the frame and the ratio between the moments of inertia of the column and beam sections, it was concluded that no single boundary condition was ideal.
2) The expected moments and axial forces at the base of the columns were large and could not be transferred to the strong floor of the laboratory through the column base plate alone. Some degree of moment transfer to a base beam was required.
3) A stiff base is representative of conditions at the ground story of a building. Infills generally fail at the bottom story first, possibly creating a story mechanism at that level. Therefore, a fixed base boundary condition was considered more critical.
4) Most previous experimental research programs on infill behavior have used a stiff base, and hence this boundary condition was chosen to maintain consistency with existing experimental data for infill behavior.

Lateral load was applied on the frame at the level of centroid of top beam using twin 100-kip hydraulic actuators with a stroke of ± 8 in., placed symmetrically on either side of the plane of the frame and connected to the rigid reaction wall of the laboratory. The actuators were controlled manually through a compressed air-driven hydraulic pump.

4.4 LOADING PROTOCOL

The testing procedure for the AAC-infilled frame specimen is in-plane quasi-static loading. ATC-63 (2007), the 75% draft report of the ATC-63 methodology, provides recommendations for determination of displacement control loading protocol for testing of structural components, and those recommendations were used to develop the displacement-controlled loading protocol for the bare frame and the AAC-infilled steel moment frame specimens. These recommendations are not continued in ATC-63 (2008) because the fundamental criterion of the latter document is that the protocol be appropriate and that "there is no unique or best loading history."

4.4.1 Recommendations by ATC-63 (2007) for displacement-controlled loading protocol

The following steps are recommended by ATC-63 (2007) for establishing a displacement-controlled loading protocol for testing of structural components:

1) Select the deformation quantity to be used to control the loading history.
2) Select Δ_m, the targeted maximum deformation amplitude of the loading history, defined as the amplitude at which it is anticipated that the load-deformation response exhibits a negative tangent stiffness for first time.
3) Estimate Δ_0, the smallest amplitude that is judged to contribute to cumulative damage, that is, the amplitude of the smallest cycle of the loading history. This amplitude should not be larger than $0.05\Delta_m$, unless it can be demonstrated that cumulative damage commences at a larger amplitude.

4) Develop a loading history that consists of step-wise increasing cycles, with Δ_m (or a value close to it) being the amplitude of the largest cycle and a value close to Δ_0 being the amplitude of the smallest cycle.

   a) There should be at least 10 steps of increasing amplitudes in the loading history and at least two cycles per amplitude, that is, there should be a minimum of twenty cycles before the target maximum amplitude Δ_m (or a value close to it) is reached.

   b) Decide on a rate of increase in the deformation amplitude of the steps of the loading history.

5) The loading history should be continued beyond the amplitude Δ_m by using increments of amplitude of $\alpha \Delta_m$. A value of $\alpha = 0.3$ is recommended.

6) The loading history should be continued until the resistance of the specimen has deteriorated to less than 50% of the maximum resistance. If a test is terminated before this limit state is attained, then it should be assumed (for modeling purposes) that the specimen resistance deteriorates to zero following the maximum amplitude executed in the test.

4.4.2 Loading protocol for bare frame and AAC-infilled frame specimen

For the bare frame and the AAC-infilled frame specimen, the lateral deflection of the frame at the level of centroid of the top beam is used to control the loading history. The draft MSJC infill design provisions for stiffness and strength of infills are based on Flanagan (2001), which suggests that infills reach their maximum lateral capacity at a deflection of 1 in. Therefore, Δ_m in the displacement protocol prescribed by ATC-63 (2007) is taken to be 1 in. Also, it is reasonable to expect that the resistance of the infill would have fallen below 50% of its maximum lateral capacity at a deflection of 2 in. Therefore, the amplitude of the displacement cycles is gradually increased to a maximum value of 2 in. Although a deflection of 2 in. (1.4% drift) may not be substantial for the steel frame, it is substantial for the AAC infill panel because infills have generally been observed to undergo significant deterioration at this drift level. At each displacement

amplitude, three cycles are performed, than the two cycles recommended by ATC-63 (2007). The displacement amplitudes are selected so that more than 20 cycles are completed at the end of the 1-in. deflection amplitude. The proposed displacement-controlled loading protocol for the bare frame and the AAC infilled frame specimen is depicted in Figure 4.4. In Figure 4.5 is shown the same protocol in terms of drift ratio. The maximum drift under design ground motions permitted by ASCE (2005) for steel moment frames is 2.5%. Therefore, the proposed loading protocol can be considered about half as severe as what a bare steel moment frame would be expected to experience in a design-basis earthquake (DBE).

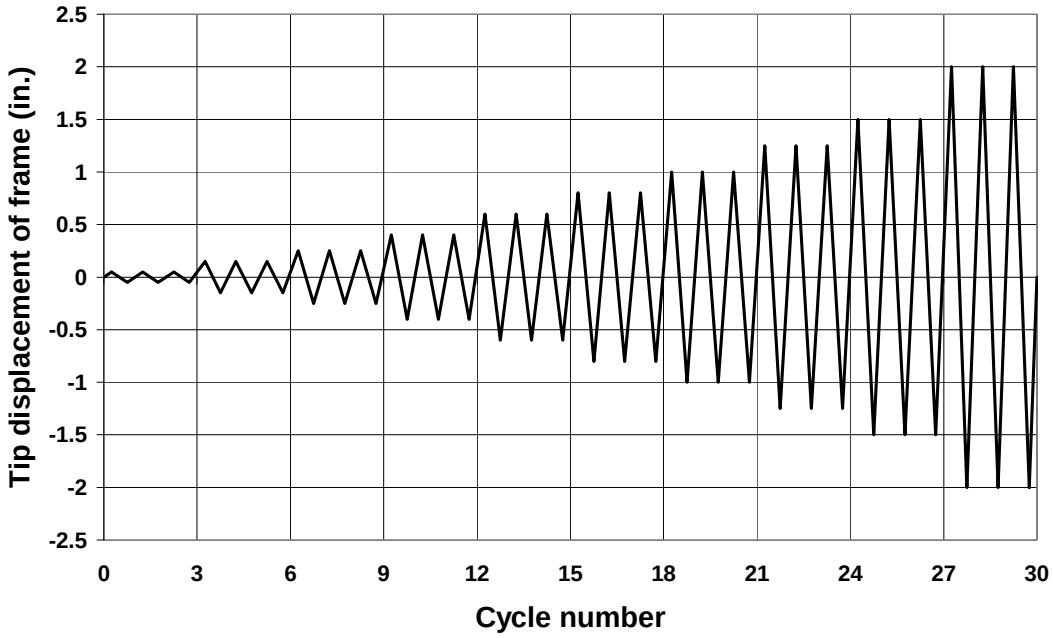

Figure 4.4: Displacement loading protocol for quasi-static testing of bare steel moment frame (ATC-63 2007)

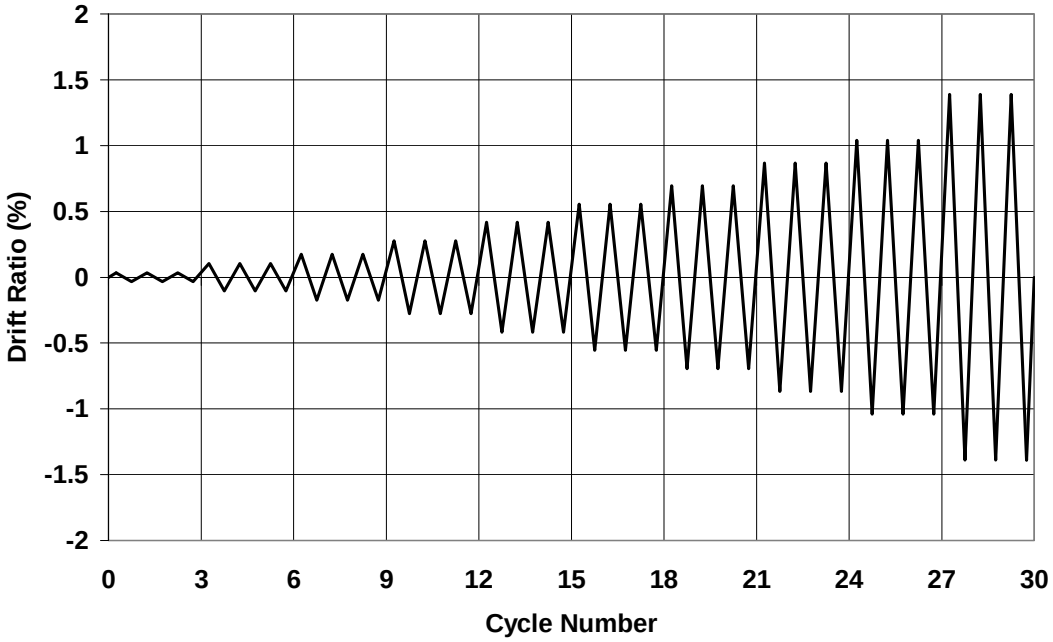

Figure 4.5: Displacement loading protocol for quasi-static testing of AAC-infilled steel moment frame

4.5 INSTRUMENTATION AND DATA ACQUISITION

Various measurements were made during testing of the bare frame and the AAC-infilled frame. The types of instrumentation used are denoted by numbers in Figure 4.6, and described further below:

1) Lateral deflection of the frame relative to the reaction wall at the level of centroid of top beam section was measured using string potentiometers. Two string potentiometers were installed on each side of the frame for redundancy in data collection.
2) Slip of the frame at the base was measured using linear potentiometer attached to the strong floor
3) Diagonal deformation of the infill panel was measured using wire potentiometers. Both diagonals were instrumented to ensure redundancy of data.

4) Vertical uplift of the bases of both columns was measured with respect to the strong floor using dial gauges

5) Deflection of the loading structure relative to the reaction wall was measured using a linear potentiometer

6) Strain in flanges of beams and columns at expected locations of maximum bending moment was measured using electrical resistance strain gages. At each of the four locations indicated in Figure 4.6, strain is measured using two strain gauges.

Data were acquired through a Hewlett-Packard 3852 scanner. Analog-to-digital conversion was carried out by a National Instruments card in a Windows-based microcomputer, running under Labview©, National Instruments software for data acquisition and analysis. Digitized data were obtained in text format and plotted using Microsoft Excel®.

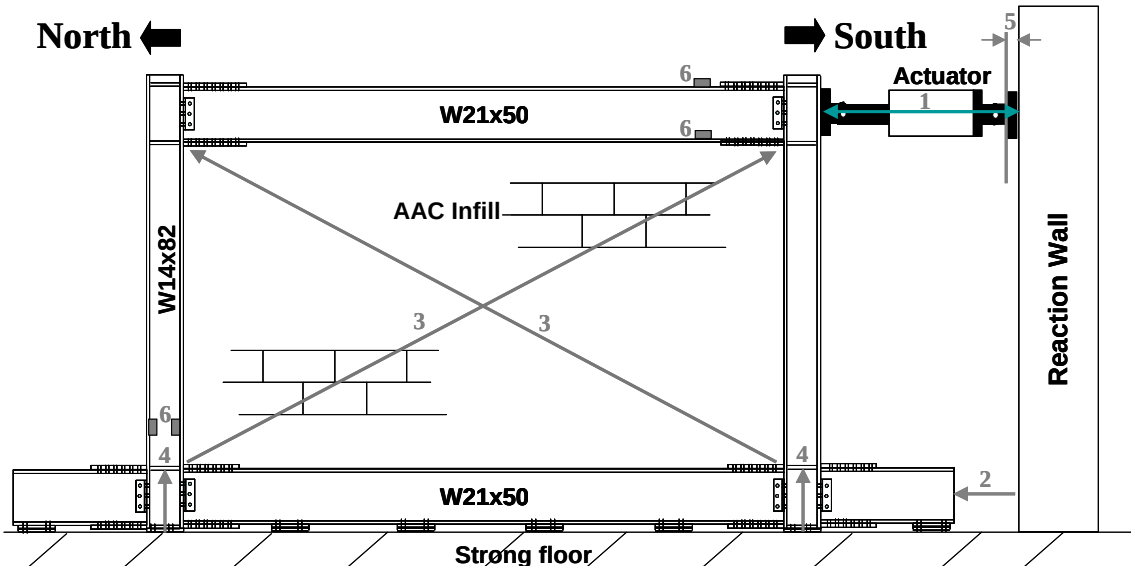

Figure 4.6: Instrumentation of test specimen

4.6 BARE FRAME TEST

The bare steel frame before testing is shown in Figure 4.7. The cyclic lateral force-deflection response of the bare steel frame obtained from the test is shown in Figure 4.8. Yielding in column flanges near the region labeled as ‘6’ in Figure 4.6 was observed during and after cycles of 1.5-in. (1.04 % drift) deflection amplitude. This was inferred from flaking of the lime-wash that had been painted at these locations (Figure 4.9). The lateral load-deflection response of the frames did not depict a clear yield point due to Bauschinger’s effect. Although pinched response due to bolt slip is typical of steel frames with flange cover-plate connection, it is not prominent for this steel frame.

Figure 4.7: Bare steel moment frame before test

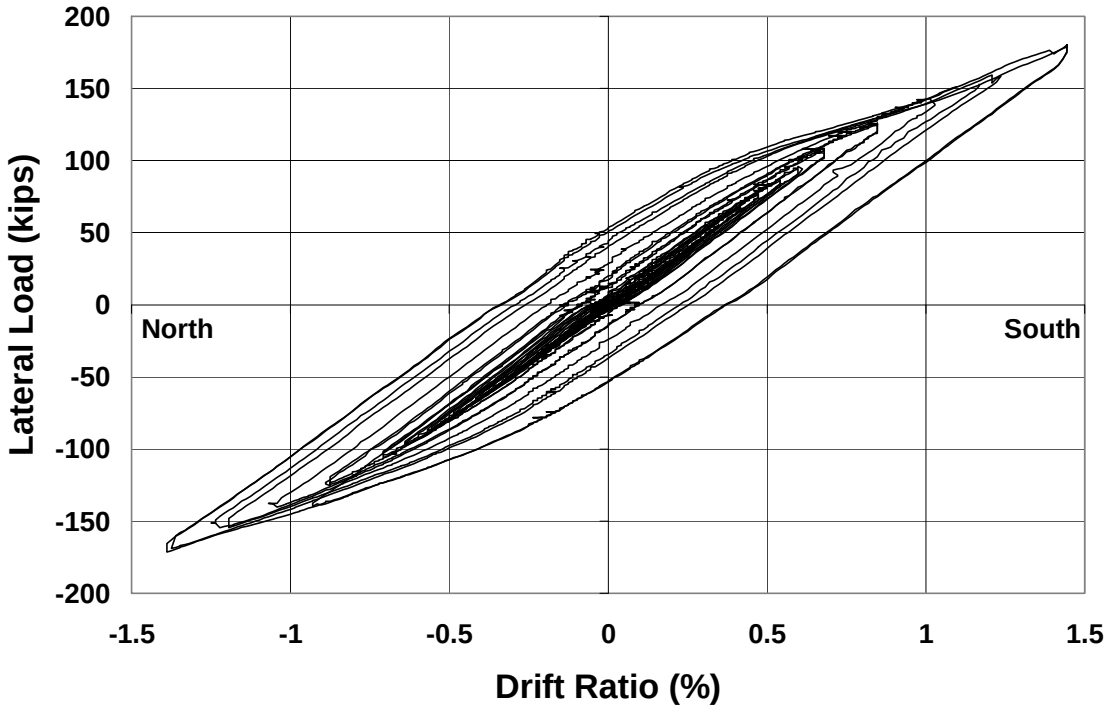

Figure 4.8: Lateral load-deflection response of bare steel frame

Figure 4.9: Yielding in column flanges during bare frame test near region labeled as '6' in Figure 4.6

4.7 CONSTRUCTION OF AAC INFILL

At the end of the bare frame test, the steel frame was returned to a plumb position, and the AAC infill was constructed within it (Figure 4.10), using Class 4 AAC blocks measuring 8 x 8 x 24 in., supplied by Xella Mexicana (Monterrey, Mexico). This strength class and these dimensions are commonly used for AAC wall elements. The AAC infill, 8-in. thick, was concentric with the plane of the steel frame, and was placed by an experienced contractor furnished by Xella Mexicana. A leveling course of mortar corresponding to ASTM C270, Type S, cement-lime, by proportion, was mixed with a small amount of thin-bed mortar and placed between the lower steel beam and the first course of AAC. Subsequent courses were laid with full bed and head joints using thin-bed mortar supplied by Xella Mexicana, and prepared according to the mortar manufacturer's instructions. The infill was fitted tightly against the bounding frame elements. The gaps between the infill and the top beam of the frame, and between the infill and the bolted connections in the corners of frame, were tightly packed with the leveling mortar, mixed with a small amount of thin-bed mortar to improve adhesion between the AAC and the steel frame. Chips in blocks and remaining gaps in the wall were patched using repair mortar and thin-bed mortar. The AAC infilled-frame specimen before testing is shown in Figure 4.11.

Figure 4.10: Construction of AAC infill

Figure 4.11: AAC-infilled frame specimen before testing

4.8 COMPRESSIVE STRENGTH OF AAC USED FOR AAC-INFILLED FRAME SPECIMEN

The compressive strength of the AAC units used to construct the infill was verified according to ASTM C1386-07. Three AAC cube specimens, obtained from the

top, middle and bottom of the batch of AAC blocks used to construct the infill, were tested. The dimensions of the testing surface, failure load and compressive strength obtained from the test for the specimens are presented in Table 4-2. The reported dimensions of the testing surface are within a tolerance of 0.0035 in. per 4 in. as required by ASTM C1386-07. The average compressive strength of the AAC, reported to the nearest 10 psi, was obtained as 650 psi, greater than the specified compressive strength of 580 psi for Class 4 AAC.

Table 4-2: Compressive strengths of AAC cube specimens (ASTM C1386)

Specimen	Dimensions of loaded surface (in. x in.)	Failure load (lbs)	Compressive strength (psi)
1	3.995 x 3.995	10440	654.1
2	3.985 x 4.015	10070	629.8
3	4.005 x 4.010	10850	675.6

4.9 AAC-INFILLED FRAME TEST

After construction, the AAC infill was allowed to cure for about a month, and was then tested. This section presents the experimental results and observations from that test.

4.9.1 Overall behavior of infilled frame specimen

In Figure 4.12 is shown the AAC-infilled frame specimen after testing. Although the infill cracked severely at all corners and spalled at isolated locations, its in-plane load-deflection behavior remained stable without abrupt changes, and it showed no out-of-plane instability.

Figure 4.12: AAC-infilled frame after testing

4.9.2 Load-deflection results from AAC infilled frame test and bare-frame test

In Figure 4.13 is shown the lateral in-plane load-deflection response of the AAC-infilled frame specimen, and in Figure 4.14, the same information with that of the bare frame superposed. Even at a lateral deflection of 2 in. (1.4% drift), the AAC infill had not failed. The test was stopped to limit yielding of the steel frame.

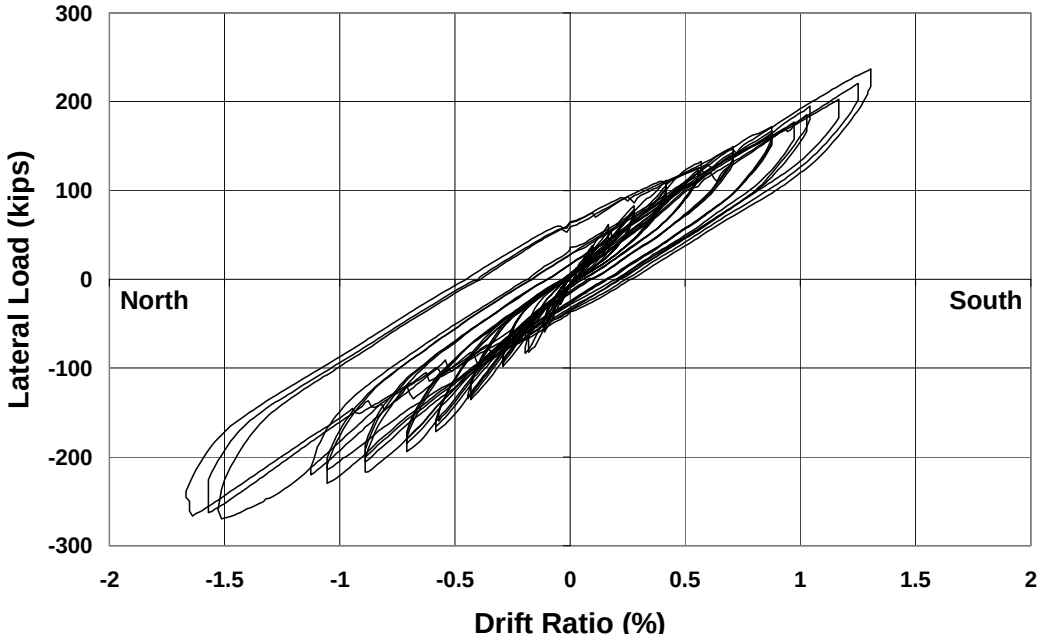

Figure 4.13: Lateral load-deflection response of AAC-infilled frame

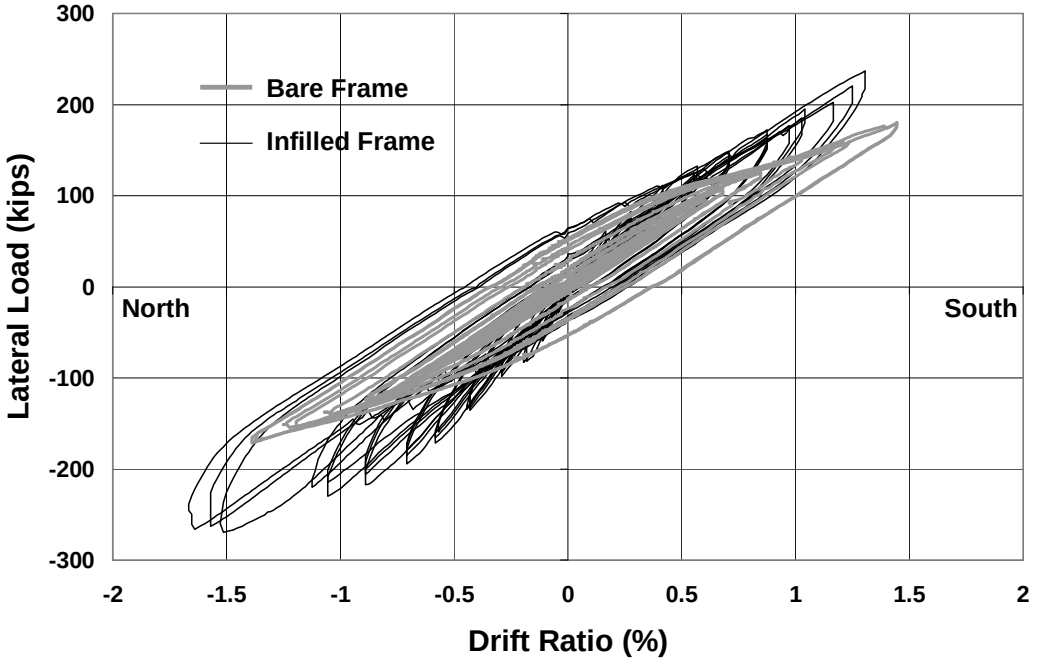

Figure 4.14: Superposed lateral-load deflection response of bare frame and of AAC-infilled frame

4.9.3 Cracking pattern in AAC infill

The cracking pattern in the AAC-infilled frame specimen after testing is shown in Figure 4.15. Cracks shown in black formed during displacements towards the north (Figure 4.6) and cracks shown in grey, during displacements towards the south. The formation of diagonal compression struts in the infill could be inferred from the presence of an increasing concentration of cracks along the diagonals. The intensity of cracking was more severe at the top corners of the frame than at the bottom corners. This is because at the top of the frame, the infill contacted the frame only at the corners where the strut seemed to extend about 3 ft on either side of the diagonal. At the bottom of the frame, the infill contacted the entire length of the bottom steel beam because the bottom steel beam was fixed to the strong floor at 4-ft intervals and remained horizontal throughout the test.

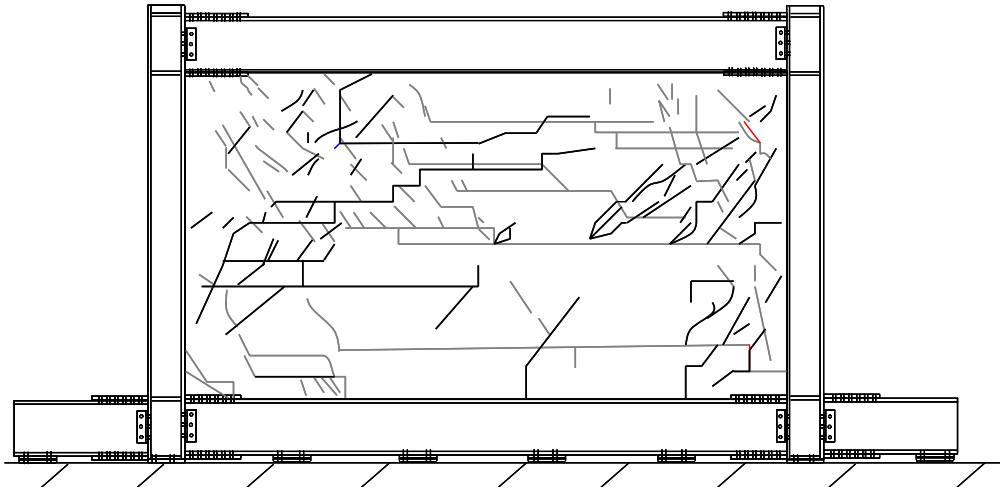

Figure 4.15: Cracking pattern in AAC-infilled frame specimen after test

Previous research on AAC (Tanner 2003) reports that AAC blocks are weaker than the thin-bed mortar used between courses and faces of AAC blocks. Therefore, for the AAC infill, diagonal cracks were expected to go through the AAC blocks rather than stair-step along the thin-bed mortar joints. In the test, however, some stair-stepped cracks formed initially along mortar joints. After these cracks stabilized and a diagonal strut formed, subsequent cracks were primarily diagonal, and passed through AAC blocks.

Because the compression strut degraded primarily through diagonal cracking, the AAC infill had a stable inelastic response without abrupt changes in lateral strength. The infilled-frame test was stopped before the crushing of the diagonal strut or other failure mode could be observed for the infill.

4.9.4 Further discussion of specimen behavior during infilled frame test

4.9.4.1 Bolt slip in steel frame

During the second cycle of reversed cyclic loading to a nominal deflection of 1.5 in. (1.04% drift) and continuing through cycles to a nominal deflection of 2 in. (1.39% drift), the steel frame made loud popping noises, accompanied by sudden jolts. These were inferred to be due to bolts slipping and coming suddenly into bearing against the bolt holes.

4.9.4.2 Correction of readings from string potentiometers

During the jolts noted above, the linear string potentiometers measuring the lateral deflection of the frame at the level of the top beam moved, and consequently their readings for the lateral deflection of the frame were corrupted for these cycles. However, the string potentiometers measuring the diagonal deformation of the infill panel (labeled '3' in Figure 4.6) did not move. The deformation in the diagonal string potentiometers can be geometrically related to the measured average deflection of the infilled frame by the following relationship:

$$\Delta_{diagonalsp} = \Delta_{average} \cos\theta$$

where,

$\Delta_{diagonalsp}$ = deformation in diagonal string potentiometers

$\Delta_{average}$ = measured average lateral deflection of the frame

θ = angle of diagonal string potentiometers with the horizontal

Although the ratio between the readings of the diagonal string potentiometers and the average deflection of the frame was not consistently equal to $\cos\theta$ at all deflection

amplitudes, for any particular deflection the ratio was observed to remain constant at all cycles preceding bolt slip. For example, for a lateral deflection of 0.4 in. (0.28% drift), the ratio was observed to be about 0.904 (than the expected value of 0.857 for $\cos\theta$) at all cycles preceding the bolt slip. Based on this consistency, the readings from the diagonal potentiometers were used to correct the average lateral deflection of the infilled frame at cycles affected by bolt slip. The load-deflection curve of Figure 4.13 reflects this correction.

4.9.5 Asymmetry of infilled frame response

The lateral load-deflection response of the infilled frame and consequently that of the infill was asymmetric, as shown in Figure 4.13 and Figure 4.18. There are two reasons for this:

1) The first and more important reason is that the infill itself behaved asymmetrically. The infill had less lateral strength towards the south side than the north. This was accompanied by more diagonal cracking close to the top left corner of the frame than at the top right corner, as shown in Figure 4.15.
2) The second reason is that the applied loading history had an unintentional asymmetry. The magnitude of this asymmetry was different at cycles preceding bolt slip and cycles after bolt slip in the steel frame. This is explained below:
    a) *Asymmetry in cycles before bolt slip in the frame:* Twisting of the south column was inferred from recorded data, which was characterized by an initial twist, with subsequent changes in twist being proportional the applied load. The initial twist was probably due to initial differential friction in the hydraulic rams, and subsequent changes in twist were probably caused by slight accidental eccentricity between the applied lateral load and the plane of the frame. The twist resulted in differential readings in the two string potentiometers measuring the lateral deflection of the frame relative to the reaction wall at the level of the centroid of the top beam, a plan view of this is shown in Figure 4.16. The magnitude of

this differential reading in the string potentiometers was about 0.04 in. (0.03% drift) at low load levels and a maximum of 0.1 in. (0.07% drift) at higher load levels. Its effect was to produce in String Potentiometer 1a a lower displacement reading towards north or a greater displacement reading towards south than the average displacement of the frame. Because String Potentiometer 1a was used to control the displacement history of the specimen, during each cycle the frame was consistently pushed to an average displacement that was greater by at most 0.05 in. (0.035% drift) towards the north than towards the south. Because this difference is small, the resulting asymmetry of load-deflection response of the AAC infill was significant only at small deflection amplitudes less than about 0.15 in (0.1% drift).

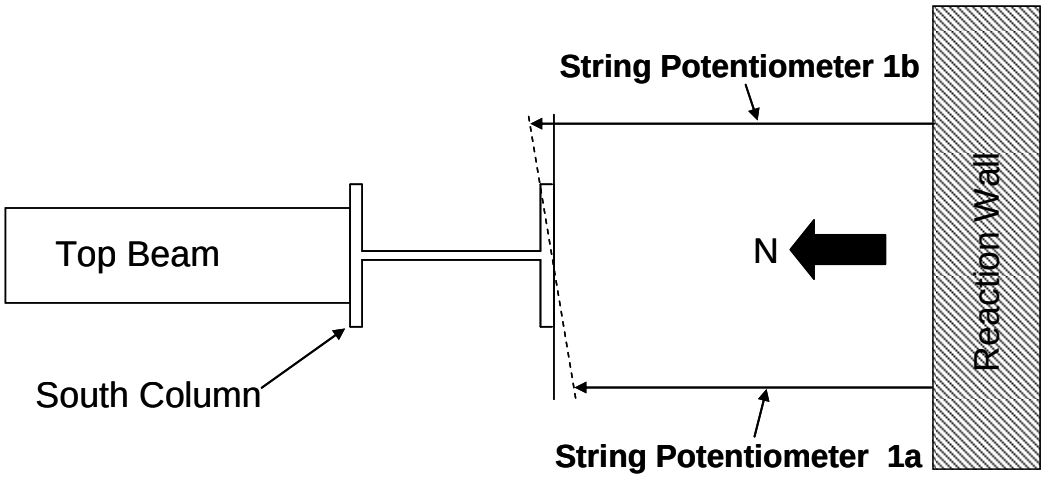

Figure 4.16: Differential reading in string potentiometers used to measure lateral deflection of frame due to twist in south column (plan view)

b) Asymmetry in cycles affected by bolt slip in the frame: As mentioned in Sections 4.9.4.1 and 4.9.4.2, the string potentiometers measuring lateral deflection moved suddenly during the jolts caused by bolt slip in the steel frame. The effect of these movements was to produce, in the string

potentiometers used to measure lateral deflection of the frame, smaller deflection readings towards the north and correspondingly greater deflection readings towards the south than were actually applied. This is illustrated in Figure 4.17. The extent of the error in the reading was not known during the test, but was later determined to have incrementally increased to maximum of about 0.35 in. (0.24% drift) during the several jolts that were witnessed. Since the displacement history of the frame was controlled using readings from string potentiometer labeled '1a' in Figure 4.17, it resulted in asymmetry in the loading history during these cycles, with the frame being pushed farther on the north side than the south. This asymmetry was significant: during cycles of nominal 2-in. (1.39% drift) deflection amplitudes, the maximum deflection of the frame was 2.4 in. (1.67% drift) to the north, compared with only 1.9 in. (1.32% drift) to the south, as evident from Figure 4.13.

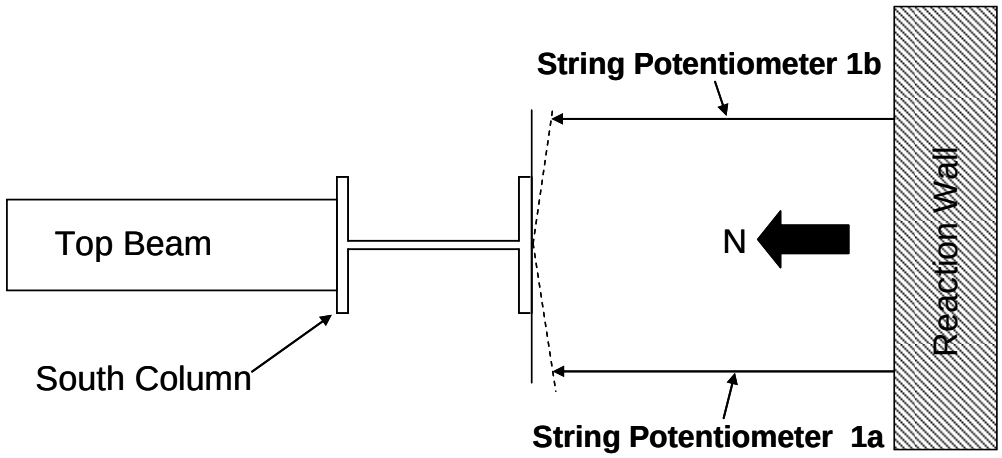

Figure 4.17: Movement of string potentiometers measuring lateral deflection of frame due to jolts from bolt slip (plan view)

4.9.6 Derived lateral load-deflection response of AAC infill

To determine the structural response of the AAC infill alone, the lateral load-deflection response of the bare frame (Figure 4.8) is subtracted from that of the AAC-

infilled frame (Figure 4.13), and the resulting response of the AAC infill is shown in Figure 4.18.

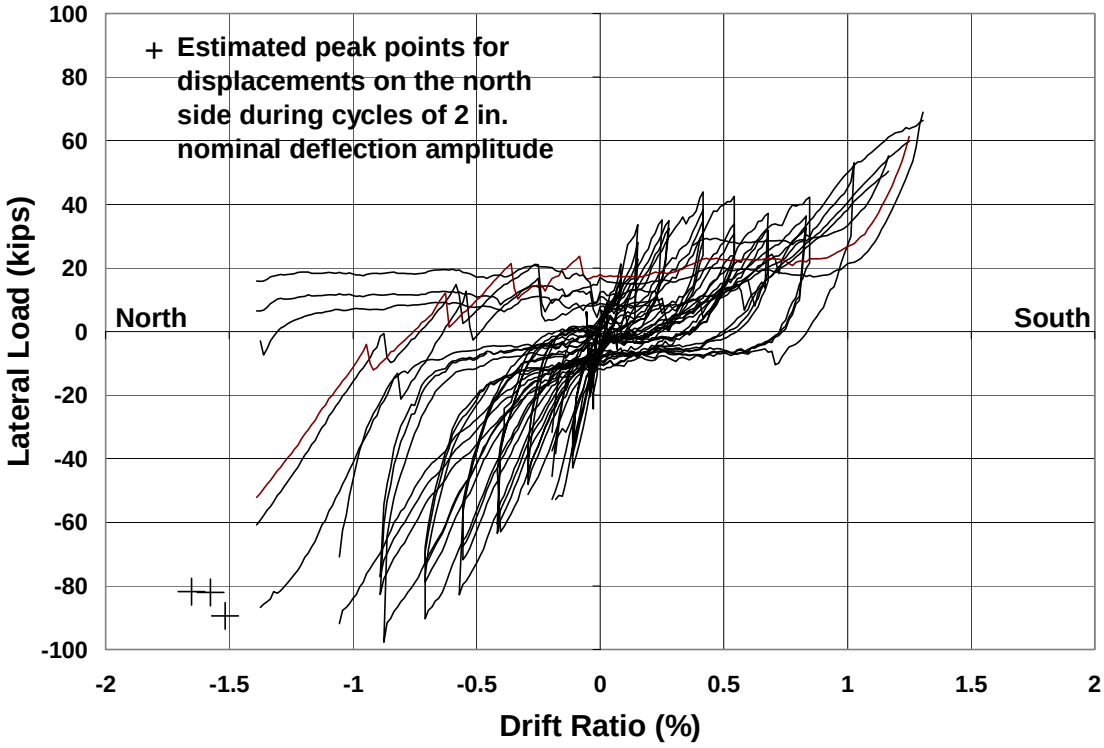

Figure 4.18: Lateral load-deflection response of AAC infill

During cycles to a nominal deflection of 2 in. (1.39% drift), the asymmetry in displacement loading protocol explained in Section 4.9.5 caused the infilled frame to be subjected to larger northward deflections than the previously tested bare frame (Figure 4.14). Because the response of the infill is obtained as the difference in responses of bare and infilled frames, the response of the infill in the north direction during these cycles could not be determined for deflections of the infilled frame greater than those previously reached by the bare frame. However, the peak responses of the infill were estimated by visually extrapolating the response of the bare frame as illustrated in Figure 4.19. The estimated peak responses are indicated in Figure 4.18.

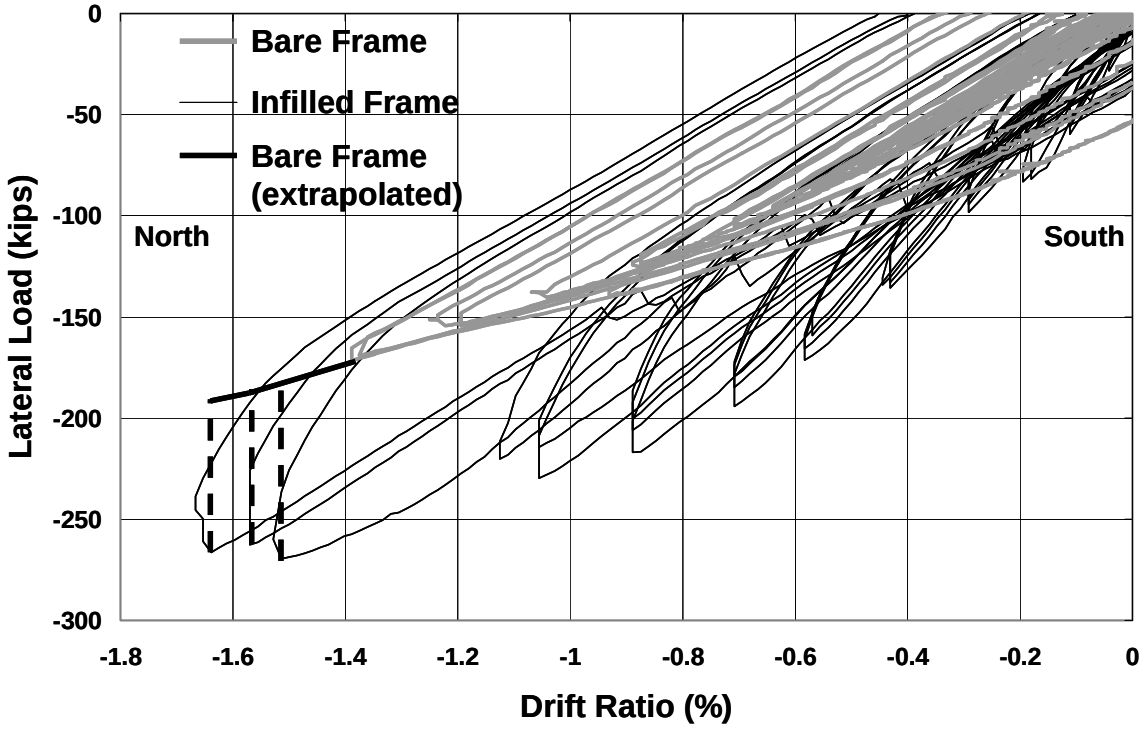

Figure 4.19: Estimating peak response of AAC infill for displacement on the north side during cycles of nominal 2-in. (1.39% drift) deflection amplitude

4.9.7 Reliability of corrected experimental data

In Section 4.9.4.1 is described the procedure to correct lateral deflections of the infilled frame specimen at cycles affected by bolt slip using data from the string potentiometers measuring the diagonal deformation of the frame (labeled "3" in Figure 4.6). To validate this procedure, it is applied to compute the lateral deflection of the infilled frame specimen at cycles preceding the jolts to nominal deflections of 1 in. (0.69% drift), 1.25 in. (0.87% drift) through the first cycle for nominal deflection of 1.5 in. (1.04% drift). The resulting lateral load-deflection response of the AAC-infilled frame specimen is compared in Figure 4.20 and matches well with that obtained directly from the experiment using data from string potentiometers labeled "1" in Figure 4.6. Hence, the procedure used to correct the lateral deflection of the AAC-infilled frame specimen during cycles affected by bolt slip is valid. The corrected lateral load-deflection response

of the frame shown in Figure 4.13 starting second cycle of reversed cyclic loading to a nominal deflection of 1.5 in. (1.04% drift) and continuing through cycles to a nominal deflection of 2 in. (1.39% drift) is reliable.

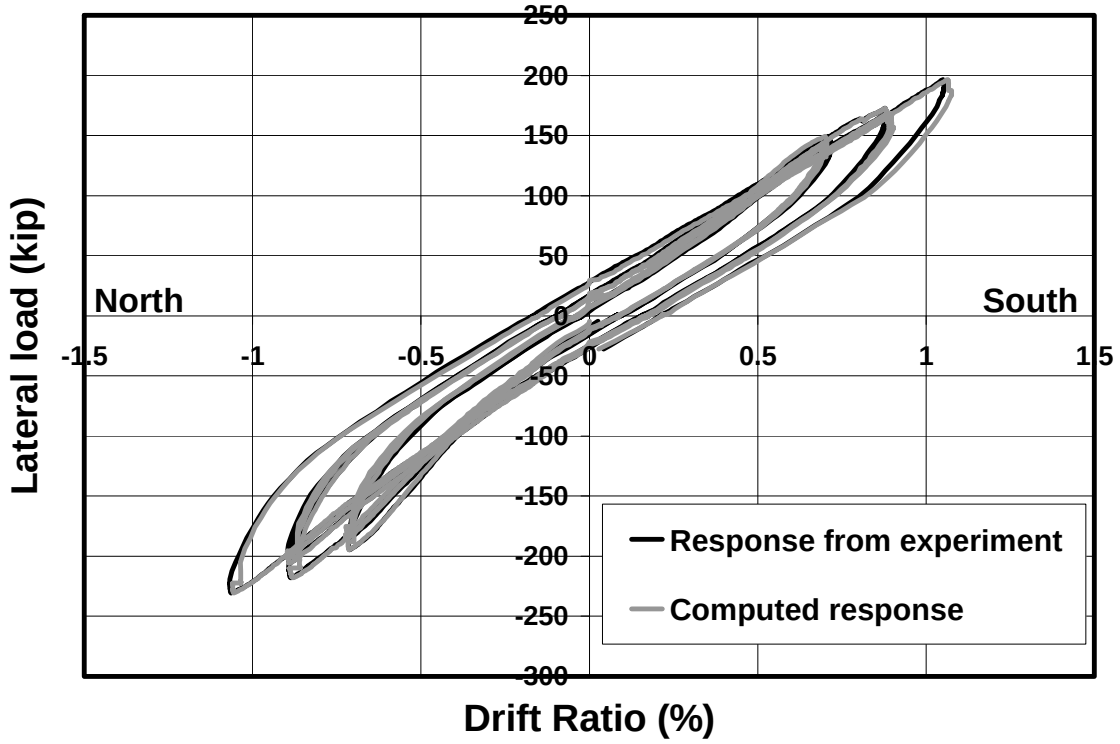

Figure 4.20: Comparison of lateral load-deflection response of the infilled frame specimen computed using procedure of Section 4.9.4.2 with that obtained directly from the experiment at cycles preceding bolt slip

4.9.8 Comparison of strain measurements for bare and infilled frames

To infer the extent to which bending moments in the frame members were affected due to interaction with the infill, strain in beam and column flanges were recorded at expected locations of maximum bending moment (Figure 4.6) during the bare and infilled framed tests. At each of these locations shown in Figure 4.6, strains were measured using two strain gauges. Strains from bare and infilled frame tests are compared in Figure 4.21 to Figure 4.24. Some strain gauges failed during the tests, and

data from them are not reported. Strains in beam flanges during the infilled frame test did not exceed 1.4 times those measured during the bare frame test at the same lateral deflection. Strains in column flanges during infilled frame test did not exceed 1.15 times those recorded during the bare frame test at the same lateral deflection.

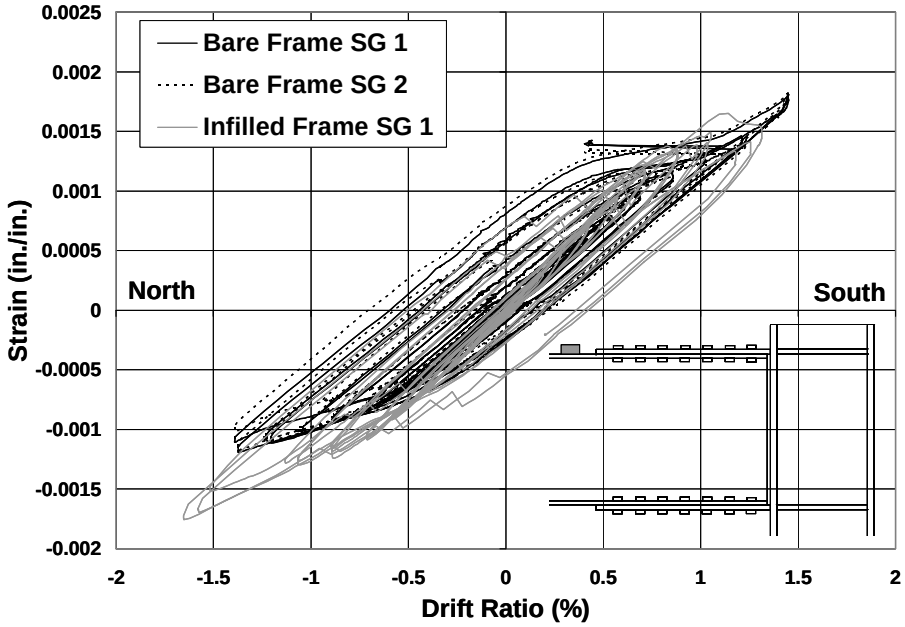

Figure 4.21: Strain in top flange of top beam (Figure 4.6) for bare and infilled frames

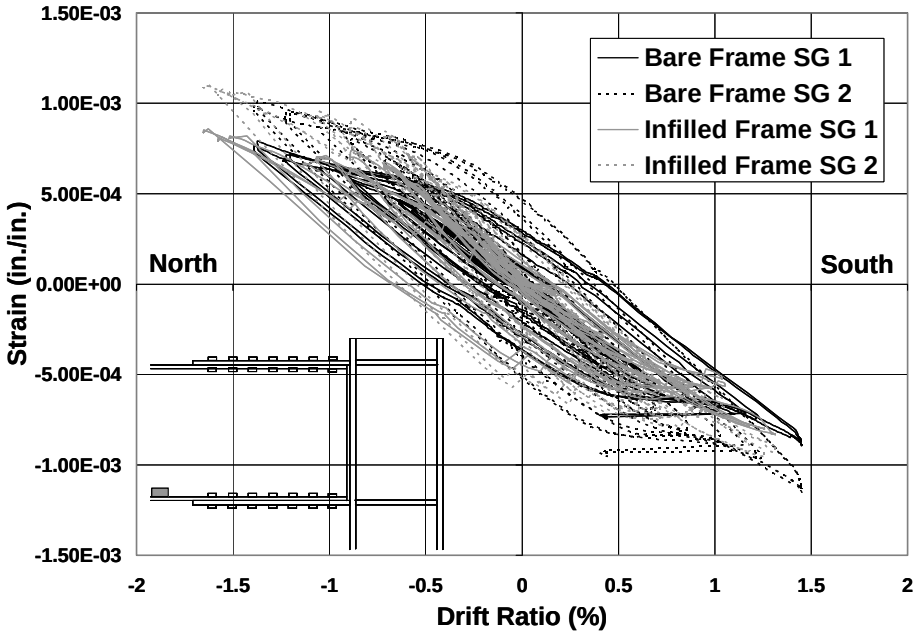

Figure 4.22: Strain in bottom flange of top beam (Figure 4.6) for bare and infilled frames

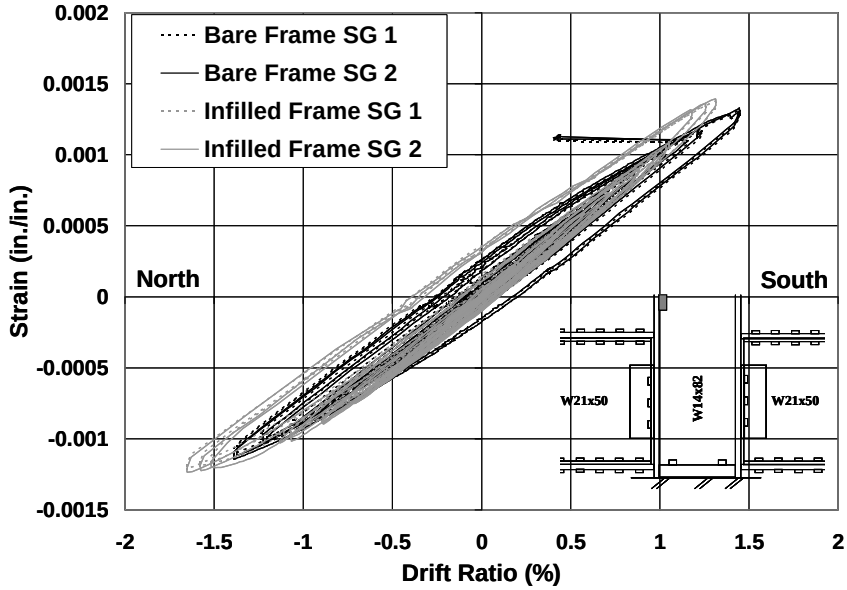

Figure 4.23: Strain in left flange of left column (Figure 4.6) for bare and infilled frames

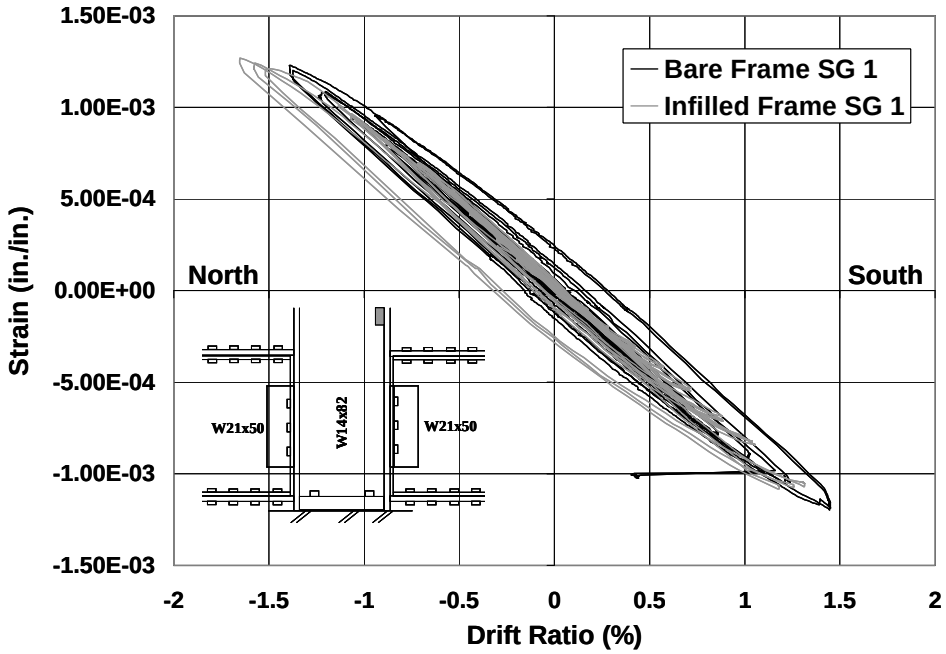

Figure 4.24: Strain in right flange of column (Figure 4.6) for bare and infilled frames

4.10 SUMMARY OF CHAPTER

To determine the stiffness, strength and hysteretic load-deflection behavior of a typical steel moment frame with an AAC infill, a typical steel moment frame was designed, constructed, and tested at the Ferguson Structural Engineering Laboratory of the University of Texas at Austin. The frame was then infilled with AAC masonry, and re-tested using the same protocol. The test setup, infilled frame specimen and testing procedure are described. Test results are presented for the AAC-infilled frame and compared with corresponding results for the bare frame. The lateral load-deflection response of the AAC infill is derived by subtracting the response of the bare steel frame from that of the AAC-infilled frame. The AAC infill cracked diagonally, but did not crush or exhibit out-of-plane instability.

CHAPTER 5
Significance of experimental results

5.1 INTRODUCTION AND SCOPE OF CHAPTER

The principal objectives of the experimental investigation of the AAC-infilled steel moment frame specimen described in Chapter 4 are to evaluate the applicability of the draft MSJC infill design provisions to AAC infills, and to develop the hysteretic data necessary for calibration of analytical models according to the ATC-63 (2008) methodology. This chapter deals with the first of those objectives. The MSJC draft provisions are reviewed; they are applied to the AAC infill in the infilled frame specimen; and their applicability to AAC infills is checked by comparing their predictions with experimental results.

5.2 APPLICATION OF DRAFT MSJC INFILL PROVISIONS TO THE AAC-INFILLED FRAME SPECIMEN

5.2.1 Calculated stiffness of AAC infill

According to the draft MSJC design provisions for infills, the infill is idealized as an equivalent strut (Figure 2.10) whose width is given by:

$$w_{strut} = \frac{0.3}{\lambda_{strut} \cos\theta}$$

Equation 5-1

MSJC draft infill design provisions Equation (X-1)

and

$$\lambda_{strut} = \sqrt[4]{\frac{E_m \; t_{\text{inf } ill} \; \sin 2\theta}{4 \; E_{col} \; I_{col} \; h_{\text{inf } ill}}}$$

Equation 5-2

MSJC draft infill design provisions Equation (X-2)

where

w_{strut} = width of equivalent strut, in.

λ_{strut} = relative stiffness parameter for equivalent strut, in.$^{-1}$

E_{col} = modulus of elasticity of confining columns, psi

E_m = modulus of elasticity of the masonry infill material, psi

h_{infill} = height of infill, in.

t_{infill} = thickness of infill, in.

I_{col} = in-plane moment of inertia of confining columns, in.^{4}

θ = angle between the diagonal of the infill panel and the horizontal

To use the draft MSJC procedure for AAC infills, E_m is taken as E_{AAC}. According to the MSJC Code (2008), the modulus of elasticity of AAC is calculated as:

$$E_{AAC} = 6500\left(f_{AAC}'\right)^{0.6}$$

Equation 5-3

From Section 1.8 of MSJC Code (2008a)

where

f_{AAC}' = specified compressive strength of AAC (580 psi for Class 4 AAC)

Therefore,

$$E_{AAC} = 6500\left(f_{AAC}'\right)^{0.6} = 6500(580)^{0.6} = 296{,}000\ psi = 296\ ksi$$

For the AAC-infilled frame specimen of this dissertation,

$$\theta = Tan^{-1}\left(\frac{h_{story}}{\ell_{bay}}\right) = Tan^{-1}\left(\frac{144}{240}\right) = Tan^{-1}\left(0.600\right) = 31.0 \text{ deg}$$

$\cos\theta = 0.857$

$\sin 2\theta = 0.883$

The specified thickness of the infill is

$$t_{\text{inf }ill} = 8\ in.$$

The height of the infill is given by

$$h_{\inf\ ill} = h_{story} - t_{beam} = 144\ in. - 20.8\ in. = 123.2\ in.$$

where

t_{beam} = specified depth of beam, in.

The elastic modulus of the steel column is

$$E_{col} = 29000\ ksi\ ,$$

and the in-plane moment of inertia of the column (W14x82) is

$$I_{col} = 881\ in.^4$$

Therefore

$$\lambda_{strut} = \sqrt[4]{\frac{E_{AAC}\ t_{\inf\ ill}\ \sin 2\theta}{4\ E_{col}\ I_{col}\ h_{\inf\ ill}}} = \sqrt[4]{\frac{296\ ksi \times 8\ in. \times 0.883}{4 \times 29000\ ksi \times 881\ in.^4 \times 123.2\ in.}} = \frac{0.0200}{in.}$$

and the width of equivalent strut is

$$w_{strut} = \frac{0.3}{\lambda_{strut} \cos\theta} = \frac{0.3}{0.0200\ in.^{-1} \times 0.857} = 17.5\ in.$$

The axial stiffness of the equivalent strut is

$$\frac{A_{strut}\ E_{AAC}}{L_{strut}} = \frac{17.5 \times 8\ in.^2 \times 296\ ksi}{\sqrt{(144^2 + 240)^2}\ in.} = 148\ \frac{kip}{in.}$$

where

A_{strut} = area of the equivalent strut

L_{strut} = diagonal length of the equivalent strut between centers of beam-column connections

The corresponding horizontal stiffness of the infill is

$$\frac{A_{strut}\ E_{AAC}}{L_{strut}} \cos^2\theta = = 148 \times 0.857^2 = 109\ \frac{kip}{in.}$$

5.2.2 Calculated lateral strength of AAC infill

According to the draft MSJC design provisions for infills, the lateral strength of an infill is the least of:

(a) $H_n = 6\ f_m'\ t_{infill}$ ***Equation 5-4***

MSJC draft infill design provisions, Equation (X-3)

and

(b) The calculated horizontal component of the force in the equivalent strut at a horizontal racking displacement of 1.0 in. (25 mm)

and

(c) $H_n = \frac{V_n}{1.5}$ ***Equation 5-5***

MSJC draft infill design provisions, Equation (X-4)

where

H_n = nominal horizontal strength of the infill (kips)

V_n = smallest nominal shear strength from Section 3.2.4 of MSJC (2008), calculated along a bed joint

f_m' = specified compressive strength of masonry (ksi)

t_{infill} = specified thickness of the infill (in.),

and the constant (6) in Equation 5-4 has units of in.

Equation 5-4 represents the lateral strength of the infill from corner or diagonal crushing failure mode, and Equation 5-5 represents the lateral strength of the infill due to horizontal shear failure along a bed joint.

(a) Using Equation 5-4 and the specified compressive strength of AAC, f'_{AAC}, the horizontal strength of the infill is computed as

$$H_n = 6\, f'_m\, t_{\inf ill} = 6\, f'_{AAC}\, t_{\inf ill} = 6\ in. \times 0.580\ ksi \times 8\ in. = 27.9\ kips$$

(b) The horizontal stiffness of the equivalent strut representing the AAC infill is obtained as 109 kip/in. in the previous section. Therefore, the calculated horizontal component of the force in the equivalent strut at a horizontal racking displacement of 1.0 in. is 109 kip.

(c) Section 3.2.4 of MSJC (2008) requires that V_n be calculated as the smallest of the following:

$$V_n = 3.8\, A_n \sqrt{f'_m} \qquad \textbf{\textit{Equation 5-6}}$$

$$V_n = 300\, A_n \qquad \textbf{\textit{Equation 5-7}}$$

$$V_n = 56\, A_n + 0.45\, N_u \qquad \textbf{\textit{Equation 5-8}}$$

where

A_n = net area of the infill, $in.^2$

N_u = factored compressive force acting normal to the shear surface, *psi*

The length of the infill panel is given by:

$$L_{\inf ill} = L_{bay} - D_{col} = 240\ in. - 14.3\ in. = 225.7\ in.$$

where,

L_{bay} = length of the bay of the frame

D_{col} = depth of the columns of the frame

The thickness of the infill panel is 8 in. Therefore, the net area of the infill panel is:

$$A_n = 225.7\ in. \times 8\ in. = 1806\ in.^2$$

In Equation 5-6, f_m' is taken as f_{AAC}'. In Equation 5-8, the axial compressive force in the infill is conservatively ignored. V_n is computed using Equation 5-6, Equation 5-7 and Equation 5-8 as:

$$V_n = 3.8\ A_n \sqrt{f_m'} = 3.8 \times 1806 \times \sqrt{580} = 165{,}000\ psi = 165\ kip \qquad \text{Equation 5-6}$$

$$V_n = 300\ A_n = 300 \times 1806 = 542{,}000\ psi = 542\ kip \qquad \text{Equation 5-7}$$

$$V_n = 56\ A_n + 0.45\ N_u = 56 \times 1806 = 101{,}000\ psi = 101\ kip \qquad \text{Equation 5-8}$$

The minimum value of V_n from Equation 5-6, Equation 5-7 and Equation 5-8 is 101 kip. Accordingly, using Equation 5-5, the lateral strength of the infill due to horizontal shear failure along a bed joint is computed as

$$H_n = \frac{V_n}{1.5} = \frac{101\ kip}{1.5} = 67.3\ kip$$

Therefore, using the least lateral strength from (a), (b) and (c), the lateral strength of the AAC infill is determined as 27.9 kip, and the corresponding diagonal compressive strength of the infill is

$$P_n = \frac{H_n}{\cos\theta} = \frac{27.9\ kips}{0.857} = 32.6\ kips$$

The commentary to the draft MSJC infill design provisions suggests that the lateral drift at this strength is approximately 1 in. This corresponds to an axial strain in the equivalent strut of

$$\varepsilon_{strut} = \frac{1\,in. \times \cos\theta}{L_{strut}} = \frac{1\,in. \times 0.857}{\sqrt{(144^2 + 240^2}\,in.} = 0.003,$$

which is close to the expected crushing strain of AAC (Tanner 2003).

5.3 EXPERIMENTAL RESULTS FOR AAC-INFILLED FRAME SPECIMEN VERSUS PREDICTIONS BY DRAFT MSJC INFILL DESIGN PROVISIONS

5.3.1 Observed stiffness versus predictions by draft MSJC provisions for infills

According to the draft MSJC provisions for infills, the stiffness of the infill, computed using Equation 5-1, is based on a horizontal displacement of approximately 0.5 in. (0.35% drift for the AAC-infilled frame test setup). The stiffness of the AAC infill from the experiment used for comparison with the prediction by draft MSJC infill design provisions is evaluated as the secant stiffness at deflection amplitude of 0.5 in. Because the infilled frame specimen was not subjected to a nominal 0.5-in. deflection amplitude cycle, this is obtained as an average of the measured secant stiffness at cycles with nominal deflection amplitudes of 0.4 in. (0.28% drift) and 0.6 in. (0.42% drift). The secant stiffness at these deflection amplitudes was nearly same as the tangent stiffness, as shown in Figure 4.18.

Table 5-1 and Table 5-2 present the secant stiffnesses of the AAC infill panel in the north and south directions during cycles to nominal deflections of 0.4 in. (0.28% drift) and 0.6 in. (0.42% drift), and the average of those values. The horizontal stiffness of the AAC infill panel, computed as the average of average stiffness at nominal deflections of 0.4 in. and 0.6 in., is 108.6 kip/in. for northward displacement and 76.8 kip/in. for southward displacement. The corresponding prediction by the draft MSJC infill provisions is 109 kip/in (Section 5.2.1). The measured stiffnesses in the north and south direction are, respectively, 1.0 and 0.7 times that predicted by the MSJC draft infill design provisions. This agreement is deemed reasonable, and it is concluded that the draft MSJC infill provisions can be used to estimate the lateral in-plane stiffness of AAC infills for design purposes.

Table 5-1: Secant stiffness (kip/in.) of AAC infill panel at cycles to nominal deflection of 0.4 in. (0.28% drift)

Cycle number	North	South
1	112.5	97.5
2	114.6	87.2
3	109.1	81.2
Average	**112.1**	**88.6**

Table 5-2: Secant stiffness (kip/in.) of AAC infill panel at cycles to nominal deflection of 0.6 in. (0.42% drift)

Cycle number	North	South
1	108.6	73.2
2	105.8	63.7
3	100.9	58.4
Average	**105.1**	**65.1**

5.3.2 Observed strength of AAC infill versus predictions by draft MSJC infill design provisions

Although the infill did not fail during the test, its lateral resistance reached a plateau at cycles to a nominal deflection of 2 in. (1.39% drift). The maximum lateral strengths of the infill for northward and southward displacements were 97.7 kips and 68.9 kips, respectively (Figure 4.18), corresponding to lateral deflections of 1.26 in. (0.875% drift) and 1.88 in. (1.30% drift), respectively.

Using the specified strength $f_{AAC}^{'}$, the draft MSJC infill design provisions, predict the lateral strength of the AAC infill as 27.9 kips (Section 5.2.2). The measured strength

of the AAC infill in the north and south directions, 97.7 kips and 68.9 kips respectively, are 3.5 and 2.5 times this prediction. Therefore, the draft MSJC infill provisions may be used to conservatively estimate the lateral in-plane strength of AAC infills for design purposes. Expected strengths should be obtained by multiplying the MSJC nominal strengths by a factor of about 3.5.

5.4 SUMMARY OF CHAPTER

In this chapter, the draft MSJC infill design provisions for stiffness and strength of infills are reviewed and checked against the observed response of the AAC-infilled frame specimen tested in this dissertation. While there is good agreement between the stiffness predicted by the draft provisions and that observed in the experiment, the strength predicted by the draft provisions using the specified compressive strength of AAC is conservative by a factor of at least 2.5 with respect to strength obtained from the experiment. Therefore, the draft MSJC infill design provisions for stiffness and strength of infill are applicable to AAC infills for design purposes. Design rules for AAC infills can be proposed based on those draft MSJC provisions, and can be used in applying the ATC-63 methodology to AAC-infilled steel moment frames.

A reliable validation of the draft MSJC infill provisions for AAC infills definitely requires more tests on AAC-infilled frame specimens. This is particularly true for establishing the statistical distribution of strengths of AAC infills. The equations to establish stiffness of AAC infills are less sensitive due to the fourth root involved in calculation of the equivalent strut parameter, λ, and may require fewer tests for validation than the equations for strength of AAC infills.

CHAPTER 6
Analytical modeling of archetypical infilled steel moment frames

6.1 INTRODUCTION AND SCOPE OF CHAPTER

In this chapter, the development of analytical models of archetypical infilled steel moment frames is described, based on ATC-63 (2008). The analytical models are developed and used in OpenSees (OpenSees 2006), a structural analysis framework for non-linear static and dynamic analysis. The hysteretic behavior of infills is modeled using the equivalent strut method introduced in Chapter 2. The force-deformation behavior of the equivalent struts is represented using the Ibarra-Krawinkler hysteretic model, also introduced in Chapter 2, and calibrated to fit the observed behavior of AAC and conventional masonry infills. Finally, the proposed analytical modeling procedures for archetypical infilled steel moment frames are demonstrated in OpenSees by simulating the lateral load-deflection response of the AAC-infilled steel moment frame specimen discussed in Chapter 4.

6.2 OPENSEES AS A STRUCTURAL ANALYSIS FRAMEWORK

The OpenSees program, developed at the PEER Center operated by the University of California at Berkeley (OpenSees 2006), provides a wide range of structural component and material models, many of which were embedded in OpenSees during the development of the ATC-63 methodology. This makes OpenSees a natural choice for the work described here. Using OpenSees, models of archetypical infilled steel moment frames are developed and applied as prescribed by the ATC-63 methodology.

6.3 GENERAL RECOMMENDATIONS OF ATC-63 (2008) FOR ANALYTICAL MODELING OF STEEL MOMENT FRAMES USING OPENSEES

ATC-63 (2008) contains example applications involving steel and reinforced concrete moment frames. The specific procedures used to model those frames with OpenSees were discussed with the authors of those example applications[1]. This is particularly true of the steel moment frame discussed in Section 10.2 of ATC-63 (2008). Those procedures are presented below and are used in this dissertation.

The example applications in ATC-63 (2008) model expected locations of plastic hinges using point plasticity springs, which are referred to as "zero-length elements" in OpenSees. In this dissertation, therefore, beams and columns (referred to here as structural members) in steel moment frames are modeled as a combination of one elastic beam-column element and two zero-length elements, with the zero-length elements being located at the ends of a structural member, where hinging typically occurs.

This is illustrated for a column in Figure 6.1. Thus, the effective stiffness of the structural member is represented by the combined stiffness of the zero-length elements and the elastic beam-column element. Ideally, the behavior of the zero-length elements should be rigid-plastic, so that the combined initial stiffness of the zero-length and the elastic beam-column elements would equal the elastic stiffness of the structural member. However, zero-length elements in OpenSees are required to have an initial elastic flexibility, which cannot be arbitrarily low for reasons of numerical stability. Therefore, the zero-length elements are modeled with initial stiffness of $66EI_y/L$, and the elastic beam-column elements are modeled with a moment of inertia of $1.1\ I_y$, where I_y is the moment of inertia of the structural member. This compensates for the reduction in stiffness of the structural member due to the initial elastic flexibility of the zero-length element, and makes the combined stiffness of the zero-length elements and the elastic

[1] Personal communications with Prof. Curt Haselton (California State University, Chico) and Prof. Abbie Liel (University of Colorado, Boulder)

beam-column element the same as that of the actual structural member under double curvature, as shown in Figure 6.2.

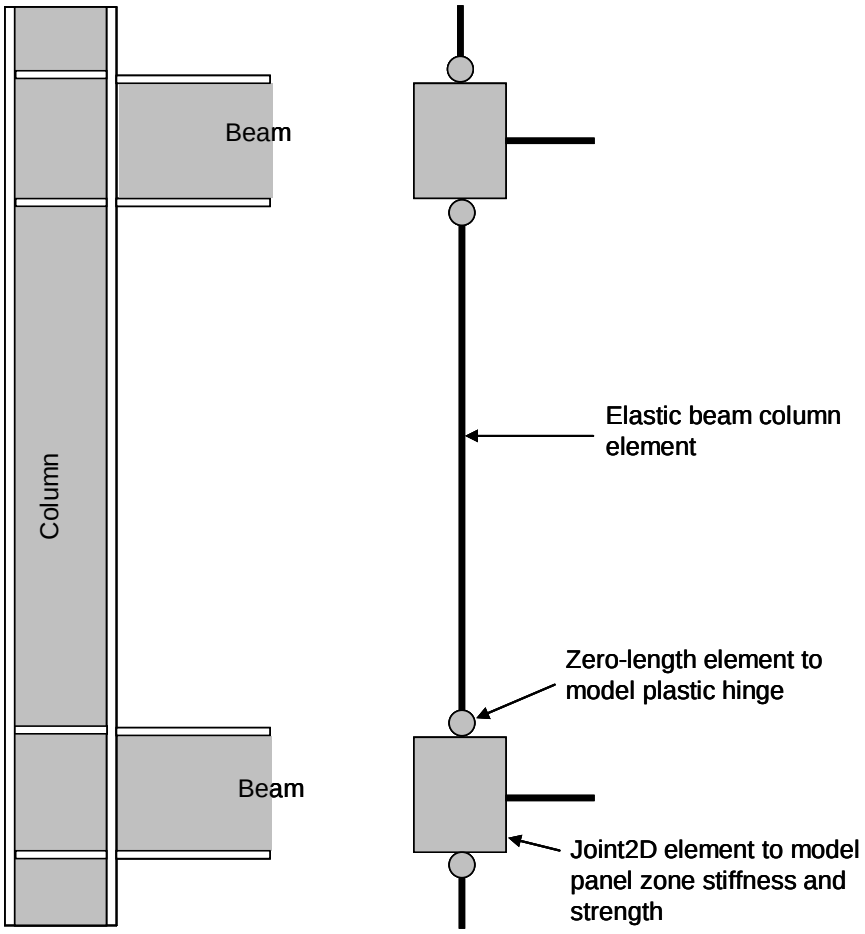

Figure 6.1: ATC-63 recommendations for modeling a structural member in OpenSees (ATC-63 2008)

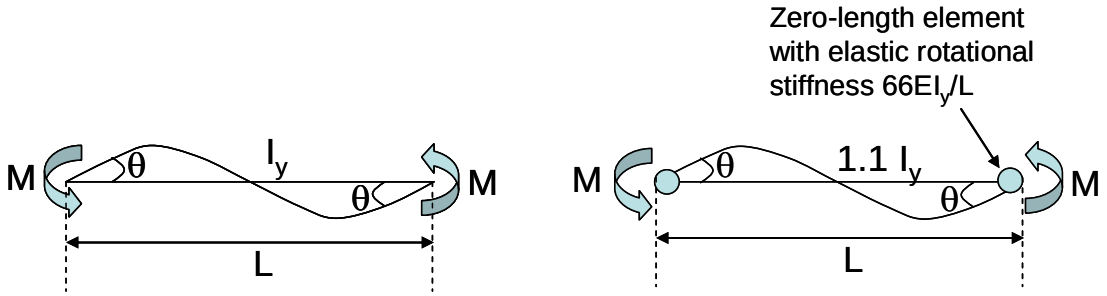

Figure 6.2: ATC-63 recommendation for elastic stiffness of zero-length and elastic beam-column element combination to model structural members in OpenSees (ATC-63 2008)

Moment-rotation properties of plastic hinges (Figure 6.3) are computed using Lignos (2007), provisionally based on data collected from Reduced Beam Section (RBS) connections. As suggested by Lignos (2007), the yield moment capacities of W-sections are computed using an expected yield strength of steel (54 ksi), and the plastic moment capacity of sections is taken as 1.05 times the expected yield moment capacity. The Ibarra-Krawinkler hysteretic model (Ibarra 2005) with bilinear hysteretic rules (Figure 6.4) is assigned to the zero-length elements.

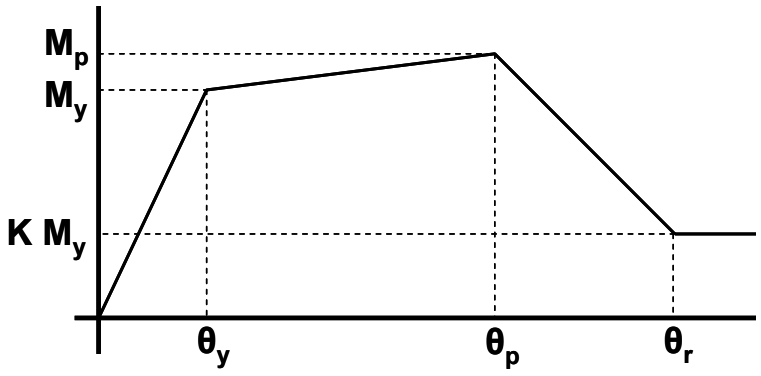

Figure 6.3: Moment-rotation properties of plastic hinges

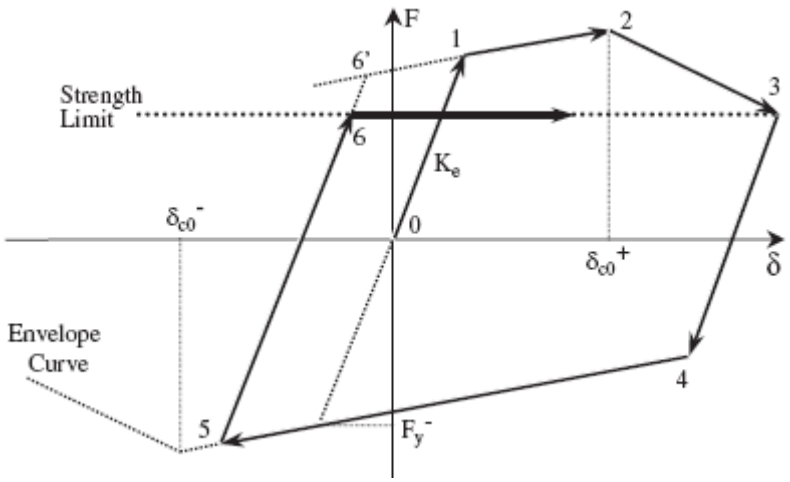

Figure 6.4: Ibarra-Krawinkler hysteretic model with bilinear hysteretic rules (Ibarra 2005)

The behavior of panel zones in beam-column joints is modeled using the Joint2D element (also known as the Altoontash-Lowes beam-column joint element) depicted in Figure 6.5 (Lowes 2003). The element characterizes the panel zone stiffness and strength using a moment-rotation relationship. Rotational springs on its faces are used to model moment-rotation behavior of plastic hinges in beams and columns and other phenomena occurring at the face of the beam-column joint (bar slip in reinforced concrete column joints, and flexibility of connections in steel frames). Because the central node of the Joint2D element is designated for internal use by the program, external elements cannot be attached to it. The rotational flexibility of the panel zone is computed by calculating the shearing deformation for a unit moment imposed on the panel, and its strength is calculated as outlined in Section J10 of AISC (2005) and in Krawinkler (1978). The Joint2D element requires a penalty-type constraint handler with a penalty factor less than 1×10^{15}.

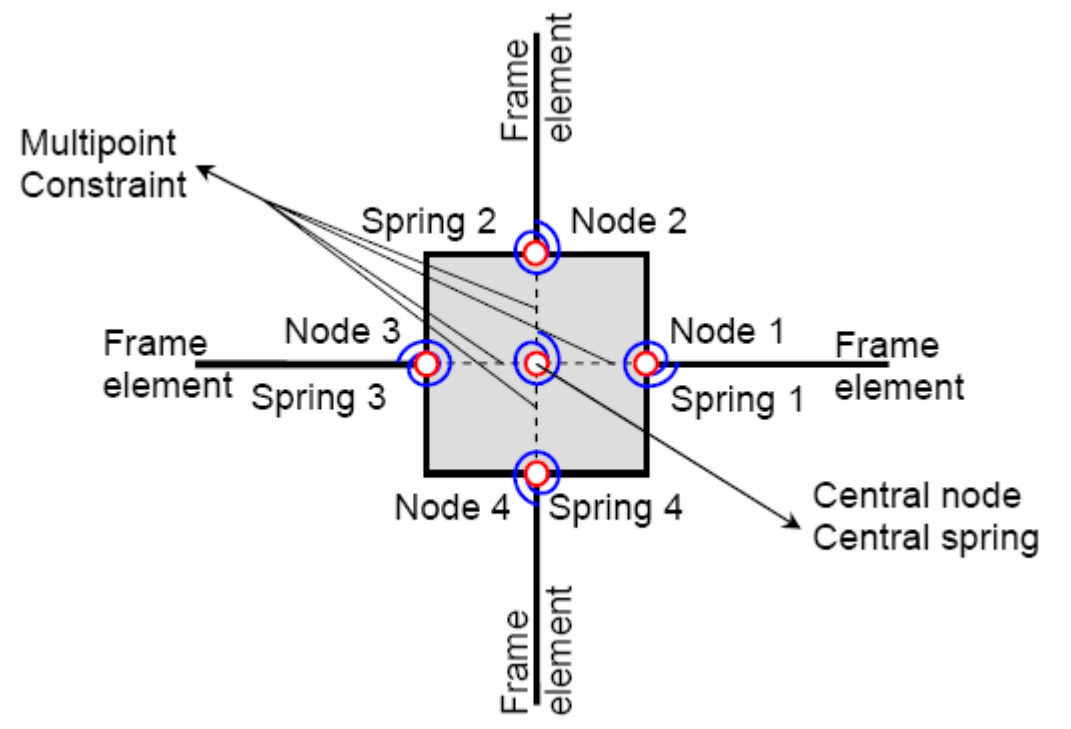

Figure 6.5: Joint2D element (Lowes 2003)

6.4 ANALYTICAL MODELING OF INFILLS

6.4.1 Equivalent strut approach

In this dissertation, infills are idealized as equivalent struts (Figure 6.6). This macro-modeling approach was introduced in Section 2.3, where its use by past researchers is presented. This approach requires much less computational effort than micro-modeling approaches such as the finite element method, yet still provides reasonable accuracy, thereby allowing easy analytical representation of multi-story, multi-bay frames. For these reasons, it is used in this dissertation to model the hysteretic behavior of infills.

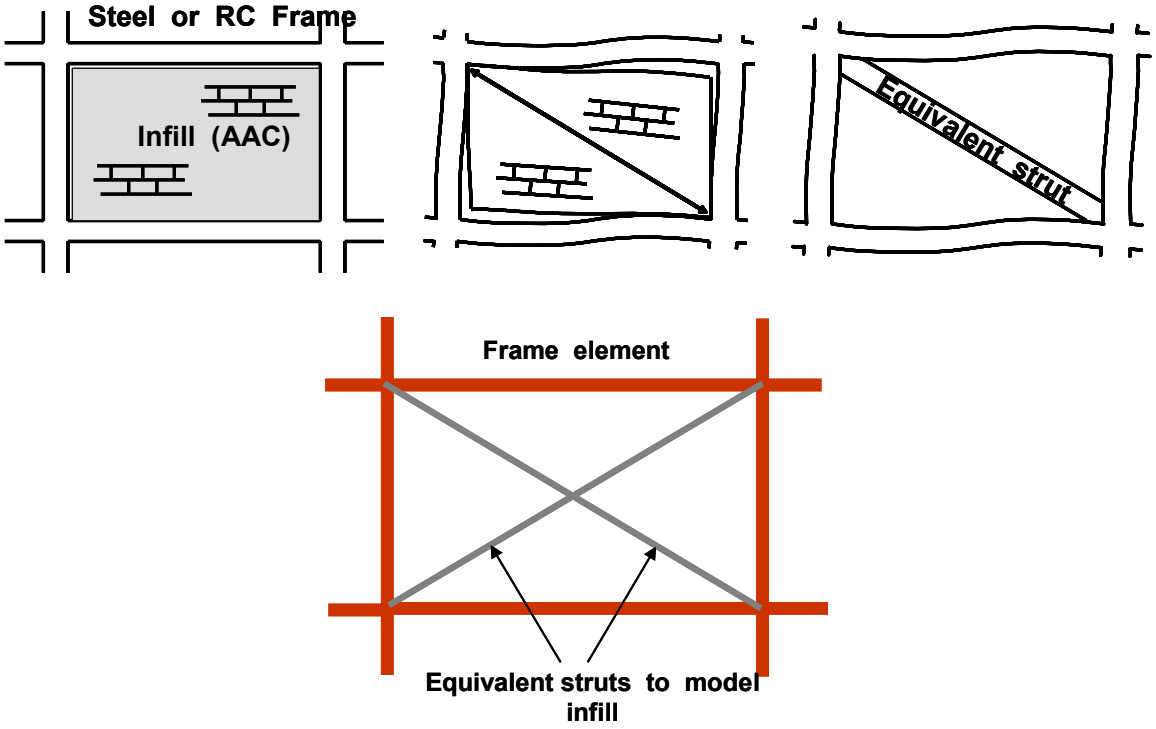

Figure 6.6: Idealization of infills using equivalent struts

In the equivalent-strut approach, the infill is represented as a combination of two compression-only truss elements, each acting independently. Each equivalent strut element is assigned an appropriate hysteretic force-deformation relationship, generally including a descending post-peak strength, in-cycle degradation, and pinching. In this dissertation, the Ibarra-Krawinkler hysteretic model with pinched hysteretic rules (Ibarra 2005) (Figure 6.7), is used for this purpose.

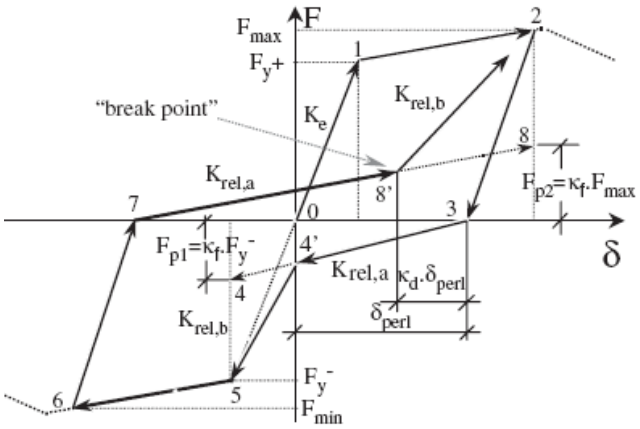

Figure 6.7: Ibarra-Krawinkler hysteretic model with pinched hysteretic rules (Ibarra 2005)

The salient features of the model are a backbone curve incorporating a residual branch with negative tangent stiffness (Figure 6.8) and parameters (k_d and k_f in Figure 6.7) to control the extent of pinching. Note from Figure 6.7 that the "backbone curve" (so termed in Ibarra 2005) is what other researchers have sometimes termed an "envelope" curve. For consistency with Ibarra (2005) and ATC-63 (2008), the designation "backbone curve" is retained in this dissertation. Cyclic degradation of strength and unloading stiffness can also be specified in the model. The following sections address the calibration of the parameters of this hysteretic model to represent the behavior of AAC and conventional masonry infills.

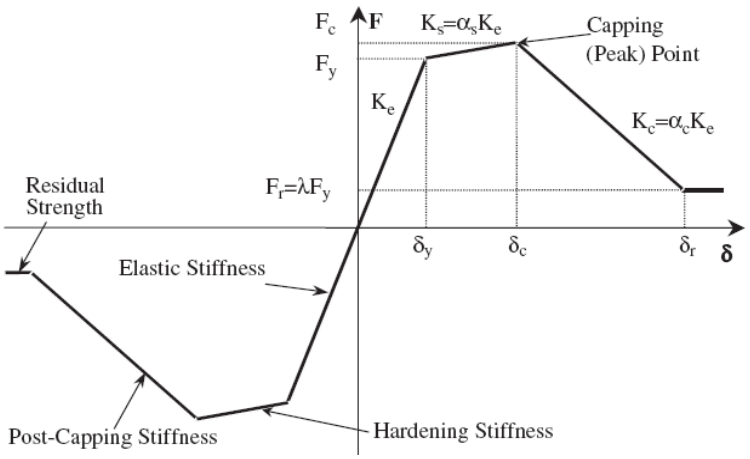

Figure 6.8: Backbone curve for Ibarra-Krawinkler hysteretic model (Ibarra 2005)

6.4.2 Modeling hysteretic behavior of AAC infills

For modeling hysteretic behavior of AAC infills, the backbone curve and other parameters of the Ibarra-Krawinkler hysteretic model are calibrated based on the experimental response of the AAC infill in the infilled frame specimen of Chapter 4. The backbone curve depicted in Figure 6.8 is calibrated to predict reasonably well the initial stiffness and strength of the AAC infill, and to visually fit the envelope of the load-deflection response of the AAC infill obtained from the test. The proposed parameters for the backbone curve are shown in Figure 6.9. The initial elastic stiffness of the backbone curve (K_e in Figure 6.8) is taken as twice the stiffness predicted by Equation 5-1 (Chapter 5) of the draft MSJC infill design provisions, because this seemed to agree well with the initial stiffness obtained from the test. The initial elastic portion of the backbone is terminated at half the lateral strength of the infill because this seemed to predict well the cracking strength of the infill, and this determines the point (δ_y, F_y) in Figure 6.8. After this, the envelope ascends to reach the maximum strength of the infill, at a lateral deflection that produces an axial strain of 0.0054 in the equivalent strut, determining the point (δ_c, F_c) in Figure 6.8. For the AAC-infilled steel moment frame specimen of Chapter 4, this axial strain in the equivalent strut corresponds to a lateral deflection of 1.75 in. (1.22% drift).

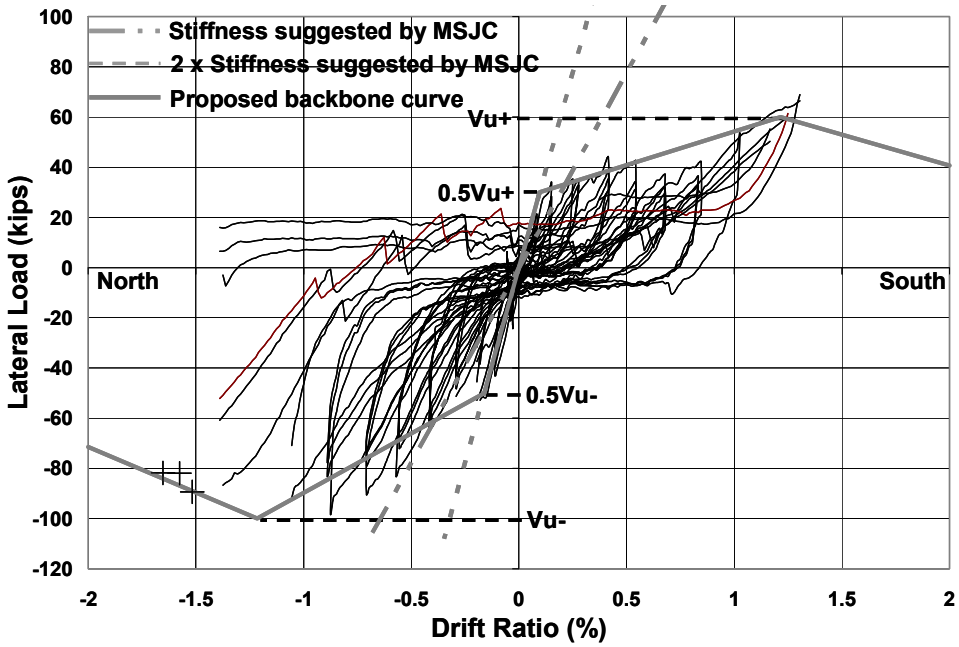

Figure 6.9: Proposed backbone curve for AAC infill

The proposed method of computing the deflection at maximum strength is based on the principle that the lateral deflection of the story in which the infill panel is located can be geometrically related to the strain in the equivalent strut by the following relation, depicted in Figure 6.10.

$$\varepsilon_{strut} = \frac{\Delta_{story} \cos\theta}{L_{strut}}$$

where,

ε_{strut} = axial strain in the equivalent strut (in./in.)

L_{strut} = diagonal length of the equivalent strut between centers of beam-column connections (in.)

Δ_{story} = lateral deflection of the story under consideration (in.)

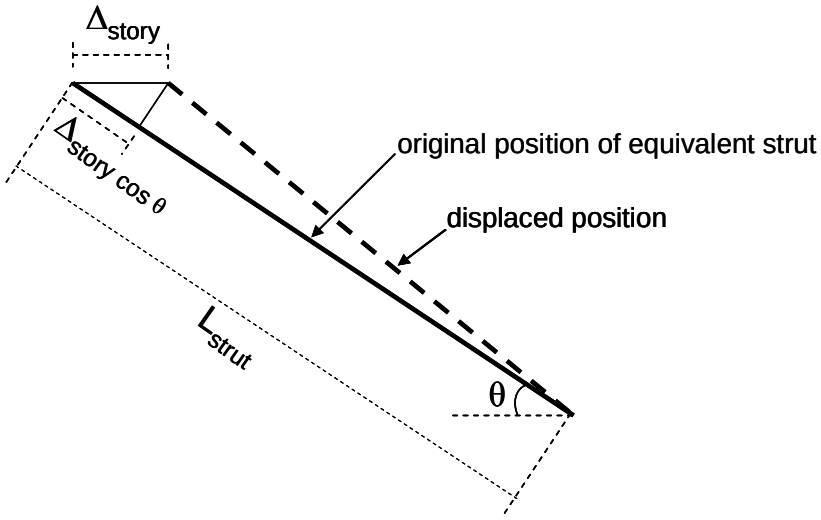

Figure 6.10: Geometrical relation between story drift and axial strain in equivalent strut

Although the equivalent strut may be expected to crush at the story drift corresponding to the maximum useful strain of the infill material, sliding along mortar joints during initial stages of loading alters the geometry of the infill, and increases the story drift required to crush the equivalent strut. For the AAC infill in the infilled frame specimen, peak strength seemed to be attained at a strain of 0.0054 in the equivalent strut, and this is adopted for analytical modeling of AAC infills.

The descending branch of the AAC infill could not be determined from the experimental results of Chapter 4, because that testing did not go to story drifts high enough to produce a descending branch. However, available literature (Flanagan 1999, 2001, Al-Chaar 2002) suggests significant post-peak strength of infills. Therefore, as suggested by Flanagan (1999), the descending branch is taken so that the strength of the AAC infill drops to 75% of its peak strength at 1.5 times the deflection at peak strength. This is used to determine the value of α_c for the backbone curve (Figure 6.8).

In-cyclic degradation of stiffness and strength of the equivalent strut is not modeled, because monotonic behavior of the AAC infill is not known. The lateral load-deflection response of the AAC infill obtained from the test (Figure 6.9) includes in-cycle

degradation. Therefore, parameters of the Ibarra-Krawinkler hysteretic model were set so that the hysteretic response of the AAC infill could be reproduced without explicit modeling of in-cyclic degradation of strength and stiffness. On this basis, the values of the pinching parameters k_f and k_d were set as 0.15 and 0.5, respectively.

As shown in Figure 6.11, the lateral force-deflection response of the AAC infill obtained from the test is reasonably well predicted by the Ibarra-Krawinkler hysteretic model with the proposed backbone curve and hysteretic parameters. Therefore, this calibrated model is used in the rest of this dissertation to model the hysteretic behavior of AAC infills in archetypical AAC-infilled steel moment frames.

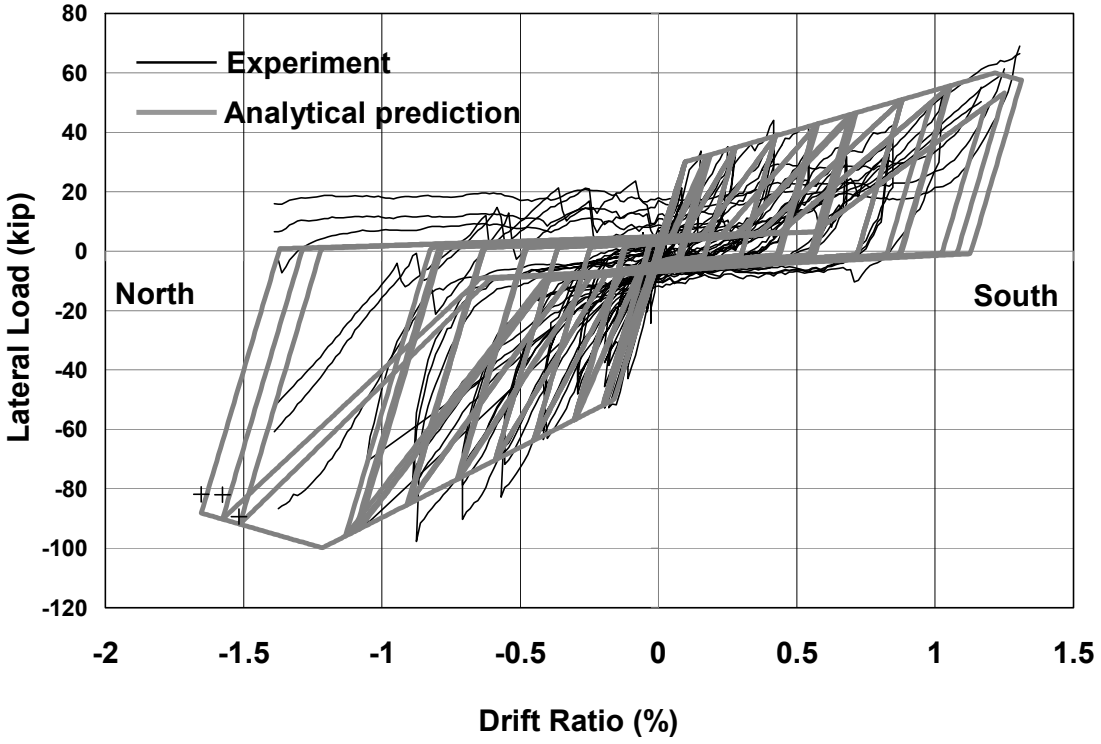

Figure 6.11: Prediction of hysteretic response of AAC infill by Ibarra-Krawinkler hysteretic model

6.4.3 Modeling hysteretic behavior of conventional masonry infills

In this dissertation, archetypical steel moment frames infilled with conventional masonry are evaluated using the ATC-63 methodology. This requires analytical modeling of the hysteretic behavior of conventional masonry infills, accomplished as just described for AAC infills, using equivalent struts and the Ibarra-Krawinkler hysteretic model. This section addresses determination of the backbone curve and parameters of the Ibarra-Krawinkler hysteretic model for conventional masonry infills (specifically, clay masonry infills). Unlike for AAC infills, however, the parameters of the hysteretic model are determined based on published experimental data for conventional masonry infills.

6.4.3.1 Initial stiffness of the infill panel

The initial stiffness of the clay masonry infill panel determines K_e (Figure 6.8) for the backbone curve of the Ibarra-Krawinkler hysteretic model. Flanagan (2001) recommends computation of the stiffness of infills using the following equation:

$$w_{strut} = \frac{\pi}{C\,\lambda_{strut}\cos\theta} \qquad \textbf{Equation 6-1}$$

In Equation 6-1, C is an empirical constant that depends on the limit state of the infill and varies with lateral deflection of the infill. For a given limit state of the infill, the value of C is nearly the same for all types of infill materials. Other parameters of Equation 6-1 are same as those in Equation 5-1 of the draft MSJC infill design provisions (Chapter 5).

To compute the initial stiffness of the infill, Flanagan (2001) recommends that the value of C be taken as 5. This makes the initial stiffness of the clay masonry infill about twice that obtained using Equation 5-1 of the draft MSJC infill design provisions. The same observation is made for analytical modeling of AAC infills in Section 6.4.2, where the initial stiffness of the AAC infill from the experiment is twice that predicted by Equation 5-1.

In using Equation 6-1, the elastic modulus of clay masonry, E_m, is computed as prescribed in Section 1.8 of the MSJC Code (MSJC 2008a):

$$E_m = 700\ f_m'$$

Although the MSJC code requires use of the specified strength of clay masonry f_m' in the formula above, the expected value of E_m was obtained using the tested compressive strength of the clay masonry infill, f_m.

6.4.3.2 Cracking strength

The cracking strength of the clay masonry infill determines F_y in Figure 6.8 for the backbone curve of the Ibarra-Krawinkler hysteretic model.

Panagiotakos (1993) takes the cracking strength as 0.77 times the capping strength, noting that this provided the best agreement with their experimental results. Dolsek (2002) assumes cracking strength to be half the capping strength, while Dolsek (2008) takes it as 0.6 times the capping strength. From experimental testing of AAC infills in this research, a cracking strength of about half the capping strength could be deduced.

Based on tests conducted on structural clay tile infills, Flanagan (1999) proposes that the mean cracking strength of infills be computed as:

$$H_{cr} = K_{cr}\ L\ t\ \sqrt{f_m}$$

where,

H_{cr} = mean cracking strength of the infill panel in N

K_{cr} = 0.066

L = length of the infill panel in mm

t = thickness of the infill panel in mm

f_m = compressive strength of masonry in MPa

In this dissertation, the cracking strength of clay masonry infills was first computed using the equation proposed by Flanagan (1999). However, this generally resulted in a computed cracking strength of about half of its capping strength. Therefore,

for simplicity the cracking strength of clay masonry infill was taken as exactly half of the capping strength for analytical modeling.

6.4.3.3 Lateral strength

The lateral strength of the infill panel determines F_c (Figure 6.8) for the backbone curve of the Ibarra-Krawinkler hysteretic model. The mean lateral strength of a clay masonry infill is computed using the simplified formula proposed by Flanagan (2001) for corner crushing strength of the infill:

$$H_{ult} = K_{ult}\ t\ f_m$$

Based on 58 tests on infills reported in literature, 12 of which were performed on clay infills, Flanagan (2001) proposes mean values for K_{ult} for different types of infills as summarized in Table 6-1. For clay masonry infill, Flanagan (2001) proposes a mean value of 201 mm for K_{ult}, which predicts mean lateral strength of clay masonry infills with a coefficient of variation of 4.6%. In US customary units, this value for K_{ult} would be 7.9 in. Therefore, in US customary units, the mean lateral strength of clay masonry infills can be computed as:

$$H_{ult,clay,mean} = 7.9\ t\ f_m\ (kip)$$

Table 6-1: K_{ult} for different types of infills (Flanagan 2001)

Specimen Characteristics		Statistical Results of K_{ult}		
Infill masonry type	Frame	Number of tests	Mean (mm)	Coefficient of variation (%)
Clay tile	Steel	18	246	23.5
Brick	Steel	12	191	17.1
(with outlier removed)		11	201	4.6
Concrete	Steel	19	259	17.3
Concrete	Concrete	10	257	23.3
Clay tile and concrete combined	Steel and concrete	47	253	20.7
All	All	58	243	21.2

For analytical modeling, the lateral strength of clay masonry infill is computed at one standard deviation less than the mean strength proposed by Flanagan (2001). Accordingly, the lateral strength of a clay masonry infill panel is computed as:

$$H_{ult,clay} = 7.9 \times (1 - \frac{4.6}{100})\ t\ f_m = 7.5\ t\ f_m$$

Lateral strength of the infill governed by shear failure along bed joint is not considered, because this failure mode is not consistent with modeling infill behavior using the equivalent strut approach, and was not observed for the AAC-infilled frame tested in this investigation.

6.4.3.4 Strain at peak strength

The strain at peak strength of clay masonry infill determines δ_c (Figure 6.8) for the backbone curve of the Ibarra-Krawinkler hysteretic model. This strain can also be represented as an interstory drift as presented in Section 6.4.2 and Figure 6.10.

Based on available experimental data, however, Flanagan (1999, 2001) reports that crushing of infills correlates better with lateral deflection than with drift ratio. He suggests that the lateral deflection at crushing of the infill be taken as 25 mm (~ 1 in.). Based on finite element studies validated by experimental results, Combescure (2000) suggests the strain in the equivalent strut at crushing to be 0.005. Dolsek (2002) assumes the interstory to be about 0.5% to 0.6% at maximum strength of the infill. He notes that this assumption "was between the values suggested according to Combescure (2000) and Crisafulli (2000)." Dolsek (2008) assumes that the maximum capacity of the infill was reached at a interstory drift of about 0.2%.

Section 3.3.2 of the MSJC code (MSJC 2008a) prescribes the maximum usable strain of clay masonry as 0.0035, and Section A.3 of that document prescribes the maximum usable strain of AAC as 0.003. Since the maximum useful strains for clay masonry and AAC are comparable, the previous experimental observation that the strain in the equivalent strut is 0.0054 near the capping strength of the AAC infill, this same value may be applicable to clay masonry infills as well.

These methods are applied to the infilled steel moment frame specimen of Chapter 4 and compared in Table 6-2 in terms of the strain in the equivalent strut and the interstory drift at crushing.

Table 6-2: Axial strain in equivalent strut and interstory drift at capping strength of infill

Author	Axial strain in equivalent strut	Interstory drift
Dolsek (2008)	0.0009	0.20%
Dolsek (2002)	0.0022-0.0026	0.50-0.60%
Flanagan (1999, 2001)	0.0030	0.69%
Combescure (2000)	0.0050	1.13%
From testing of AAC infills in this dissertation	0.0054	1.23%

In this dissertation, the proposal of Flanagan (1999, 2001) is used to estimate the strain in the equivalent strut at capping strength of the clay masonry infill, for the following reasons:

1) his proposal is simple;
2) it results in a value of crushing strain in the equivalent strut for clay masonry that agrees with the 2008 MSJC value for maximum useful strain; and
3) its estimation of the strain in the equivalent strut and the horizontal drift at crushing seems to lie near the middle of all observations.

6.4.3.5 Post-peak strength

The post-peak strength of the clay masonry infill determines α_c and δ_r (Figure 6.8) for the backbone curve of the Ibarra-Krawinkler hysteretic model. While many recommendations are available in literature for the post-peak strength of clay masonry infills, these are somewhat arbitrary and vary widely. Panagiotakos (1993) takes the ratio of the stiffness of the descending branch to the initial stiffness as a negative 0.5%. Flanagan (1999) proposes that "a conservative post-peak approach is to reduce the in-plane infill strength to 75% of peak at an in-plane drift of 1.5 times the displacement at

peak strength." Based on finite element studies validated by experimental results, Combescure (2000) suggests the strain at the end of the descending branch to be 0.015. Dolsek (2002) assumes that the stiffness of the descending branch is equal to a negative 5% of the initial stiffness. Dolsek (2008) assumes the slope of the descending branch based on a ratio of 5 between the displacement at the end of the descending branch and the displacement at capping strength.

Regardless of these inconsistencies, published literature also indicates that the slope of the descending branch does not significantly affect the collapse capacity of infilled frames under strong ground motions (Dolsek 2004, Krawinkler 2007).

Since other parameters for the backbone curve of clay masonry infills were determined using recommendations by Flanagan (1999, 2001), for sake of consistency those recommendations are followed for the slope of the descending branch as well. Thus, the slope of the descending branch of clay masonry infill is determined by reducing the in-plane strength of the infill to 75% of its capping strength at an in-plane displacement of 1.5 times that at capping strength.

6.4.3.6 Residual strength

The residual strength of clay masonry infills beyond the descending branch is assumed to be 0.3 times the capping strength of the infill.

6.4.3.7 Pinching parameters

Panagiotakos (1993) used a hysteretic model that is similar to the Ibarra-Krawinkler hysteretic model with pinched hysteretic rules. The parameters β and γ used by Panagiotakos' (1993) model are similar to the parameters k_f and k_d (Figure 6.7) respectively in the Ibarra-Krawinkler hysteretic model. Panagiotakos reports values of 0.1 and 0.8 for β and γ, respectively.

The values of pinching parameters k_f and k_d for the Ibarra-Krawinkler hysteretic model that best represent the behavior of the AAC infill in the infilled frame specimen

described in Chapter 4 are 0.15 and 0.5, respectively. These values are comparable to those used by Panagiotakos (1993), and are used for clay masonry infills as well.

6.4.3.8 In-cycle stiffness and strength degradation

Current published literature contains no reliable quantification for in-cycle degradation of stiffness and strength of clay masonry infills, and such an exercise is beyond the scope of this dissertation. Therefore, in-cycle degradation of strength and stiffness of clay masonry is not considered in the analytical model of this dissertation.

6.5 DEMONSTRATION OF ANALYTICAL MODELLING PROCEDURES FOR ARCHETYPICAL INFILLED STEEL MOMENT FRAMES

The analytical modeling procedures presented in previous sections for archetypical infilled steel moment frames are demonstrated by using OpenSees to simulate the response of the AAC-infilled steel moment frame specimen of Chapter 4 (Figure 4.1). It is easier and more convincing to demonstrate the procedures for a simple and experimentally established case such as the AAC-infilled frame specimen before applying the procedures to a more realistic frame. Such an exercise also provides an opportunity to validate the use of component and hysteretic models in OpenSees.

6.5.1 Analytical model of steel moment frame test setup

The analytical model of the steel moment frame test setup is developed in OpenSees using the procedures described in Section 6.3. The test setup uses flange cover plate moment connections, and plastic hinges are expected to form in the top beam in the rows of bolts farthest from the column faces. For the columns, the expected location of plastic hinges is just above the bottom connection near the region labeled as “6” in Figure 4.6. The moment-rotation properties of the W-sections of the test setup are taken from Lignos (2007), because no similar recommendations exist for flange cover plate connections. Schneider (2002) discusses analytical modelling of flange cover plate connections, but does not provide precise guidelines for computing their moment-rotation

properties. Also, the conditions of a plastic hinge in flange cover plate connections are similar to those in Reduced Beam Section connections (of primary interest to Lignos), because for both types of connection the plastic hinges occur away from column faces, at changes in beam cross-section.

The flexibility of flange cover plates is computed assuming equal shear in all bolts connecting the flange cover plate to the beam flange, and this flexibility is modeled using a rotational spring. Because the test setup did not exhibit loss of stiffness or strength due to bolt slip during the bare frame test (Figure 4.8), slip between flange cover plates and beam flanges is not modeled. This is to be expected, because the bolt holes are only 1/16 in. larger than the bolt diameter, and the bolts come into bearing as soon as they slip. During the infilled frame test, however, some of the bolts slipped randomly and came into bearing against the cover plates, resulting in kinks in the load-deflection curve (Figure 4.13), as explained in Section 4.9.4. It is not possible to capture such localized behavior in the analytical model.

The analytical model of the test setup developed using these procedures is shown in Figure 6.12, and is referred to in this chapter as Model 1.

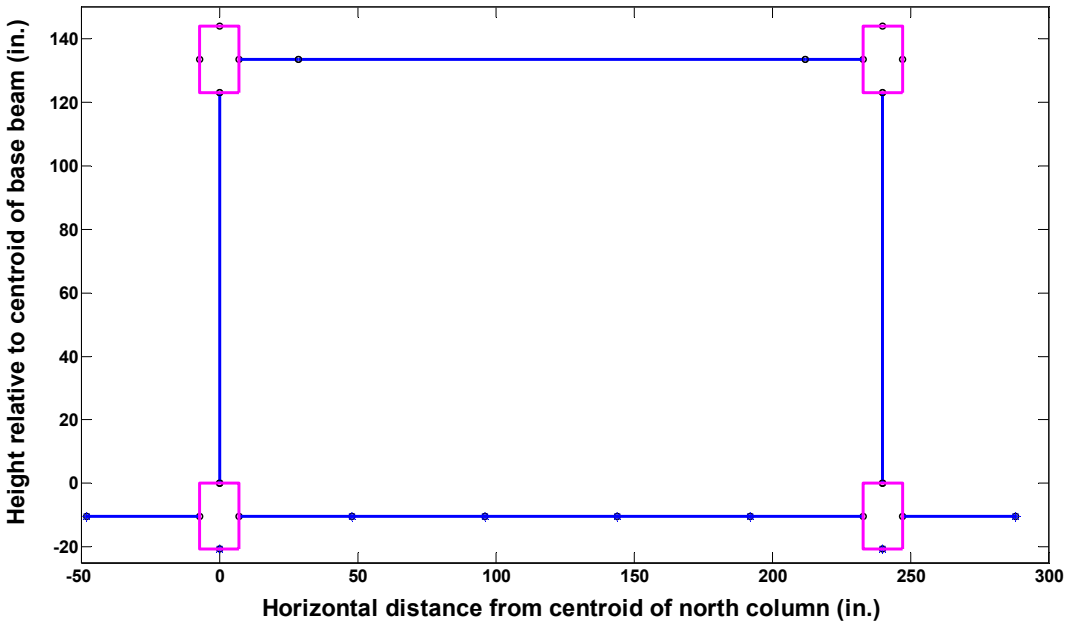

Figure 6.12: Model 1 - Model of bare frame

6.5.2 Analytical modeling of AAC-infilled frame specimen

The analytical model of the AAC-infilled frame specimen is developed by including in Model 1 the model for the AAC infill, using the approach described in Section 6.4.26.4. To overcome the inability to connect other elements to the center node of the Joint2D (Section 6.3), the following two modelling strategies were tried:

1) Model 2: In this model, the beam-column joint is modeled using stiff flexural elements whose stiffness is calibrated so that initial stiffness of Model 2 is the same as that of Model 1. Thereafter, the equivalent strut representing the infill spans diagonally across the frame between centers of beam-column joints (Figure 6.13)

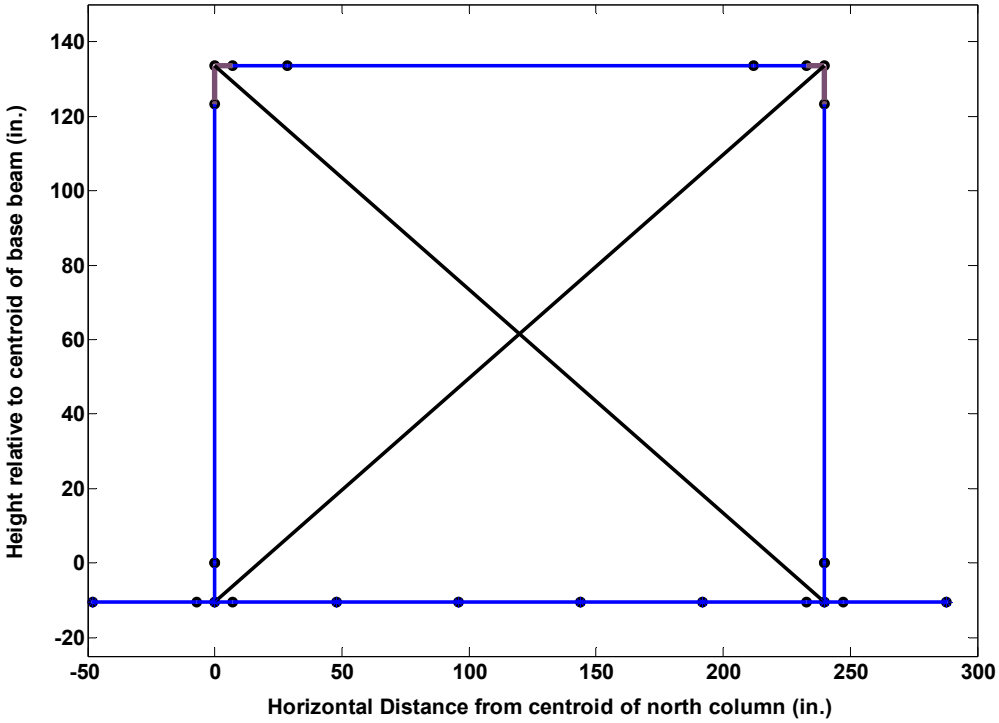

Figure 6.13: Model 2 of infilled frame specimen

2) Model 3: This model is same as Model 1, with the addition of an independent node at the center of the beam-column joint, connected to the nodes on the faces of the Joint2D element (Figure 6.5) using stiff axial links (Figure 6.14). As the deformed geometry of the Joint2D element is expected to be a parallelogram, the axial links do not contribute to stiffness or stength. The equivalent strut representing the infill is connected to that new node -column joint.

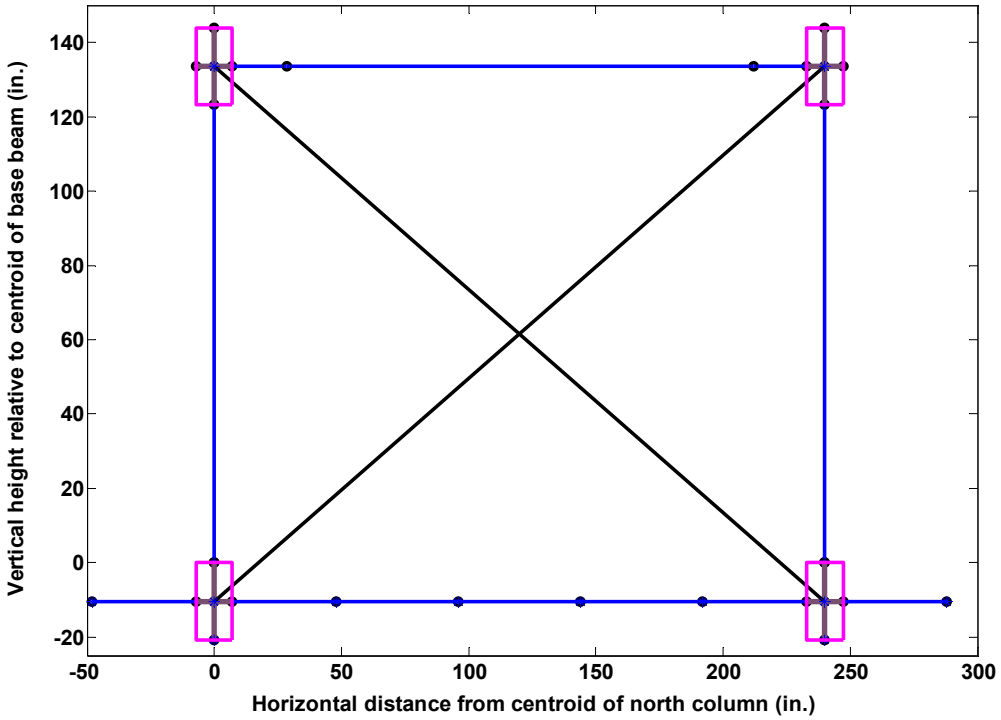

Figure 6.14: Model 3 of infilled frame specimen

The behavior of the bare frame test setup is predicted using Models 1, 2 and 3. With Models 2 and 3, the equivalent struts representing the AAC infill are omitted. Behavior of the infilled frame test setup is predicted using Models 2 and 3. Based on these predictions, the procedure used for either Model 2 or 3 is selected to construct analytical models of archetypical infilled steel moment frames in this dissertation. These are explained further below.

6.5.3 Analyses of bare frame test setup

Model 1, Model 2 and Model 3 were analyzed using pushover and static cyclic analysis to predict behavior of the bare frame test setup. Results from the pushover analysis are presented in Figure 6.15, and results from static cyclic analysis are presented in Figure 6.16.

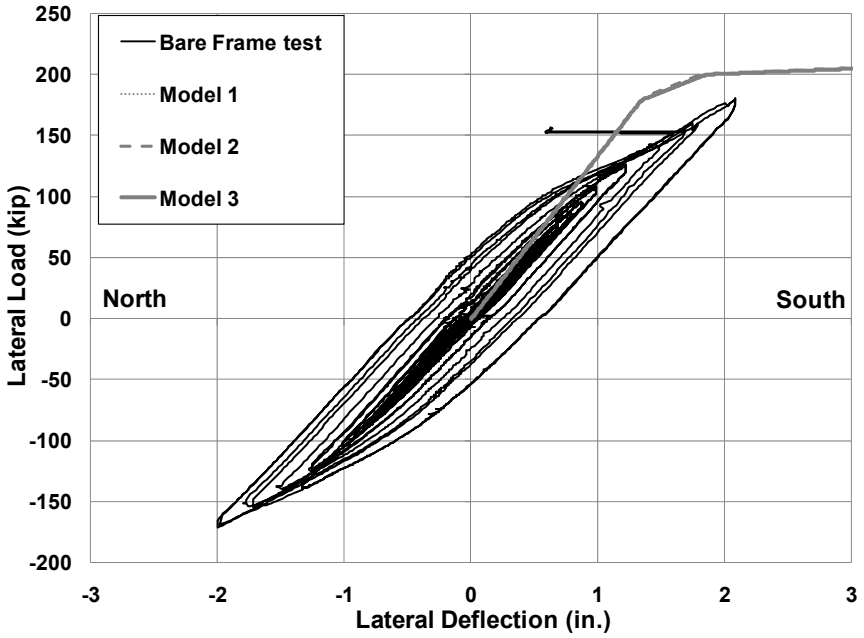

Figure 6.15: Pushover curves for bare frame test setup from Models 1, 2 and 3

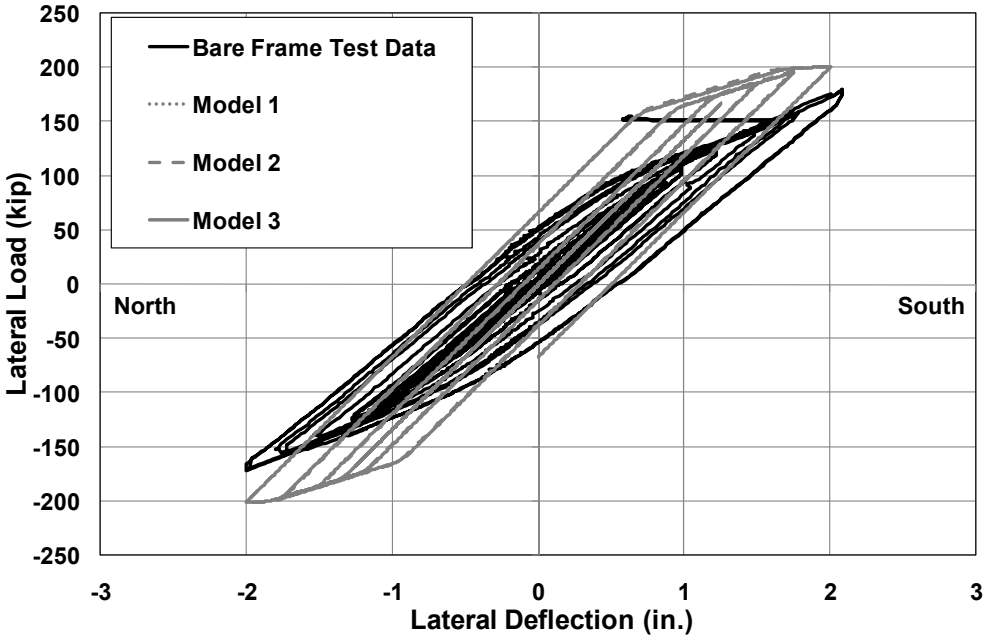

Figure 6.16: Static cyclic analysis of bare frame test setup with Models 1, 2 and 3

All three models predicted identical bare frame behavior. The predicted initial stiffness of the bare frame is slightly greater than the experimental result. This is

probably because the analytical models did not include shearing deformations, or because the analytical models for the moment connections between beams and columns of the test setup and the connections between the strong floor and the base beam were stiffer than their real-world counterparts. Because the bare frame test setup did not reach its ultimate strength during the bare frame test (Section 4.6), the analytically predicted strength of the bare frame cannot be compared with the observed strength. However, the analytically predicted strength of the bare frame does approach the observed strength at higher deflections. Differences between the analytical prediction and experimental result are probably due mainly to modeling of moment-rotation behavior of plastic hinges using Ibarra-Krawinkler hysteretic model with bilinear hysteretic rules. Such simple rules cannot capture the reduction in stiffness of the frame during inelastic response as influenced by Bauschinger's effect, by the gradual spread of yielding along the length of structural members at plastic hinge locations, and by the residual stresses from the manufacturing process.

Because Models 1, 2 and 3 give identical predictions for behavior of the bare frame, the axial links used in Model 3 to connect the equivalent struts to the centers of the beam-column joints evidently do not contribute to the stiffness of the beam-column joints or the frame. Because the predictions of Model 2 are identical to predictions of Model 3, in cases where the joint panel zone is not expected to yield, the beam-column joint can simply be modeled using rigid bending elements as in Model 2.

6.5.4 Analysis of AAC-infilled frame specimen

As shown in Figure 6.17, the quasi-static cyclic response of the AAC-infilled frame specimen is reasonably well predicted using Models 2 and 3. Differences between the analytical predictions and the experimental results for the infilled frame are mainly due to differences analytical predictions and experimental results for the bare frame (Figure 6.16).

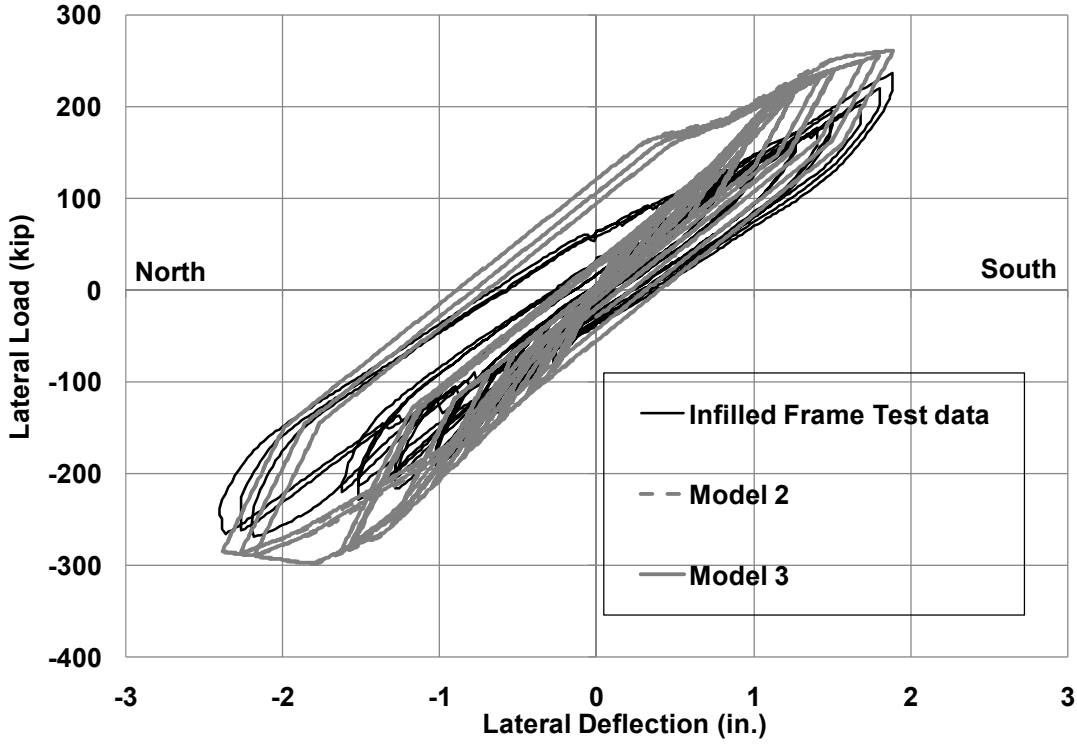

Figure 6.17: Static cyclic analysis of AAC-infilled steel moment frame specimen using models 2 and 3

Models 2 and 3 give identical predictions for the behavior of the infilled frame specimen. This shows that the approach used in Model 3 can be reliably used in OpenSees to connect equivalent struts (representing infills) to the Joint2D element. Therefore, this approach is adopted in this dissertation for developing analytical models of archetypical infilled steel moment frames in OpenSees.

6.6 SUMMARY OF CHAPTER

In this chapter, the approach for development of analytical models of archetypical infilled steel moment frames is presented. The analytical models are developed and analyzed in OpenSees (OpenSees 2006), a structural analysis framework for non-linear static and dynamic analysis. For analytical modeling of steel moment frames, the recommendations of the ATC-63 methodology are presented and adopted here.

The hysteretic behavior of infills is modeled using an equivalent strut whose hysteretic force-deformation behavior is described using the Ibarra-Krawinkler hysteretic model (Ibarra 2005). For AAC infills, the parameters of that model are calibrated against the AAC infill in the infilled frame specimen of Chapter 4. For conventional masonry infills, the parameters of that model are calibrated based primarily on Flanagan (2001).

Infilled steel moment frames are modeled in OpenSees using equivalent struts connected to independently established central nodes in the Joint2D element of OpenSees. These modeling procedures are demonstrated and verified by applying them to the AAC-infilled steel moment frame specimen presented in Chapter 4, and are shown to predict reasonably well the response of this infilled frame specimen compared to experimental results. Based on this demonstration, it is concluded that the proposed modeling procedures can be used to develop OpenSees analytical models for archetypical infilled steel moment frames as part of the ATC-63 methodology.

CHAPTER 7
Study of ATC-63 methodology using example steel moment frame

7.1 INTRODUCTION AND SCOPE OF CHAPTER

In this chapter, an example steel moment frame presented in ATC-63 (2008) is re-evaluated as part of the author's familiarization with the ATC-63 methodology. Such an exercise was felt necessary because the ATC-63 methodology is elaborate, with many details that can be best understood through an example. The results obtained from the re-evaluation are compared with those published in ATC-63 (2008). Based on that comparison, conclusions are drawn and comments on the ATC-63 methodology are presented. The methodology is then used to evaluate seismic design factors for infilled steel moment frames.

7.2 STEEL MOMENT FRAME USED FOR STUDY

One example in ATC-63 (2008) involves evaluation of seismic design factors for a four-story steel moment frame, shown in Figure 7.1.

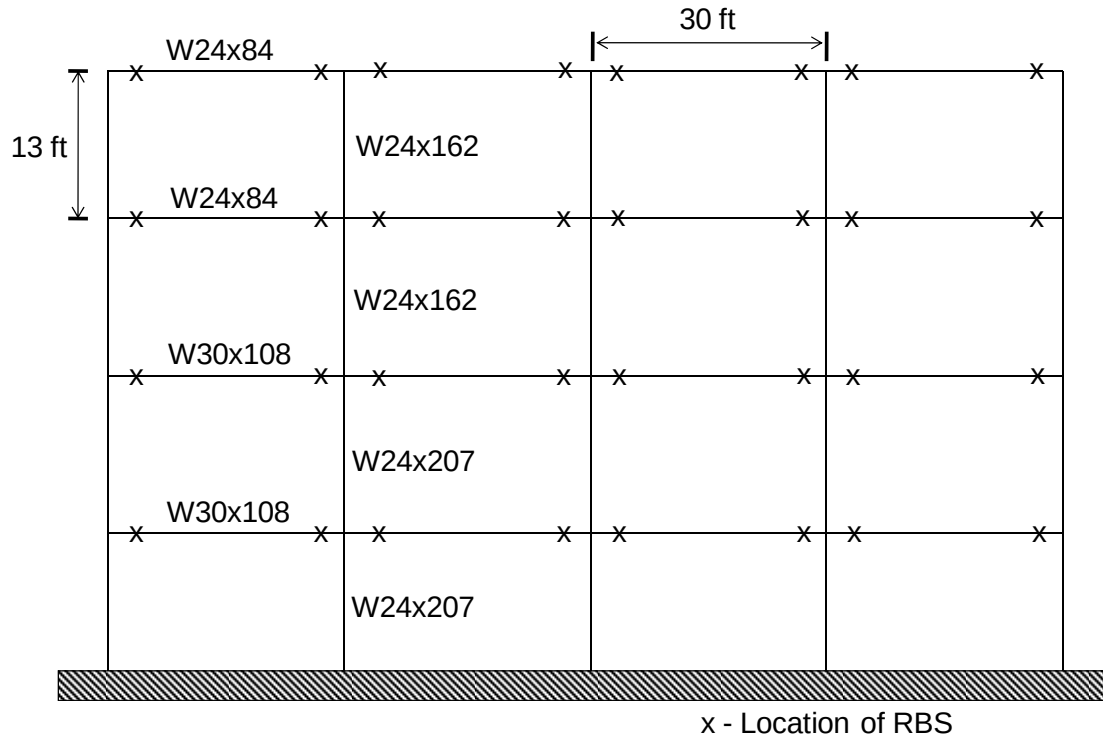

Figure 7.1: Four-story steel moment frame from ATC-63 (2008)

According to Section 10.2 of ATC-63 (2008) ("SMF" stands for "special moment frame"):

> This example focuses on assessment of a single steel SMF building, which in concept could be one of many index archetype configurations serving to describe the full archetype design space for all steel SMFs. The procedures applied to this one building would be extended to the full set of index archetype models in order to evaluate the entire class of steel SMFs…
>
> …The steel SMF archetype design analyzed in this example (Figure 10-1) is one of four perimeter moment frames that comprise the seismic-force resisting system of a four-story building. The building is designed assuming a high seismic site located in Seismic Design Category D, based on T = 0.94 second and an MCE spectral demand, S_{MT}, of 0.96g

(corresponding to Dmax). The structure has a design base shear, V = 0.08W. As designed according to ASCE/SEI 7-05 and AISC 2005, beams range in size from W24 to W30 (Figure 10-1), and are governed by minimum stiffness (drift limit) requirements. The RBS sections have 45% flange reduction. W24 columns are sized to satisfy the connection panel zone strength requirements without the use of web doubler plates. As such, they automatically satisfy other requirements, including the strong-column weak-beam (SCWB) requirement. The resulting SCWB ratio is about 2.5 times larger than the minimum requirement. This large column overstrength reflects a possible design decision that is representative of current practice in California; however, it implies that this example will not necessarily demonstrate the lower-bound performance of code-conforming steel SMFs…

…This structure is judged to have primarily two collapse modes: (1) sidesway collapse associated with beam and column hinging, and (2) collapse triggered by ductile fracture in one or more reduced beam section. The nonlinear response history analyses were run using the OpenSees (OpenSees 2006) software, employing elements with concentrated inelastic springs to capture flexural hinging in beams and columns and an inelastic (finite size) joint model for the beam-column panel zone.

Based on a separate communication with the author of this section of ATC-63 (2008), the RBS were located at 15 in. from the face of the column flanges[1]. Since the design base shear ratio is 0.08, corresponding to a MCE-level spectral demand of 0.96g, it can be deduced that the trial value of the response reduction factor, *R*, used for design of the steel moment frame is 8. According to Chapter 12 of ASCE7-05, this trial value of *R* classifies the frame as a "special steel moment frame." The corresponding value from

[1] Personal communication, Prof. Abbie Liel, University of Colorado, Boulder, September 18, 2008.

ASCE7-05 for the overstrength factor, Ω_o, is 3.0, and the value for the deflection amplification factor, C_d, is 5.5. From now on in this dissertation, this steel moment frame is referred to as "the ATC-63 steel moment frame."

7.3 ANALYTICAL MODEL OF THE ATC-63 STEEL MOMENT FRAME

For re-evaluation in this dissertation, the analytical model of the ATC-63 steel moment frame developed in OpenSees generally using the procedures described in Section 6.3, is depicted in Figure 7.2. Important aspects of the modeling are presented in the following sections.

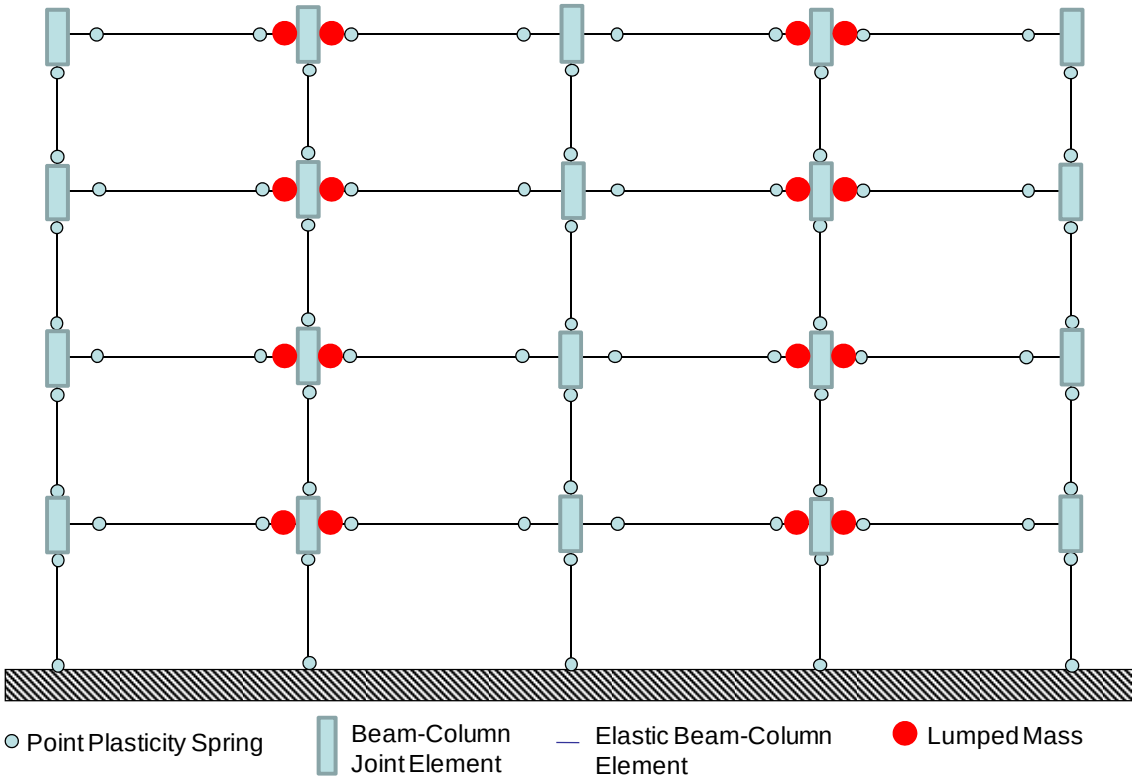

Figure 7.2: Analytical model of ATC-63 steel moment frame

7.3.1 Modeling moment-rotation behavior of plastic hinges in ATC-63 steel moment frame

Plastic hinges in beams are assumed to form at the RBS whose properties are used to calculate the moment capacity. The properties of W-sections and the moment-rotation parameters for the backbone curve of the Ibarra-Krawinkler hysteretic model (Figure 6.3) to model plastic hinges in these sections are presented in Table 7-1. Table 7-1 also presents the parameters computed using Lignos (2007) to model stiffness and strength deterioration of the plastic hinges.

Table 7-1: Properties and modeling parameters for steel W-sections (units: kip, in.)

Section	**W24x162**	**W24x207**	**W24x84**	**W30x108**
Area	47.7	60.7	24.7	31.7
D	25	25.7	24.1	29.8
b_f	12.955	13.0	9.02	10.5
t_f	1.22	1.57	0.77	0.760
t_w	0.705	0.870	0.47	0.545
I_x	5170	6820	2370	4470
Z_x	414	606	224	346
k_x	10.4	10.6	9.79	11.9
I_y	443	578	94.4	146
Z_y	68.4	137	32.6	43.9
k_y	3.05	3.08	1.95	2.15
L_b	156	156	120	120
Expected F_y	55	55	55	55
Moment-rotation parameters from Lignos (2007)				
θ_p	0.025	0.031	0.016	0.015
θ_r	0.18	0.20	0.17	0.16
Deterioration parameters from Lignos (2007)				
Λ_s	3.32	5.61	1.82	1.39
$E_t = \Lambda_s * M_y$	32058	51982	19406	17979
Length of member	131.9	126.2	299	298.3
$\delta_y [M_y/(6EI/L)]$	0.0038	0.0035	0.0061	0.0052
$\gamma_s = E_t / (M_y * \delta_y)$	877	1581	296	267

In Table 7-2, the moment-rotation parameters obtained in this dissertation for the backbone curve of the Ibarra-Krawinkler hysteretic model are compared with those reported in ATC-63 (2008). In a personal communication with the author of Section 10.2 of ATC-63 (2008), it was determined that a probable reason for the difference in the two sets of moment-rotation parameters is that those reported in ATC-63 (2008) were based on initial work by Lignos and that might not have been completely consistent with the final published results of Lignos (2007). From this personal communication, it was also found that the peak-oriented hysteretic rule (Ibarra 2005) is used with the Ibarra-Krawinkler hysteretic model in ATC-63 (2008) for modeling behavior of plastic hinges. In this dissertation, however, it is considered more appropriate to use the bilinear hysteretic rule discussed in Ibarra (2005) for this purpose. Hence, analyses are performed using both sets of hysteretic rules, and are then compared. The peak-oriented hysteretic rule is used with moment-rotation parameters labeled as "ATC-63 (2008)" in Table 7-2, while the bilinear hysteretic rule is used with moment-rotation parameters labeled as "Lignos (2007)". This is summarized in Table 7-3.

Table 7-2: Moment-rotation parameters for W-sections obtained using Lignos (2007) and those used in ATC-63 (2008)

Section	M_y (kip-in.)	$M_p/M_y^{+(-)}$	$\theta_p^{+(-)}$ (rad)	θ_r (rad)	K	γ	E_t (kip-in.)	c
Lignos (2007)								
W24x162	25740	1.05	0.025	0.18	0.4	877	85239	1
W24x207	33330	1.05	0.031	0.20	0.4	1581	186824	1
W24x84	8310	1.1 (1.05)	0.016	0.17	0.4	296	15140	1
W30x108	13294	1.1 (1.05)	0.015	0.16	0.5	267	18439	1
ATC-63 (2008)								
W24x162	25740	1.05	0.025	0.35	0.4	330	32058	1
W24x207	33330	1.05	0.03	0.3	0.4	440	51982	1
W24x84	8310	1.1 (1.05)	0.025 (0.020)	0.17	0.4	380	19406	1
W30x108	13294	1.1 (1.05)	0.022 (0.016)	0.15	0.5	260	17979	1

Table 7-3: Combinations of moment-rotation parameters and hysteretic rules used for plastic hinges in evaluation of the ATC-63 steel moment frame

Combination	Source of moment-rotation parameters	Hysteretic rule
1	Lignos (2007)	Bilinear
2	ATC-63 (2008)	Peak-oriented

7.3.2 Modeling beam-column joint behavior

Panel zones of beam-column joints are modeled as outlined in Section 6.3. Table 7-4 presents the calculation of stiffness and strength of panel zones in beam-column joints of the ATC-63 steel moment frame.

Table 7-4: Calculations for rotational stiffness and strength of panel zone in beam-column joints of the ATC-63 steel moment frame

Section	W24x162	W24x207
D_{col} (in.)	25.00	25.70
t_w (in.)	0.705	0.870
F_y (ksi)	55	55
D_{beam} (in.)	24.10	29.80
E (ksi)	29000	29000
G (ksi)	11154	11154
Rotational stiffness of panel zone (kip-in./rad) = $G\, D_{col}\, D_{beam}\, t_w$	4737740	7431790
R_n (kip) for $P_r \le 0.75\, P_c$ (AISC 2005)	661	844
Moment capacity of panel zone (kip-in.) = $R_n\, D_{beam}$	15930	25160

7.3.3 Mass and damping

Lumped masses equivalent to the seismic weight reported in ATC-63 (2008) are assigned to each story at the locations shown in Figure 7.2. Table 7-5 gives the seismic mass and gravity load at each floor level (Floor 1 coincides with the ground level). P-delta effects from gravity loads in columns are considered because they can increase ductility demand in the columns and are essential to simulate collapse. Rayleigh damping, consistent with that used for the ATC-63 steel moment frame in ATC-63 (2008), is specified so that the first and third modes have 2% damping. Table 7-6 presents the Rayleigh damping parameters and their calculation.

Table 7-5: Gravity load and seismic mass associated with stories of the ATC-63 steel moment frame

Floor	Gravity Load (kips)	Mass (kip-sec^2/in.) (g = 386 in./sec^2)
5 (roof)	1045	2.71
4	940	2.44
3	940	2.44
2	940	2.44

Table 7-6: Rayleigh damping parameters used for dynamic analyses of the ATC-63 steel moment frame

Parameter	Value
ω_1 (rad/sec)	5.87
ω_3 (rad/sec)	40.5
ξ_1	0.0200
ξ_3	0.0200
Rayleigh constant - *a* (associated with mass matrix)	0.205
Rayleigh constant - *b* (associated with stiffness matrix)	0.0010

7.3.4 Non-simulated collapse modes

Section 3.6.4 introduces non-simulated collapse modes and their consideration in the analysis of archetypical structures. For evaluation of the ATC-63 steel moment frame, apart from considering sidesway collapse mechanism, ATC-63 (2008) considers non-simulated collapse due to ductile fracture of RBS in beams. However, re-evaluation of the frame considering only sidesway collapse mechanism is sufficient to understand all the steps of the ATC-63 methodology. Therefore, non-simulated collapse modes due to ductile fracture of RBS in beams are not considered in this re-evaluation.

7.4 RESULTS AND COMPARISON WITH ATC-63 (2008)

7.4.1 Fundamental period

The ATC-63 methodology prescribes that the limiting fundamental period of the structure be calculated using Section 12.8.2 of ASCE7-05. Because the ATC-63 steel moment frame is evaluated using the response spectrum for SDC D_{max} in ATC-63 (2008), which has S_{MS} and S_{M1} as 1.5 g and 0.9 g respectively, the value of C_u from Table 12.8.1 of ASCE (2005) is 1.4. Therefore, the prescribed fundamental period of the ATC-63 steel moment frame is

$$T = C_u \, T_a = 1.4 \times 0.028 \times (13 \times 4)^{0.8} = 0.925 \text{ sec}$$

The corresponding MCE spectral demand ($S_{MT}[T]$) is:

$$S_{MT}[T] = \frac{S_{M1}}{T} = \frac{0.9}{0.925} = 0.973 \; g$$

In ATC-63 (2008), $S_{MT}[T]$ for the ATC-63 steel moment frame is reported as 0.96 g.

The fundamental period of the ATC-63 steel moment frame obtained in this dissertation from eigenvalue analysis is 1.07 sec, less than the value of 1.28 sec stated in ATC-63 (2008). Through a personal communication[2] with the author of Section 10.2 of ATC-63 (2008), it was learned that the model developed for ATC-63 (2008) used slightly higher values for seismic mass than stated in ATC-63 (2008), and that this could be the reason for the difference in the fundamental period from eigenvalue analysis.

7.4.2 Pushover analysis

As outlined in Section 3.6.2, pushover analysis is performed on the analytical model of the ATC-63 steel moment frame using both combinations of moment-rotation parameters and hysteretic rules listed in Table 7-3. Figure 7.3 presents results from the

[2] Personal communication with Prof. Abbie Liel, University of Colorado Boulder

pushover analyses, and Figure 7.4 presents the pushover curve reported in ATC-63 (2008). The two curves are quite close to each other.

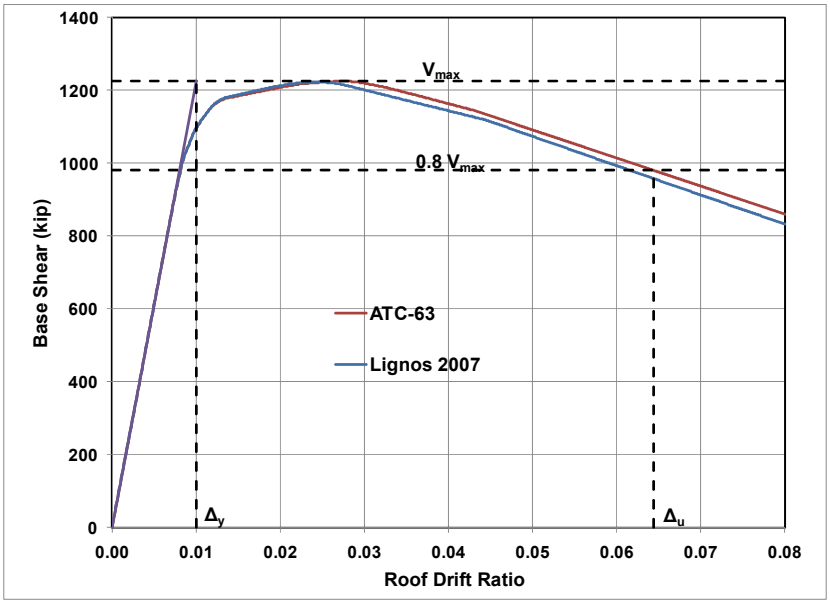

Figure 7.3: Pushover curve for the ATC-63 steel moment frame (this dissertation)

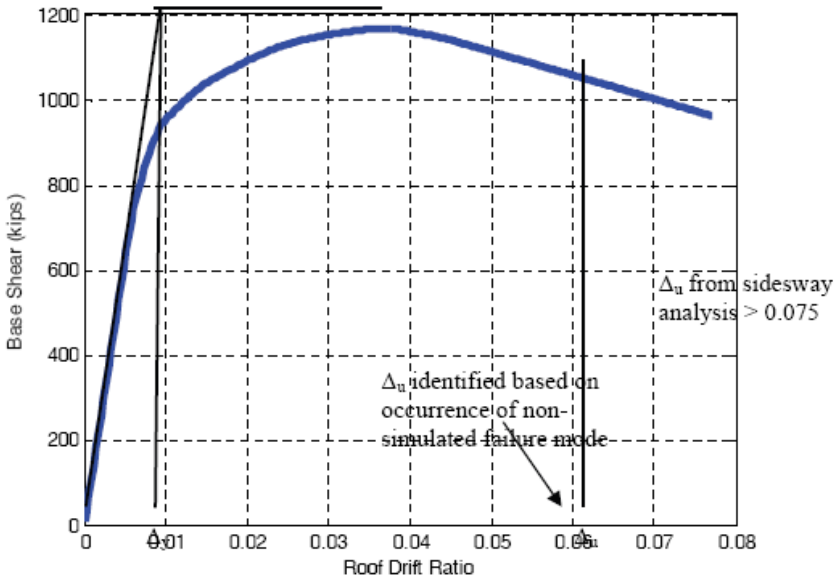

Figure 7.4: Pushover curve of the ATC-63 steel moment frame (ATC-63 2008)

Over-strength and ductility factors for the ATC-63 steel moment frame are calculated from the pushover curve obtained using Combination 1 of the moment-rotation parameters and hysteretic rules in Table 7-3. The over-strength factor is obtained as 3.6 neglecting material over-strength, and as 4.0 including material over-strength. It is reported as 3.4 in ATC-63 (2008). However, the maximum base shear is obtained in this dissertation as 1225 kips, close to 1150 kips reported in ATC-63 (2008). Therefore, it is assumed that the over-strength factor of 3.4 reported in ATC-63 (2008) does not include material over-strength, and the value of 3.6 obtained in this dissertation neglecting material over-strength is in close agreement with that value.

As outlined in Figure 3.6, the ductility factor considering sidesway collapse mechanism is calculated to be 6.4, while it is reported as approximately 7.5 in ATC-63 (2008). The ductility factor is also determined considering non-simulated collapse mode of fracture at a plastic rotation of 0.063 in RBS of beams. The ductility factor for this non-simulated collapse mode was obtained as 6.3 less than the 7.2 reported in ATC-63 (2008).

7.4.3 IDA and collapse margin ratio

IDA, as described in Section 3.6.3, is performed for the ATC-63 steel moment frame using both combinations of moment-rotation parameters and hysteretic rules listed in Table 7-3. Figure 7.5 depicts results from IDA using Combination 1 of moment-rotation parameters and hysteretic rules from Table 7-3. The spectral intensity, $S_{CT}[T]$, that causes collapse of the frame under half of the ground motions is found to be 2.14 g. The corresponding *CMR* for $S_{MT}[T]$ of 0.96 g, is calculated as 2.2.

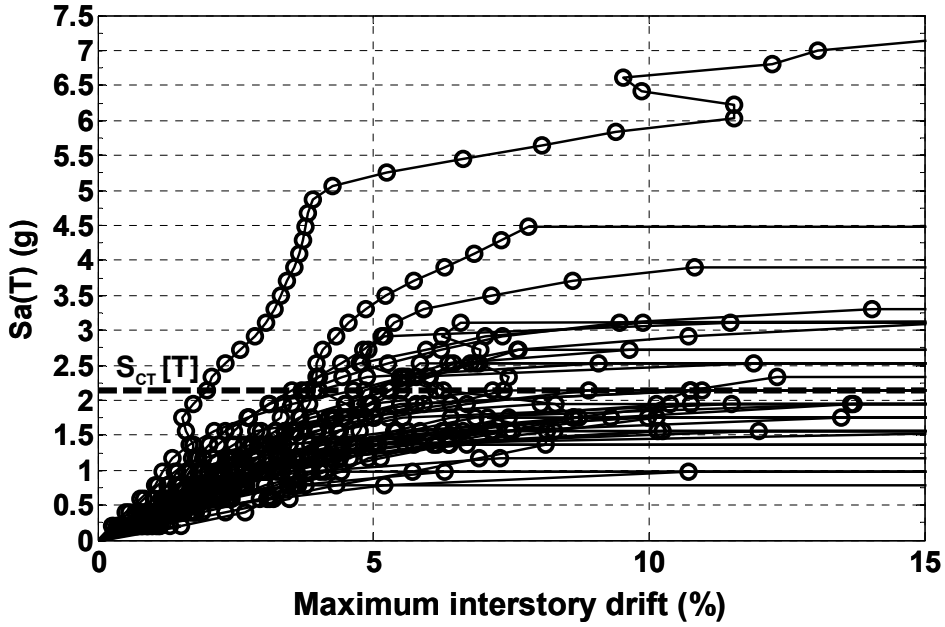

Figure 7.5: Results from IDA for the ATC-63 steel moment frame using Combination 1 of moment-rotation parameters and hysteretic rule in Table 7-3 (this dissertation)

Similarly, Figure 7.6 presents results from IDA using Combination 2 of the moment-rotation parameters and hysteretic rules in Table 7-3. $S_{CT}[T]$ that causes collapse of the frame under half of the ground motions is again obtained as 2.14 g, and the corresponding *CMR* is 2.2. Apparently, the same values are obtained for $S_{CT}[T]$ and *CMR* using both combinations of moment-rotation parameters and hysteretic rules in Table 7-3.

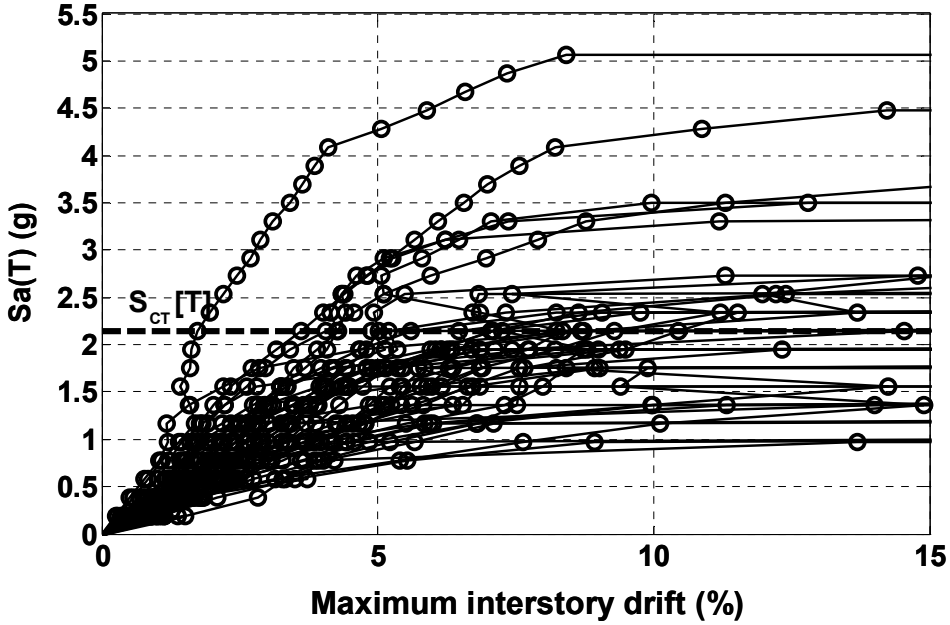

Figure 7.6: Results from IDA for the ATC-63 steel moment frame using Combination 2 of moment-rotation parameters and hysteretic rule in Table 7-3 (this dissertation)

Figure 7.7 presents results from IDA for the ATC-63 steel moment frame as reported in ATC-63 (2008). $S_{CT}[T]$ is reported as 2.36 g, and *CMR* is reported as 2.5.

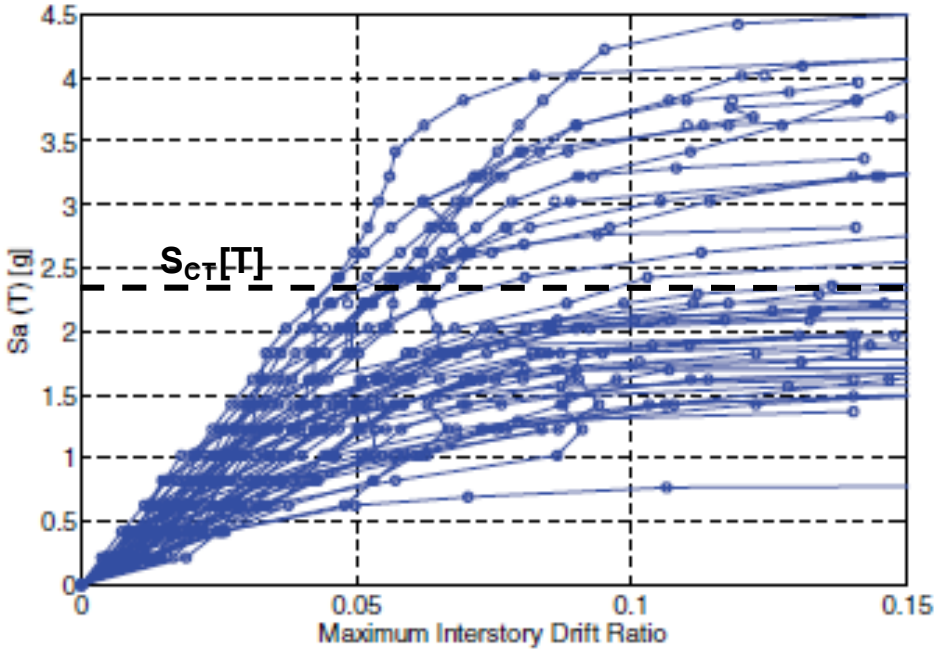

Figure 7.7: IDA results for ATC-63 steel moment frame from ATC-63 (2008)

Table 7-7 summarizes the results from analysis of the ATC-63 steel moment frame in this dissertation and compares them with the corresponding results from ATC-63 (2008).

Table 7-7: Summary of results obtained from analysis of the ATC-63 steel moment frame

Result type	**This dissertation**	**ATC-63 (2008)**
Fundamental period from eigenvalue analysis	1.07	1.28
Over-strength factor	3.6	3.4
Ductility factor from sidesway collapse	6.4	~7.5
Ductility factor from fracture of RBS	6.3	7.2
CMR using Combination 1 of moment-rotation parameters and hysteretic rules from Table 7-3	2.2	

CMR using Combination 2 of moment-rotation parameters and hysteretic rules from Table 7-3	2.2	2.5

7.4.4 *SSF* and adjusted collapse margin ratio

The *SSF* for the ATC-63 steel moment frame is determined as outlined in Section 3.7.1. Corresponding to a ductility of 6.4 from pushover analysis, and a fundamental period of 0.925 sec, the *SSF* is 1.40. Corresponding to a *CMR* of 2.2 and a *SSF* of 1.40, the adjusted collapse margin ratio (*ACMR*) is 3.1.

7.4.5 Rating of uncertainties for the ATC-63 steel moment frame

In this section, the various uncertainties outlined in Section 3.7.2 are rated for the ATC-63 steel moment frame.

7.4.5.1 Record-to-record uncertainty

The ATC-63 methodology recommends that the lognormal distribution standard deviation parameter associated with record-to-record uncertainty (β_{RTR}) be taken as 0.4. As mentioned in Section 3.7.3, β_{RTR} due to record-to-record uncertainty can be also be determined directly from the results of IDA by computing the lognormal distribution standard deviation parameter of the collapse scaling factors. Accordingly, for the 44 collapse scaling factors obtained for the ATC-63 steel moment frame from IDA, the lognormal distribution standard deviation parameter is determined as 0.43, close to the value of 0.4 published in ATC-63 (2008).

7.4.5.2 Design uncertainty

The ATC-63 steel moment frame is designed according to the existing consensus design provisions (AISC 2005), which have evolved based on research conducted over several decades. These provisions prescribe comprehensive procedures for analysis, design and fabrication of steel buildings. Nevertheless, variations in the final design of an archetypical structure are possible due to different intermediate choices made during

design process. Hence, uncertainty related to design requirements is rated as "good," and the corresponding lognormal distribution standard deviation parameter (β_{DR}) is taken as 0.3.

7.4.5.3 Test data uncertainty

Lignos (2007) and Krawinkler (1978), used for modeling hysteretic behavior of components of the ATC-63 steel moment frame, are based on extensive and reliable experimental data. Therefore, the test data used for calibration of component analytical models is rated as "good," and the corresponding lognormal distribution standard deviation parameter (β_{TD}) is taken as 0.3.

7.4.5.4 Modeling uncertainty

As presented in previous sections, differences exist between this dissertation and ATC-63 (2008) at every stage of the evaluation of the ATC-63 steel moment frame. Moment-rotation parameters for plastic hinges were determined using the same recommendations (Lignos 2007), yet the value of these parameters differed, sometimes significantly (Table 7-2). Analytical models for ATC-63 (2008) as well as this dissertation were developed and analyzed in the same structural analysis program using identical modeling techniques. Nevertheless, results differ by more than 10% for all analysis cases (eigenvalue, pushover analysis and IDA). Reasons for this are not clear. The models were developed by two different individuals. This suggests that regardless of the sophistication of the analytical models and the methods to determine the parameters required by those models, analytical results could vary considerably due to analytical choices as well as analytical errors. Considering these, modeling uncertainty for the ATC-63 steel moment frame is rated as "fair," and the corresponding lognormal distribution standard deviation parameter (β_{MDL}) as taken as 0.45.

7.4.5.5 Total system uncertainty

To summarize, β_{RTR} , β_{DR} , β_{TD} and β_{MDL} for the ATC-63 moment frame are determined as 0.4, 0.3, 0.3 and 0.45, respectively, and the lognormal distribution standard deviation parameter for the total uncertainty in the collapse capacity is obtained as 0.75.

7.4.6 Minimum value of ACMR for acceptable performance

For the performance of an archetypical structure to be acceptable, the ATC-63 methodology requires that the probability of collapse at MCE be less than 10%. From Table 7-3 of ATC-63 (2008), corresponding to β_{TOT} of 0.75, this minimum value of *ACMR* is 2.61. The *ACMR* calculated here (3.1) exceeds 2.61, indicating that the ATC-63 steel moment frame performs acceptably according to the ATC-63 methodology.

7.4.7 Collapse fragility curve

In Figure 7.8 is shown the collapse fragility curve obtained for the ATC-63 steel moment frame using various combinations of *CMR* and uncertainty. The collapse fragility curve obtained by considering *CMR* and only record-to-record uncertainty (β_{RTR} of 0.4) closely matches the cumulative probability of collapse scaling factors from IDA. Figure 7.8 also shows that considering uncertainties in performance evaluation has the effect of flattening the collapse fragility curve.

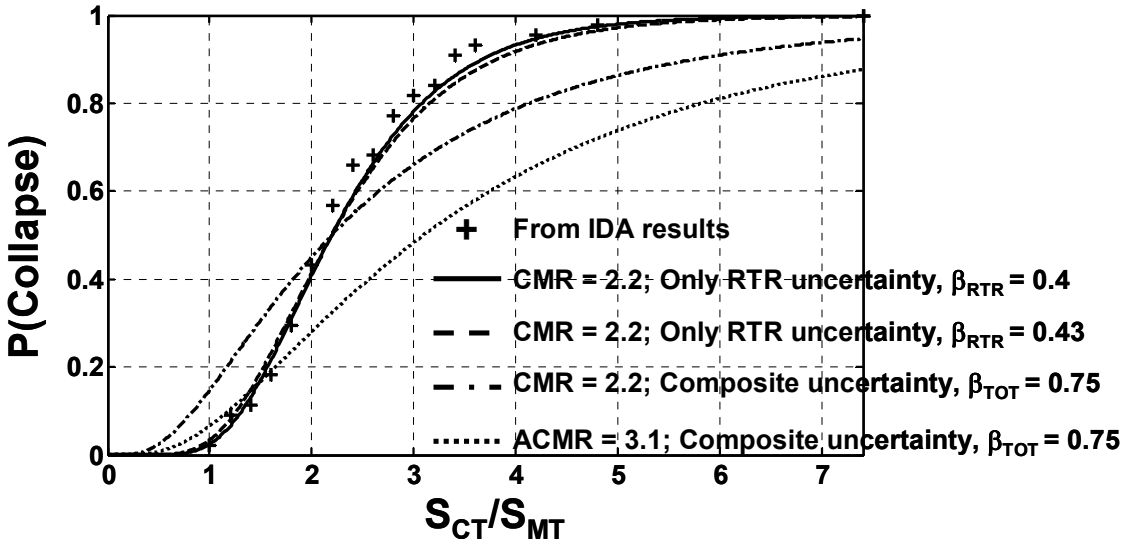

Figure 7.8: Collapse fragility curves for ATC-63 steel moment frame (this dissertation)

7.4.8 Uncertainty parameters and collapse fragility curve in ATC-63 (2008)

According to Section 10.2 of ATC-63 (2008):

The collapse fragility is now computed based on both simulated and non-simulated collapse modes…..The combined collapse fragility is illustrated in Figure 10-7, where the composite uncertainty is $\beta_{TOT} = 0.60$, as determined from Table 7-3. In this figure, the horizontal-axis fragility parameter, S_{CT}, is normalized by MCE demand, S_{MT}, to permit direct comparison of the collapse margin ratio (CMR) for the structure with and without consideration of non-simulated fracture induced failure modes. For this structure, the net result of including the fracture-induced collapse is to reduce the collapse margin ratio (CMR) by 32%, from 2.5 for the simulated side-sway-only case to 1.9. The conditional probability of collapse at the MCE increases from 8% to 14%. (Note: these margins and the collapse probabilities do not include the spectral shape factor, which is considered in the evaluation of acceptance criteria.)

Finally, the combined fragility data, reflecting the likelihood of both simulated and non-simulated collapse, should be compared to the acceptance criteria, as specified in Chapter 7. For this structure, the spectral shape factor (SSF) of 1.43 is determined from Table 7-1b with T = 0.94 seconds and μ_c = 7.2, which the increases collapse margin ratio from 1.9 to 2.8, thus easily satisfying the acceptance criteria given in Section 7.6. Here, acceptance is based on a total system collapse uncertainty of β_{TOT} = 0.60, which provides an acceptable collapse margin ratio of 2.16, as given in Table 7-2.

In Figure 7.9 is shown the collapse fragility curve for the ATC-63 steel moment frame reported in ATC-63 (2008).

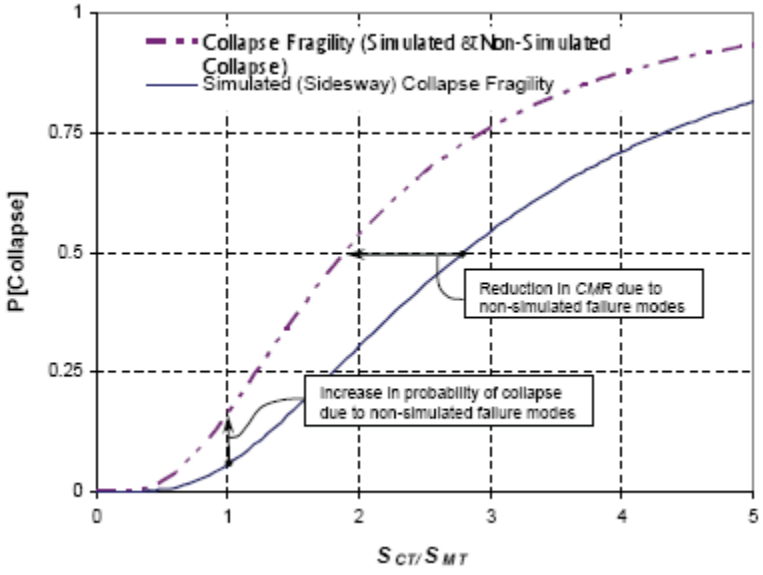

Figure 7.9: Collapse fragility curve from ATC-63 (2008) for the ATC-63 steel moment frame

In ATC-63 (2008), since β_{TD} , β_{MDL} and β_{TOT} are reported as 0.3, 0.3 and 0.6 respectively, it can be deduced that the uncertainty related to design requirements was rated as "superior" and the corresponding β_{DR} is 0.2. ATC-63 (2008) does not explicitly state the *ACMR* obtained considering only sidesway collapse mechanism (that is, without

considering non-simulated collapse modes). However, it does give the corresponding *CMR* as 2.5, and the *SSF* as 1.43. From these, the ACMR obtained in ATC-63 (2008) considering only sidesway collapse mechanism can be computed as 3.6. Table 7-8 provides a summary of the uncertainty and collapse fragility curve parameters obtained in this dissertation and ATC-63 (2008).

Table 7-8: Comparison of uncertainty and collapse fragility curve parameters obtained in this dissertation and in ATC-63 (2008)

Parameter	Value from this dissertation	Value from ATC-63 (2008)
Uncertainty parameters		
Record-record uncertainty	$\beta_{RTR} = 0.4$	$\beta_{RTR} = 0.4$
Design requirements uncertainty	Good ($\beta_{DR} = 0.3$)	Superior ($\beta_{DR} = 0.2$)
Test Data uncertainty	Good ($\beta_{TD} = 0.3$)	Good ($\beta_{TD} = 0.3$)
Modeling uncertainty	Fair ($\beta_{MDL} = 0.45$)	Good ($\beta_{MDL} = 0.3$)
Total system uncertainty	$\beta_{TOT} = 0.75$	$\beta_{TOT} = 0.6$
Collapse margin ratio		
CMR	2.2	2.5
ACMR	3.1	3.6
Probability of Collapse at MCE		
With *CMR* and considering only record-to-record variability ($\beta_{RTR} = 0.4$)	2.4%	1.1%
With *CMR* and considering all uncertainties (β_{TOT})	15%	6.3%
With *ACMR* and considering all uncertainties (β_{TOT})	6.6%	1.7%

7.4.9 Validity of trial response reduction factor

Since the probability of collapse at MCE of the ATC-63 steel moment frame is obtained as less than 10%, the frame meets the performance criteria (Section 3.7.5) prescribed by the ATC-63 methodology. This indicates the validity of the trial value of 8 used for the response reduction factor, *R*, in the design of this frame.

7.4.10 Comments on effect of *SSF*

The *CMR* obtained in this dissertation (2.2) was lower than that reported in ATC-63 (2008) (2.5), and the uncertainties in estimating collapse were more critically evaluated in this dissertation. Nevertheless, for the trial value of *R* assumed for design (Section 7.2), the ATC-63 steel moment frame still meets the performance criteria prescribed by the ATC-63 methodology. This is because of the effect of the *SSF*, which makes the *ACMR* greater than the *CMR*. From Table 7-1 of ATC-63 (2008) it can be said that the magnification of the *CMR* by the *SSF* is greater for a system with greater ductility and period. Therefore, the final result (pass/fail) from application of the ATC-63 methodology is less sensitive to variations in modeling and performance-evaluation parameters for systems with high ductility or long periods, than for systems with low ductility or short periods.

7.4.11 Comments on differences in results between this dissertation and ATC-63 (2008)

Previous sections address the differences in results obtained in this dissertation and those presented in ATC-63 (2008) from application of the ATC-63 methodology to the ATC-63 steel moment frame. Some differences exist because of the way in which the ATC-63 methodology has been developed. Because supporting studies (such as Lignos 2007) were conducted concurrently with the development of ATC-63 methodology, model parameters currently reported in ATC-63 (2008) may not be same as those used when the ATC-63 steel moment frame was studied by the ATC-63 team. Because a complete evaluation of even a single archetype using the methodology takes much time

and effort, it is not feasible to repeat the evaluation to match every changing reference. Therefore, an exact agreement in results from evaluation of the ATC-63 steel moment frame between ATC-63 (2008) and this dissertation may not be possible. It is not necessary, however, provided that the trial value of R assumed for design of the frame meets the performance criteria prescribed by the ATC-63 methodology.

7.5 SUMMARY OF CHAPTER

In this chapter, the ATC-63 steel moment frame reported in Section 10.2 of ATC-63 (2008) has been re-evaluated using the ATC-63 methodology. Through this exercise, modeling of steel moment frames for collapse evaluation and the general aspects of the ATC-63 methodology have been well understood. Results obtained in this dissertation are compared with those reported in ATC-63 (2008) and found to be close enough so that the ATC-63 steel moment frame meets the performance criteria prescribed by the ATC-63 methodology for the trial value of response reduction factor (R) assumed for design. It is observed that an exact agreement is results may not be necessary as long as the overall conclusion from application of the methodology remains the same. With this experience, the ATC-63 methodology can be applied with confidence to evaluate seismic design factors of infilled ATC-63 steel moment frames.

CHAPTER 8
Development of archetypical infilled steel moment frames

8.1 INTRODUCTION AND SCOPE OF CHAPTER

In this chapter, archetypical infilled steel moment frames are developed for evaluation by the ATC-63 methodology. The ATC-63 steel moment frame, discussed in Chapter 7 and considered an archetypical steel moment frame, is infilled to obtain the archetypical infilled steel moment frames. The infill configurations used to develop archetypical infilled steel moment frames, introduced in Section 3.4.1, are the uniformly infilled configuration and the open ground story configuration. Infill cases for the archetypical infilled steel moment frames are selected based on preliminary pushover analysis of the ATC-63 steel moment frame with infills of varying strength.

8.2 STEEL MOMENT FRAME USED TO DEVELOP ARCHETYPICAL INFILLED STEEL MOMENT FRAMES

The ATC-63 steel moment frame discussed in Chapter 7 (Figure 7.1) is used to develop archetypical infilled steel moment frames for reasons outlined below:

- The ATC-63 steel moment frame was extensively evaluated in ATC-63 (2008), and in this sense is a known quantity. Further use of that frame here enhances the usefulness of this dissertation to other investigators.
- The ATC-63 steel moment frame is a reasonable choice for an archetypical steel moment frame, as acknowledged by Section 10.2 of ATC-63 (2008). Therefore, when ATC-63 steel moment frame is infilled with typical materials used as infills, it is reasonable to expect the resulting frame to be an archetypical infilled steel moment frame.

- The ATC-63 steel moment frame was evaluated in Chapter 7 as a bare frame, and was shown to meet the performance criteria of the ATC-63 methodology. Therefore, performance of the bare ATC-63 steel moment frame can be used as a benchmark to assess the effect of infills on the behavior and performance of the corresponding archetypical infilled steel moment frames.
- The ATC-63 steel moment frame has been evaluated using the ATC-63 methodology for seismic design category D_{max}, the highest seismic design category addressed by the methodology. This makes the ATC-63 steel moment frame especially useful, because evaluating a structural system for the highest seismic design category generally suffices to prove its applicability to lower seismic design categories. This previous work, combined with a similar evaluation (in the highest seismic design category) of the archetypical infilled steel moment frames developed in this chapter, can cover the performance of infilled steel moment frames in all seismic design categories addressed by the ATC-63 methodology.

8.3 APPROACH FOR SELECTION OF ARCHETYPICAL INFILLED STEEL MOMENT FRAMES

From initial results of pushover analysis of the ATC-63 steel moment frame with AAC infill in uniformly infilled and open ground story configurations, it was observed that the presence of AAC infills did not lead to story mechanisms in the frame. This is contrary to what has been observed for infilled frames in general, and is believed due to the relatively low in-plane strength of AAC infills compared to the collapse capacity of the bare frame. Based on this observation, pushover analysis is performed on the ATC-63 steel moment frame with infills of varying strength to study the effect of infill strength on frame behavior. Both uniformly infilled frames and open ground story frames are considered. The same lateral load profile used for pushover analysis of the bare ATC-63 steel moment frame (Section 7.4.2) is also used for pushover analysis of the AAC-infilled frames. Results and conclusions from these pushover analyses are presented in this

section, and form the basis for selection of the infill cases to be used with the ATC-63 steel moment frame for development of archetypical infilled steel moment frames.

In general, results from pushover analysis may not represent actual structural response during ground motions, even when performed with an appropriate lateral load profile. This is especially true of the pushover analysis performed in this section for infilled frames, because the lateral load profile used is the one selected for the bare frame. Infilled frames have a shorter fundamental period and different characteristic deflected shapes than the original bare frame, and hence require a different lateral load profile for pushover analysis. While IDA can capture behavior more reliably, it requires much greater time and effort than pushover analysis. To avoid spending time unnecessarily, archetypical infilled steel moment frames for ATC-63 evaluation have to be carefully selected. Pushover analysis is vital to this selection, because it provides rapid information about the general behavior of infilled frames.

8.3.1 Pushover analysis of uniformly infilled frames with varying infill strengths

The ATC-63 steel moment frame is uniformly infilled and subjected to pushover analysis. The strength of the infill panels is varied to study the effect of that variation on frame behavior. The analytical model of the uniformly infilled ATC-63 steel moment frame is shown in Figure 8.1, and the model is developed using the procedures discussed in Chapter 6. The infill cases considered for the pushover analysis are presented in Table 8-1. Infills are placed in all four bays of the ATC-63 steel moment frame, except for Infill Case 1, in which only the central two bays are infilled. Infill Cases 1 and 2 are considered to involve Class 4 AAC masonry units with nominal dimensions of 8 x 8 x 24 in. The hysteretic force-deformation behavior of the AAC infill is taken as that presented in Section 6.4.2 (Figure 6.11) for the AAC infill of the infilled-frame specimen, except that the stiffness of the AAC infill and the strain in the equivalent strut at peak strength of the AAC infill are re-computed in the context of the ATC-63 steel moment frame. For other infill cases, the backbone curve of the Ibarra-Krawinkler hysteretic force-deformation model is obtained by proportionately increasing the assumed strength and stiffness of the

AAC infill by an appropriate factor. For each infill case, in Table 8-1 are summarized the shear strength of an infill panel and the total shear strength of infills in each story.

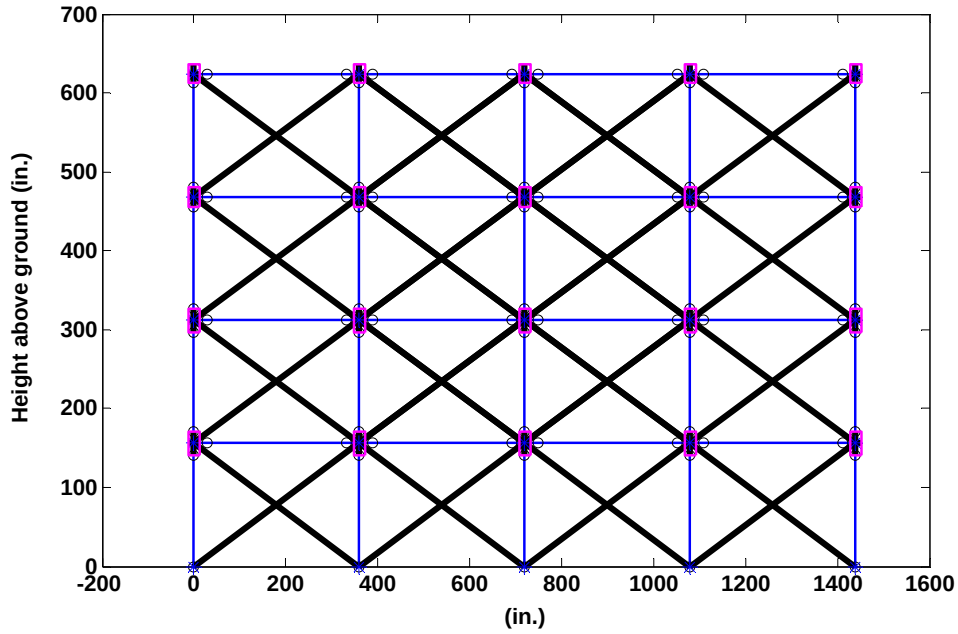

Figure 8.1: Analytical model of ATC-63 uniformly infilled steel moment frame with infill in all bays

Table 8-1: Horizontal shear strengths of infills for different infill cases

Infill Case	Strength of infill panel (kip)	Ratio of infill panel strength compared to strength of AAC infill	Total shear strength of infills in each story (kip)
1	97.4	1	194.8
2	97.4	1	389.6
3	194.8	2	779.2
4	292.2	3	1168.8
5	389.6	4	1558.4
6	487.0	5	1948.0
7	584.4	6	2337.6
8	779.2	8	3116.8
9	974.0	10	3896.0

In Figure 8.2 are presented the pushover curves (base shear versus roof drift ratio) for the bare frame and for the uniformly infilled frames with different infill cases. In Figure 7.3 is presented the ultimate roof drift ratio, Δ_u, reached by the bare frame during the pushover analysis as determined by the ATC-63 methodology (Section 3.6.2). In Figure 8.3, the displacement profiles of the bare frame and the uniformly infilled frames are compared at the ultimate roof drift ratio of the bare frame determined from pushover analysis (Section 7.4.2). In the legend of these figures, alongside the label identifying the infill case, also presented is a quantity called “infill strength ratio,” to be defined shortly.

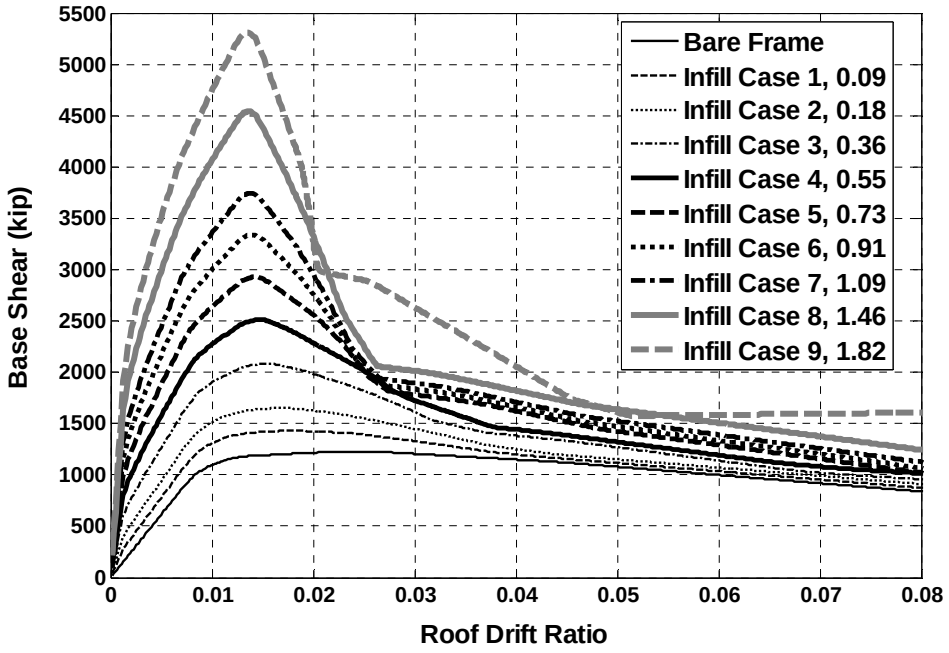

Figure 8.2: Pushover curves for uniformly infilled frames

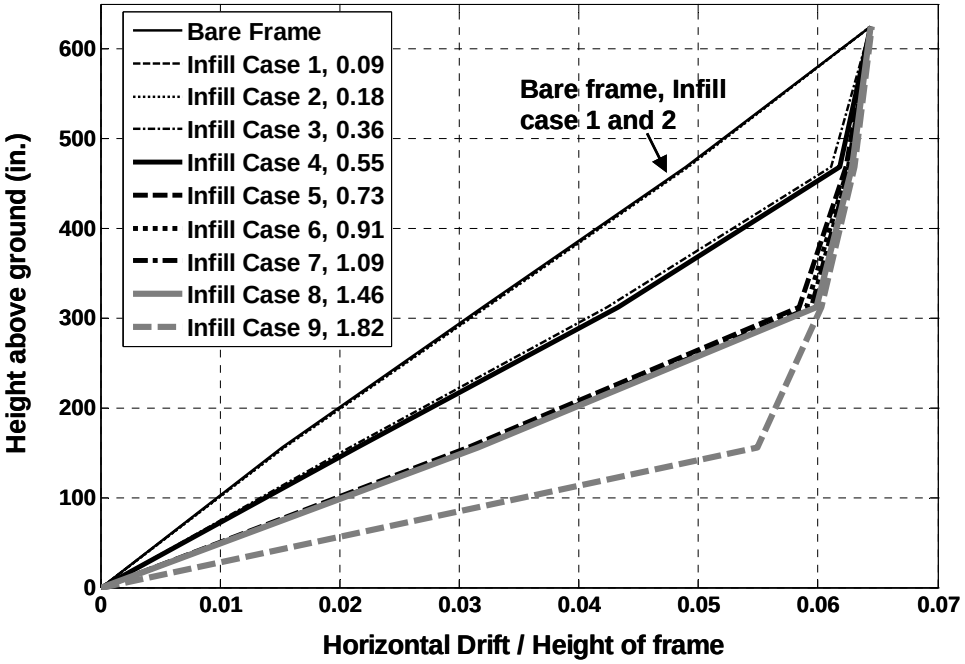

Figure 8.3: Displaced profile of uniformly infilled frames compared at ultimate roof displacement of bare frame

As shown in Figure 8.3 the displacement profile of the bare frame is a straight line, denoting a collapse mechanism characterized by formation of a plastic hinges in beams at each story level and in columns at the base of the frame. In contrast, the displacement profiles for many of the uniformly infilled frames show a "kink," denoting the formation of hinges in the columns of the frame at that level, and concentrating the failure mechanism of the frame below the level of the kink. As the lateral in-plane strength of the infill increases, the story level at which columns hinge drops, eventually reaching the first elevated floor. At that point, hinges form both at the top and bottom of the ground story, leading to a concentration of the failure mechanism there. This is commonly referred to as a weak ground story mechanism.

8.3.2 Pushover analysis of open ground story frame with varying infill strengths

After observing the results from pushover analyses of uniformly infilled frames, it was of interest to see if results would be similar for open ground story frames. The pushover analysis is repeated for the ATC-63 steel moment frame with an open ground story for the same infill cases presented in Table 8-1. The analytical model of the ATC-63 steel moment frame with an open ground story is depicted in Figure 8.4.

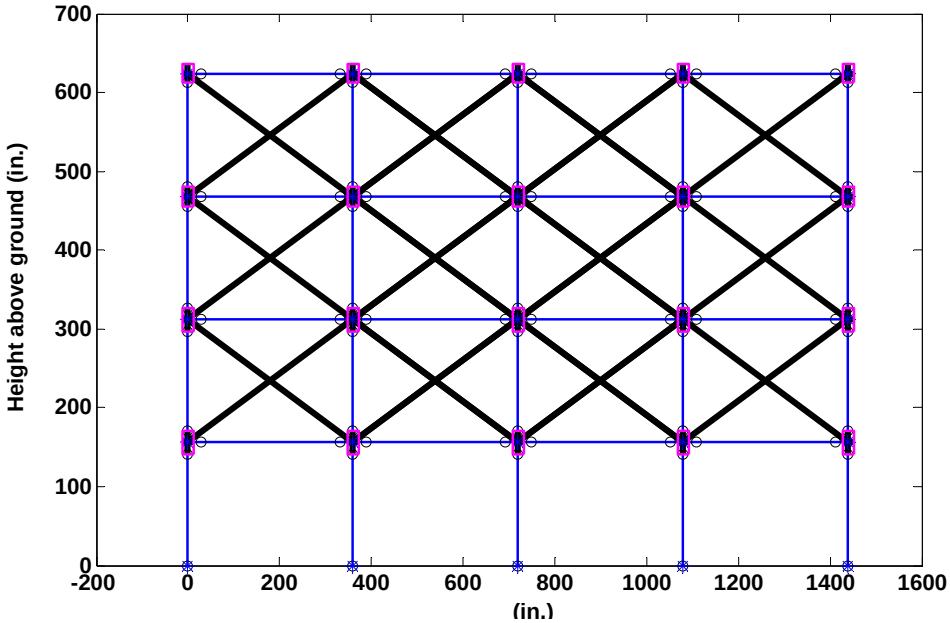

Figure 8.4: Analytical model of open ground story frame

In Figure 8.5 are presented pushover curves for the bare frame and for open ground story frames. As for uniformly infilled frames, Figure 8.6 is a comparison of the displacement profiles for the bare frame and for the open ground story frames at the ultimate roof drift ratio of the bare frame. For the open ground story frames, the effect of increasing strength of infills is similar to that for the uniformly infilled frames, except that the formation of hinges in columns progresses faster towards the ground story reaching it at Infill Case 7 (rather than Infill Case 9 for the uniformly infilled frames).

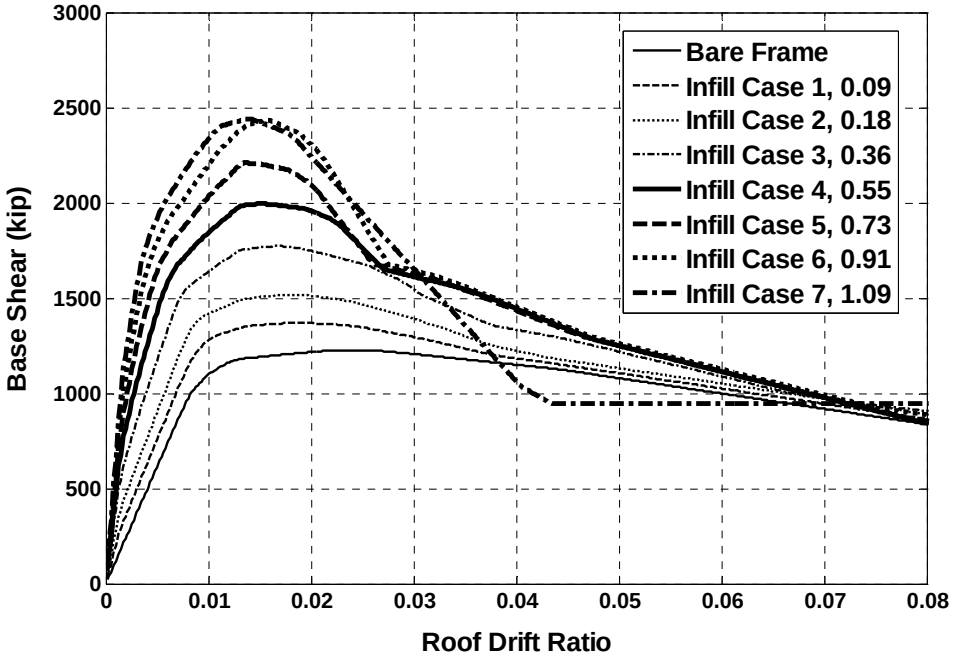

Figure 8.5: Pushover curves for open ground story frames

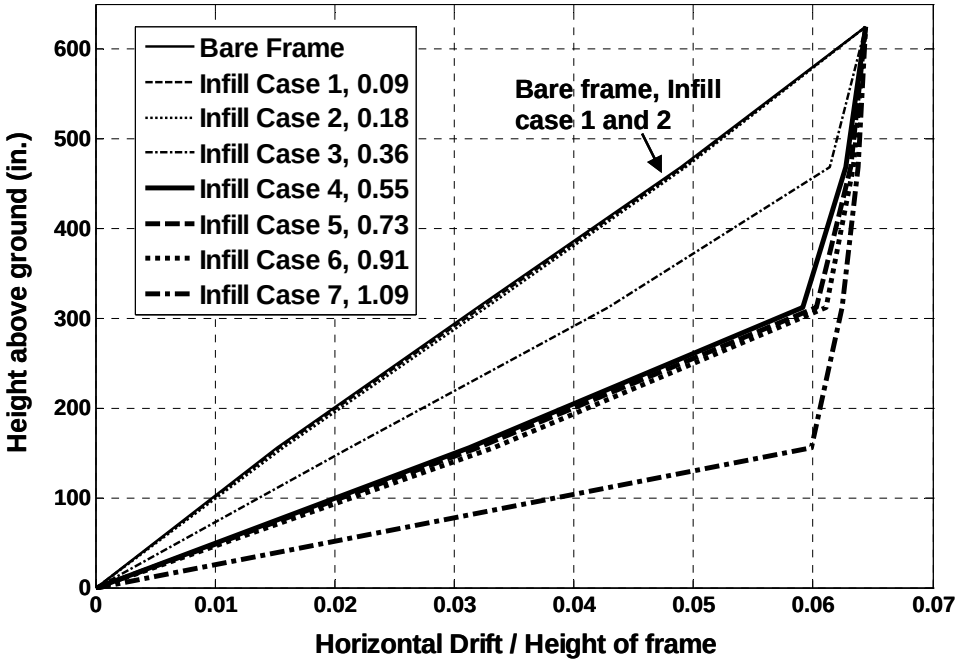

Figure 8.6: Displaced profile of open ground story frames compared at the ultimate roof displacement of bare frame

8.3.3 Relationship between infill strength and frame failure mechanism

Results of the foregoing pushover analyses for the ATC-63 steel moment frame with uniform AAC infills and open ground story infills indicate that the failure mechanism of the infilled frame depends in general on the ratio of the story shear strength of the infills to the story shear strength of the bare frame. In this dissertation, this ratio is termed the "infill strength ratio." It is shown later to have fundamental importance for the seismic behavior of infilled frames.

The story shear strength of the bare frame is computed using Equation 8-1, considering a story mechanism that leads to hinges at the top and bottom of columns at that story (Figure 8.7). If axial loads in columns are significant, then their effect on plastic moment capacity of column sections should be considered.

$$F_{story\ mechanism} = \frac{\sum M_p}{h} \qquad \textbf{\textit{Equation 8-1}}$$

where,

$F_{story\ mechanism}$ = shear strength of the story under consideration

M_p = plastic moment capacity of columns at the story under consideration

h = height of the story under consideration

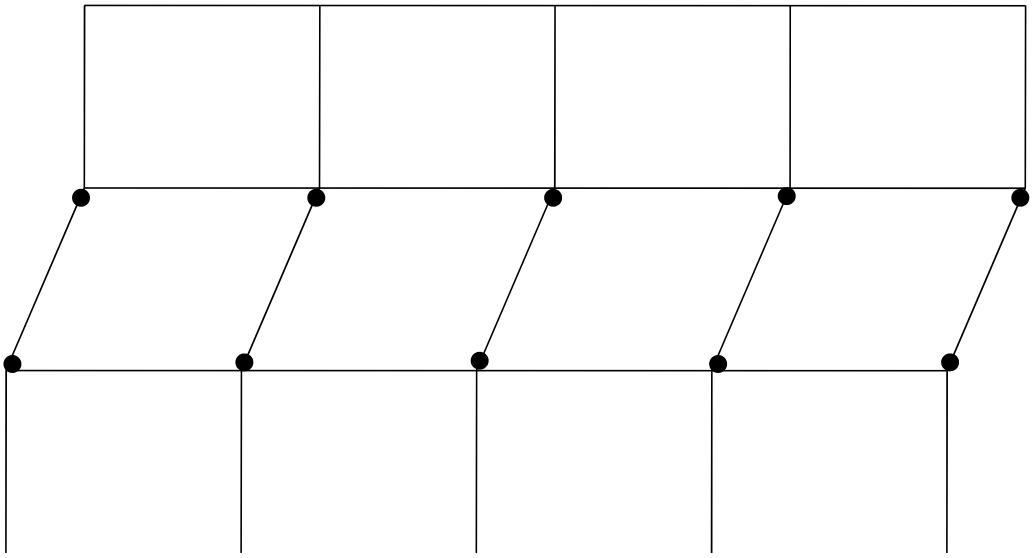

Figure 8.7: Story mechanism used to calculate story shear strength of bare frame

As shown in Figure 7.1, the ATC-63 steel moment frame is designed using two tiers of column sizes, W24x207 at the first and second stories and W24x162 at the third and fourth stories. In Table 8-2 are presented the plastic moment capacities of these W-sections computed using expected yield strength of steel (55 ksi) and the corresponding story shear strength of the bare frame computed using Equation 8-1. The axial load in the columns of the ATC-63 steel moment is not significant, and its effect is ignored in computing the plastic moment capacity of the column sections.

Table 8-2: Plastic moment capacity of columns and story shear strength of bare ATC-63 steel moment frame

Story	Column W-section	Column section plastic moment capacity (kip-in.)	Story shear strength (kip)
1, 2	W24x207	33330	2137
3, 4	W24x162	25740	1650

In Table 8-3 are presented the infill strength ratios for each infill case of Table 8-1. Those ratios are also indicated in Figure 8.2, Figure 8.3, Figure 8.5 and Figure 8.6.

Table 8-3: Infill strength ratios for infill cases of Table 8-1

Infill case	Infill strength ratio	
	Story 1, 2	Story 3, 4
1	0.09	0.12
2	0.18	0.24
3	0.36	0.47
4	0.55	0.71
5	0.73	0.94
6	0.91	1.18
7	1.09	1.42
8	1.46	1.89
9	1.82	2.36

Referring to Figure 8.3 and Table 8-3, the following statements can be made for the uniformly infilled ATC-63 steel moment frame:

1) If the infill strength ratio is less than about 0.35, the presence of infills does not change the failure mechanism, which involves hinging in beams and at column bases.
2) When the infill strength ratio reaches about 0.35 (Infill Case 3), the presence of the infill begins to change the failure mechanism of the frame, from hinging in beams and at column bases, to story mechanisms involving column hinging at multiple levels of the lower stories.
3) When the infill strength ratio reaches about 1 (Infill Case 6), infills significantly change the failure mechanism of the frame, concentrating it in the bottom half of the frame.

4) When infill strength ratio reaches about 2 (Infill Case 9), infills consistently lead to ground story mechanisms.

For the open ground story frame, referring to Figure 8.5 and Figure 8.6, the following statements can be made:

1) If the infill strength ratio is less than about 0.35 (Infill Case 3), the presence of infills does not change the failure mechanism, which involves hinging in beams and at column bases.
2) If the infill strength ratio is between 0.35 and 1, the failure mechanism becomes progressively concentrated in the lower stories.
3) If the infill strength ratio reaches about 1 (Infill Case 7), infills consistently lead to ground story mechanisms.

8.4 SELECTION OF INFILL CASES FOR ATC-63 EVALUATION

Based on observations from the pushover analyses of the previous section, the infill cases to be used with the ATC-63 steel moment frame for evaluation by the ATC-63 methodology are selected to represent a broad range of infill strength ratios. Accordingly, three infill cases are selected: the first, with an infill strength ratio below 0.35, the second, with a ratio of about 0.5; and the third, with a ratio of about 1. For the first case, AAC infilling is a natural choice because of its low strength. In particular, the first case can be represented by an infill made of 8-in. thick Class 4 AAC units. For the second and third cases, conventional masonry is a more natural choice because of its higher strength. In particular, the second and third cases can be represented by conventional (clay) masonry with specified compressive strengths of 4 ksi and thicknesses of 8 and 12 in., respectively. These are summarized in Table 8-4. The conventional masonry cases also correspond to specific thicknesses of concrete masonry. This is discussed later in this dissertation. For now, to reduce confusion, the conventional masonry cases are associated with physical thickness of clay masonry only.

Table 8-4: Infill cases considered for ATC-63 evaluation

Infill case	Infill Material	Thickness of infill (in.)	Specified compressive strength (psi)
1	AAC, Class 4	8	580
2	Conventional masonry (clay)	8	4000
3	Conventional masonry (clay)	12	4000

8.4.1.1 Properties of AAC infill for ATC-63 evaluation

For ATC-63 evaluation of archetypical AAC-infilled steel moment frames, the hysteretic force-deformation behavior of the 8-in. thick Class 4 AAC infill is modeled as described in Section 6.4.2. Related calculations to determine the backbone curve of the Ibarra-Krawinkler hysteretic model for the AAC infill are presented in the Appendix.

Based on the preliminary observation that behavior of the frame and its failure mechanism deteriorate with increasing infill strength, the strength of the AAC infill for this evaluation is conservatively taken as the maximum shear strength obtained from the AAC infill in the infilled frame specimen whose testing is described in Chapter 4. That specimen also had 8-in. thick Class 4 AAC infill, and its lateral strength was 97.4 kip. That same value is therefore taken as the lateral strength of AAC infills for this ATC-63 evaluation of archetypical AAC-infilled steel moment frames.

The resulting total horizontal shear strength of the four AAC infills in each story of the ATC-63 steel moment frame is 390 kip. Corresponding to this infill shear strength and the shear strength of the bare frame presented in Table 8-2, the infill strength ratio of the ATC-63 steel moment frame is computed as 0.18 and 0.24 at the bottom and upper column tiers, respectively.

8.4.1.2 Properties of conventional masonry infill for ATC-63 evaluation

Conventional masonry proposed to be used for ATC-63 evaluation of archetypical conventional masonry infilled steel moment frames has a specified strength, f_m', of 4 ksi. By Table 1 of MSJC 2008a, this can be achieved using Type S mortar and clay masonry units with a tested strength of 11.5 ksi. The corresponding actual strength of masonry, f_m, is assumed as 6 ksi.

The hysteretic force-deformation behavior of conventional masonry infills is modeled as described in Section 6.4.3. Related calculations to determine the backbone curve of the Ibarra-Krawinkler hysteretic model for 8-in. and 12-in. conventional masonry infills are presented in the Appendix.

For the 8-in. conventional masonry infill, the shear strength of each infill panel is computed to be 362 kip. The total shear strength of 4 infill panels at a story of the ATC-63 steel moment frame is equal to 4 times this value of 362 kips, or 1448 kips. For this shear strength of the AAC infill and the story shear strength of the bare frame presented in Table 8-2, the infill strength ratio is computed to be 0.68 and 0.88 at the bottom and upper stories, respectively, of the ATC-63 steel moment frame.

For the 12-in. conventional masonry infill, the lateral shear strength of each infill panel is computed to be 543 kip. The total shear strength of 4 infill panels at a story of the ATC-63 steel moment frame is 2172 kips. This corresponds to an infill strength ratio of 1.01 and 1.30 at the bottom and upper stories, respectively, of the ATC-63 steel moment frame.

8.4.1.3 Summary of infill cases for ATC-63 evaluation

Table 8-5 provides a summary of the infill cases considered for ATC-63 evaluation and the corresponding infill strength ratios at the bottom stories of the ATC-63 steel moment frame. The infill cases provide a broad range of infill strength ratios whose effect on the performance of the ATC-63 steel moment frame can be comprehensively evaluated.

Table 8-5: Infill strength ratio for different infill cases at the bottom story of the steel moment frame

Infill case	Infill type	Infill thickness (in.)	Infill strength ratio
1	AAC, Class 4	8	0.18
2	Conventional masonry	8	0.68
3	Conventional masonry	12	1.01

8.5 ARCHETYPICAL INFILLED STEEL MOMENT FRAMES FOR ATC-63 EVALUATION

Starting with the ATC-63 steel moment frame, and infilling all bays with the infill cases presented in Table 8-5, results in three archetypical infilled steel moment frames for the uniformly infilled configuration, and three more for the open ground story configuration. This total of 6 archetypical infilled steel moment frames is summarized in Table 8-6, along with the terminology used to describe each of these infilled frames in the rest of this dissertation.

Table 8-6: Archetypical infilled steel moment frames

Infill material	Infill Configuration	
	Uniformly infilled frames	**Open ground story frames**
8-in. thick Class 4 AAC	AAC uniformly infilled frame	AAC open ground story frame
8-in. thick conventional masonry	8-in. thick conventional masonry uniformly infilled frame	8-in. thick conventional masonry open ground story frame
12-in. thick conventional masonry	12-in. thick conventional masonry uniformly infilled frame	12-in. thick conventional masonry open ground story frame

8.5.1 Trial seismic design factors

Based on the previous observation that for lower ratios of infill strength to frame strength the original mechanism of the bare frame was not altered, it was decided to use the same trial seismic design factors for the infilled frames, as are currently mandated by ASCE7-05 for the bare frame (Section 7.2). This is an important assumption, and its validity will later be re-visited.

8.6 SUMMARY OF CHAPTER

In this chapter, archetypical infilled steel moment frames are developed for evaluation by the ATC-63 methodology, by infilling the bare ATC-63 steel moment frame presented in Chapter 7. A preliminary pushover analysis of the ATC-63 steel moment frame with varying infill strengths revealed that the ratio of story shear strength of infills to the story shear strength of bare frame is an important parameter affecting the behavior of infilled frames. This ratio is defined as the "infill strength ratio" in this dissertation. In general, it is observed that increasing infill strength ratio progressively deteriorates the performance of the frame, leading to story mechanisms that concentrate the failure mechanism of the frame in only a few stories near the ground.

Based on this observation, three infill cases are selected to develop archetypical infilled steel moment frames, representing a broad range of infill strength ratios: 8-in. thick Class 4 AAC; 8-in. thick conventional masonry; and 12-in. thick conventional masonry. These selected infill cases are used with the ATC-63 steel moment frame to develop three archetypical infilled steel moment frames for the uniformly infilled configuration, and three more for the open ground story configuration. Later in this dissertation, these archetypical infilled steel moment frames are evaluated using the ATC-63 methodology, and seismic design factors are determined for infilled steel moment frames.

CHAPTER 9
IDA for infilled frames

9.1 INTRODUCTION TO CHAPTER

In this chapter, procedures for IDA are specialized for application to infilled steel moment frames. Local shear failures in structural members of a frame due to frame-infill interaction forces are considered as non-simulated collapse modes, and rules are formulated for identifying those non-simulated collapse modes during IDA.

9.2 FUNDAMENTAL PERIOD USED FOR DETERMINING INTENSITY OF GROUND MOTIONS

In Section 3.6.3, procedures were introduced for performing IDA of archetypical structures. A fundamental feature of IDA is scaling of ground-motion intensities, determined as the spectral intensity at the fundamental period of the archetypical structure (as prescribed by ASCE7-05), until the ground motions cause collapse of the archetypical structure.

The bare ATC-63 steel moment frame and the archetypical infilled steel moment frames have different fundamental periods, however, due to their different stiffnesses. If ground motion intensities are scaled at the respective fundamental periods of the bare ATC-63 steel moment frame and archetypical infilled steel moment frames, the IDA plots and intermediate results cannot be directly compared. Therefore, in this dissertation, for all archetypical infilled steel moment frames, ground motion intensity during IDA is scaled at the fundamental period of the bare ATC-63 steel moment frame. This makes the IDA results comparable for both archetypes. If required, a spectral intensity determined at the fundamental period of the ATC-63 steel moment frame can readily be converted to the spectral intensity at the fundamental period of the corresponding archetypical infilled steel moment frame.

9.3 NON-SIMULATED COLLAPSE MODES IN INFILLED FRAMES

When the infill acts as a diagonal strut, it causes local shear forces in frame members (Figure 2.8), which add to the shear forces due to frame action. If the combined shears exceed the shear capacity, the frame member can fail locally in shear. This possibility could not be directly considered in the analysis, for the following two reasons:

1) Failure due to shear is not included in the analytical model used for frame members (Section 6.3); and
2) Equivalent struts representing infills connect to the center of beam-column joints, and transfer their axial forces as point loads to the frame (Figure 6.6). Therefore, interaction forces between the infill and the frame members (Figure 2.8) could not be considered in the analytical model.

Using data from the IDA, however, and as explained in Section 3.6.4, the ATC-63 methodology can address local shear failures in frame members as non-simulated collapse modes. The remainder of this section explains how this was done for infilled frames in this dissertation.

For the archetypical infilled steel moment frames, axial forces in equivalent struts representing infills were monitored during IDA. Actually, at any particular story, the forces in equivalent struts are similar (Figure 9.1), and hence it was sufficient to monitor the axial forces in the equivalent struts of only one central bay. Because the shears in the interior columns of a particular story are nearly identical, and because the shear in the interior columns always exceeded the shear in the exterior columns, only the shear in Column Line 3 of Figure 9.1 was monitored. Because the shears in beams of interior bays at a particular story were nearly identical, beam shear was monitored in only one of the interior bays. Because the shears in beams of exterior bays at a particular story were nearly identical, beam shear was monitored in only one of the exterior bays.

At each instant of the IDA, the appropriate component of the axial force in the equivalent struts is added to shear force in frame members due to frame action alone, as

shown in Figure 2.8. This gives the total shear force in frame members due to frame action plus frame-infill interaction forces.

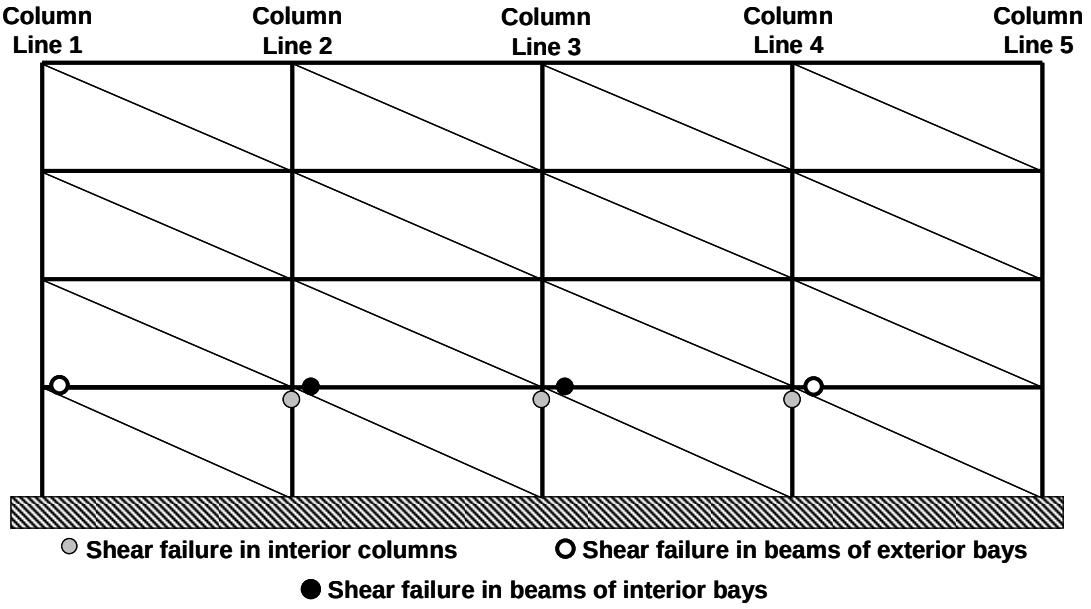

Figure 9.1: Non-simulated collapse modes in infilled frames: simultaneous shear failures in frame members

At any particular story, because the forces in the equivalent struts and shear forces in interior columns are nearly uniform, a shear failure in Column Line 3 is considered to indicate a shear failure in Column Line 2 and Column Line 4 as well. Similarly, a shear failure in the beam of one of the interior bays is considered to be shear failure in beams of all interior bays, and a shear failure in the beam of one of the exterior bays is considered to be shear failure in beams of all exterior bays (Figure 9.1). Shear failure in such a large number of structural members can significantly impair the stability of the structure and can effectively be treated as the failure of the structure itself.

During IDA, however, local shear failures due to frame-infill interaction forces may not occur at all spectral intensities for a particular ground motion. In the IDA of this dissertation, if local shear failure is detected at more than one spectral intensity for a particular ground motion, then non-simulated collapse is considered to occur at the

second (higher) of these spectral intensities. This is illustrated in Figure 9.2, in which the solid dots indicate spectral intensities causing non-simulated collapse. Ground Motion 1, which causes local shear failure at more than one collapse spectral intensity during IDA, is considered to cause non-simulated collapse at the spectral intensity corresponding to the second blue dot. Ground Motion 2, which causes local shear failure at only one spectral intensity during IDA, is not considered to cause non-simulated collapse.

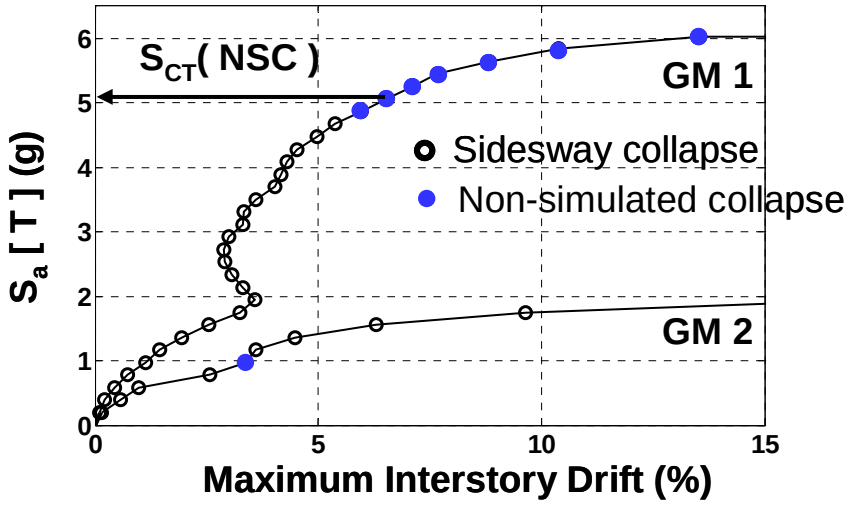

Figure 9.2: Rule for determination of non-simulated collapse of archetypical infilled steel moment frames due to local shear failure in structural members during IDA

9.4 SUMMARY OF CHAPTER

In this chapter, procedures for IDA are specialized for application to infilled frames. To make results for infilled frames comparable to those of the corresponding bare frame, ground motion intensity for all archetypical infilled steel moment frames is scaled at the fundamental period of the ATC-63 steel moment frame. Local shear failures in frame members due to frame-infill interaction forces are considered as non-simulated collapse. If local shear failure is detected at more than one spectral intensity for a particular ground motion during IDA, non-simulated collapse is considered to occur under that ground motion, at the second (higher) spectral intensity causing local shear failure.

CHAPTER 10
ATC-63 evaluation of archetypical infilled steel moment frames

10.1 INTRODUCTION AND SCOPE OF CHAPTER

In this chapter, the archetypical infilled steel moment frames developed in Chapter 8 are analyzed and evaluated using the ATC-63 methodology described in Sections 3.6 and 3.7. First, the AAC uniformly infilled frame is evaluated, because the research project associated with this dissertation primarily focuses on AAC-infilled steel moment frames. Then the archetypical frames, uniformly infilled with conventional masonry, are evaluated. Finally, the archetypical infilled frames with an open ground story are evaluated. Results from these evaluations are presented, and are later used to propose seismic design factors and design guidelines for infilled steel moment frames. In this and later chapters, and particularly in figures, the ATC-63 steel moment frame is sometimes referred to simply as the "bare frame."

10.2 ATC-63 EVALUATION OF ATC-63 MOMENT FRAME, UNIFORMLY INFILLED WITH AAC MASONRY

In this section, the ATC-63 moment frame, uniformly infilled with AAC masonry (Table 8-6), is evaluated using the ATC-63 methodology, and the results are presented.

10.2.1 Fundamental period of AAC uniformly infilled frame by ASCE7-05

The fundamental period of the AAC uniformly infilled frame is determined as described in Section 3.6.1, as the limiting period ($C_u T_a$) prescribed by Section 12.8.2 of ASCE7-05. While ASCE7-05 provides no recommendation regarding fundamental period, T_a, of infilled frames, its Section 12.8.2.1 does provide the following general recommendation for all moment frames:

> Alternatively, it is permitted to determine the approximate fundamental period (T_a) in sec from the following equation for structures not exceeding 12 stories in height in which the seismic force–resisting system consists entirely of concrete or steel moment resisting frames and the story height is at least 10 ft (3 m).
>
> $$T = 0.1\,N$$

For the AAC uniformly infilled frame, the primary and most significant lateral load-resisting system is the ATC-63 steel moment frame. As will be shown later, appropriately designed AAC infills do not affect the native behavior of steel moment frames under large earthquakes. They crush early during the response of the steel moment frame, after which the steel moment frame acts as the sole lateral load-resisting system while the AAC infills act as weak energy dissipators. Therefore, it is reasonable to use the above general recommendation, and the code-defined approximate fundamental period of the AAC uniformly infilled frame is computed as 0.4 sec. The coefficient for upper limit on the calculated period, C_u, is determined by Table 12.8-1 of ASCE 7-05 as 1.4, the same as for the ATC-63 steel moment frame (Section 7.4.1). Therefore, the limiting fundamental period of the AAC uniformly infilled frame by ASCE 7-05 is:

$$T = C_u\ T_a = 1.4 \times 0.4 = 0.56 \text{ sec}$$

This is close to the fundamental period of 0.52 sec obtained analytically for the AAC uniformly infilled frame.

10.2.2 MCE-level spectral demand of AAC uniformly infilled frame

In Figure 10.1, MCE-level spectral demands are compared for the ATC-63 steel moment frame and the AAC uniformly infilled frame, based on the SDC D_{max} response spectrum of the ATC-63 methodology. Due to its shorter fundamental period, the AAC uniformly infilled frame has an elastic spectral acceleration about 1.5 times that of the ATC-63 steel moment frame.

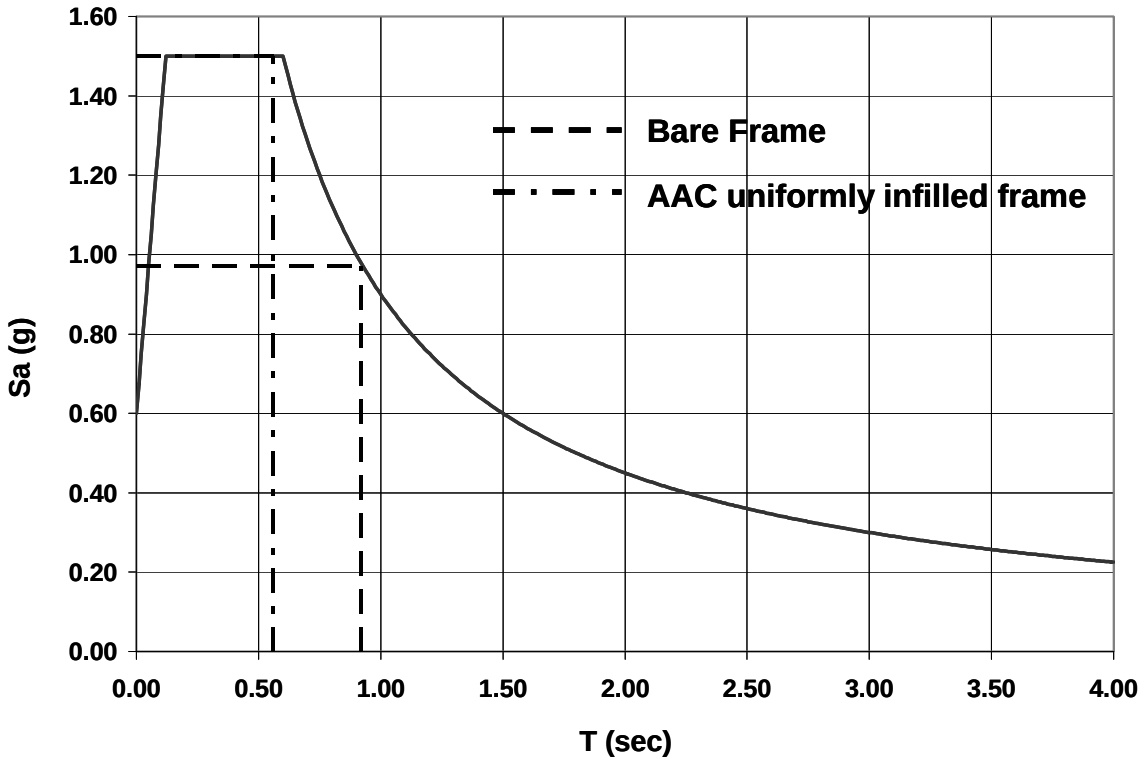

Figure 10.1: Spectral demands for ATC-63 steel moment frame and AAC uniformly infilled frame (SDC D_{max} response spectrum of ATC-63 methodology)

10.2.3 Pushover analysis

Pushover analysis was performed on the AAC uniformly infilled frame, and the results are compared with those previously obtained for the ATC-63 steel moment frame. So that the results of both analyses can be directly comparable, the same lateral load pattern is used for the AAC uniformly infilled frame as for the ATC-63 steel moment frame, and the two pushover curves are compared in Figure 10.2.

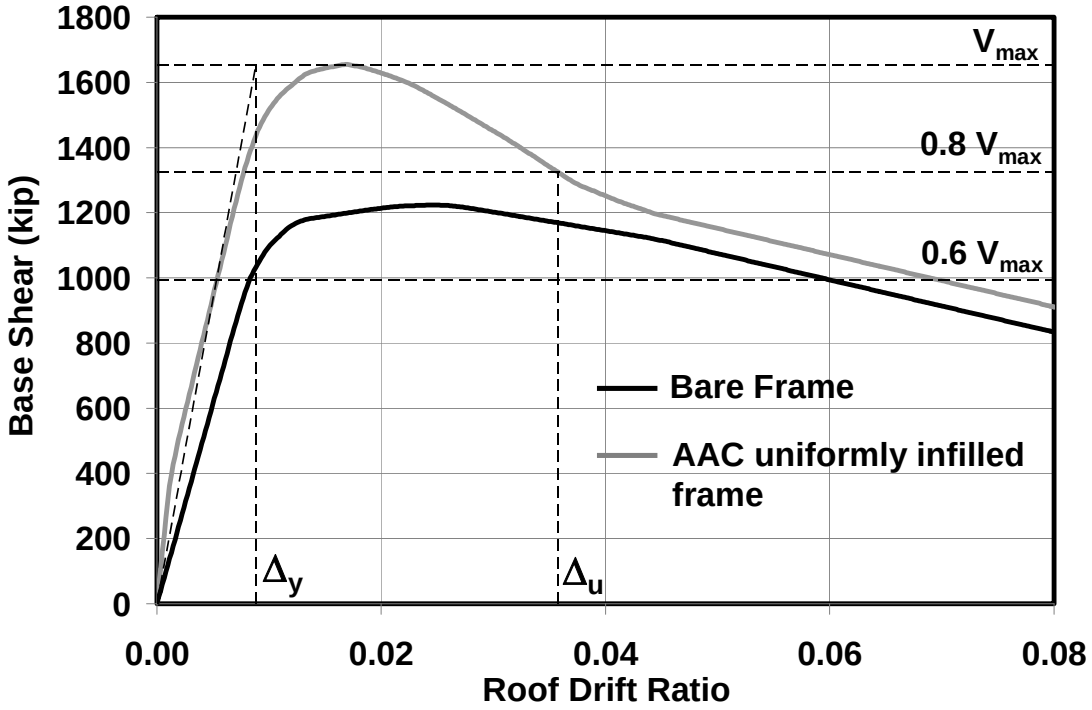

Figure 10.2: Base shear versus roof displacement from pushover analyses of ATC-63 steel moment frame and AAC uniformly infilled frame

10.2.3.1 Effect of AAC infills on initial stiffness

Referring to Figure 10.2, AAC infills increase the initial stiffness of the ATC-63 steel moment frame by a factor of 2.7. As shown in Section 10.2.1, due to this increased stiffness the AAC uniformly infilled frame experiences a spectral acceleration about 1.5 times greater than that of the ATC-63 steel moment frame during initial stages of its response. Due to the increase in initial stiffness, however, interstory drifts at low ground-motion intensities will probably still be less for the AAC uniformly infilled frame than for the ATC-63 steel moment frame.

10.2.3.2 Effect of uniform AAC infills on overstrength

As described in Section 7.2, the design base shear of the ATC-63 steel moment frame is 309.2 kip. From pushover analysis (Figure 10.2), the maximum base shear

capacity of the AAC uniformly infilled frame is 1655 kip, giving an overstrength factor (Ω) of 5.4. From pushover analysis, the ATC-63 steel moment frame had a maximum base shear capacity of 1225 kip, and a corresponding over-strength factor (Ω) of 4.0 (Section 7.4.2). The increase in base shear capacity from the bare frame to the AAC uniformly infilled frame (430 kips) is almost identical to the total shear strength of the AAC infills in each story (390 kips). This indicates that the presence of AAC infills does not change the failure mechanism of the ATC-63 steel moment frame for pushover analysis, and that the base shear strength of the bare ATC-63 steel moment frame is not reduced by the presence of the AAC infills.

10.2.3.3 Ductility of AAC uniformly infilled frame

The ductility of the AAC uniformly infilled frame is determined from the pushover analysis as described in Section 3.6.2. The displacements Δ_y and Δ_u are determined as shown in Figure 10.2, and the ductility factor is computed to be 4.1, lower than the ductility factor of 6.4 previously determined for the ATC-63 steel moment frame (Section 7.4.2).

10.2.3.4 Failure mechanism and displaced profile of AAC uniformly infilled frame

Plastic hinges formed in frame members in the AAC uniformly infilled frame at the same locations as in the ATC-63 steel moment frame (at the reduced beam sections at the ends of beams and at the bottom of ground story columns). As shown in Figure 10.3 and Figure 10.4, at every stage of the pushover analysis, the plastic hinge rotations were nearly the same as for the ATC-63 steel moment frame. In Figure 10.5, the pushover displacement profiles of the AAC uniformly infilled frame and the ATC-63 steel moment frame are compared at the ultimate roof displacement of the ATC-63 steel moment frame (Section 7.4.2). The displaced profile of the two structures remained nearly identical during all stages of the pushover analysis. This indicates that AAC infills can be proportioned so that they do not modify the native side-sway failure mechanism of steel moment frames.

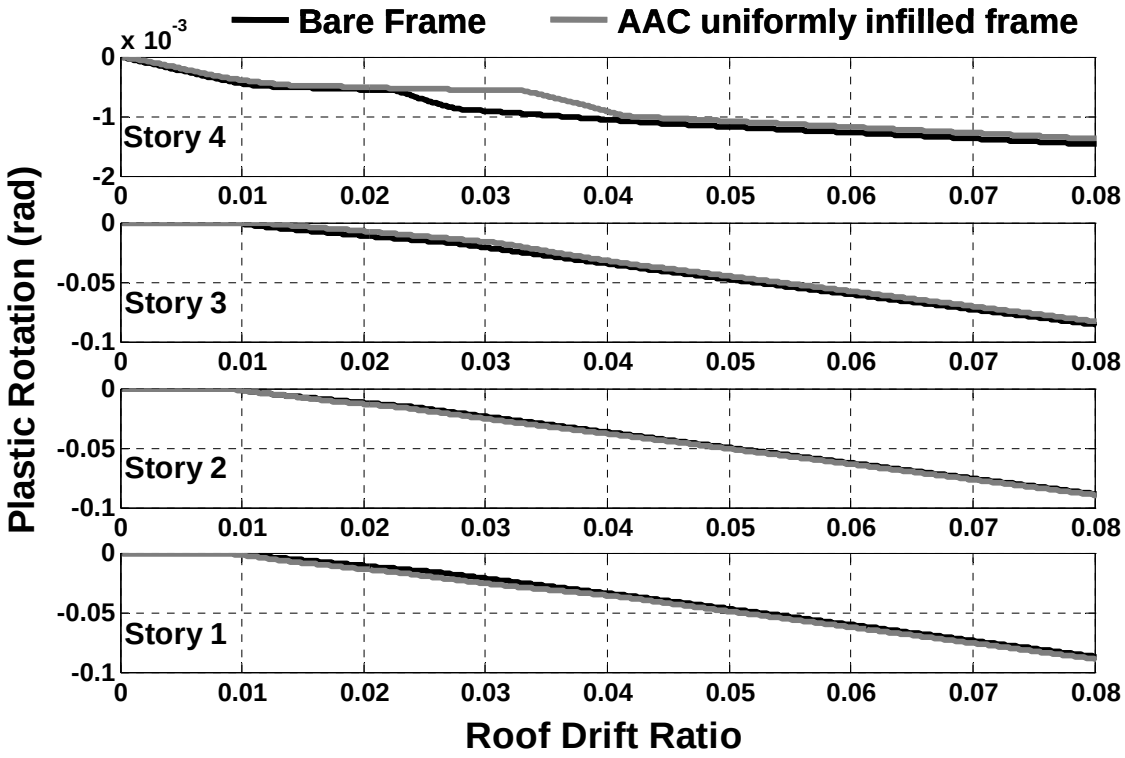

Figure 10.3: Plastic rotations in hinges at reduced beam sections during pushover analysis of ATC-63 steel moment frame and AAC uniformly infilled frame

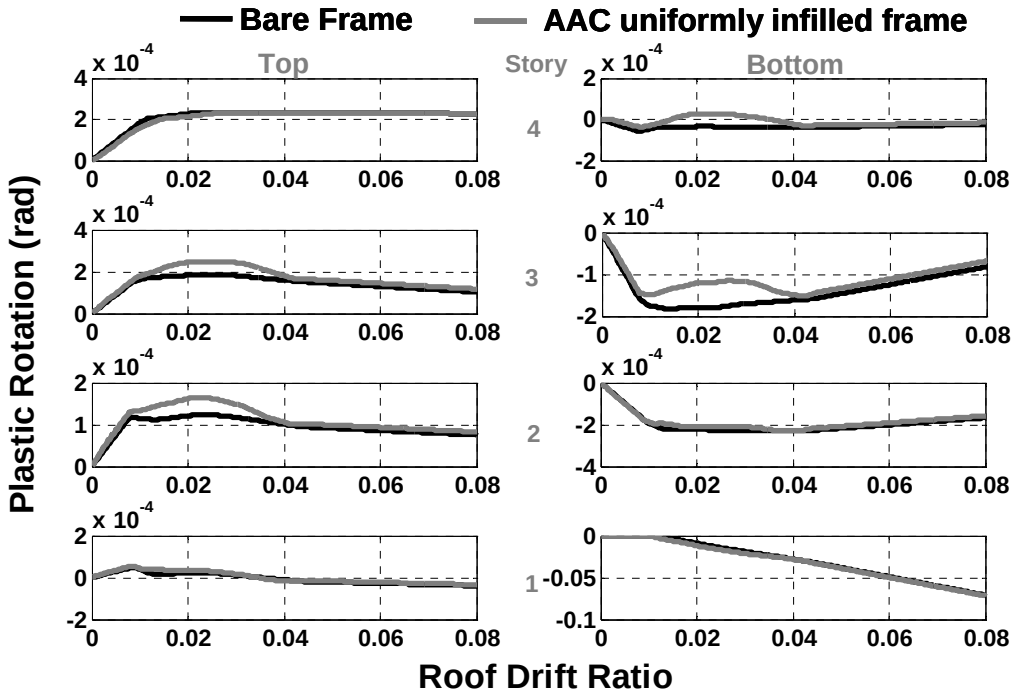

Figure 10.4: Plastic rotations at top and bottom of columns in each story during pushover analysis of ATC-63 steel moment frame and AAC uniformly infilled frame

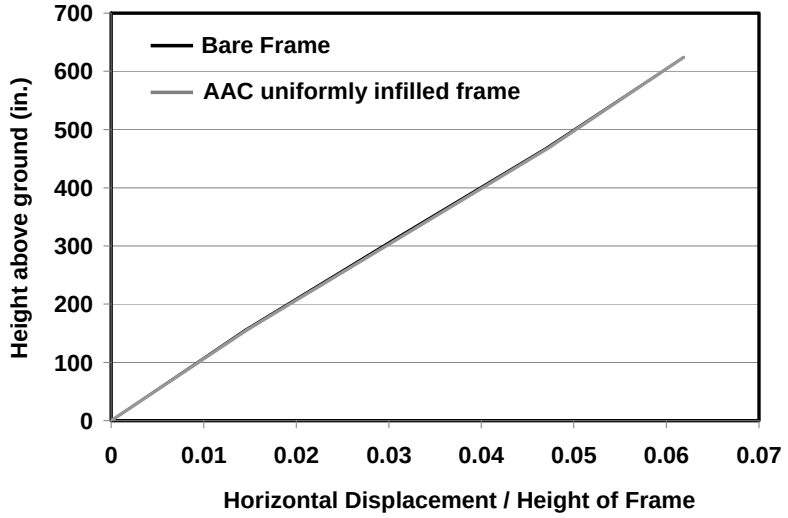

Figure 10.5: Displacement profiles of ATC-63 steel moment frame and AAC uniformly infilled frame at the ultimate roof drift of ATC-63 steel moment frame

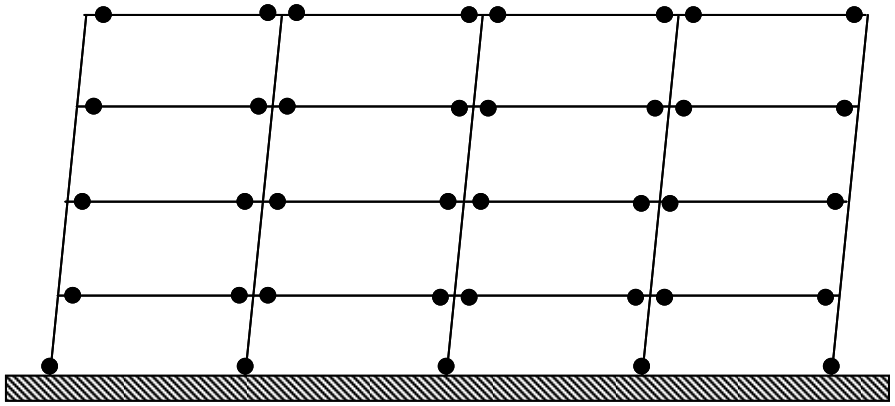

Figure 10.6: Failure mechanism of ATC-63 steel moment frame and AAC uniformly infilled frame

10.2.3.5 Axial forces in frame members of AAC uniformly infilled frame

Overturning moments produce tensions in the columns on one side of a building, and compressions on the other. As shown in Figure 10.7, these tensions and compressions are increased by the presence of infills. At each story, the increase in column axial force is equal to the vertical component of the force in the equivalent strut.

These increments in axial force cascade down each column line, increasing column axial forces from top to bottom of the building. Near the ground story, these increases can be significant and detrimental, because the flexural capacity and curvature ductility of a steel column decrease with increasing axial force (tensile or compressive). It may be necessary to address them in the design process.

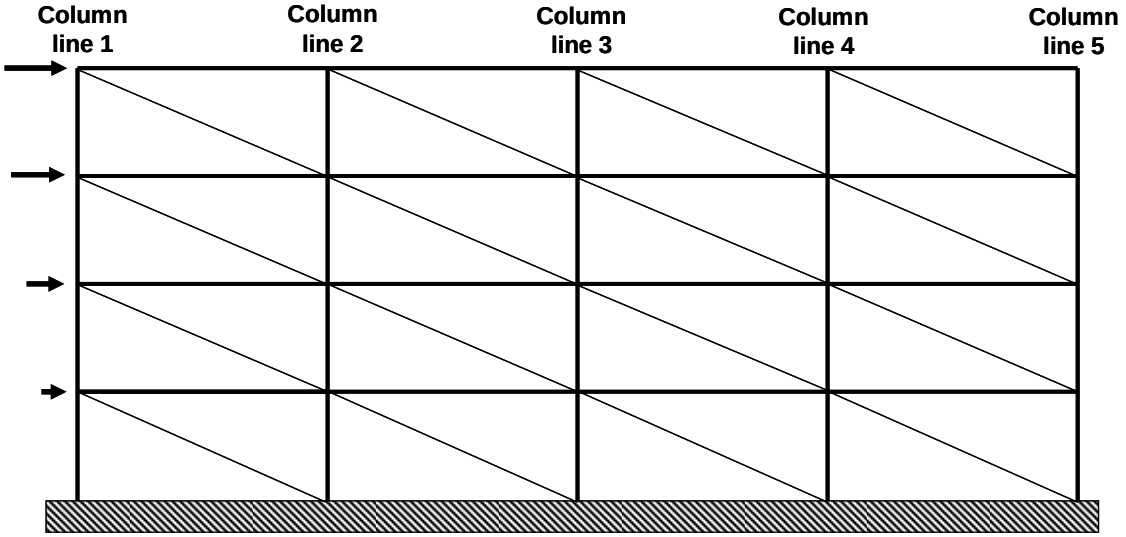

Figure 10.7: Equivalent struts active during pushover analysis of archetypical uniformly infilled frames

In exterior column lines, infills can cause significant differences in axial forces. For the AAC uniformly infilled frame, axial forces in exterior and interior columns were monitored during the pushover analysis, and are presented in Figure 10.8, along with the active equivalent struts and labeling of column lines during the pushover analysis. Compared to the ATC-63 steel moment frame, the axial forces in exterior columns of the AAC uniformly infilled frame increase progressively from top to bottom. Because the infills in all stories crushed at about the same time during the pushover analysis, the differences at each story between the maximum axial force in a particular column line of the ATC-63 steel moment frame and the same column line in the AAC uniformly infilled frame, are multiples of 40 kips (the vertical component of the axial strength of the equivalent strut). In Column Line 1, the difference in maximum axial force between the

ATC-63 steel moment frame and AAC uniformly infilled frame was equal to 40 kips at the fourth story, 80 kips at the third story, and so on down to the bottom story (Figure 10.8). For Column Line 5, in axial compression, the vertical components in the equivalent struts cascade down the columns from top of the third story. Accordingly, while the column axial force in the fourth story was nearly the same for the AAC uniformly infilled frame as for the ATC-63 steel moment frame, they differ by about 40 kip at the third story, 80 kip at the second story, and 120 kip at the ground story.

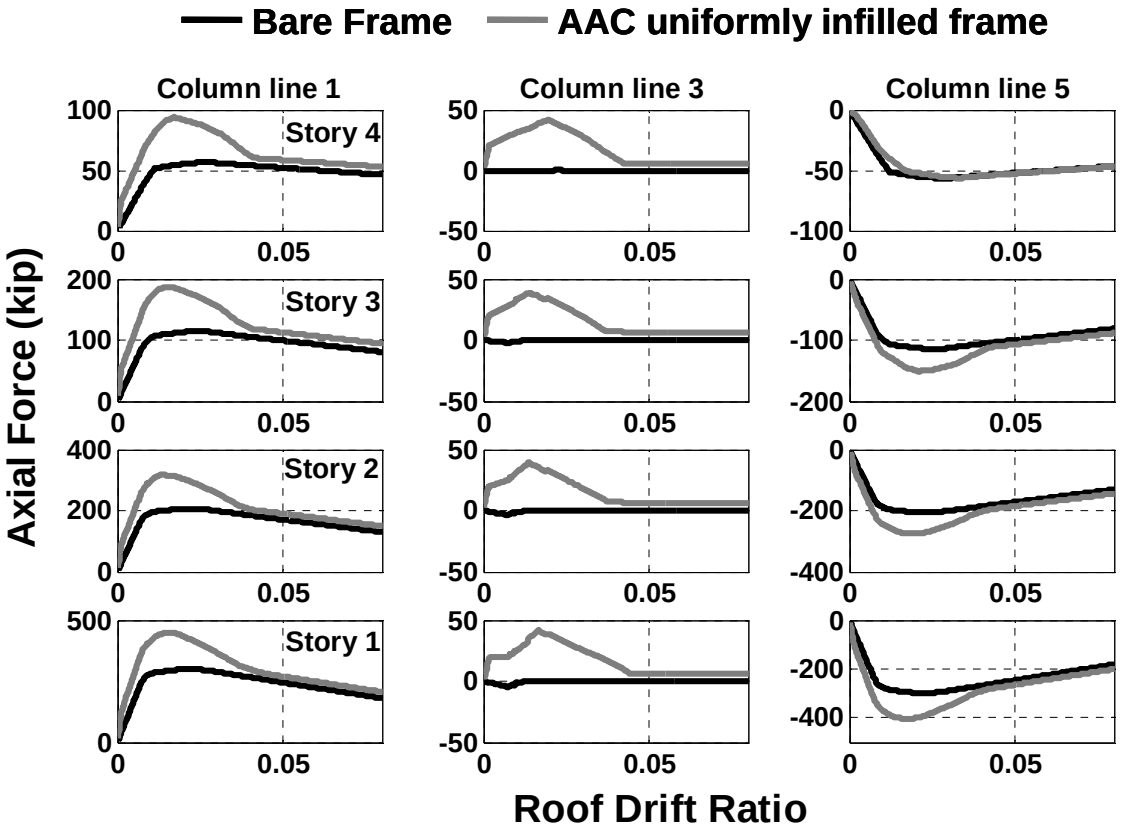

Figure 10.8: Axial forces in column lines of ATC-63 bare frame and AAC uniformly infilled frame during pushover analysis

In interior column lines, in contrast, infills do not cause significant changes in axial forces compared to the bare frame. This is because the vertical components of the

forces in the equivalent struts framing into opposite sides of an interior column tend to neutralize each other, except at the top story (Figure 10.7). For example, in Column Line 3 (Figure 10.8), the differences in axial forces between the AAC uniformly infilled frame and the ATC-63 bare frame remain nearly uniform at about 40 kips (tension).

Because of the relatively weak AAC infills, axial forces in the columns of the ATC-63 bare frame do not increase significantly due to uniform AAC infilling. The maximum increase in axial force (160 kips in tension and 120 kips in compression) are only 4.8% and 3.6%, respectively, of the concentric axial capacity of the ground story column. These increases do not significantly reduce the moment capacity or ductility of the columns.

10.2.3.6 Non-simulated collapse mode of AAC uniformly infilled frame

Non-simulated collapse due to local shear failure of frame members (Chapter 9) did not occur during the pushover analysis of the AAC uniformly infilled frame.

10.2.4 Incremental dynamic analysis

IDA (Section 3.6.3 and Section 9.2) is performed for the AAC uniformly infilled frame, and the results are presented in Figure 10.9, at the prescribed fundamental period of the ATC-63 steel moment frame. The spectral intensity that causes collapse of the AAC uniformly infilled frame under half the ground motions is 2.33 g, compared with 2.14 g for the ATC-63 steel moment frame (Section 7.4.3). Corresponding to a spectral intensity of 0.97 g at the fundamental period of the ATC-63 steel moment frame, the corresponding CMR for the AAC uniformly infilled frame is 2.4, compared to 2.2 for the ATC-63 steel moment frame. Thus, uniformly infilling the ATC-63 steel moment frame with AAC infills increases the CMR by about 10 percent.

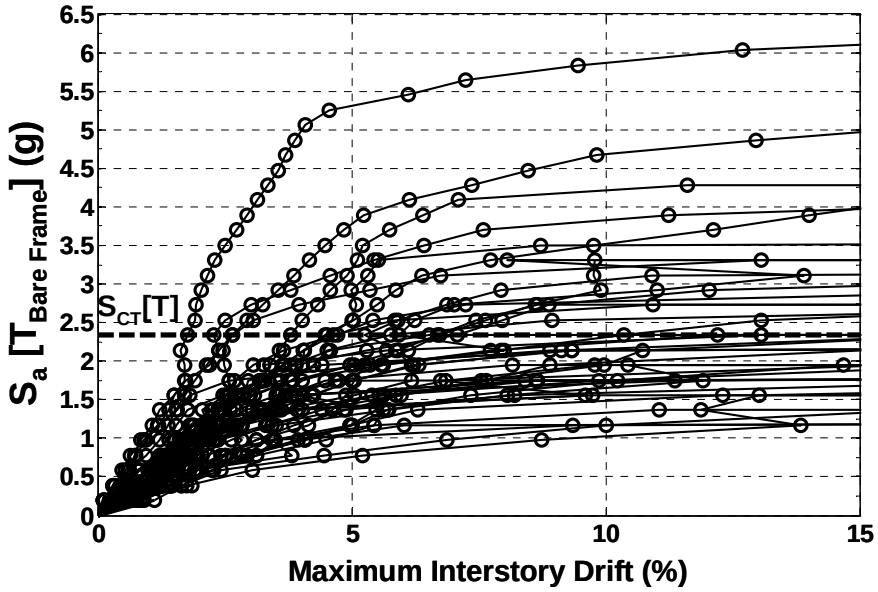

Figure 10.9: Results from IDA for ATC-63 steel moment frame with uniform AAC infill

For each of the 44 ground motions in the ATC-63 suite, the spectral intensity required to collapse the AAC uniformly infilled frame was divided by that required to collapse the ATC-63 steel moment frame. Both spectral intensities were determined at the fundamental period of the ATC-63 steel moment frame. The ratios of those intensities are plotted in Figure 10.10. Most ratios are greater than 1.0, indicating in a preliminary manner that uniform AAC infilling increases the seismic resistance of the ATC-63 bare frame. This indication is confirmed formally later in this chapter.

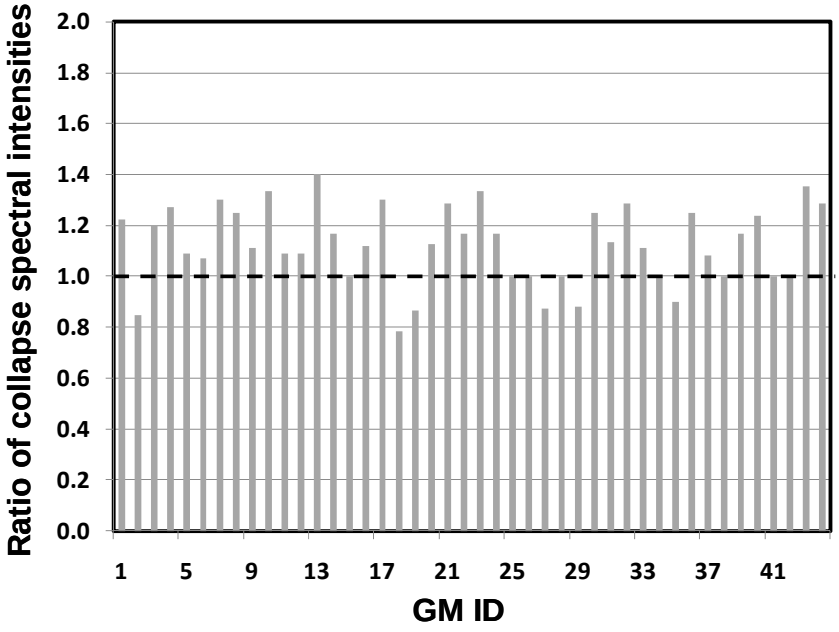

Figure 10.10: Ratios of collapse spectral intensities for AAC uniformly infilled frame and ATC-63 steel moment frame for 44 ground motions of the ATC-63 suite

The results of the IDA can also be expressed at the fundamental period of the AAC uniformly infilled frame. For the median response spectrum of the ATC-63 ground motion suite, a spectral acceleration of 2.33 g at a period of 0.92 sec (the fundamental period of the ATC-63 steel moment frame) corresponds to a spectral acceleration of 4.04 g at 0.56 sec (the fundamental period of AAC uniformly infilled frame). As shown in Figure 10.1, at that fundamental period of 0.56 sec, the MCE spectral acceleration demand on the AAC uniformly infilled frame from the SDC D_{max} response spectrum is 1.5 g. Thus, the CMR corresponding to spectral intensities determined at the fundamental period of the AAC uniformly infilled frame is 2.7, again greater than the CMR of 2.2 for the ATC-63 steel moment frame.

10.2.4.1 Non-simulated collapse modes for AAC uniformly infilled frame

Results of the IDA for the AAC uniformly infilled frame show no local shear failure in frame members, and consideration of such failure produced no change in the IDA plots of Figure 10.9. The median collapse spectral acceleration of 2.33 g (at the fundamental period of the ATC-63 steel moment frame) and the CMR of 2.4 for the AAC uniformly infilled frame were similarly unchanged.

10.2.4.2 Displaced profile at collapse during IDA

In Figure 10.11 are shown the IDA displaced profiles of the ATC-63 steel moment frame for a maximum interstory drift of 15% at any story (considered equivalent to collapse according to the ATC-63 methodology). In Figure 10.12 are shown the corresponding results for the AAC uniformly infilled frame. The two sets of profiles are similar for most ground motions, indicating that uniform AAC infilling generally does not affect the failure mechanism of the frame or lead to weak story mechanisms. As shown by arrows in Figure 10.12, AAC infills caused four cases of hinging at the top of the third-story columns, and one case of hinging at the top of the second-story columns.

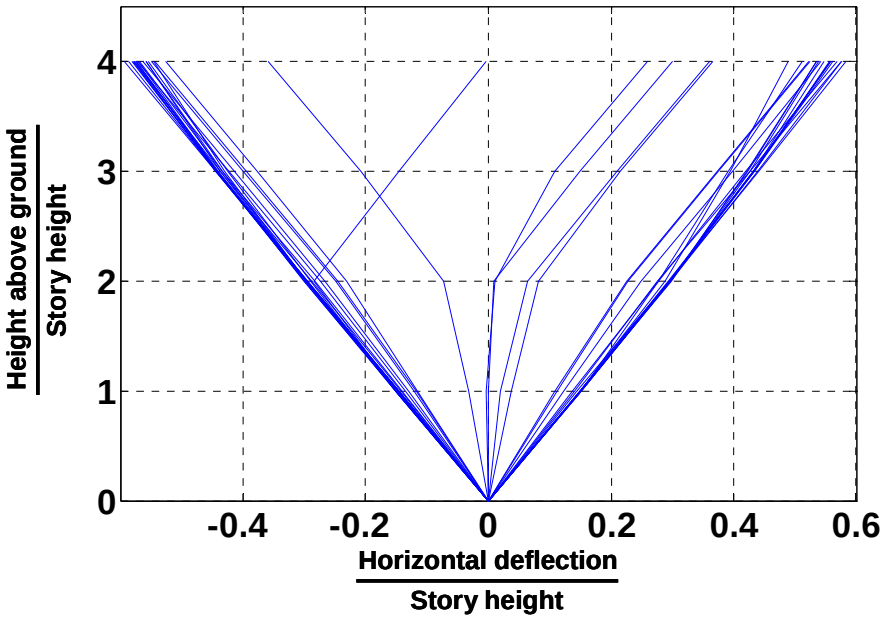

Figure 10.11: IDA displacement profiles at 15% interstory drift for ATC-63 steel moment frame

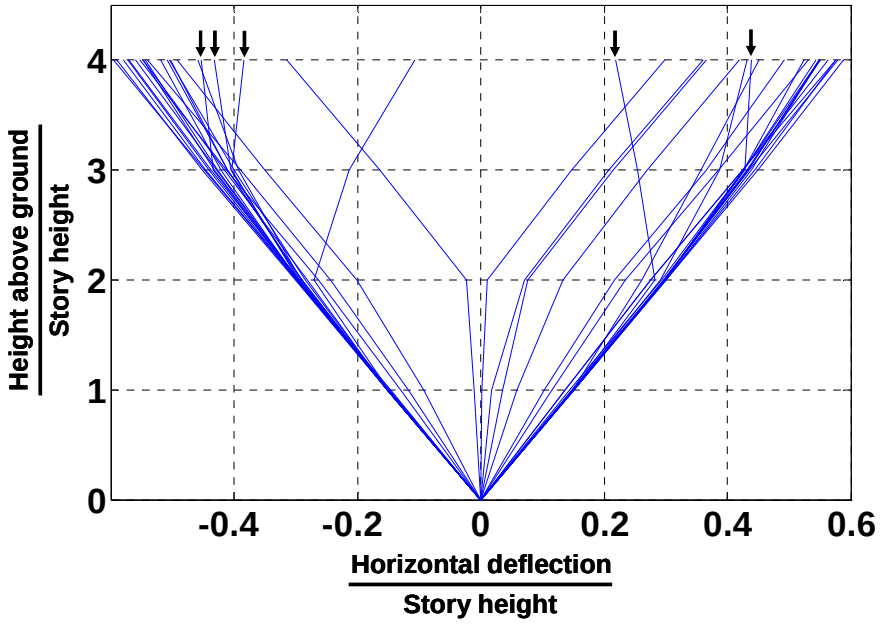

Figure 10.12: IDA displacement profile at 15% interstory drift for AAC uniformly infilled frame

10.2.4.3 Uncertainty parameters for AAC uniformly infilled frame

The uncertainties in collapse capacity of the AAC uniformly infilled frame are determined as for the ATC-63 steel moment frame in Section 7.4.5, as outlined below:

a. Record-to-record uncertainty (β_{RTR}) is taken as 0.4 as prescribed by Section 7.3.4 of ATC-63 (2008).

b. Design related uncertainty is rated as "good," and the corresponding β_{DR} is taken as 0.3, as for the ATC-63 steel moment frame, because the AAC infills are ignored in the design process.

c. Test data related uncertainty is rated as only "fair" (because the test data for the AAC infill were obtained from only a single infilled frame specimen), and the corresponding uncertainty parameter (β_{TD}) is taken as 0.45. In contrast, the quality of test data for the bare frame had been rated as "good," and the corresponding uncertainty parameter for the ATC-63 steel moment frame had been taken as 0.3.

d. Modeling uncertainty is rated as "fair" for the AAC uniformly infilled frame (because of limited experience and also because of assumptions made in modeling the hysteretic behavior of AAC infills). The corresponding parameter (β_{MDL}) is taken as 0.45.

In Table 10-1, the uncertainty parameters for the AAC uniformly infilled frame are compared with those of the ATC-63 steel moment frame. From Table 7-2 of ATC-63 (2008), the lognormal distribution standard deviation parameter for the total uncertainty in the collapse capacity of the AAC uniformly infilled frame is obtained as 0.80.

Table 10-1: Uncertainty parameters for the ATC-63 steel moment frame and for corresponding AAC uniformly infilled frame

Uncertainty parameter	Rating for the ATC-63 steel moment frame	Rating for the AAC uniformly infilled frame
Record-to-record uncertainty	$\beta_{RTR} = 0.4$	$\beta_{RTR} = 0.4$
Design requirements uncertainty	Good ($\beta_{DR} = 0.3$)	Good ($\beta_{DR} = 0.3$)
Test Data uncertainty	Good ($\beta_{TD} = 0.3$)	Fair ($\beta_{TD} = 0.45$)
Modeling uncertainty	Fair ($\beta_{MDL} = 0.45$)	Fair ($\beta_{MDL} = 0.45$)
Total uncertainty	$\beta_{TOT} = 0.75$	$\beta_{TOT} = 0.80$

10.2.4.4 Methods for determination of probability of collapse at MCE and collapse fragility curve

To enable comparison of the ATC-63 steel moment frame and the AAC uniformly infilled frame, two methods are proposed here for computing the probability of collapse and the collapse fragility curve of archetypical infilled steel moment frames. These methods differ in how the *CMR* and *SSF* are determined for the archetypical infilled steel moment frames.

1) In Method 1, the ATC-63 steel moment frame and the archetypical infilled steel moment frame are considered as two different archetypical structures, each of which is evaluated independently using the ATC-63 methodology. The *CMR* of the archetypical infilled steel moment frame is computed using the median collapse spectral intensity and MCE-level spectral demand determined at the fundamental period of that archetypical infilled steel moment frame. The *SSF* is

computed using the ductility of the archetypical infilled steel moment frame as obtained from the pushover analysis.

2) In Method 2, the archetypical infilled steel moment frame is considered as a variant of the ATC-63 steel moment frame. The *CMR* of the archetypical infilled steel moment frame is computed using the median collapse spectral intensity and MCE level spectral demand determined at the fundamental period of the ATC-63 steel moment frame. Ideally, for this method the *SSF* for the archetypical infilled steel moment frame should be taken as that of the ATC-63 steel moment frame. However, because the *SSF* decreases with decreasing ductility (as determined from pushover analysis) as well as decreasing fundamental period of the archetypical structure, using the *SSF* of the ATC-63 steel moment frame for an archetypical infilled steel moment frame may result in over-prediction of the collapse capacity of the archetypical infilled steel moment frame. For this reason, the spectral shape is taken as the average of that obtained for the ATC-63 steel moment frame and the archetypical infilled steel moment frame.

These two methods, summarized in Table 10-2, are used to determine the probability of collapse and the collapse fragility curve of the AAC uniformly infilled frame.

Table 10-2: Summary of methods for determination of probability of collapse at MCE and collapse fragility curve

Method	Fundamental period used for determination of median collapse spectral intensity and CMR	SSF
Method 1	Fundamental period of archetypical infilled steel moment frame	Same as that of the archetypical infilled steel moment frame
Method 2	Fundamental period of ATC-63 steel moment frame	Average of ATC-63 steel moment frame and archetypical infilled steel moment frame

10.2.4.5 Probability of collapse at MCE and collapse fragility curve for AAC uniformly infilled frame

Method 1 above is applied using the following steps:

1) The median collapse spectral intensity of the AAC uniformly infilled frame at its fundamental period (0.56 sec) was obtained as 4.04 g earlier in this section. The MCE-level spectral acceleration demand on the AAC uniformly infilled frame from the SDC D_{max} response spectrum of the ATC-63 methodology is 1.5 g (Figure 10.1). Therefore, the *CMR* is 2.7.
2) The spectral shape factor (*SSF*), evaluated using the ductility of 4.1 obtained from pushover analysis and fundamental period of the infilled frame of 0.56 sec is 1.25.

3) The adjusted collapse margin ratio (*ACMR*), determined as the product of the *CMR* and the *SSF*, is 3.4.
4) The uncertainty parameters for the AAC uniformly infilled frame are presented in Section 10.2.4.3. The total system uncertainty is 0.80.
5) The probability of collapse at MCE of the AAC uniformly infilled frame is 6.4 %.

Method 2 above is applied using the following steps:

1) The collapse spectral intensity of the AAC uniformly infilled frame at the fundamental period of the ATC-63 steel moment frame was determined to be 2.34 g. The MCE-level spectral acceleration demand from the SDC D_{max} response spectrum (Figure 3.5) at the fundamental period of the ATC-63 steel moment frame is 0.97g (Figure 10.1). Therefore, the *CMR* for the AAC uniformly infilled frame is 2.4.
2) The *SSF* from Table 7-1b of the ATC-63 (2008), based on the fundamental period and ductility of the ATC-63 steel moment frame, is obtained as 1.40 in Section 7.4.4. The *SSF* corresponding to fundamental period of 0.56 sec and ductility of 4.1 of the AAC uniformly infilled frame is obtained as 1.25. The *SSF* of the AAC uniformly infilled frame (computed as the average of that of the ATC-63 steel moment frame and the AAC uniformly infilled frame) is 1.33.
3) The adjusted collapse margin ratio, *ACMR*, determined as the product of the *CMR* and the *SSF*, is 3.2.
4) The total system uncertainty is 0.80.
5) The probability of collapse at MCE of the AAC uniformly infilled frame is 7.4 %.

Results obtained from both methods for the probability of collapse at MCE of the AAC uniformly infilled frame are summarized in Table 10-3.

Table 10-3: Probability of collapse at MCE of the ATC-63 steel moment frame and the AAC uniformly infilled frame

Quantity	ATC-63 steel moment frame	AAC uniformly infilled frame	
		Method 1	Method 2
CMR	2.2	2.7	2.4
SSF	1.40	1.25	1.33
ACMR	3.1	3.4	3.2
Probability of collapse at MCE	6.6 %	6.4 %	7.4 %

10.2.4.6 Collapse fragility curve for AAC uniformly infilled frame

In Figure 10.13, the collapse fragility curves obtained for the AAC uniformly infilled frame using Methods 1 and 2 are compared with that previously obtained for the ATC-63 steel moment frame. Depending on whether Method 1 or Method 2 is used, the probability of collapse is either decreased or marginally increased at ground motion intensities close to MCE. In both cases, however, it remains lower than the 20% and 10% limits of the ATC-63 methodology for individual archetypical structures and for performance groups, respectively.

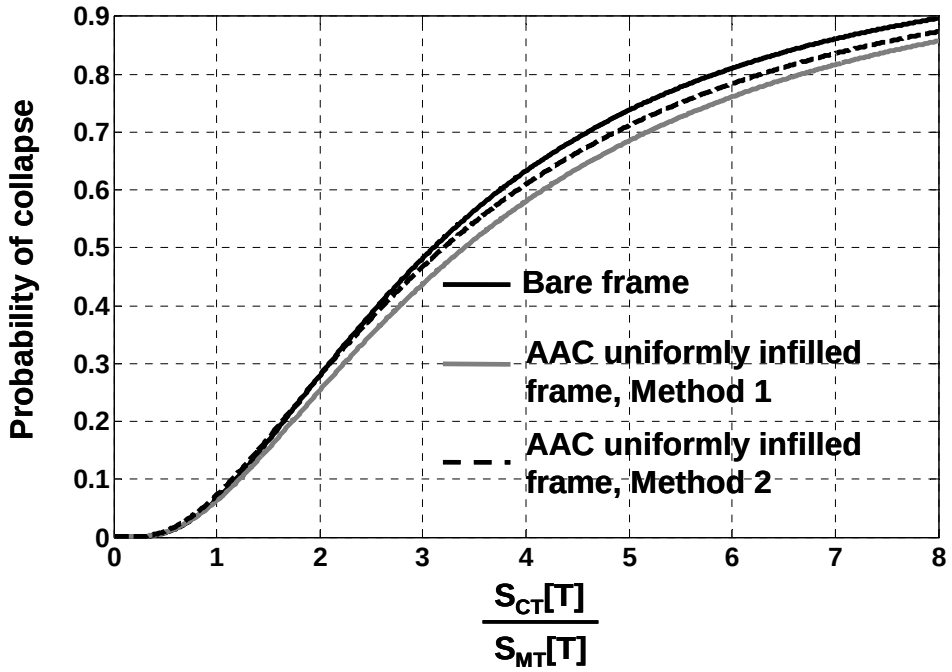

Figure 10.13: Collapse fragility curve obtained using Method 1 and Method 2 for the AAC uniformly infilled frame

10.2.4.7 Effect of uniform AAC infills at MCE- and DBE- level ground motions

As shown in Figure 10.14, the effect of uniform AAC infills on the response of the ATC-63 steel moment frame is also evaluated in terms of reduction in peak interstory drift at MCE- and DBE-level ground motions. Although this check is not required by the ATC-63 methodology, it is useful. DBE is generally defined as 0.67 times MCE by ASCE7-05. Because ground motion intensity is scaled by increments of 0.2 for the IDA of this dissertation, the closest intensity to DBE was 0.6 times MCE, and comparisons are made at this level.

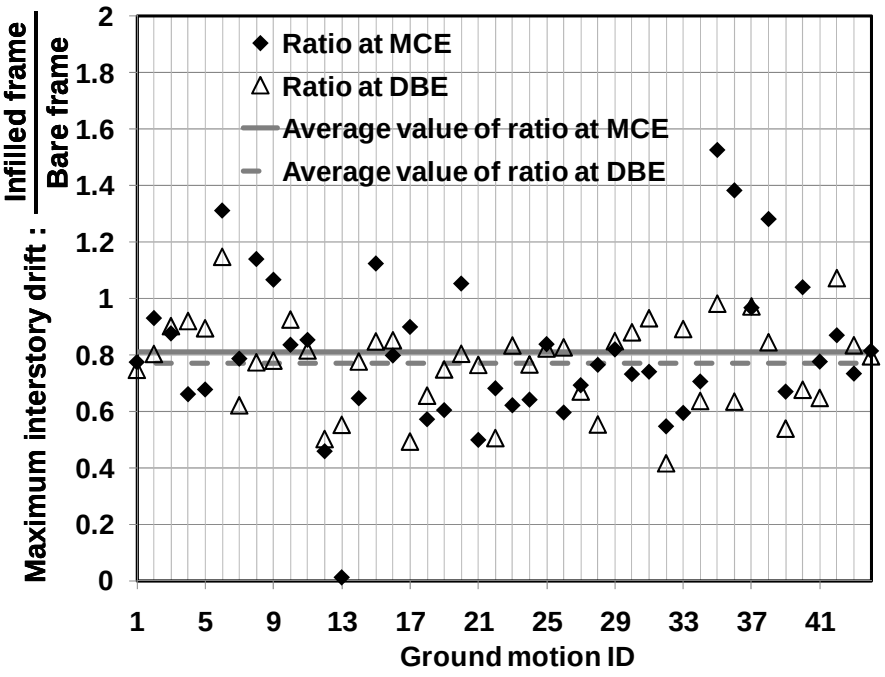

Figure 10.14: Reduction in maximum interstory drift for AAC uniformly infilled frame compared to ATC-63 steel moment frame at MCE and DBE-level ground motions

From Figure 10.14, it can be concluded that for MCE- and DBE-level ground motions, uniform AAC infills generally reduce interstory drifts by an average of about 20%.

10.3 ATC-63 EVALUATION OF ARCHETYPICAL CONVENTIONAL MASONRY UNIFORMLY INFILLED FRAMES

This section presents the ATC-63 evaluation of the 8-in. and 12-in. thick conventional masonry uniformly infilled frames (Table 8-6). Results in Section 10.2 from ATC-63 evaluation of the AAC uniformly infilled frame is also presented for comparison and completeness.

10.3.1 Fundamental period of conventional masonry uniformly infilled frames

The fundamental period of the archetypical conventional masonry uniformly infilled frames is determined, as described in Section 3.6.1, as the limiting period ($C_u T_a$) prescribed by Section 12.8.2 of ASCE7-05.

The general formula for the fundamental period of moment frames (recommended by Section 12.8.2.1 of ASCE7-05 and used previously for the AAC uniformly infilled frame) is applicable only if the frame is the sole seismic load-resisting system. Its use is difficult to justify for the conventional masonry uniformly infilled frames, because those infills have significant lateral strength and can possibly alter the native failure mechanism of the steel moment frame. Therefore, the fundamental period of the conventional masonry infilled frames is calculated using the general formula of ASCE7-05 for shear-wall buildings.

$$T_a = \frac{0.0019}{\sqrt{C_w}} h_n \qquad \textit{Equation 10-1}$$

$$C_w = \frac{100}{A_B} \sum_{i=1}^{x} \left(\frac{h_n}{h_i} \right)^2 \frac{A_i}{\left[1 + 0.83 \left(\frac{h_i}{D_i} \right)^2 \right]} \qquad \textit{Equation 10-2}$$

$$T = C_u \, T_a \qquad \textit{Equation 10-3}$$

where,

T_a = approximate fundamental period of shear walls

T = code defined limiting fundamental period

C_u = factor determined by Table 12.8-1 of ASCE7-05

h_n = height above the base to the highest level of the structure, ft

A_B = area of base of the structure, ft^2

A_i = web area of shear wall "i" in ft^2

D_i = length of shear wall "i" in ft

h_i = height of shear wall "i" in ft

x = number of shear walls in the building effective in resisting lateral forces in the direction under consideration

The factor C_u, determined by Table 12.8-1 of ASCE7-05 based on the value of design spectral acceleration at the one-second fundamental period, S_{D1}, and corresponding to seismic design category D_{max}, is 1.4.

Accordingly, the code-defined limiting fundamental periods for the 8-in. and 12-in. thick conventional masonry uniformly infilled frame are presented in Table 10-4, along with the respective fundamental periods from analytical models. The fundamental periods predicted by the analytical model decrease with increasing infill strength ratio, and are close to the limiting fundamental period from ASCE7-05.

Table 10-4: Fundamental period of archetypical uniformly infilled frames

Infill type	**Formula for determination of fundamental period by ASCE7-05**	**Code defined limiting fundamental period (sec)**	**Fundamental period from analytical model (sec)**
Bare frame	Steel moment frame	0.93	1.07
AAC, 8-in. thick	General formula for moment frames	0.56	0.52
Conventional masonry, 8- in. thick	Masonry shear wall	0.17	0.23
Conventional masonry, 12-in. thick	Masonry shear wall	0.14	0.20

10.3.2 Pushover analyses of conventional masonry uniformly infilled frames

Pushover analysis was performed on the 8-in. and 12-in. thick conventional masonry uniformly infilled frames using the same lateral load profile as for the ATC-63 steel moment frame and the AAC uniformly infilled frame. The pushover curves are compared in Figure 10.15, presented individually in Figure 10.16 and Figure 10.17, and used to obtain overstrength and ductility factors for the conventional masonry uniformly infilled frames.

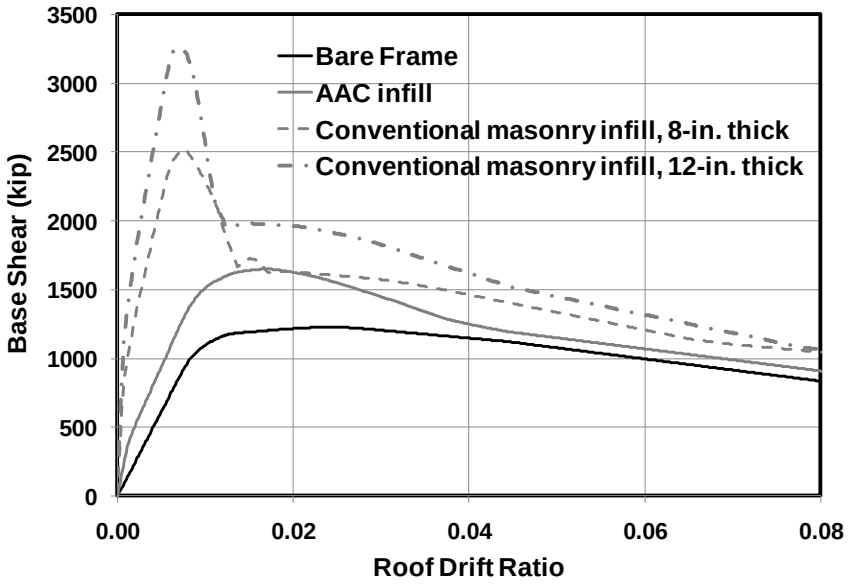

Figure 10.15: Pushover curve for archetypical uniformly infilled frames

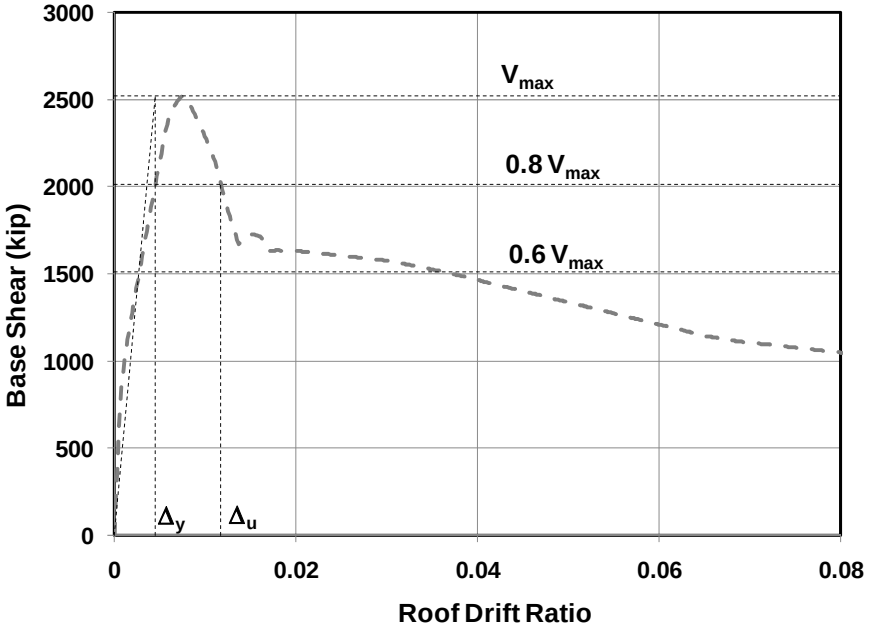

Figure 10.16: Pushover curve for 8-in. thick conventional masonry uniformly infilled frame

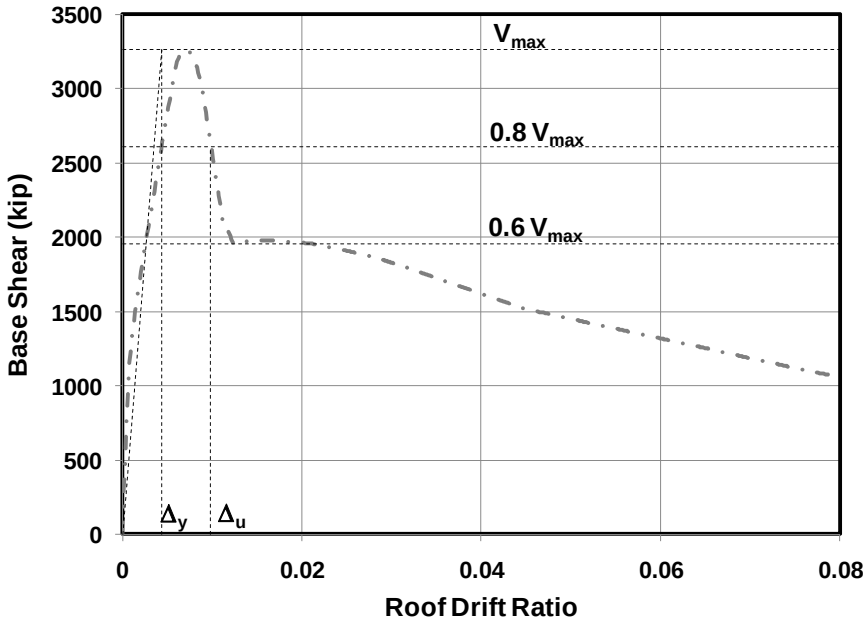

Figure 10.17: Pushover curve for 12-in. thick conventional masonry uniformly infilled frame

In Table 10-5, the stiffness, strength and ductility of the archetypical uniformly infilled frames, determined as outlined in Section 3.6.2, are compared with that of the ATC-63 steel moment frame. In general, increasing infill strength ratio progressively increases initial stiffness and strength while decreasing the ductility.

Table 10-5: Stiffness, strength and ductility of archetypical uniformly infilled frames from pushover analysis

Infill Type	Initial stiffness with respect to ATC-63 steel moment frame	Strength divided by design base shear	Displacement ductility
Bare frame	1.0	4.0	6.2
AAC, 8-in. thick	2.7	5.3	4.1
Conventional masonry, 8-in. thick	10.1	8.1	2.6
Conventional masonry, 12-in. thick	12.5	10.5	2.3

10.3.2.1 Failure mechanism and displaced profile

Plastic rotations in beam and column hinges during the pushover analysis of the ATC-63 steel moment frame and the archetypical uniformly infilled frames are shown in Figure 10.18 and Figure 10.19. In Figure 10.20 are compared the displaced profiles of the ATC-63 steel moment frame and the archetypical uniformly infilled frames at the ultimate roof drift ratio of the ATC-63 steel moment frame (Section 7.4.2).

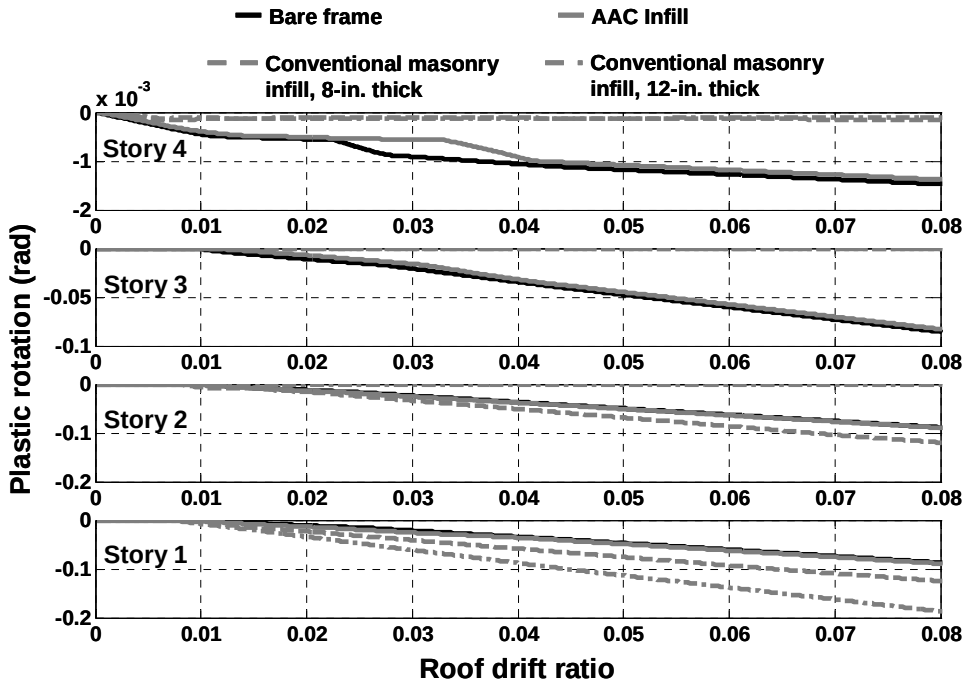

Figure 10.18: Plastic rotation in beams during pushover analysis of archetypical uniformly infilled frames

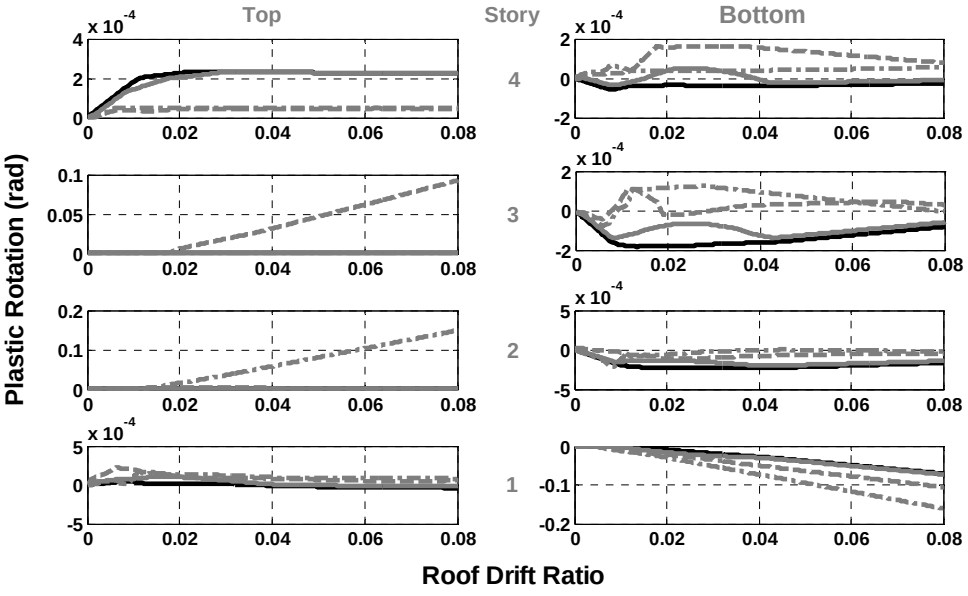

Figure 10.19: Plastic rotation in columns of steel moment frame during pushover analysis of archetypical uniformly infilled frames

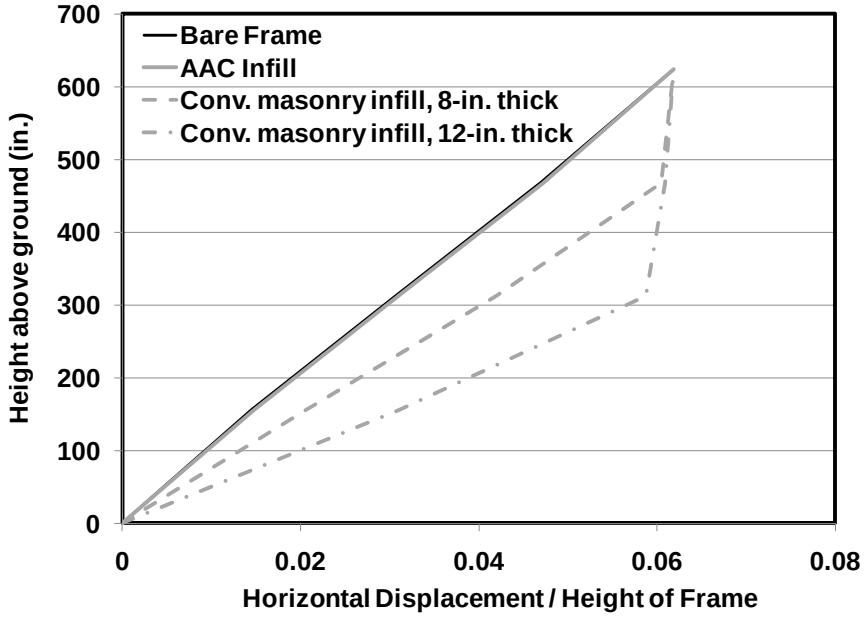

Figure 10.20: Displacement profile of archetypical uniformly infilled frames from pushover analyses

From the plastic rotations in hinges of beams and columns and the displaced profile of the archetypical uniformly infilled frames, the failure mechanism of the frames can be deduced. As already observed in Section 10.2.3, the presence of AAC infills did not change the failure mechanism of the frame. As shown in Figure 10.21, the failure mechanism of the 8-in. thick conventional masonry uniformly infilled frame is concentrated in the bottom three stories. For the 12-in. thick conventional masonry uniformly infilled frame, the failure mechanism is limited to the bottom two stories. This is corroborated by Figure 10.18 and Figure 10.19, in which concentration of the failure mechanism in the lower stories of the frame is seen to increase the plastic rotation demand in hinges of beams and columns in these stories compared to the ATC-63 steel moment frame. In Figure 10.21 and Figure 10.22 are shown the pushover failure mechanism of the 8-in. thick conventional masonry uniformly infilled frame and the 12-in. thick conventional masonry uniformly infilled frame, respectively.

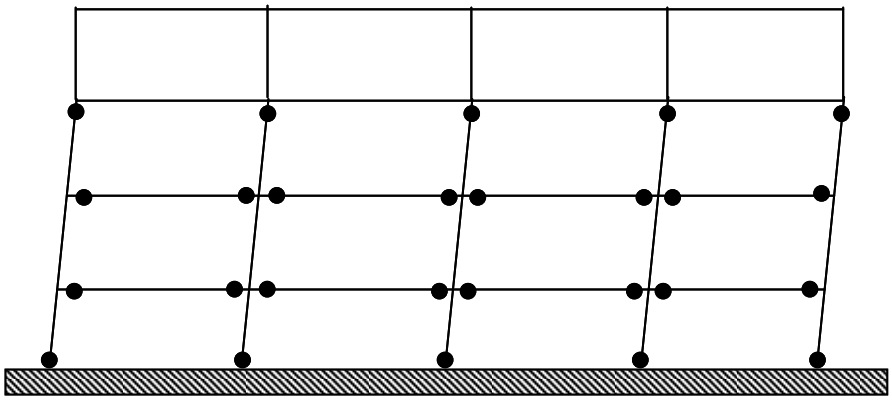

Figure 10.21: Failure mechanism of 8-in. thick conventional masonry uniformly infilled frame (pushover analysis)

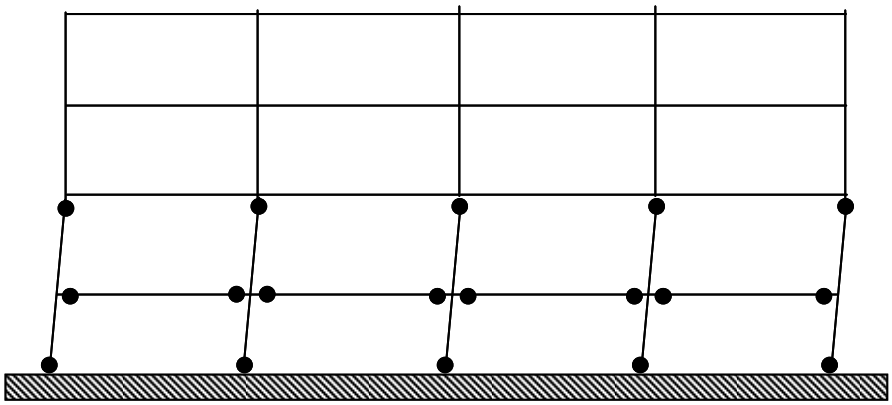

Figure 10.22: Failure mechanism of 12-in. thick conventional masonry uniformly infilled frame (pushover analysis)

10.3.2.2 Effect of conventional masonry infills on axial forces in columns

The axial strengths of the equivalent struts of the 8-in. and 12-in. thick conventional masonry infills are 394 kip and 591 kip, respectively (Section 8.4.1.2), and the corresponding vertical components of the strut forces are 157 kip and 235 kip, respectively.

In Figure 10.23 are shown the variations in axial forces in columns during the pushover analysis of 8-in. and 12-in. thick conventional masonry uniformly infilled frames. Column Lines 1, 3 and 5 are as defined in Figure 10.7. The trend in those

variations is similar to that observed in the case of the AAC uniformly infilled frame, although some differences are apparent, as discussed below.

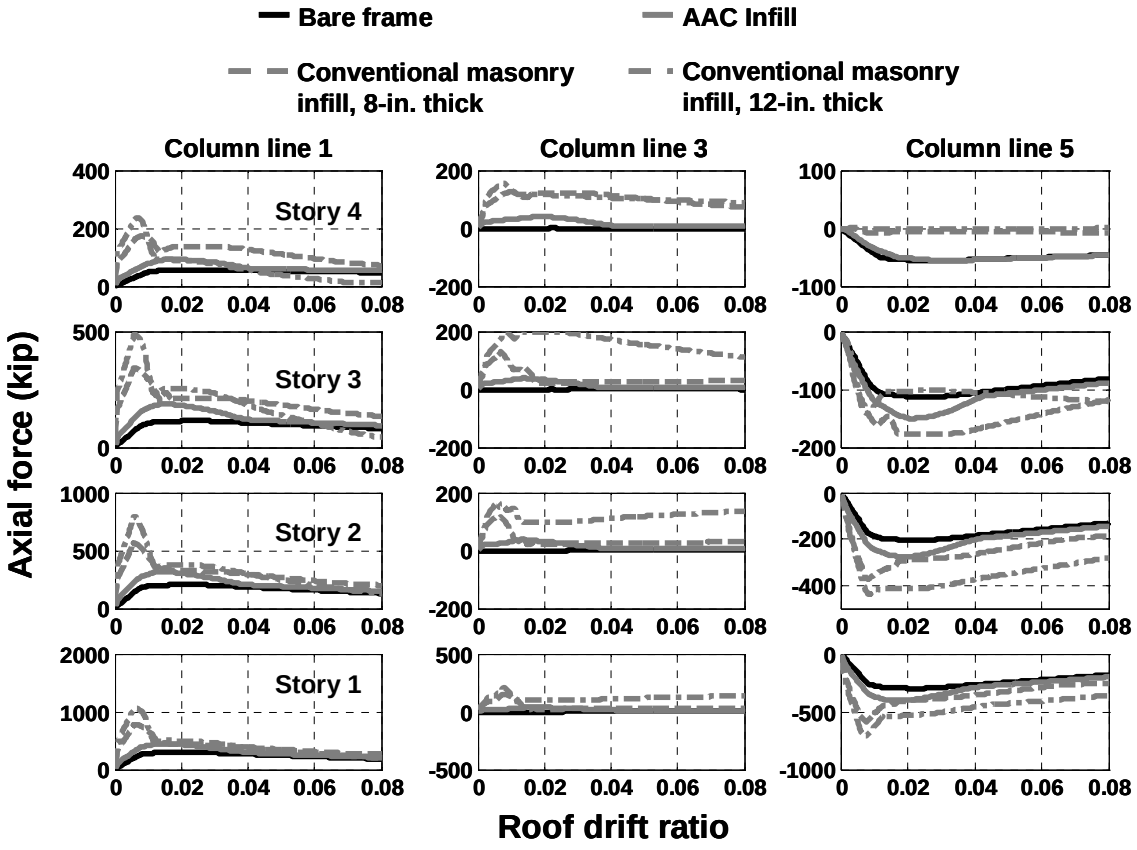

Figure 10.23: Variation in axial forces of columns during pushover analysis of archetypical uniformly infilled frames

In Column Line 1, maximum axial force generally increase from top to bottom. In contrast to the case of AAC uniformly infilled frame, however, the increase between two adjacent stories relative to the ATC-63 steel moment frame is consistently less than the vertical component of the axial strength of the infill. The first reason for this is that the infills did not crush completely at the upper stories, and those upper stories did not participate in the failure mechanism of the frame. The second reason is that axial force in the columns due to frame action is generally less than in the ATC-63 steel moment frame, because the failure mechanism of the frame does not involve beam hinging at all stories.

For Column Line 3, the axial force in columns is nearly the same at all stories, because opposing axial forces from equivalent struts framing from adjacent bays into a beam-column joint (Figure 10.7) tend to neutralize each other except at the top story. Therefore, the axial force in the top story column is carried down to the bottom stories.

The trend in axial forces in columns of Column Line 5 was similar to that of Column Line 1. The only difference was that the axial force in the column at the top story, primarily due to frame action, was negligible for both the 8-in. and 12-in. thick conventional masonry uniformly infilled frames, indicating that the most of the lateral load at the top story is carried by infill strut action.

Because conventional masonry infills are generally stronger than AAC masonry infills, they cause greater increases in column axial forces. The maximum increase in axial force relative to the ATC-63 steel moment frame in the ground story of Column Line 1, is about 500 kip and 800 kip for the 8-in. and 12-in conventional masonry uniformly infilled frames, respectively. These are 17% and 27%, respectively, of the axial capacity of the ground story columns. Such large increases in axial force may be difficult to handle in design.

10.3.2.3 Non-simulated collapse modes for conventional masonry uniformly infilled frames

The occurrence of non-simulated collapse due to local shear failure in frame members was monitored during the during pushover analysis. For the 8-in. thick conventional masonry uniformly infilled frame, the shear capacity of frame members was not exceeded. For 12-in. thick conventional masonry uniformly infilled frame, the shear capacity of columns was exceeded in the bottom three stories. The first such exceedance occurred in the ground story columns at a roof drift ratio of 0.0057, and reduced the ductility of the 12-in. thick conventional masonry uniformly infilled frame from 2.3 to 1.3.

10.3.2.4 Comments on results from pushover analysis of archetypical conventional masonry uniformly infilled frames

From pushover analysis, it has been determined that conventional masonry infills change the failure mechanism of the ATC-63 steel moment and cause local shear failure in frame members due to frame-infill interaction. This suggests that the collapse capacity of the ATC-63 steel moment frame may be reduced due to occurrence of story mechanisms and local shear failure in frame member. It will be useful to compare to what degree these observations are reflected in IDA.

10.3.3 Incremental dynamic analysis of conventional masonry infilled frames

In Figure 10.24 and Figure 10.25 are shown results from IDA for the 8-in. and 12-in. conventional masonry uniformly infilled frames. The *CMR* is 2.6 and 2.7, respectively, greater than the 2.2 obtained previously for the ATC-63 moment frame, and also greater than the 2.4 obtained previously for the AAC uniformly infilled frame. This shows that if only global sidesway failure mechanism of the frame is considered for collapse evaluation, increasing the infill strength ratio increases the collapse capacity. However, large increases in infill strength ratio produce only a small increase in the *CMR*.

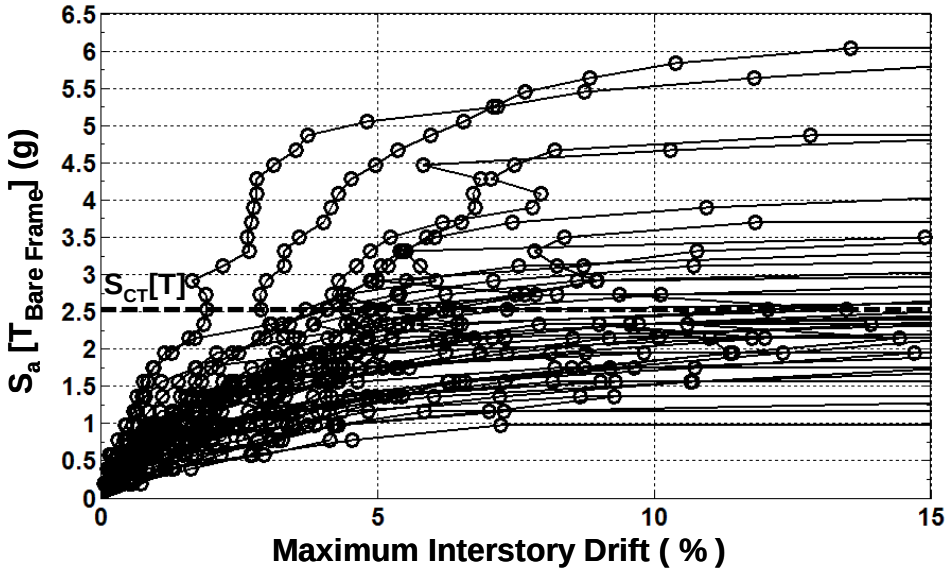

Figure 10.24: IDA results for 8-in. thick conventional masonry uniformly infilled frame

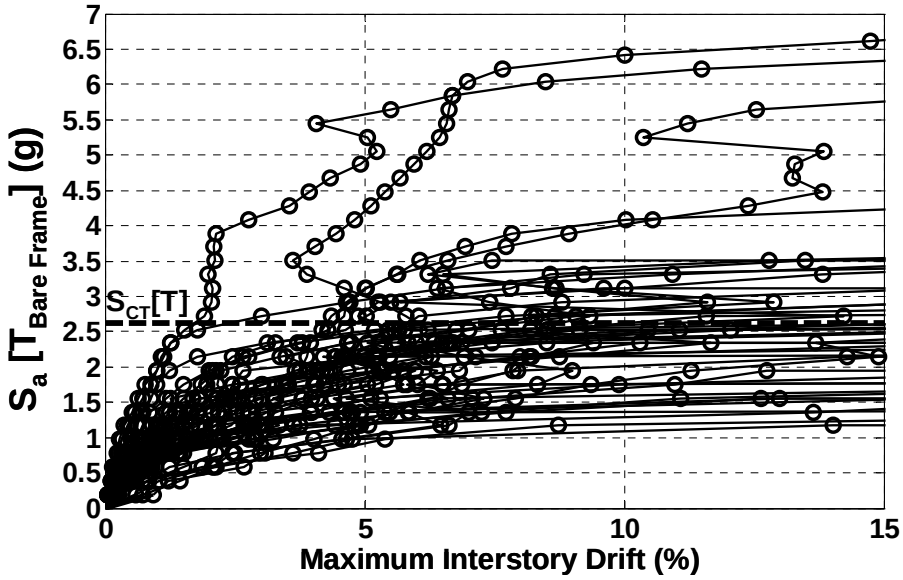

Figure 10.25: IDA results for 12-in. thick conventional masonry uniformly infilled frame

In Figure 10.26 and Figure 10.27 are shown the ratios of collapse spectral intensities of the 8-in. and 12-in. thick conventional masonry uniformly infilled frames, divided by those of the ATC-63 steel moment frame for the 44 ground motions of the ATC-63 suite. While the maximum collapse spectral intensity ratio is about 1.8, it is as low as 0.6 for some ground motions. In general, uniformly infilling the ATC-63 steel moment frame with conventional masonry infills does not produce consistent benefits. This is in contrast to the results shown for the AAC uniformly infilled frame in Figure 10.10.

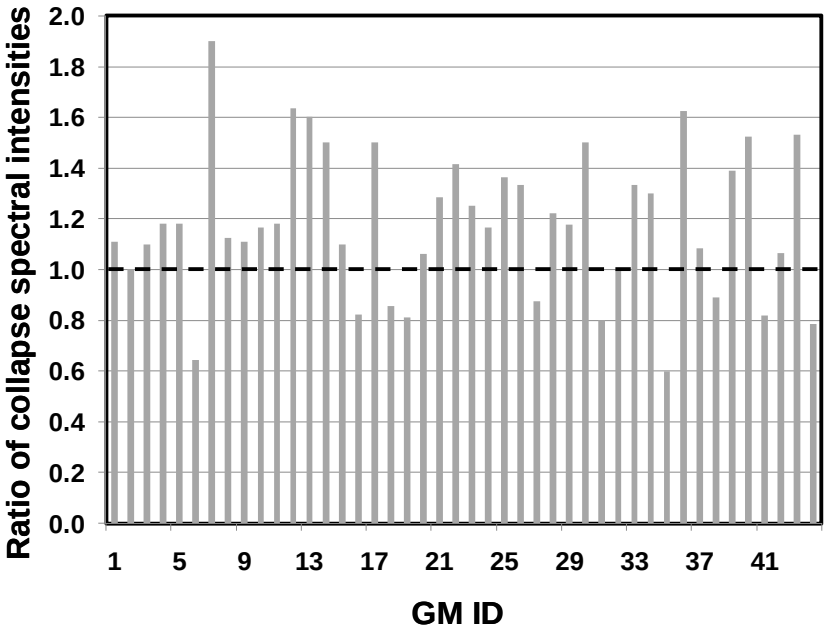

Figure 10.26: Ratios of collapse spectral intensities of 8-in thick conventional masonry uniformly infilled frame to those of the ATC-63 steel moment frame

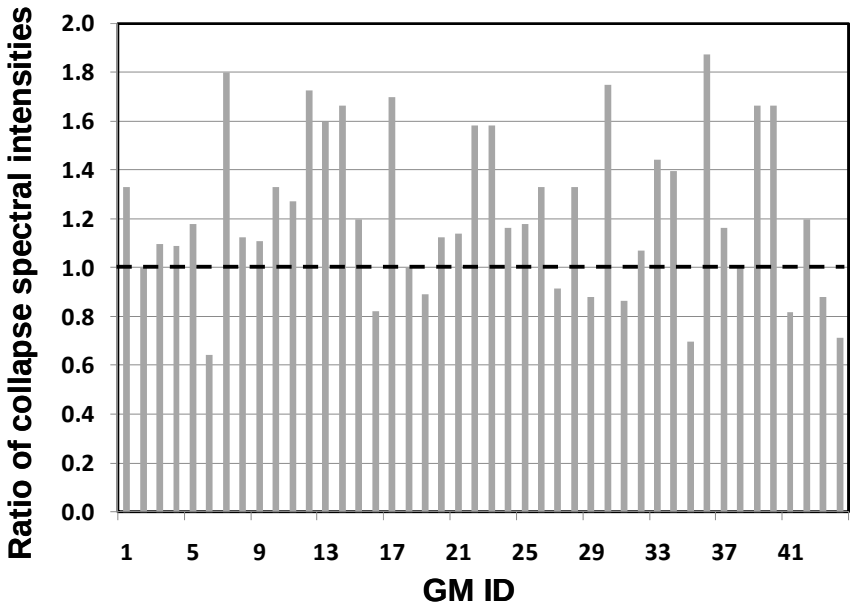

Figure 10.27: Ratios of collapse spectral intensities of 12-in thick conventional masonry uniformly infilled frame to those of the ATC-63 steel moment frame

10.3.3.1 Non-simulated collapse modes for conventional masonry infilled frames

In Figure 10.28 and Figure 10.29, respectively, are shown the IDA curves considering non-simulated collapse modes (Chapter 9) for 8-in. thick and 12-in. thick conventional masonry uniformly infilled frame.

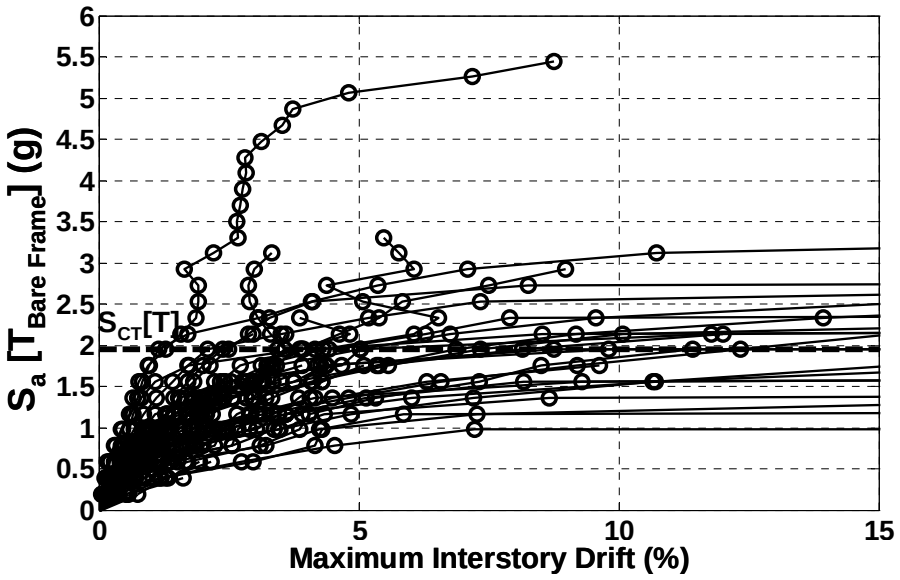

Figure 10.28: IDA results considering non-simulated collapse for 8-in. thick conventional masonry uniformly infilled frame

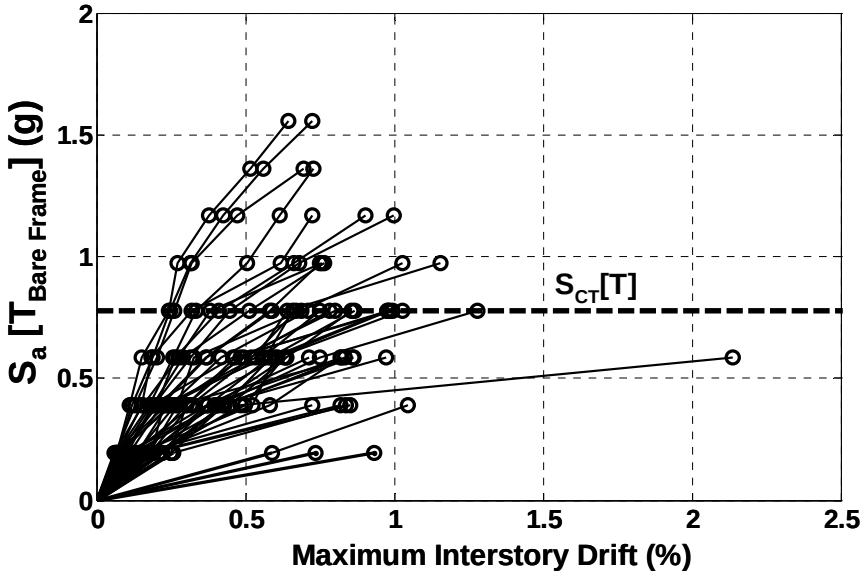

Figure 10.29: IDA results considering non-simulated collapse for 12-in. thick conventional masonry uniformly infilled frame

For the 8-in. thick conventional masonry uniformly infilled frame, local shear failure generally occurred in the bottom two stories and sometimes in the third and fourth stories as well. For the 12-in. thick conventional masonry uniformly infilled frame, local shear failure generally occurred in columns at all stories. The shear capacities of beams were never exceeded, probably because the vertical component of the infill force was limited by the large aspect ratio (story height divided by bay width) of the infill. Therefore, the local shear failures predicted by pushover analysis in Section 10.3.2.3 are also observed from IDA, to an even greater extent. IDA predicts local shear failures for the 8-in. thick conventional masonry uniformly infilled frame, while pushover analysis does not.

Table 10-6 presents the *CMR* obtained for the archetypical uniformly infilled frames considering non-simulated collapse modes.

Table 10-6: Median collapse spectral intensity and CMR for the archetypical uniformly infilled frames with and without non-simulated collapse modes

Infill type	Considering only sidesway collapse		Including local shear failure as non-simulated collapse mode	
	Median collapse spectral intensity at fundamental period of the ATC-63 steel moment frame	CMR	Median collapse spectral intensity at fundamental period of the ATC-63 steel moment frame	CMR
Bare frame	2.14	2.2	2.14	2.2
AAC, 8-in. thick	2.34	2.4	2.34	2.4
Conventional masonry, 8- in. thick	2.53	2.6	1.95	2.0
Conventional masonry, 12-in. thick	2.63	2.7	0.78	0.8

In Figure 10.30 and Figure 10.31 are shown the ratios of collapse spectral intensities (including non-simulated collapse modes) of the 8-in. and 12-in. thick conventional masonry uniformly infilled frames, divided by those of the ATC-63 steel moment frame, for 44 ground motions of the ATC-63 suite. The inconsistent effects of uniform infilling with conventional masonry, noted earlier in this section, are even more evident when non-simulated collapse modes are considered. Some spectral intensity ratios show more scatter, and many are now lower than 1.0.

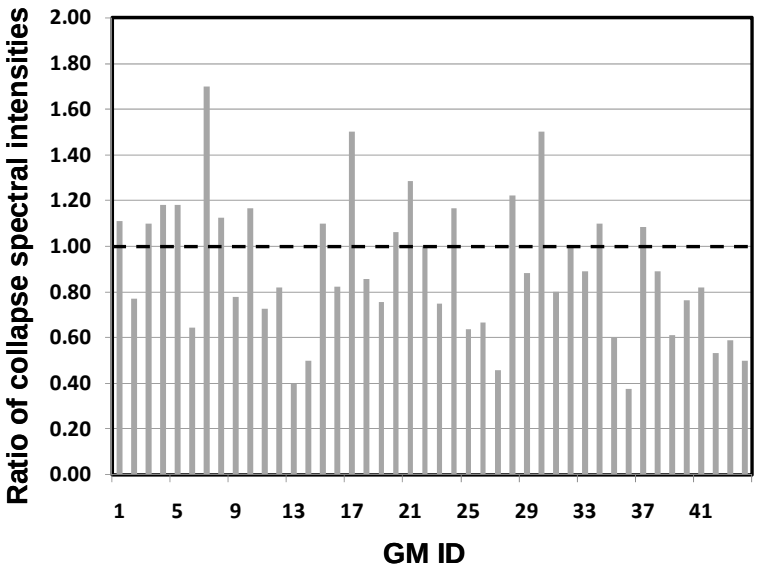

Figure 10.30: Ratios of collapse spectral intensities of 8-in. thick conventional masonry uniformly infilled frame to those of the ATC-63 steel moment frame considering non-simulated collapse modes

As shown in Figure 10.31, results for the 12-in. conventional masonry infills are particularly telling. Strong infills cause non-simulated shear failures, dramatically decreasing the spectral intensity required to cause collapse.

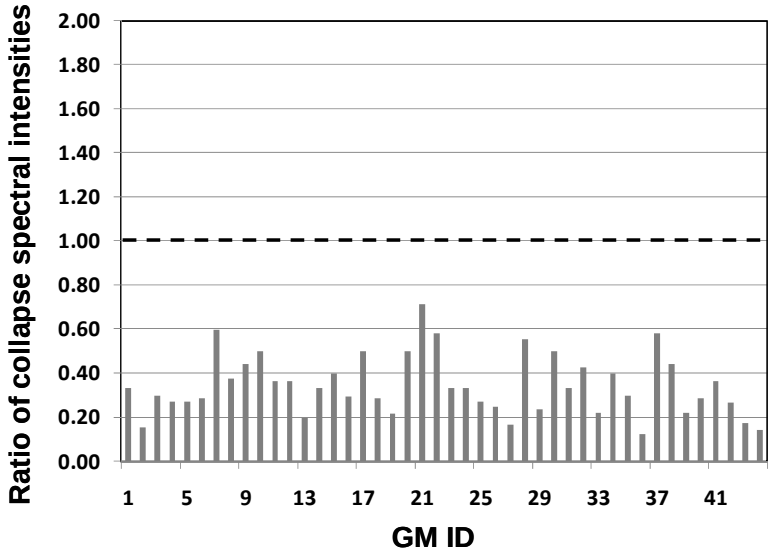

Figure 10.31: Ratios of collapse spectral intensities of 12-in. thick conventional masonry uniformly infilled frame to those of the ATC-63 steel moment frame considering non-simulated collapse modes

From the results of the IDA considering local shear failure as non-simulated collapse modes, the following observations can be made:

1) Local shear failures did not occur for AAC uniformly infilled frame. Therefore, uniformly placed infills in uniformly infilled steel moment frames can be proportioned so that local shear failures are avoided.

2) When local shear failures were considered as non-simulated collapse mode, the *CMR* decreased from 2.6 to 2.0 for 8-in. thick conventional masonry uniformly infilled frame, and from 2.7 to 0.8 for 12-in. infills. Therefore, increasing infill strength ratios lead to a higher probability of local shear failures in frame elements.

3) Strong infills cause local shear failure in frame members even at moderate ground motions. This is particularly evident from Figure 10.29 for the 12-in. thick conventional masonry uniformly infilled frame, which caused local shear failure

in frame members at ground motion intensities much less than the MCE-level spectral demand on the ATC-63 steel moment frame (0.93 g).

4) These observations are consistent with anecdotal evidence (from real earthquakes and experimental investigations) that infills can cause local shear failure in frame members.

10.3.3.2 Displaced profile at collapse during IDA for conventional masonry infilled frame

In Figure 10.32 and Figure 10.33 are shown the displaced profile of the 8-in. and 12-in. thick conventional masonry uniformly infilled frames respectively, when interstory drift exceeded 15% during IDA for each of the 44 ground motions of the ATC-63 suite. This was presented in Figure 10.11 and Figure 10.12 for the ATC-63 steel moment frame and the AAC uniformly infilled frame, respectively. While the displacement profile for the AAC uniformly infilled frame, represents a sidesway failure mechanism distributed over the entire height of the frame, similar to that of the ATC-63 steel moment frame, the displacement profile for the 8-in. thick conventional masonry uniformly infilled frame represents a failure mechanism limited in most cases to the lower three or two stories. This is even more true for the 12-in. thick conventional masonry uniformly infilled frame, whose displacement profile is generally limited to the bottom two stories. This behavior is consistent with the results of pushover analyses (Figure 10.20). Therefore, it can be said that a high infill strength ratio leads to story mechanisms even in a frame designed according to the strong column-weak beam concept. With an infill strength ratio of 1.0, the failure mechanism is concentrated in the bottom half of the 12-in. thick conventional masonry uniformly infilled frame.

These observations made here confirm those made previously by Dolsek (2000), that story mechanisms can occur even in uniformly infilled frames. While Dolsek attributed this to ground motion intensity exceeding a certain level, the results presented here suggest that it is more fundamentally attributable to the infill strength ratio.

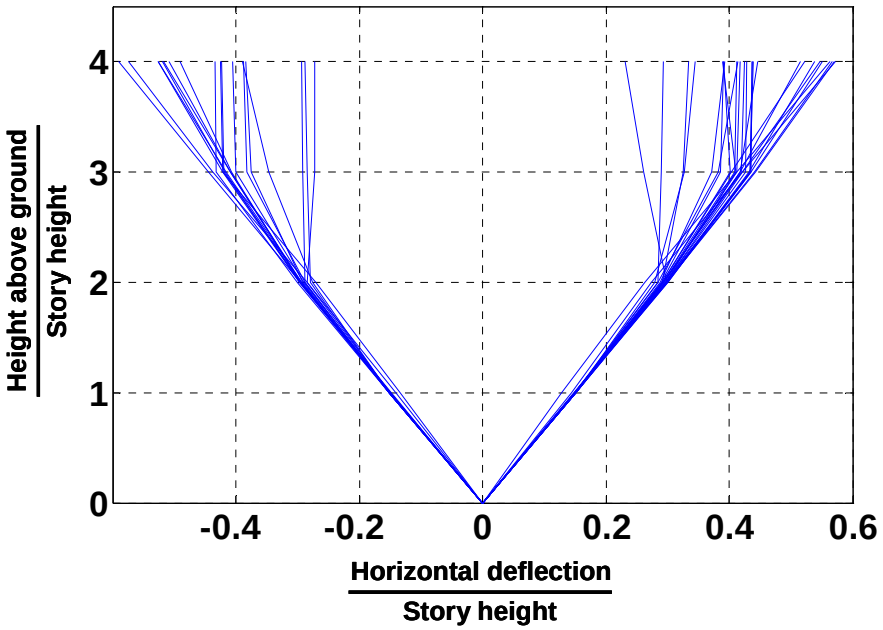

Figure 10.32: Displacement profile at 15% interstory drift of the 8-in. thick conventional masonry uniformly infilled frame from IDA

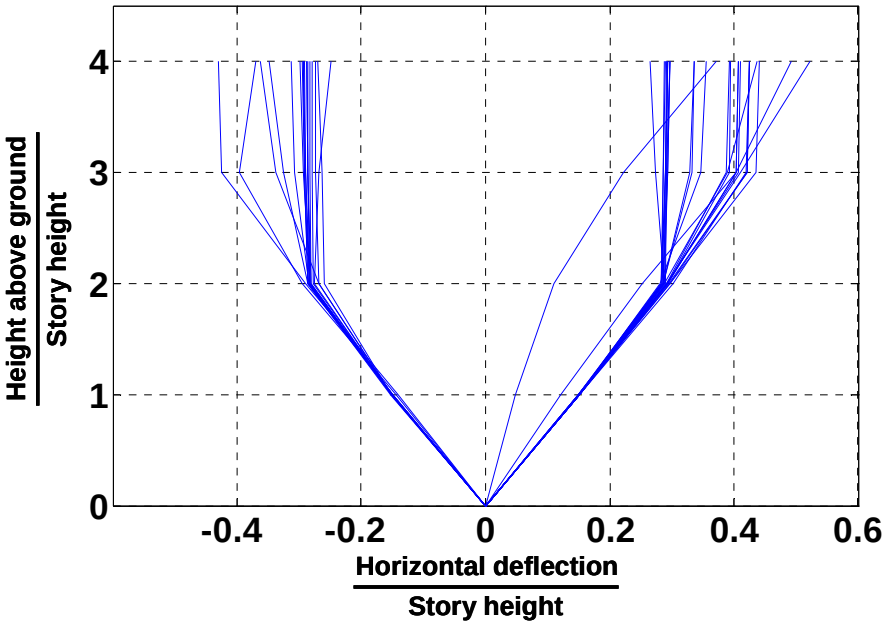

Figure 10.33: Displacement profile at 15% interstory drift of the 12-in. thick conventional masonry uniformly infilled frame from IDA

10.3.4 Uncertainties in evaluation of conventional masonry infilled frames

Uncertainties involved in ATC-63 evaluation of conventional masonry uniformly infilled frames are the same as for the AAC uniformly infilled frame (Section 10.2.4.3), are similarly justified, and are presented in Table 10-7.

Table 10-7: Uncertainties and corresponding lognormal distribution standard deviation parameter for 8-in. and 12-in. thick conventional masonry uniformly infilled frames

Infill Type	Record to record	Design related	Test data	Modeling	Total system uncertainty
Bare frame	0.4	Good (0.3)	Good (0.3)	Fair (0.45)	0.75
AAC, 8-in. thick	0.4	Good (0.3)	Fair (0.45)	Fair (0.45)	0.80
Conventional masonry, 8-in. thick	0.4	Good (0.3)	Fair (0.45)	Fair (0.45)	0.80
Conventional masonry, 12-in. thick	0.4	Good (0.3)	Fair (0.45)	Fair (0.45)	0.80

10.3.5 Probability of collapse at MCE and collapse fragility curve for conventional masonry infilled frames

The probability of collapse at MCE and the collapse fragility curve for the 8-in. and 12-in. thick conventional masonry uniformly infilled frames are evaluated using Methods 1 and 2 (Section 10.2.4.4) and are presented below, including the effects of non-simulated-collapse modes.

10.3.5.1 Method 1

In Table 10-8 are presented the *SSF*, *ACMR* and probability of collapse at MCE computed using Method 1 for the 8-in. and 12-in. thick conventional masonry uniformly infilled frames. In Figure 10.34 are shown the corresponding collapse fragility curves, plotted using *ACMR* as the median, and the total system collapse uncertainty as the lognormal standard deviation parameter, of the lognormal distribution of collapse spectral intensities. The probability of collapse at MCE for the 8-in. and 12-in. thick conventional masonry uniformly infilled frames is obtained as 9.4% and 48%, much larger than the 6.6% obtained for the ATC-63 steel moment frame.

Table 10-8: SSF, ACMR and probability of collapse at MCE for 8-in. and 12-in. thick uniformly infilled frames using Method 1

Infill type	*CMR*	*SSF*	*ACMR*	Probability of collapse at MCE
Bare frame	2.2	1.40	3.10	0.066
AAC, 8-in. thick	2.7	1.25	3.37	0.064
Conventional masonry, 8-in. thick	2.4	1.18	2.87	0.094
Conventional masonry, 12-in. thick	0.9	1.16	1.05	0.480

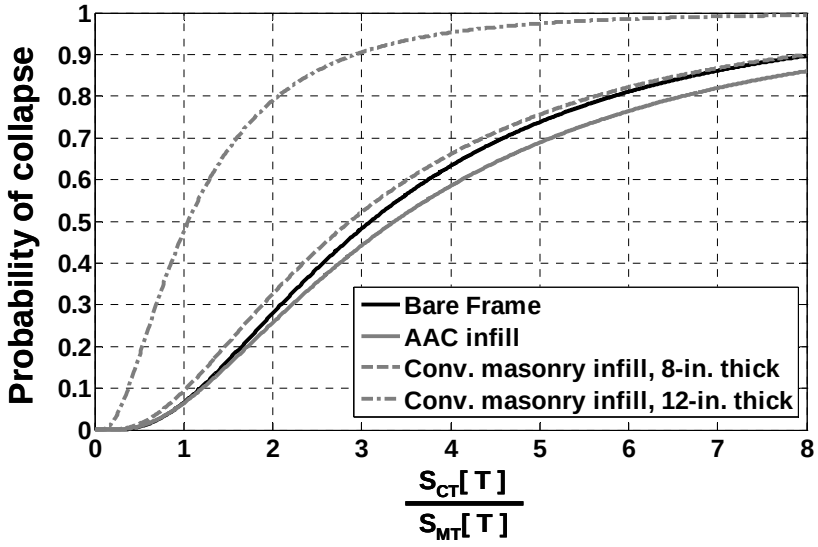

Figure 10.34: Collapse fragility curves using Method 1 for uniformly infilled frames

10.3.5.2 Method 2

In Table 10-9 are presented the *SSF*, *ACMR* and probability of collapse at MCE computed using Method 2 for the 8-in. and 12-in. thick conventional masonry uniformly infilled frames. In Figure 10.35 are shown the resulting collapse fragility curve. The probability of collapse at MCE for the 8-in. and 12-in. thick conventional masonry uniformly infilled frames using Method 2 is obtained as 12% and 49%, again much higher than the 6.6% obtained for the ATC-63 steel moment frame.

Table 10-9: SSF, ACMR and probability of collapse at MCE for uniformly infilled frames using Method 2

Infill type	*CMR*	*SSF*	*ACMR*	Probability of collapse at MCE
Bare frame	2.2	1.40	3.10	0.066
AAC, 8-in. thick	2.4	1.33	3.19	0.074
Conventional masonry, 8-in. thick	2.0	1.29	2.58	0.12
Conventional masonry, 12-in. thick	0.8	1.28	1.03	0.490

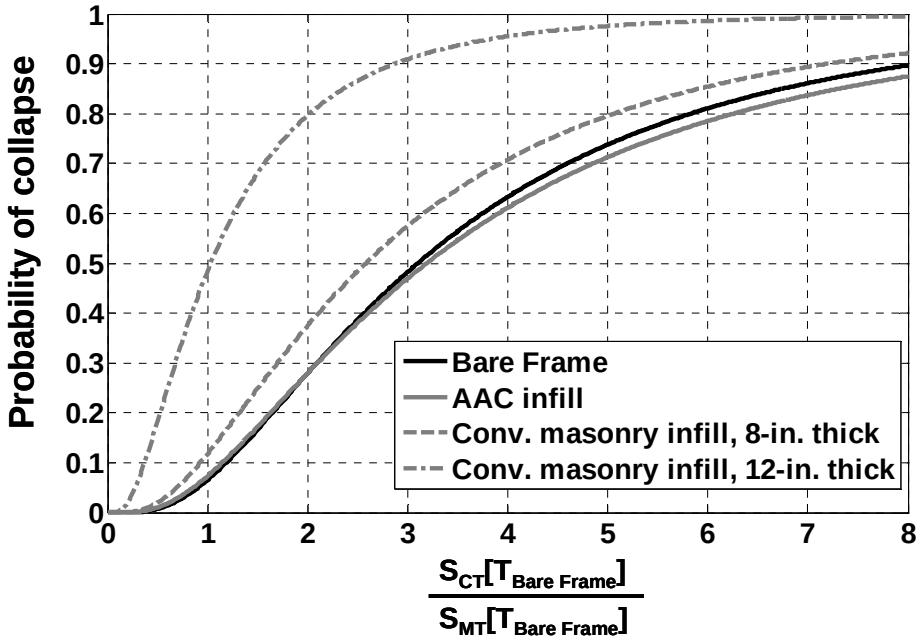

Figure 10.35: Collapse fragility curves using Method 2 for uniformly infilled frames

10.3.5.3 Summary of observations from Methods 1 and 2

As shown in Table 10-8 and Table 10-9, stronger infills generally increase the probability of collapse at MCE, primarily because they cause local shear failure in frame members, which greatly decreases the *CMR*. This is particularly true for 12-in. thick conventional masonry uniformly infilled frame.

10.3.6 Performance at MCE and design level ground motions

In Figure 10.36 and Figure 10.37, respectively, reductions in interstory drift (compared to the ATC-63 steel moment frame) are shown for the 8-in. and 12-in. thick conventional masonry uniformly infilled frames, at MCE- and DBE-level ground motions. Increasing infill strength ratios generally reduce maximum interstory drifts.

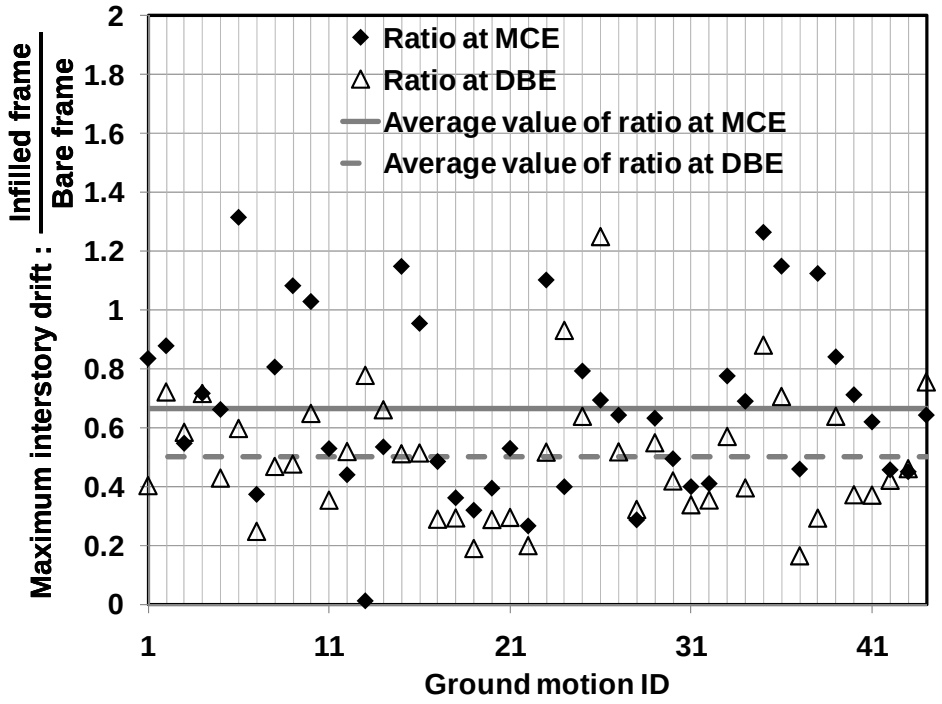

Figure 10.36: Reduction in maximum interstory drifts for 8-in. thick conventional masonry uniformly infilled frame compared to the ATC-63 steel moment frame

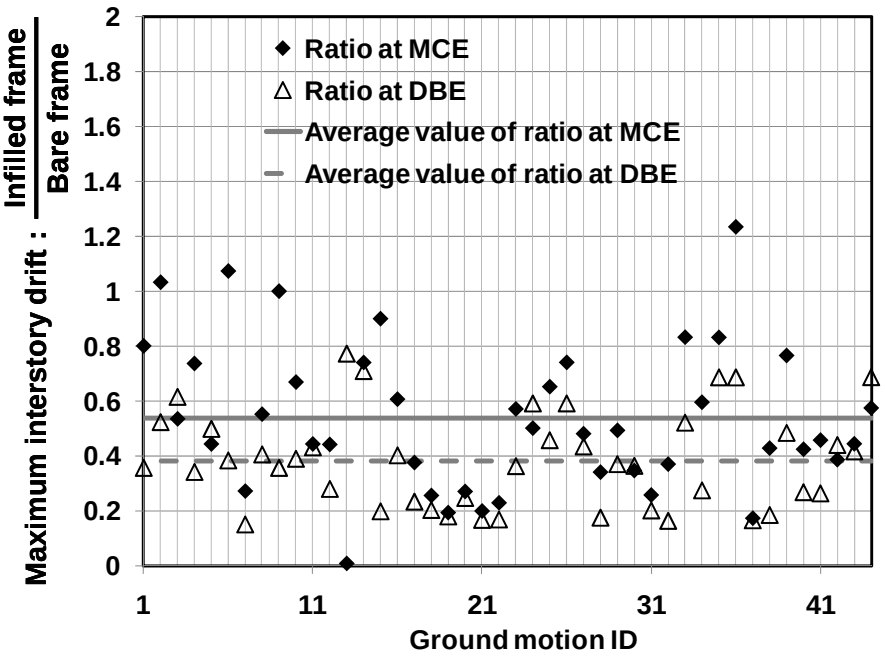

Figure 10.37: Reduction in maximum interstory drift for 12-in. thick conventional masonry uniformly infilled frame compared to the ATC-63 steel moment frame

In Table 10-10 are presented the percentages of ground motions for which local shear failures occurred in 8-in. and 12-in. thick conventional masonry uniformly infilled frames at MCE- and DBE-level ground motions. As before, DBE is taken as 0.6 MCE. Although conventional masonry infills generally reduce maximum interstory drift at these ground motion intensities, they also dramatically increased the percentage of local shear failures, particularly for the 12-in. thick conventional masonry uniformly infilled frame.

Table 10-10: Percentages of ground motions producing local shear failure at DBE- and MCE-level ground motions during IDA

Infill Type	Percentage of local shear failures at DBE	Percentages of local shear failures at MCE
AAC, 8-in. thick	0%	0%
Conventional masonry, 8-in. thick	7%	7%
Conventional masonry, 12-in. thick	41%	84%

10.4 ATC-63 EVALUATION OF ARCHETYPICAL OPEN GROUND STORY FRAMES

In this section, the ATC-63 evaluation is repeated for archetypical open ground story frames (Table 8-6), using the procedures described in Sections 3.6 and 3.7.

10.4.1 Fundamental period of open ground story frames

Because ASCE7-05 does not provide recommendations for computing the fundamental period of open ground story frames, the same procedures are used as in Section 10.2.1 and Section 10.3.1 for uniformly infilled frames.

As before, because the steel moment is the only significant lateral load resisting system of the AAC open ground story frame, the fundamental period of the AAC open ground story frame is determined using the general recommendation of ASCE7-05 for moment frames presented in Section 10.2.1. For 8-in. and 12-in. thick conventional masonry open ground story frames, the fundamental period is determined using the general recommendation of ASCE7-05 for shear walls as presented in Section 10.3.1. For the archetypical open ground story frames, C_u is determined by Table 12.8-1 of ASCE7-05, and is 1.4, the same as for the ATC-63 steel moment frame and the archetypical uniformly infilled frames,.

In Table 10-11, the code-defined limiting fundamental period for the archetypical open ground story frames is compared with the corresponding fundamental period determined analytically. The ASCE7-05 formulas give good estimates for the AAC open ground story frame, but underestimate the fundamental period of the conventional masonry open ground story frames.

Table 10-11: Fundamental period of archetypical open ground story frames

Infill type	Formula used for determination of fundamental period	Code-defined limiting fundamental period (sec)	Fundamental period from analytical model (sec)
Bare frame	Steel moment frame	0.93	1.07
AAC, 8-in. thick	General formula for moment frames	0.56	0.61
Conventional masonry, 8- in. thick	Masonry shear wall	0.17	0.43
Conventional masonry, 12-in. thick	Masonry shear wall	0.14	0.42

10.4.2 Pushover analysis of open ground story frames

Pushover analysis was performed on the archetypical open ground story frames using the same lateral load profile as for the ATC-63 steel moment frame (Section 7.4.2). The pushover curves are presented together in Figure 10.38, and individually in Figure 10.39, Figure 10.40 and Figure 10.41. The latter figures include the corresponding

calculations of over-strength and ductility factors according to the ATC-63 methodology (Section 3.6.2)

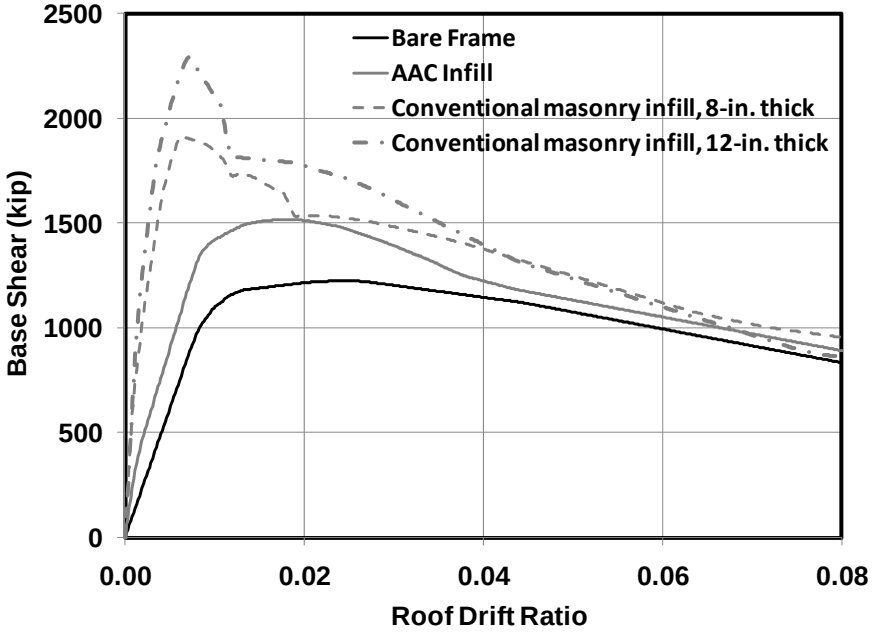

Figure 10.38: Pushover curves for archetypical open ground story frames

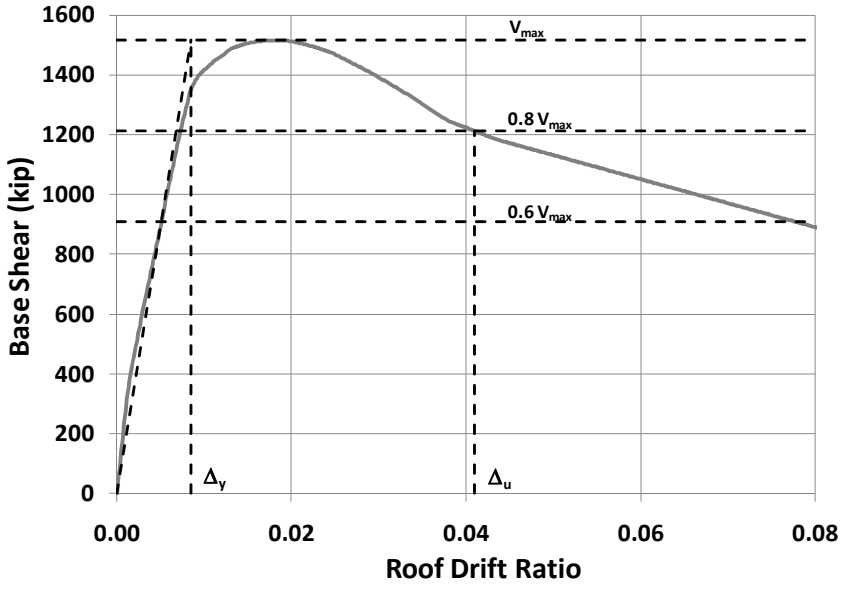

Figure 10.39: Determination of over-strength and ductility factors for the AAC open ground story frame

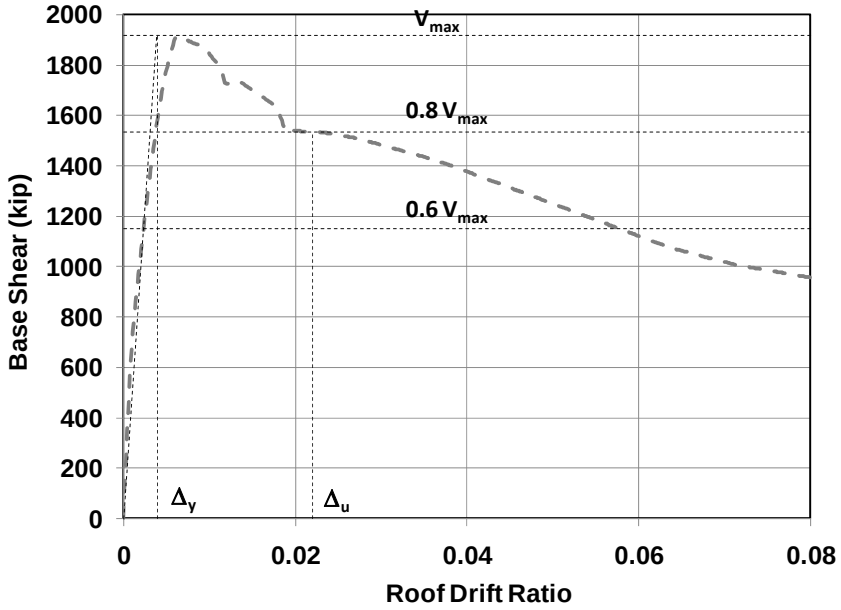

Figure 10.40: Determination of over-strength and ductility factors for the 8-in. thick conventional masonry open ground story frame

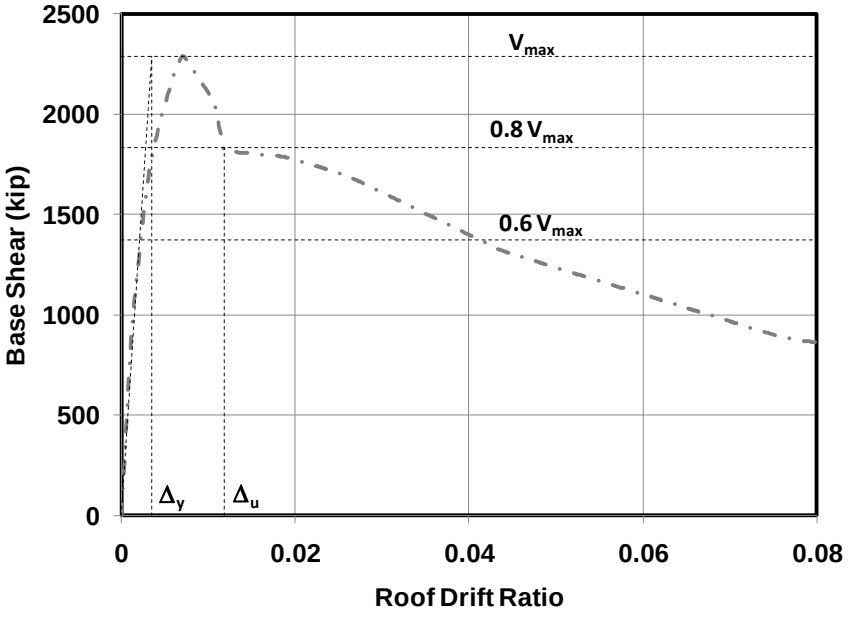

Figure 10.41: Determination of over-strength and ductility factors for the 12-in. thick conventional masonry open ground story frame

In Table 10-12 are presented the stiffness, strength and ductility of the archetypical open ground story frames. Trends are generally similar to those observed for archetypical uniformly infilled frames (Table 10-5): increasing infill strength ratios cause increased initial stiffness and strength, while decreasing ductility. The lone exception was the 8-in. thick conventional masonry open ground story frame, whose ductility was greater than that of the AAC open ground story frame. This is because the yield roof drift ratio (determined using the recommendations of the ATC-63 methodology) decreased much more than the ultimate roof drift ratio for the 8-in. thick conventional masonry open ground story frame. In contrast, the yield roof drift ratio did not decrease much more than the ultimate roof drift ratio for the AAC open ground story frame .

Table 10-12: Stiffness, strength and ductility of open ground story frames from pushover analysis

Infill Type	Initial stiffness with respect to ATC-63 steel moment frame	Strength divided by design base shear	Displacement ductility
Bare frame	1.0	4.0	6.2
AAC, 8-in. thick	2.4	4.9	4.8
Conventional masonry, 8-in. thick	6.0	6.2	5.6
Conventional masonry, 12-in. thick	6.5	7.3	3.3

10.4.2.1 Failure mechanism and displaced profile of open ground story frames

In Figure 10.42, the displacements profiles of the ATC-63 steel moment frame and archetypical open ground story frames are compared at the ultimate roof drift ratio of the ATC-63 steel moment frame (Section 7.4.2). In Figure 10.43 and Figure 10.44 are shown the plastic rotations in beam and column hinges, respectively, during the pushover analysis of the archetypical open ground story frames.

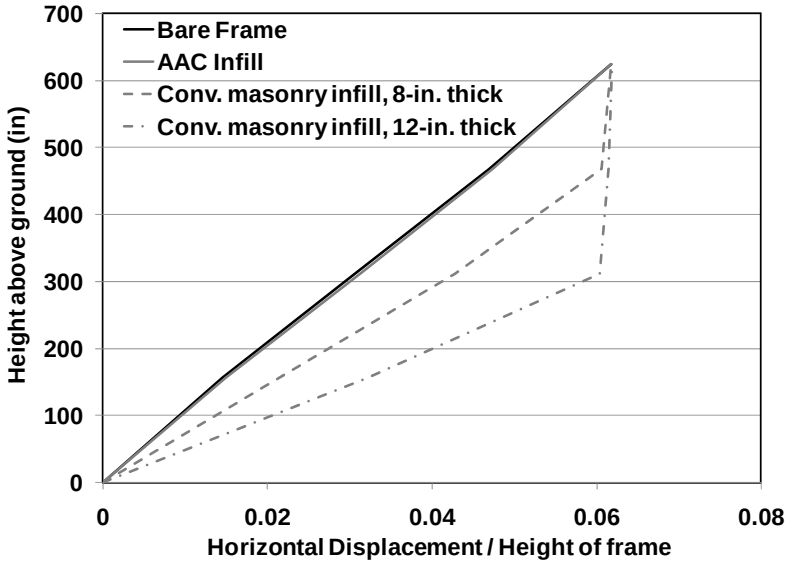

Figure 10.42: Displacement profiles of ATC-63 steel moment frame and archetypical open ground story frames from pushover analysis

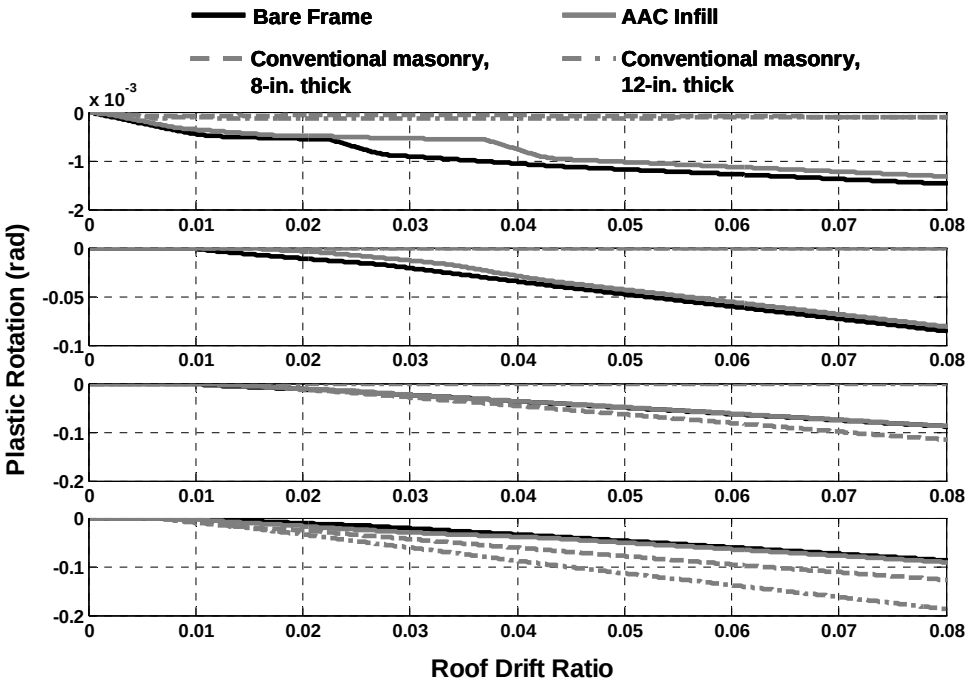

Figure 10.43: Plastic rotation in beam hinges during pushover analysis of archetypical open ground story frames

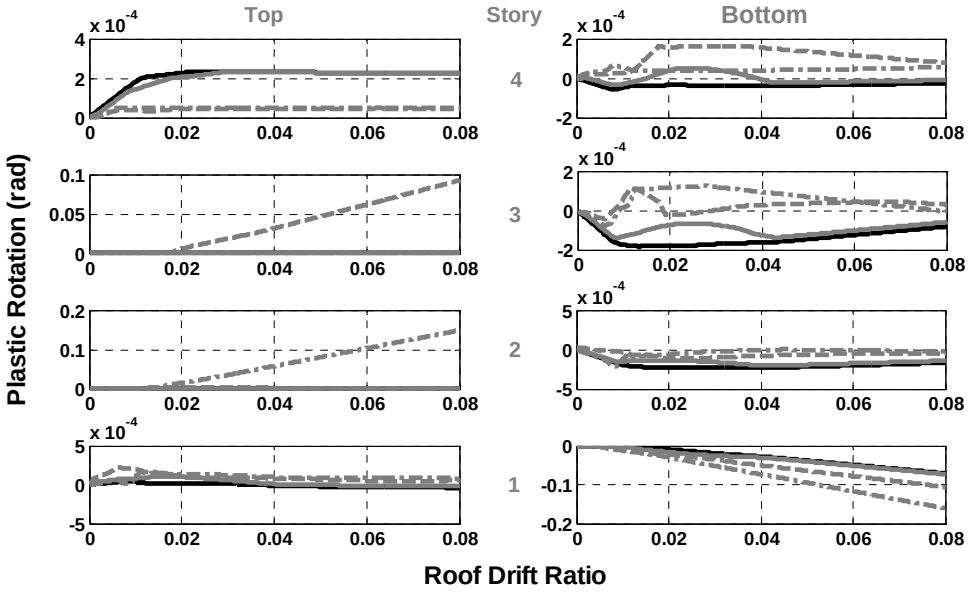

Figure 10.44: Plastic rotation in columns during pushover analysis of archetypical open ground story frames

Using the observations of plastic rotation in hinges of beams and columns and the displacement profile, the failure mechanisms of the archetypical open ground story frames can be determined. In Figure 10.6 the failure mechanism of the AAC open ground story frame is seen to be the same as that of the ATC-63 steel moment frame. The failure mechanisms of 8-in. and 12-in. thick conventional masonry open ground story frames are the same as those of the corresponding archetypical uniformly infilled frames, as shown in Figure 10.21 and Figure 10.22, respectively.

An important observation is that the failure mechanisms of the ATC-63 steel moment frame and AAC open ground story frame are almost identical. This means that even with an open ground story, it is possible to design infills that will not change the native failure mechanism of the frame. For increasing infill strength ratios, the failure mechanism becomes progressively concentrated in the lower stories of the frame. For an infill strength ratio of 1.0 (12-in. thick conventional masonry open ground story frame), failure mechanism is concentrated in lower half of frame, similar to what was also observed in Section 10.3.2.1 for archetypical conventional masonry uniformly infilled frames. In Figure 10.43 and Figure 10.44, this concentration of failure mechanism is shown to increase the plastic rotation demand in the beams and columns in the bottom stories of the frame. Also, contrary to popular belief, a ground story mechanism did not form even in the case of 12-in. thick conventional masonry open ground story frame, corresponding to an infill strength ratio of 1.01. Further studies using pushover analysis showed that a ground story mechanism would form at infill strength ratios above about 1.1.

10.4.2.2 Effect of conventional masonry infills on axial forces in columns (open ground story)

In Figure 10.45 are shown the variation in axial forces in columns of archetypical open ground story frames during pushover analysis. These are similar to those presented in Section 10.3.2.2 for the corresponding uniformly infilled frames, except of course at

the ground story, which is not infilled in the open ground story case. In Figure 10.7 are shown the active equivalent struts during pushover analysis of the archetypical open ground story frames, and the definitions of Column Lines 1, 3 and 5.

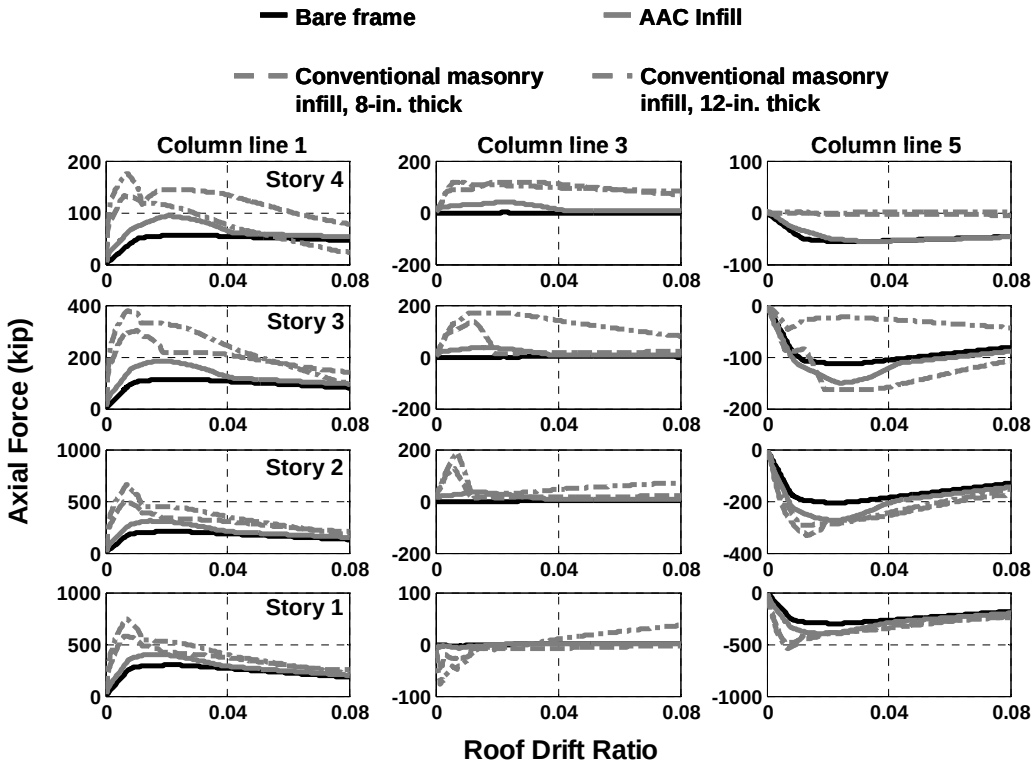

Figure 10.45: Axial forces in columns of archetypical open ground story frames during pushover analysis

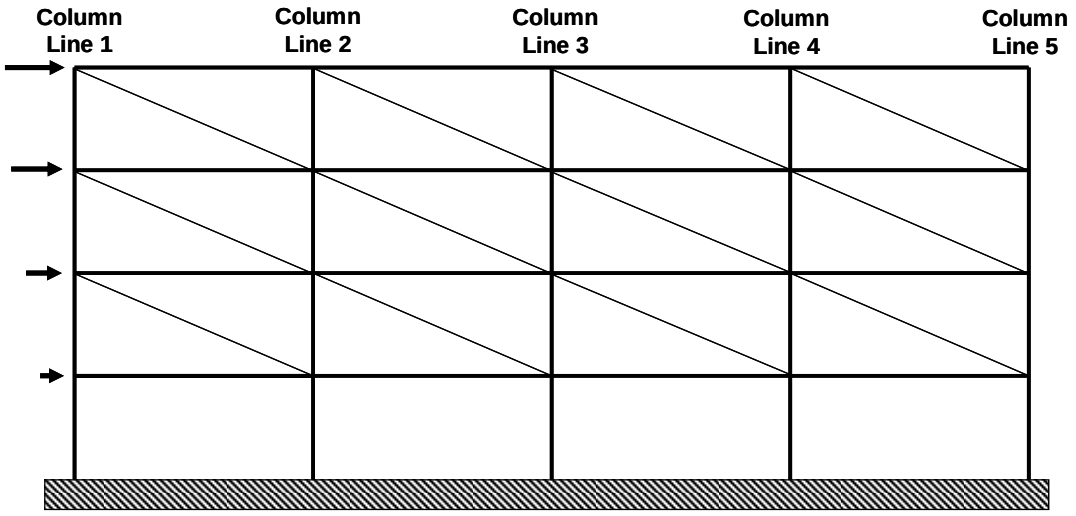

Figure 10.46: Active equivalent struts during pushover analysis of archetypical open ground story frames

For the AAC open ground story frame, the maximum increase in column axial forces between adjacent stories in Column Lines 1 and 5, relative to the ATC-63 steel moment frame, is consistent with the vertical component of the axial strength of the infill, 40 kips. The maximum increase in axial force of ground story columns compared to the ATC-63 steel moment frame is about 105 kip in Column Line 1 and 95 kip in Column Line 5. For Column Line 3, the maximum axial force in columns is nearly the same at all stories, except at the ground story, where it is almost zero. This is because opposing axial forces from equivalent struts framing from adjacent bays into a beam-column joint (Figure 10.7) tend to neutralize each other, except at the top and ground stories.

For 8-in. and 12-in. thick conventional masonry open ground story frames, axial forces in the columns of Column Lines 1 and 5 increase similarly to those of the corresponding archetypical conventional masonry uniformly infilled frames. Column axial forces generally increase from top story to bottom. However, the increase between two adjacent stories (relative to the ATC-63 steel moment frame) is consistently less than the vertical component of the axial strength of the equivalent strut representing the infill.

The reasons for this are same as those presented for archetypical conventional masonry uniformly infilled frames.

The maximum increase in axial force in the exterior columns of the AAC open ground story frame relative to the ATC-63 steel moment frame is 105 kip (ground story column in Column Line 1), or 3.5% of the axial capacity of the bottom story column. For the 8-in. and 12-in thick conventional masonry open ground story frames, the maximum increases are 290 kip and 450 kip respectively, about 9.5% and 15% of the axial capacity of the column. Therefore, the axial forces in exterior columns for conventional masonry open ground story frames increase significantly compared to the axial capacities of those columns, and may be difficult to handle in design. Increases in axial forces in interior columns are not significant.

10.4.2.3 Non-simulated collapse modes for open ground story frames

Local shear failure of frame members due to frame-infill interaction forces was checked from the results of the pushover analysis of archetypical open ground story frames. For all infill cases, local shear failure in frame members did not occur, and ductility of the archetypical open ground story frame from pushover analysis remained the same as that determined using the global sidesway collapse mechanism.

10.4.3 Incremental dynamic analysis of open ground story frames

In Figure 10.47, Figure 10.48 and Figure 10.49 are shown the results from IDA for the archetypical open ground story frames.

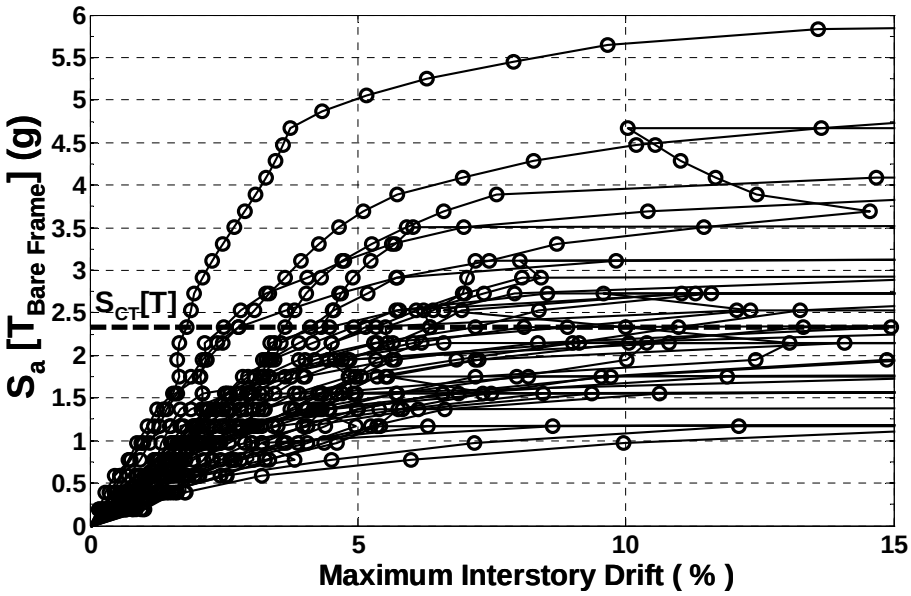

Figure 10.47: IDA results for the AAC open ground story frame

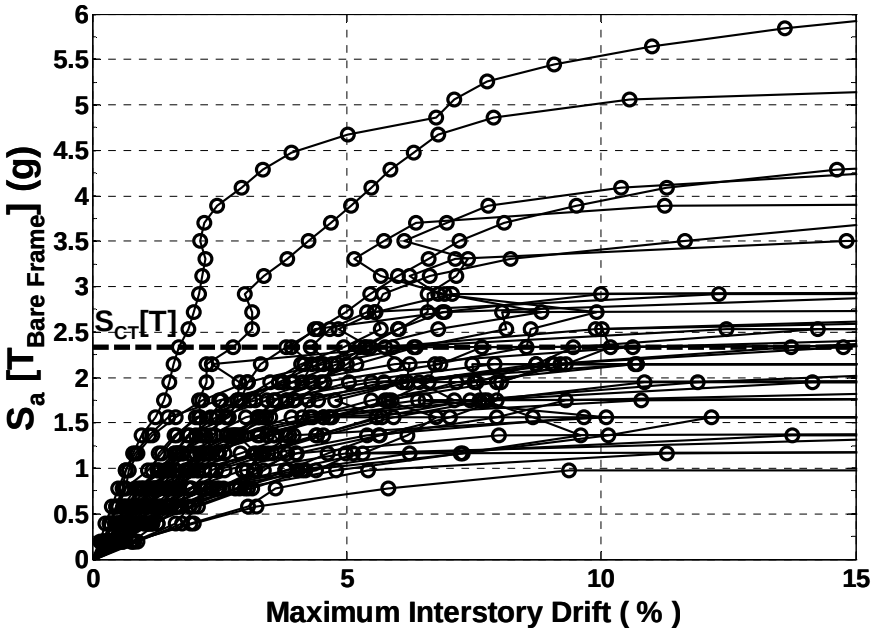

Figure 10.48: IDA results for the 8-in. thick conventional masonry open ground story frame

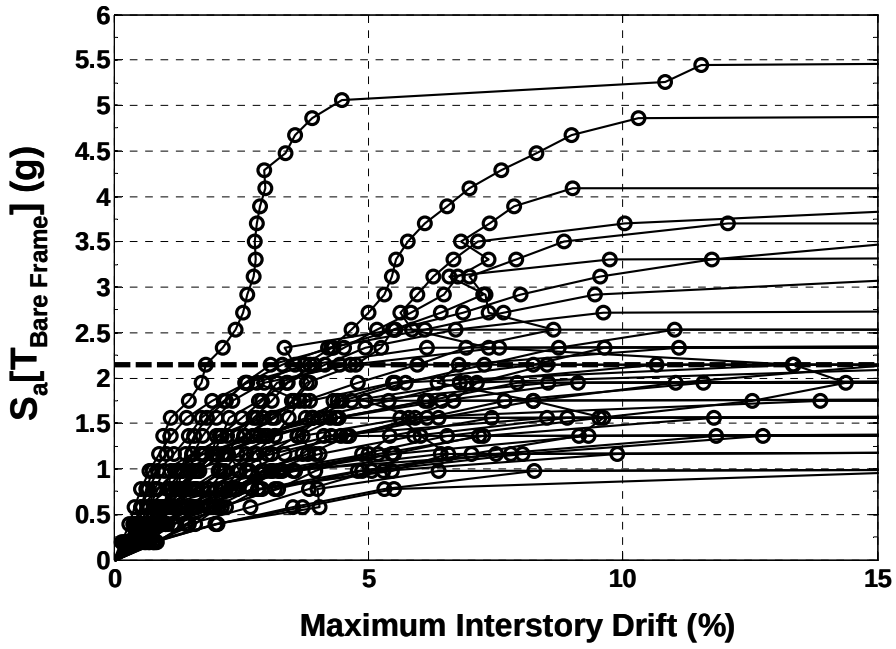

Figure 10.49: IDA results for the 12-in. thick conventional masonry open ground story frame

In Table 10-13 are presented the median collapse spectral intensity and the corresponding *CMR* determined at the fundamental period of the ATC-63 steel moment frame from these analyses. Stronger infills lead to greater decreases in the *CMR* for open ground story frames as compared to the corresponding uniformly infilled frames: constant at 2.4 for AAC infills; decreasing from 2.6 to 2.4 for 8-in. thick conventional masonry infills; and decreasing from 2.7 to 2.2 for 12-in. thick conventional masonry infills. These decreases are caused by increasing formation of story mechanisms.

Table 10-13: CMR for the archetypical open ground story frames, with and without non-simulated collapse modes

Infill type	Considering only sidesway collapse		Including local shear failure as non-simulated collapse mode	
	Median collapse spectral intensity at fundamental period of ATC-63 steel moment frame	***CMR***	**Median collapse spectral intensity at fundamental period of ATC-63 steel moment frame**	***CMR***
Bare frame	2.14	2.2	2.14	2.2
AAC, 8-in. thick	2.34	2.4	2.34	2.4
Conventional masonry, 8- in. thick	2.34	2.4	2.34	2.4
Conventional masonry, 12-in. thick	2.14	2.2	1.56	1.6

In Figure 10.50, Figure 10.51 and Figure 10.52 are shown the ratios of collapse spectral intensities of the archetypical open ground story frames to those of the ATC-63 steel moment frame, for the 44 ground motions of the ATC-63 suite. Comparison of Figure 10.50 and Figure 10.10 suggests that AAC infills with an open ground story are even more consistent than uniform AAC infills in improving the collapse capacity of the ATC-63 steel moment frame. Comparison of Figure 10.51 with Figure 10.26, and comparison of Figure 10.52 with Figure 10.27, suggests that in contrast, conventional masonry infills with an open ground story do not consistently improve the collapse capacity of the ATC-63 steel moment frame. This is becomes even more true as the infill thickness increases.

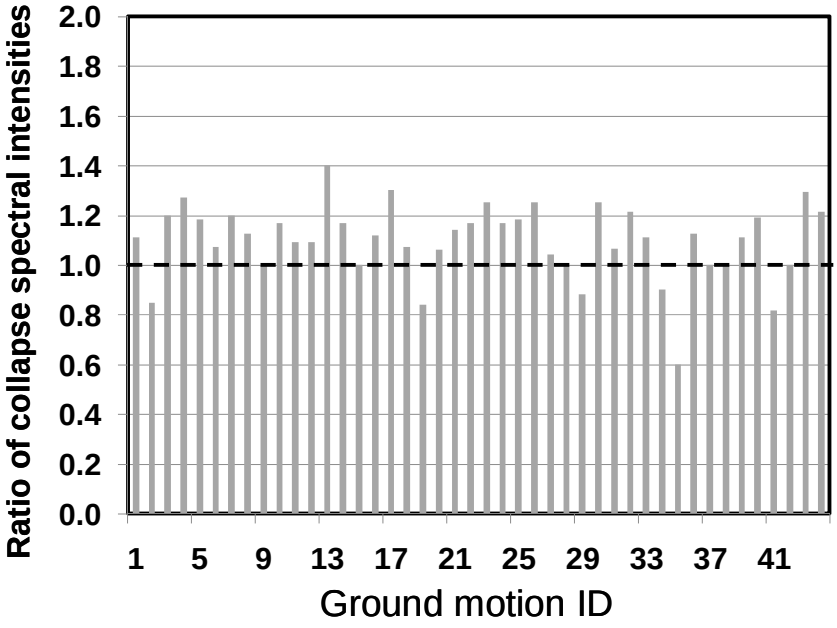

Figure 10.50: Ratios of collapse spectral intensities of AAC open ground story frame to those of ATC-63 steel moment frame for 44 ground motions of ATC-63 suite

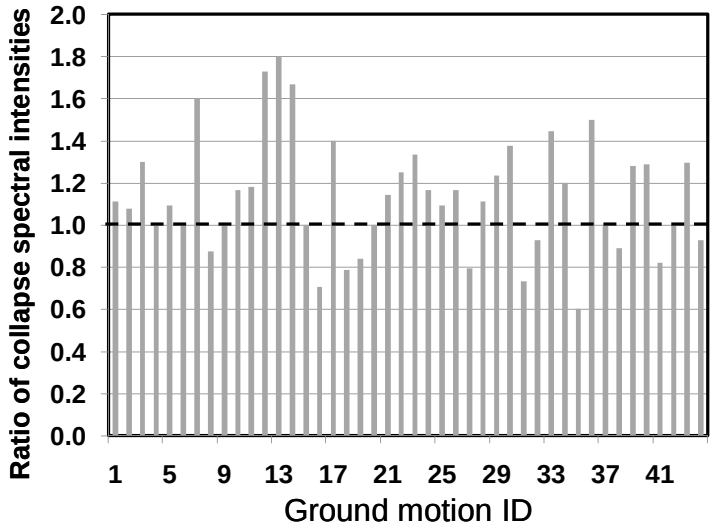

Figure 10.51: Ratios of collapse spectral intensities of 8-in. thick conventional masonry open ground story frame to those of ATC-63 steel moment frame for 44 ground motions of ATC-63 suite

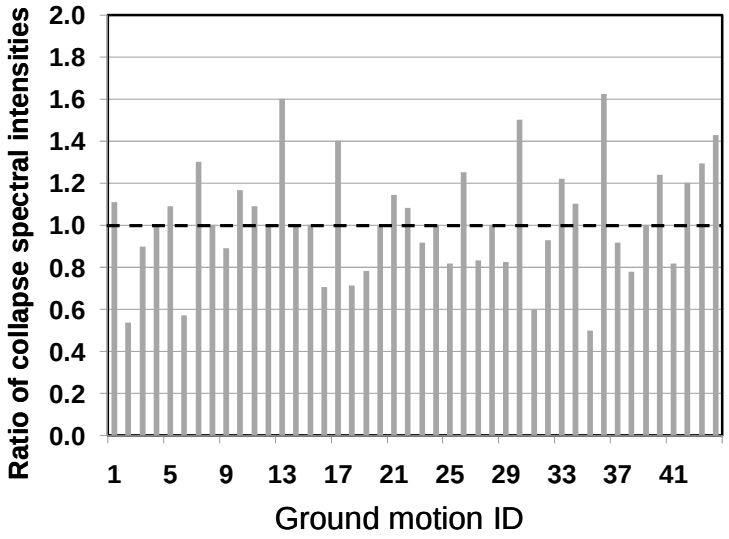

Figure 10.52: Ratios of collapse spectral intensities of 12-in. thick conventional masonry open ground story frame to those of ATC-63 steel moment frame for 44 ground motions of ATC-63 suite

10.4.3.1 Non-simulated collapse modes

Non-simulated collapse modes are not detected for the AAC open ground story frame, and hence the IDA curves considering non-simulated collapse modes remain the same as shown in Figure 10.47. In Figure 10.53 and Figure 10.54 are shown results from IDA considering non-simulated collapse modes for the 8-in. 12-in. thick conventional masonry open ground story frames, respectively. Table 10-13 presents the corresponding *CMR*. For the 8-in. conventional masonry infill with an open ground story, consideration of non-simulated collapse did not change the previous *CMR* of 2.4, even though non-simulated collapse occurred in 9 out of 44 ground motions of the ATC-63 suite. For the 12-in. thick conventional masonry infill with an open ground story, consideration of non-simulated collapse modes decreased the *CMR* from 2.2 to 1.6.

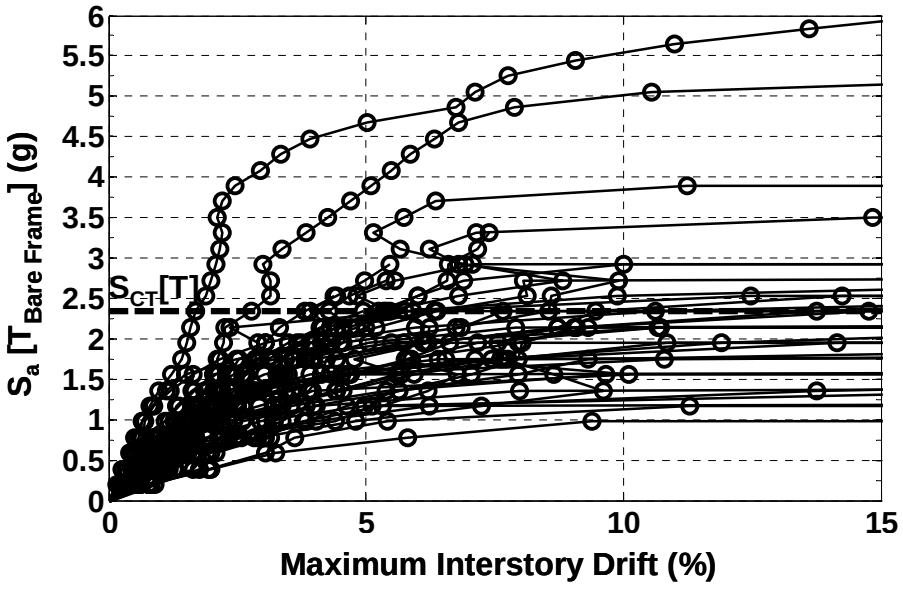

Figure 10.53: IDA results considering non-simulated collapse for open ground story frame with 8-in. thick conventional masonry infill

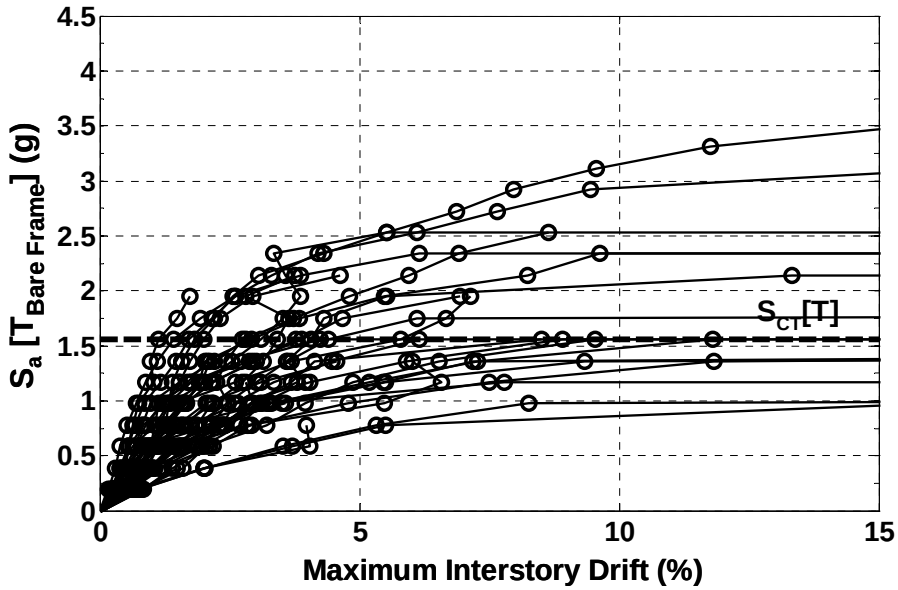

Figure 10.54: IDA results considering non-simulated collapse for open ground story frame with 12-in. thick conventional masonry infill

For the 8-in. thick conventional masonry open ground story frame, local shear failure occurred only in the second- and third-story columns. For the 12-in. thick conventional masonry open ground story frame, local shear failure generally occurred in the second- and third story columns, and sometimes also in the fourth-story columns. This is similar to what was observed for archetypical conventional masonry uniformly infilled frames.

However, the decrease in *CMR* due to local shear failures is not as severe for the open ground story frames as for the uniformly infilled frames. One reason for this is that the open ground story frames have no infill at the ground story, where story shear is highest. For this same reason, local shear failure generally occurs later in the IDA for the conventional masonry open ground story frames than for the conventional masonry uniformly infilled frames. Another reason is that the archetypical conventional masonry open ground story frames generally have a longer fundamental period than the corresponding conventional masonry uniformly infilled frames, probably resulting in lower spectral acceleration demand and lower base shear.

In Figure 10.55 and Figure 10.56 are shown the ratios of collapse spectral intensities, considering non-simulated collapse modes, of the 8-in. and 12-in. thick conventional masonry open ground story frames divided by those of the ATC-63 steel moment frame for the 44 ground motions of the ATC-63 suite. Since non-simulated collapse modes were not detected for the AAC open ground story frame, those ratios are identical to those in Figure 10.50. As with conventional masonry uniformly infilled frames, consideration of non-simulated collapse modes leads to less-consistent improvement in collapse spectral intensities in conventional masonry open ground story frames, compared with the ATC-63 steel moment frame.

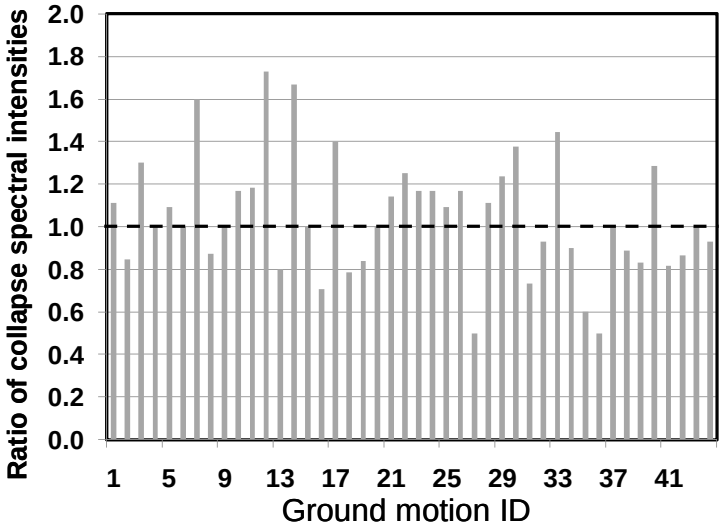

Figure 10.55: Ratios of collapse spectral intensities (including non-simulated collapse) of 8-in. thick conventional masonry open ground story frame and ATC-63 steel moment frame

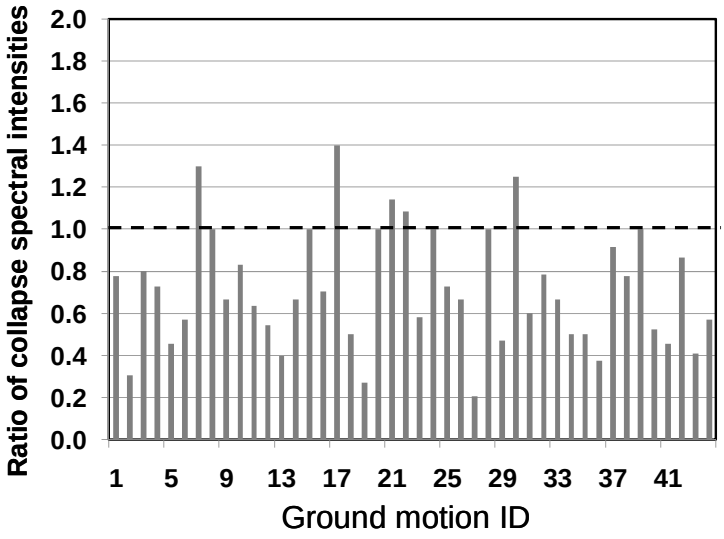

Figure 10.56: Ratios of collapse spectral intensities (including non-simulated collapse) of the 12-in. thick conventional masonry open ground story frames and ATC-63 steel moment frame

10.4.3.2 Displacement profile at collapse during IDA

In Figure 10.57, Figure 10.58 and Figure 10.59 are shown, respectively, the displacement profiles of the AAC open ground story frame and the 8-in. and 12-in. thick conventional masonry open ground story frames, when interstory drift exceeded 15% for each of the 44 ground motions of the ATC-63 suite during IDA.

For the AAC open ground story frame, the failure mechanism is generally distributed over the entire height of the frame, except for a few cases in which it is limited to the lower three stories. This is similar to that observed for the AAC uniformly infilled frame (Figure 10.12).

For the 8-in. thick conventional masonry open ground story frame, the failure mechanism is limited in most cases to the lower three or two stories. This is similar to the 8-in. thick conventional masonry uniformly infilled frame (Figure 10.32), but with more cases in which the failure mechanism is concentrated in the bottom two stories.

The displaced profile of the 12-in. thick conventional masonry open ground story frame corroborates the empirical observation that infilled frames with an open ground story often fail in real earthquakes by formation of a weak ground story mechanism. This behavior did not occur, however, for 8-in. thick conventional masonry open ground story frame. The difference lies in the infill strength ratio, which is 1.01 for the 12-in. infill, and 0.68 for the 8-in. infill. Infill strength ratios close to 1.0 seem almost to ensure the formation of weak ground story mechanisms. Interestingly, this was not captured in Section 10.3.2 for the pushover analysis of the same 12-in. infill.

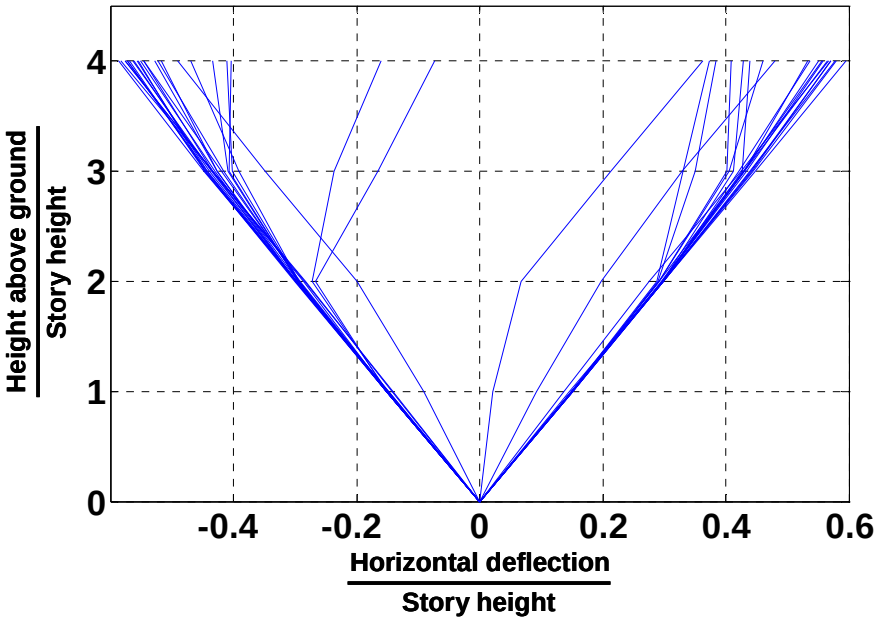

Figure 10.57: Displaced profiles of AAC open ground story frame at a maximum interstory drift of 15% during IDA

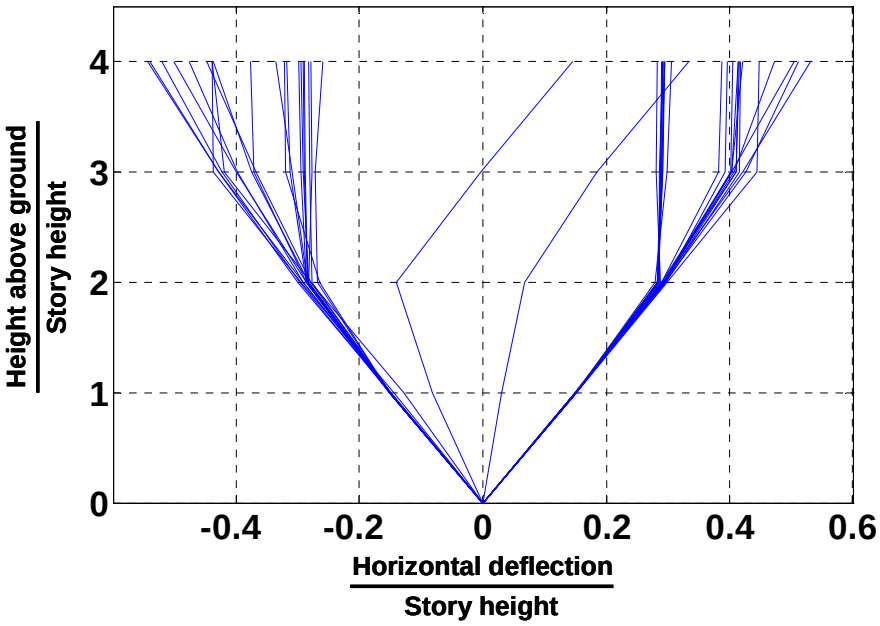

Figure 10.58: Displaced profiles of 8-in thick conventional masonry open ground story frame at a maximum interstory drift of 15% during IDA

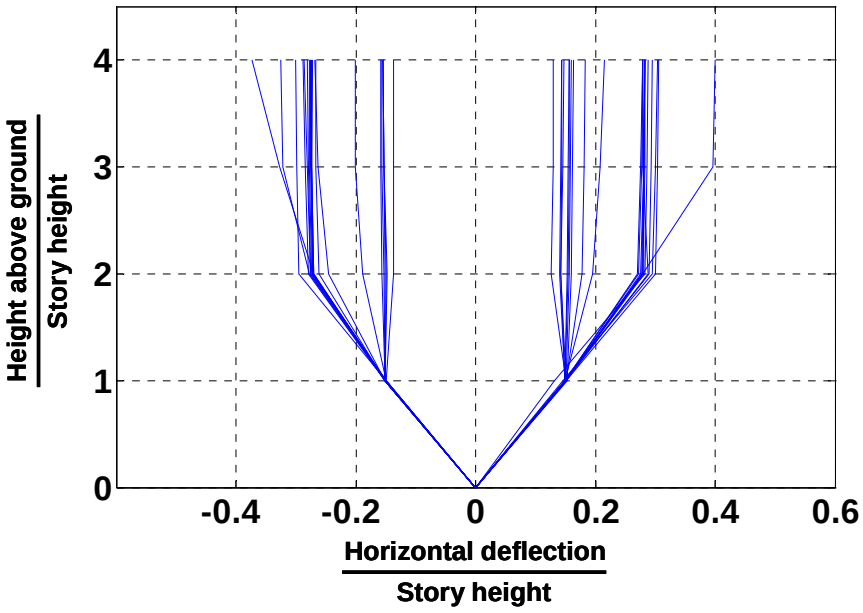

Figure 10.59: Displaced profiles of 12-in thick conventional masonry open ground story frame at a maximum interstory drift of 15% during IDA

10.4.4 Uncertainties in evaluation of open ground story frames

Uncertainties involved in collapse capacity of the archetypical open ground story frames are the same as for the archetypical uniformly infilled frames, as presented and explained in Section 10.3.4.

10.4.5 Probability of collapse at MCE and collapse fragility curve

The probability of collapse at MCE and the collapse fragility curve for the archetypical open ground story frames are evaluated using both methods described in Section 10.2.4.4, including non-simulated collapse modes in the evaluation of collapse spectral intensities. Computations and results using each method are presented below.

10.4.5.1 Method 1

In Table 10-14 are presented the *SSF*, *ACMR* and probability of collapse at MCE for the open ground story frames, computed using Method 1. In Figure 10.60 depicts the corresponding collapse fragility curve, plotted using the *ACMR* and the total system collapse uncertainty as the median and the lognormal distribution standard deviation parameter, respectively.

Table 10-14: SSF, ACMR and probability of collapse at MCE using Method 1 for archetypical open ground story frames

Infill type	*CMR*	*SSF*	*ACMR*	Probability of collapse at MCE
Bare frame	2.2	1.40	3.10	0.066
AAC, 8-in. thick	2.7	1.27	3.42	0.062
Conventional masonry, 8-in. thick	2.9	1.29	3.76	0.049
Conventional masonry, 12-in. thick	1.8	1.22	2.20	0.160

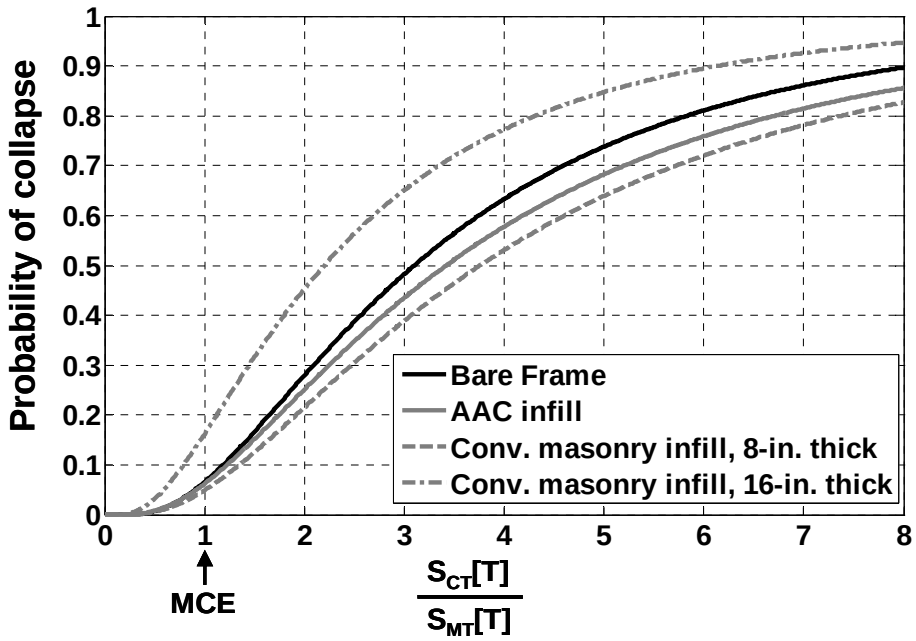

Figure 10.60: Collapse fragility curves for archetypical open ground story frames using Method 1

The probability of collapse at MCE of the AAC open ground story frame is evaluated using Method 1 as 6.2%. This is slightly less than for the ATC-63 steel moment frame (6.6%), even though test data related uncertainty was rated more critically for infilled frames. This is even less than that the probability of collapse of the corresponding AAC uniformly infilled frame, which was obtained as 6.4% using Method 1. This is because of the increased ductility and fundamental period of the AAC open ground story frame compared to AAC uniformly infilled frame, which resulted in a higher *SSF* and corresponding higher *ACMR*.

The probability of collapse at MCE of the 8-in. thick conventional masonry open ground story frame was obtained as 0.049. This is less than that of the ATC-63 steel moment frame (6.6%) and also less than that of the corresponding 8-in. thick conventional masonry uniformly infilled frame (9.6%). It is also less than that of the AAC open ground story frame (6.2%). This is due to the higher *CMR* obtained using

Method 1 by evaluating spectral intensities at the fundamental period of the infilled frame and also due to higher ductility from the pushover analysis, which gave a higher *SSF* and also a higher *ACMR*. The 8-in. thick conventional masonry open ground story frame had the least probability of collapse at MCE of all the archetypical infilled steel moment frames evaluated in this dissertation.

The probability of collapse at MCE for 12-in. thick conventional masonry open ground story frame is 16%, the highest among the archetypical open ground story frames and higher than that of the ATC-63 steel moment frame. It is lower, however, than that obtained for the corresponding 12-in. thick conventional masonry uniformly infilled frame (48%), mainly because the uniformly infilled frames experienced a drastic reduction in *CMR* due to non-simulated collapse modes.

10.4.5.2 Method 2

In Table 10-15 are presented the *SSF*, *AMCR* and probability of collapse at MCE computed using Method 2 for the archetypical open ground story frames. In Figure 10.61 is shown the resulting collapse fragility curve. The results using Method 2 are similar to those using Method 1. The only exception is that the probability of collapse at MCE for the AAC open ground story frame and the 8-in. thick conventional masonry open ground story frame, 0.072 and 0.071 respectively, are slightly greater than that of the ATC-63 steel moment frame (6.6%).

Table 10-15: SSF, ACMR and probability of collapse at MCE using Method 2 for archetypical open ground story frames

Infill type	*CMR*	*SSF*	*ACMR*	Probability of collapse at MCE
Bare frame	2.2	1.40	3.10	0.066
AAC, 8-in. thick	2.4	1.34	3.22	0.072
Conventional masonry, 8-in. thick	2.4	1.35	3.23	0.071
Conventional masonry, 12-in. thick	1.6	1.31	2.10	0.180

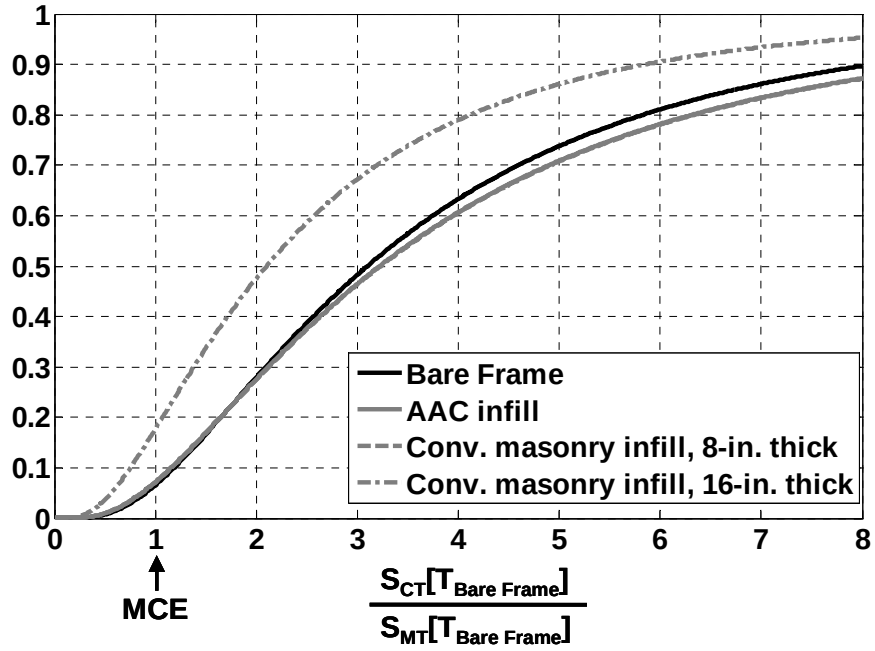

Figure 10.61: Collapse fragility curves for archetypical open ground story frames by Method 2

10.4.5.3 Qualitative observations based on the foregoing

The above results obtained above lead to a useful qualitative observation. Contrary to what might be generally expected, and also contrary to anecdotal evidence from real earthquakes, the probability of collapse at MCE of archetypical open ground story frames is generally less than that of corresponding archetypical uniformly infilled frames. There are two reasons for this. The first reason is that ductility from pushover analysis is greater for open ground story frames than for the corresponding uniformly infilled frames, resulting in greater *SSF* and *ACMR* for the open ground story frames. The second reason is that the reduction in *CMR* due to consideration of local shear failure as a non-simulated collapse mode is less for open ground story frames, than for uniformly infilled frames.

10.4.6 Performance at ground motion intensities corresponding to MCE and DBE

The reduction in maximum interstory drift for the archetypical open ground story frames relative to the ATC-63 steel moment frame at spectral intensities corresponding to MCE and DBE is now computed, as for the archetypical uniformly infilled frames. Results are presented in Figure 10.62 for the AAC open ground story frame, and in Figure 10.63 and Figure 10.64 for the 8-in and 12-in. thick conventional masonry open ground story frames, respectively.

The AAC open ground story frame and the 8-in. thick conventional masonry open ground story frame have much lower interstory drift than the ATC-63 steel moment frame. For the AAC open ground story frame, the average reduction is about 20% at MCE as well as DBE, and for the 8-in. thick conventional masonry open ground story frame, the average reduction is 20% at MCE, and 30% at DBE (taken as 0.6 MCE). For the 12-in. thick conventional masonry open ground story frame, in contrast, interstory drifts are higher in many cases than for the ATC-63 steel moment frame. This is due primarily to the increasing formation of weak ground story mechanisms. It reinforces the previous observation that an infill strength ratio of about 1.0 probably marks the onset of

degradation in performance of open ground story frames due to formation of a weak ground story.

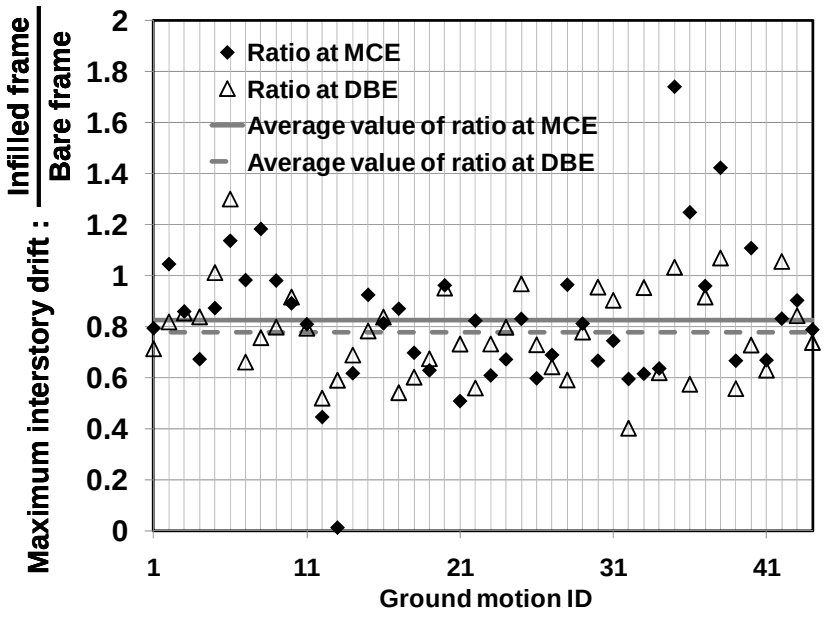

Figure 10.62: Reduction in maximum interstory drift for the AAC open ground story frame compared to ATC-63 steel moment frame

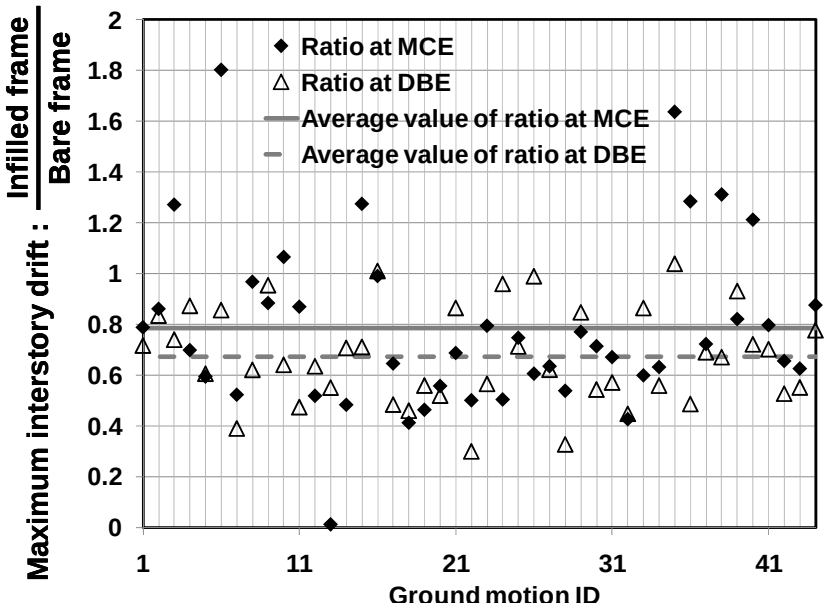

Figure 10.63: Reduction in maximum interstory drift for the 8-in. thick conventional masonry open ground story frame compared to ATC-63 steel moment frame

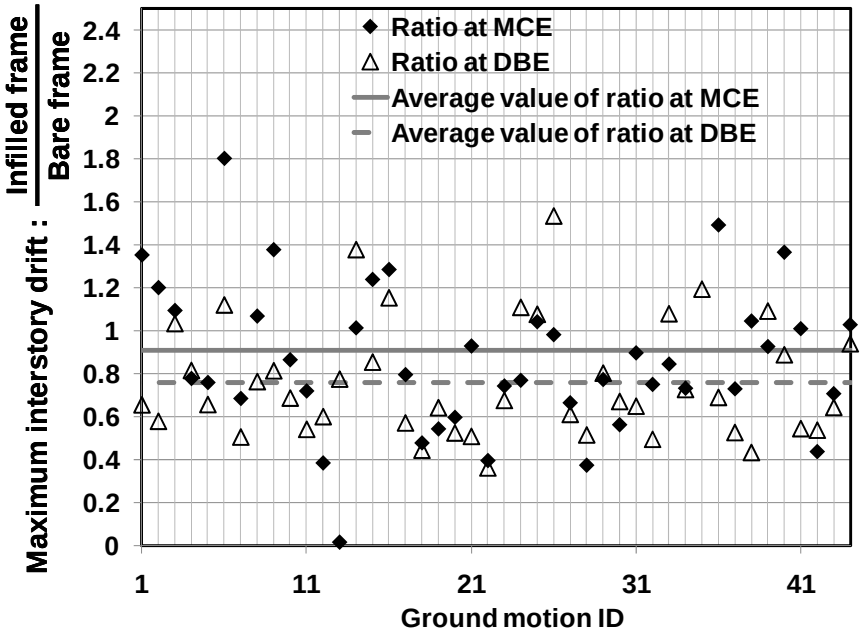

Figure 10.64: Reduction in maximum interstory drift for the 12-in. thick conventional masonry uniformly open ground story frame compared to ATC-63 steel moment frame

In Table 10-16 is presented the percentage of local shear failures in archetypical open ground story frames due to frame-infill interaction forces at ground motion intensities corresponding to MCE and DBE. The percentages of local shear failures are lower for open ground story frames than for corresponding uniformly infilled frames.

Table 10-16: Percentages of shear failure in open ground story frames at ground motion intensities corresponding to MCE and DBE during IDA

Infill Type	Percentage of shear failures at 0.6 MCE	Percentage of shear failures at MCE
AAC, 8-in. thick	0%	0%
Conventional masonry, 8-in. thick	0%	5%
Conventional masonry, 12-in. thick	5%	20%

10.5 CONFIDENCE IN RESULTS FROM ATC-63 EVALUATION OF AAC-INFILLED FRAMES

The analytical model for hysteretic behavior of AAC infills is developed in Section 6.4.2 by calibrating the Ibarra-Krawinkler hysteretic model to experimental results from only the single AAC-infilled frame specimen described in Chapter 4. Even though the model was calibrated using only one specimen, the calibration is believed to be reliable, for several reasons. First, the initial monotonic stiffness of the AAC infill is taken as twice the stiffness obtained from draft MSJC equations, which is consistent with experimental data reported in Flanagan (2001) for other types of infills. Second, the cracking strength of AAC infills is taken one-half the capping strength, which is generally consistent with published research (Section 2.3.3 and Section 6.4.3.2). Third, the values of the hysteretic pinching parameters (k_f and k_d in Figure 6.7) seem realistic, and are comparable to those used by other researchers (Panagiotakos 1993). Variations in their values are not expected to significantly change results from ATC-63 evaluation of AAC-infilled frames.

In contrast to these aspects of the calibration, the assumption for the slope of the descending branch of the backbone curve, characterized by α_c in Figure 6.8, is arbitrary. To determine the sensitivity of the results from ATC-63 evaluation to this assumption, a second IDA is performed for the AAC uniformly infilled frame, using a descending branch with a slope twice that used for the first IDA of Section 10.2.4. In Figure 10.65, the two descending branches are compared.

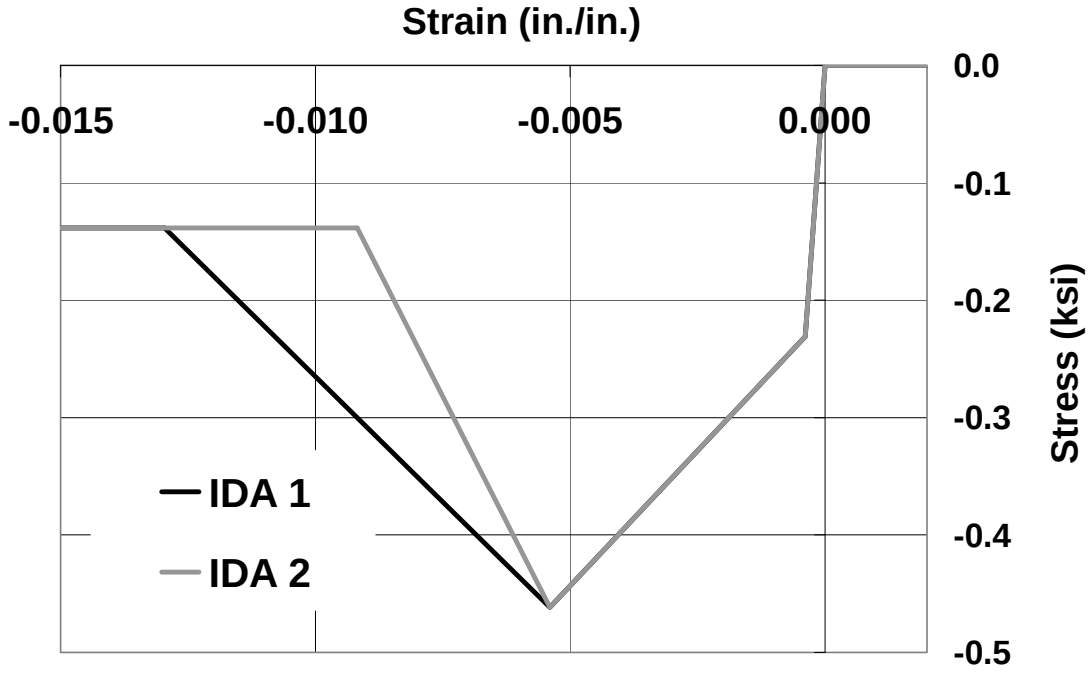

Figure 10.65: Stress-strain of equivalent strut representing AAC infill for first and second IDA of the AAC uniformly infilled frame

The results from the second IDA, shown in Figure 10.66, are nearly identical to those presented in Figure 10.9 for the first IDA. While the collapse spectral intensity generally remained the same for most ground motions, it decreased by 10% for eleven ground motions and increased by 10% for two ground motions. The CMR remained the same at 2.4, as obtained in Section 10.2.4 from the first IDA. Therefore, the results from

ATC-63 evaluation of the archetypical AAC-infilled frames do not seem sensitive to the assumed slope of the descending branch of the backbone curve for the AAC infill.

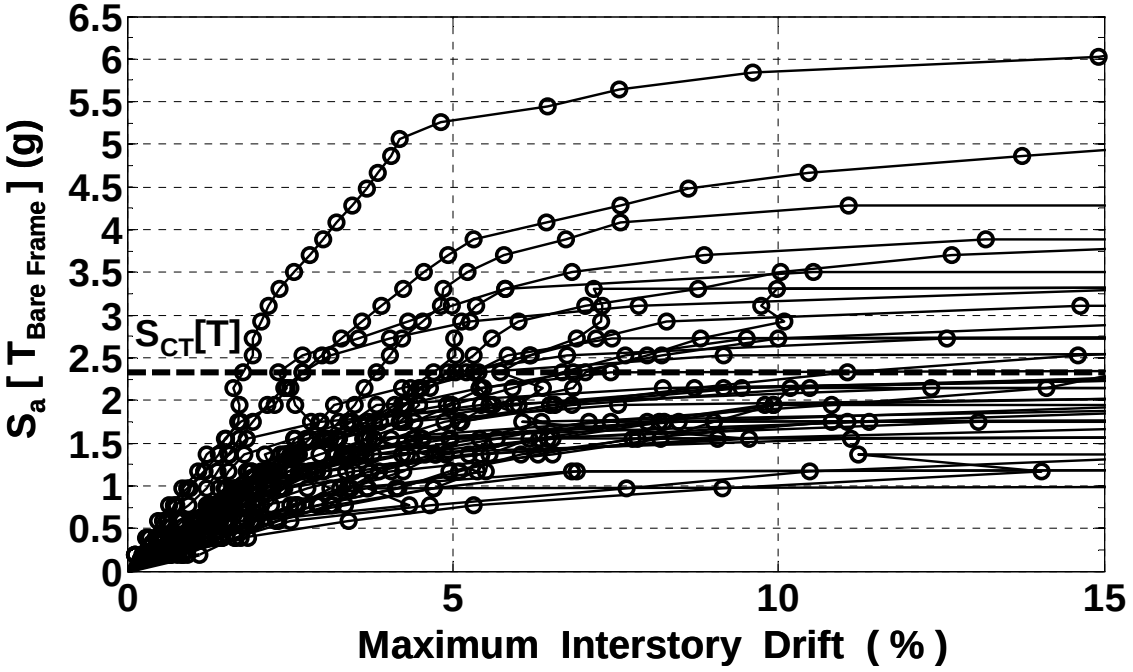

Figure 10.66: Results from second IDA for ATC-63 steel moment frame with uniform AAC infill

Another parameter arbitrarily assumed for the analytical model of AAC infills is the residual strength of the backbone curve, taken to be 0.3 times the maximum strength of the infill. Results from IDA are not expected to be sensitive to residual strength if it is only a small fraction of the maximum strength of the infill. This is because the magnitude of reloading stiffness of the infill becomes insignificant at large displacements. However, future investigations should explicitly determine sensitivity of IDA results to the residual strength of AAC infills.

Another issue that raises concerns about results from IDA for the archetypical AAC-infilled steel moment frames is the mismatch in the maximum drift reached in the experiment on the AAC infilled frame specimen and IDA. While in IDA collapse is defined as exceedance of 15% interstory drift, the AAC-infilled frame specimen

described in Chapter 4 used to develop a nonlinear hysteretic model for AAC infills was subjected to a maximum lateral drift of about 1.5% (Figure 4.11). However, it has been shown in this section that the results from IDA for the archetypical AAC-infilled steel moment frames are not sensitive to the slope of the descending branch of the backbone curve. As explained previously in this section, the results are also not expected to be sensitive to the assumed residual strength if it is only a small fraction of the maximum strength of the infill. Therefore, mismatch in maximum drift reached during IDA and that reached during testing of the AAC-infilled frame specimen is not likely to change the general nature of results obtained from ATC-63 evaluation of the archetypical AAC-infilled steel moment frames.

In summary, the calibration of the nonlinear model used for the ATC-63 evaluation of AAC infilled frames is generally reliable, even though it is based on a single test.

10.6 DISCUSSION OF PERFORMANCE GROUPS

As explained in Section 3.4.1, the ATC-63 methodology permits categorization of the archetypical structures into performance groups. The archetypical infilled steel moment frames evaluated in this dissertation can be categorized either by configuration (uniform versus open ground story) or by material (AAC infills versus conventional masonry infills).

As noted throughout this chapter, however, such categorization would not be useful. The fundamental point is that the effects of infilling on the seismic performance of steel moment frames are characterized by infill strength ratio. This is independent of configuration (uniform versus open ground story), and also independent of material (because a particular strength ratio can in principle be achieved with an appropriate thickness of any masonry material). In the remainder of this dissertation, therefore, infilled steel moment frames are distinguished by infill strength ratios rather than performance groups.

10.7 SUMMARY OF CHAPTER

In this chapter, the archetypical infilled steel moment frames developed in Chapter 8 have been analyzed and evaluated using ATC-methodology. Results from these evaluations have been presented. The concept of performance groups is not considered for the archetypical infilled steel moment frames, because the behavior of the archetypical infilled steel moment frames is found to be characterized by infill strength ratio rather than infill configuration or infill material.

CHAPTER 11
Synthesis and discussion of results from ATC-63 evaluation of archetypical infilled steel moment frames

11.1 INTRODUCTION AND SCOPE OF CHAPTER

In this chapter, results from application of the ATC-63 methodology to the archetypical infilled steel moment frames, developed in Chapter 8 and analyzed in Chapter 9, are synthesized and discussed. Based on the results, seismic design factors are proposed for AAC-infilled steel moment frames, and design guidelines are outlined for the such infills and of the frame members bounding them. The extension of these seismic design factors and accompanying design guidelines to uniformly infilled frames and open ground story frames in general is suggested.

11.2 SUMMARY OF PROBABILITIES OF COLLAPSE AT MCE OF ARCHETYPICAL INFILLED STEEL MOMENT FRAMES

In Table 11-1 are summarized the probabilities of collapse at MCE of archetypical infilled steel moment frames. All infilled frames except the 12-in. thick conventional masonry uniformly infilled frame meet the performance criteria of "probability of collapse at MCE less than 20%" prescribed by the ATC-63 methodology for individual archetypical structures. In particular, the probability of collapse at MCE is generally less than 10% for the archetypical AAC-infilled steel moment frames. These observations are independent of whether the ATC-63 evaluation of the infilled frame is conducted using the ASCE7-05 prescribed fundamental period of the original bare frame ("Method 1"), or of the infilled frame ("Method 2").

Table 11-1: Probabilities of collapse at MCE for archetypical infilled steel moment frames

Infill Type	Method 1 (Section 10.2.4.4)		Method 2 (Section 10.2.4.4)	
	Uniformly infilled frame	Open ground story frame	Uniformly infilled frame	Open ground story frame
Bare frame	0.066	0.066	0.066	0.066
AAC, 8-in. thick	0.064	0.062	0.074	0.072
Conventional masonry, 8-in. thick	0.094	0.049	0.12	0.071
Conventional masonry, 12-in. thick	0.480	0.160	0.490	0.180

11.3 SYNTHESIS OF RESULTS FROM ATC-63 EVALUATION OF AAC UNIFORMLY INFILLED FRAME

In Table 11-2 are presented the observations from ATC-63 evaluation of the AAC uniformly infilled frame, with emphasis on the most important observations. Accompanying each observation in Table 11-2 is the section number in Chapter 10 where the observation is justified. Following the table, each observation is briefly discussed.

Table 11-2: Synthesis of results from ATC-63 evaluation of AAC uniformly infilled frame

Important observations	Other observations
o At an infill strength ratio of 0.18, the failure mechanism of bare frame remains unchanged (Section 10.2.4.2). o Probability of collapse at MCE is less than or equal to that of the original bare frame (Section 10.2.4.5). o Drift at MCE and DBE is 80% of the drift of the original bare frame (Section 10.2.4.7).	o Non-simulated collapse due to local shear failure in frame members does not occur (Section 10.2.4.1). o Maximum axial force in columns from pushover analysis increases in an insignificant and predictable manner (Section 10.2.3.5).

Important observations from Table 11-2 are further explained as follows. Uniformly infilling the ATC-63 steel moment frame with AAC infills (infill strength ratio of 0.18) did not change the failure mechanism of the original bare frame (a sidesway mechanism with column hinging at the base only, and beam hinging over the entire height of the frame). Therefore, such infills do not compromise the strength and ductility that can be obtained from frame action alone, even after the infill fails. In addition, such infills act as energy dissipators, reducing collapse probability at MCE and interstory drift at MCE and smaller ground motions.

Other observations from Table 11-2 are further explained as follows. AAC infills did not cause local shear failures in frame members due to frame-infill interaction forces, and they increased axial forces in columns in an insignificant and predictable manner. This means that the AAC infills can be added to the bare frame without changing the design process for the frame.

11.4 SYNTHESIS OF RESULTS FROM ATC-63 EVALUATION OF ARCHETYPICAL CONVENTIONAL MASONRY UNIFORMLY INFILLED FRAMES

In Table 11-3 are presented the observations from ATC-63 evaluation of the archetypical conventional masonry uniformly infilled frames, with emphasis on the most

important observations. Accompanying each observation in the table is the section number in Chapter 10 where the observation is justified. Following the table, each observation is briefly discussed.

Table 11-3: Synthesis of results from ATC-63 evaluation of archetypical conventional masonry uniformly infilled frames

Important observations	Other observations
o For the 8-in. and the 12-in. thick conventional masonry uniformly infilled frames (infill strength ratios of 0.68 and 1.01, respectively), the failure mechanism is concentrated in the lower stories (Section 10.3.3.2). o Frame members bounding infills often fail in shear ("non-simulated" collapse), significantly increasing the probability of collapse (Section 10.3.3.1). o Probability of collapse at MCE is significantly greater than for the original bare frame. This is particularly true for the 12-in thick conventional masonry uniformly infilled frame. (Section 10.3.5).	o Maximum axial force in columns from pushover analysis, increases in a significant and unpredictable manner (Section 10.3.2.2).

Important observations from Table 11-3 are further explained as follows. The infill strength ratio fundamentally determines the story mechanism, because higher infill strength ratios lead to a concentration of the failure mechanism in the lower stories of the frame. Conventional masonry infills also caused local shear failures in frame members, and the likelihood of these failures increases with increase in infill strength ratio. The 12-in. thick conventional masonry uniformly infilled frame experienced local shear failures even at ground motion intensities much lower than MCE and DBE, resulting in a significantly larger probability of collapse at MCE than for the bare frame.

Other observations from Table 11-3 are further explained as follows. Conventional masonry infills significantly increased axial forces in columns. Together with the likelihood of local shear failure in frame members, this makes it difficult to add such infills to a bare frame without changing the design process for the frame.

11.5 SYNTHESIS OF RESULTS FROM ATC-63 EVALUATION OF AAC OPEN GROUND STORY FRAMES

Results for the AAC open ground story frame are essentially identical to those presented in Section 11.3 and Table 11-2 for the AAC uniformly infilled frame. Using infills with an infill strength ratio less than about 0.35 permits an open ground story, while still reducing the probability of collapse at MCE, and also reducing drift at MCE and DBE levels.

11.6 SYNTHESIS OF RESULTS FROM ATC-63 EVALUATION OF ARCHETYPICAL CONVENTIONAL MASONRY OPEN GROUND STORY FRAMES

Results for the conventional masonry open ground story frames are similar to those presented in Section 11.311.4 for the conventional masonry uniformly infilled frames. Additional observations specific to conventional masonry open ground story frames are presented in Table 11-4, with emphasis on the most important observations. Accompanying each observation in the Table 11-4 is the section number in Chapter 10 where the observation is justified. Following the table, each observation is briefly discussed.

Table 11-4: Synthesis of results from ATC-63 evaluation of archetypical conventional masonry open ground story frames

Important observations	Other observations
o For the 12-in. thick conventional masonry open ground story frame (infill strength ratio 1.01), the failure mechanism is concentrated in the ground story (Section 10.4.3.3) o Due to onset of weak ground story mechanism, *CMR* for the 12-in. thick conventional masonry open ground story frame determined using only sidesway collapse mechanisms showed a marked decrease than the ATC-63 steel moment frame. (Section 10.4.3) o The probability of collapse at MCE of the 8-in. conventional masonry open ground story frame was the lowest among all archetypical infilled frames evaluated in this dissertation. (Table 11-1)	o The occurrence of local shear failures in 9 out of 44 ground motions of the ATC-63 suite did not reduce *CMR* of the 8-in. thick conventional masonry open ground story frame. (Section 10.4.3.1) o In general, the archetypical conventional masonry open ground story frames show much less incidence of local shear failure than corresponding uniformly infilled frames. (Section 10.4.3.1)

Important observations from Table 11-4 are further explained as follows. The 12-in. thick conventional masonry open ground story frames, with an infill strength ratio of 1.01, displayed weak ground story failure mechanisms, which are the most commonly observed behavior of open ground story frames in real earthquakes. Based on this combination of analytical and empirical evidence, an infill strength ratio of about 1 therefore probably marks the onset of the weak ground story mechanism in general in open ground story frames. Due to the formation of the weak ground story mechanism, the 12-in. thick conventional masonry open ground story frame was the only archetypical infilled steel moment that showed a decrease in *CMR* from that of the ATC-63 steel moment frame from consideration of sidesway collapse mechanism alone (without considering non-simulated failure modes). Interestingly, among all the archetypical infilled steel moment frames evaluated in this dissertation, the 8-in. thick conventional

masonry open ground story frame had the best performance in terms of probability of collapse at MCE, because its *CMR* is not reduced by non-simulated collapse modes, and also because its high pushover ductility resulted in a higher *SSF* and hence a higher *ACMR*.

Other observations from Table 11-4 are further explained as follows. The reduced incidence of local shear failures in frame members of the archetypical conventional masonry open ground story frames compared to the corresponding uniformly infilled frames is mainly due to the absence of infill in the ground story where base shear is highest, and also due to the longer fundamental period of the open ground story frames, leading to lower base shear demand.

11.7 ADDITIONAL OBSERVATIONS FROM ATC-63 EVALUATION OF ARCHETYPICAL INFILLED STEEL MOMENT FRAMES

This section contains additional observations which, though not required by the ATC-63 methodology, provide useful information on the seismic performance of infilled steel moment frames.

11.7.1 Ratios of collapse scaling factors

The ATC-63 methodology as described in ATC-63 (2008) does not provide specific guidance on how to compare the seismic performance of archetypes and variants on those archetypes. Because such comparison is at the heart of this dissertation, additional tools were developed here for this purpose. One of the most useful of these was the ratio, for each ground motion used in the IDA, of the scaling factor required to cause collapse of the variant, divided by the scaling factor required to cause collapse of the original archetype. Table 11-5 references the figures from Chapter 10 that provide this information for each of the archetypical infilled steel moment fames. In those figures, the archetypical infilled frames are considered as variants of the ATC-63 steel moment frame.

Table 11-5: Figures depicting ratio of collapse scaling factors of archetypical infilled steel moments to those of the ATC-63 steel moment frame

AAC uniformly infilled frame	Figure 10.10
8-in. thick conventional masonry uniformly infilled frame	Figure 10.26, Figure 10.30
12-in. thick conventional masonry uniformly infilled frame	Figure 10.27, Figure 10.31
AAC open ground story frame	Figure 10.50
8-in. thick conventional masonry open ground story frame	Figure 10.51, Figure 10.55
12-in. thick conventional masonry open ground story frame	Figure 10.52, Figure 10.56

From those figures, it is inferred that the collapse spectral intensity of the archetypical AAC-infilled steel moment frames is generally greater than or nearly the same as that of the ATC-63 steel moment frame. In a few cases when collapse spectral intensity was lower for the archetypical AAC-infilled steel moment frames, the ratio to that of the ATC-63 steel moment frame is not less than 0.8.

In contrast, for the archetypical conventional masonry infilled steel moment frames, the ratio of their collapse spectral intensity to that of the ATC-63 steel moment frame varies widely for 44 ground motions of the ATC-63 suite. While in some cases the ratio is 1.8, in some other cases it is about 0.6. This variation is exacerbated when local shear failure in frame members is included in the collapse evaluation.

11.7.2 Interstory drift at MCE and DBE level ground motions

During IDA, reduction in maximum interstory drift of the archetypical infilled steel moment frames compared to the ATC-63 steel moment frame at ground motion intensities corresponding to MCE and DBE was monitored. Table 11-6 gives the figures that depict this reduction for each of the archetypical infilled steel moment frames.

Table 11-6: Figures depicting reduction in maximum interstory drift in archetypical infilled steel moment frames compared to ATC-63 steel moment frame

AAC uniformly infilled frame	Figure 10.14
8-in. thick conventional masonry uniformly infilled frame	Figure 10.36
12-in. thick conventional masonry uniformly infilled frame	Figure 10.37
AAC open ground story frame	Figure 10.62
8-in. thick conventional masonry open ground story frame	Figure 10.63
12-in. thick conventional masonry open ground story frame	Figure 10.64

From these figures, it is inferred that infilling the ATC-63 steel moment frame generally reduced drift at MCE and DBE level ground motion intensities. An exception is the 12-in. thick conventional masonry open ground story frame, which displayed many instances of higher drift than the ATC-63 steel moment frame at MCE and design level ground motions. This is due to formation of a weak ground story mechanism.

11.7.3 ATC-63 results in the context of history of performance of steel moment frames

As presented in Section 2.2.1, evidence regarding performance of infilled frames during earthquakes generally pertains to infilled frames of reinforced concrete. However, the ATC-63 evaluation archetypical steel moment frames described in this dissertation is still valid. Story mechanisms due to the presence of infills are equally likely in steel and reinforced concrete moment frames. Local shear failure in frame members was handled as a non-simulated collapse mode to illustrate the possibility and effects of such failure modes in infilled frames, particularly in the case of reinforced concrete frames. In steel moment frames, although shear failure of W-sections is a ductile phenomenon that may not significantly affect performance, shear failure of associated connections between beams and columns may not be benign. Also, local shear failure in members of the archetypical infilled steel moment frames is considered for the sake of completeness, and

so that the results can be applied as well to reinforced concrete frames, for which column shear failure definitely hurts performance.

11.8 IMPLICATIONS FOR SEISMIC DESIGN FACTORS AND DESIGN GUIDELINES FOR AAC-INFILLED STEEL MOMENT FRAMES

11.8.1 Seismic response reduction factor, *R*

Archetypical AAC-infilled steel moment frames conforming to uniform and open ground story infill configurations, and evaluated using the ATC-63 methodology with a trial seismic force reduction factor (*R*) equal to that of the original bare steel moment frame, meet the performance criteria prescribed by the ATC-63 methodology. Therefore, the value of *R* prescribed for steel moment frames by ASCE7-05 is applicable to AAC-infilled steel moment frames as well. Although the archetypical AAC-infilled steel moment frames are evaluated in this dissertation for Seismic Design Category D_{max} of the ATC-63 methodology, the proposed value of *R* for AAC-infilled steel moment frames is expected to be applicable in other seismic design categories as well because the fundamental principles in the design and evaluation of the archetypical AAC-infilled steel moment frame in those seismic design categories remain the same.

The archetypical AAC-infilled frames evaluated in this dissertation had an infill strength ratio of about 0.2. From results of pushover analysis of the ATC-63 steel moment frame, an infill strength ratio of about 35% is found to mark the onset of story mechanisms. Although none of the archetypical infilled steel moment frames evaluated using the more rigorous IDA have an infill strength ratio of 35%, there is a fair correlation between infilled frame behavior observed during pushover analysis and IDA.

Therefore, the proposed value of *R* is expected to be valid for AAC-infilled steel moment frames with infill strength ratios up to about 0.35.

With an infill strength ratio of 35%, an open ground story will lie between a weak story and an extreme weak story as defined by Table 12.3-2 of ASCE7-05. Assuming that lateral strength of the bare frame at the ground story and the story above it are the same,

infills with story shear strength 35% of the bare frame will make the total lateral strength of the open ground story 26% less than the lateral strength of the story above it. In this perspective, an infill strength ratio of 35% is a practical limit serving the generally accepted definition of a weak story.

Also, examination of the relation between infill strength ratio and the results of ATC-63 evaluation show that the probability of collapse increases slowly as the infill strength ratio increases through 35 %, and that an infill strength ratio of 35 % is not a strict demarcation between desirable and undesirable infills. Nevertheless, the value of 35 % is selected here because it is reasonable.

11.8.2 System overstrength factor, Ω_0

The ATC-63 methodology requires that the value of the system overstrength factor, Ω_o, for use in design not be less than the largest average value of archetypical structure overstrength, Ω, from any performance group (Section 3.7.6). However, it has been shown in this dissertation that AAC infills do not change the native failure mechanism of the bare frame. The force resultants in frame members of an AAC-infilled steel moment frame due to frame action alone will remain same as for the bare frame. Therefore, the same over-strength factor recommended by ASCE7-05 for steel moment frames is proposed for the design of frame members of AAC-infilled steel moment frames. However, AAC infills induce additional force resultants on the frame members which should accounted for during the design process. This is addressed in a subsequent section.

11.8.3 Displacement amplification factor

The ATC-63 methodology recommends that the deflection amplification factor, C_d, of a structural system be computed using the procedure given in Section 3.7.7 of this dissertation. Although C_d could be determined using that procedure, the values recommended for C_d by ASCE7-05 for steel moment frames are based on industry-wide consensus and is generally adequate. In addition, AAC infills have been shown to reduce

drift of steel moment frames under MCE and design level ground motions. Therefore, the same value of C_d prescribed by ASCE7-05 for steel moment frames is proposed for design of AAC-infilled steel moment frames.

11.8.4 Analysis and design guidelines to consider presence of infills

For ATC-63 evaluation of the archetypical AAC-infilled steel moment frames, the original design of the ATC-63 steel moment frame was not altered to account for the addition of AAC infills. The AAC infills were simply placed in the panels of the frame. In spite of this, local shear failure in frame members was not detected during IDA of the archetypical AAC-infilled steel moment frames. This is due to the reserve shear strength of frame members beyond that required to cause plastic hinges. In addition, the maximum increase in axial force in the columns of the archetypical AAC-infilled steel moment frame compared to the ATC-63 steel moment frame is not significant, as determined from pushover analysis. Therefore, when weak infills such as AAC are used, it may be not necessary to design for additional force resultants on frame members due to the infills.

However, a simple procedure is proposed for addressing, at least in a limited way, the increased force resultants on frame members due to the presence of AAC infills. In using the proposed value of R and Ω_o, the preliminary design of the bare steel moment frame can be completed without considering the AAC infills. Each infill panel should then be modeled as a pair of equivalent diagonal struts, whose properties can be obtained using the draft MSJC infill provisions. The frame members bounding infill panels must be checked for the additional shears produced by the strut reactions. The frame columns also must be checked for the additional axial forces produced by seismic overturning due to the presence of the infill panels. This design approach is applicable to AAC-infilled steel moment frames in both uniformly infilled and open ground story configurations.

11.8.5 Illustration of proposed design approach to the ATC-63 steel moment frame with AAC infill

Infilling the ATC-63 steel moment frame with 8-in. thick Class 4 AAC units resulted in an infill strength ratio of 0.18. Therefore, the proposed design approach is applicable for Class 4 AAC infill up to a thickness of 16 in., which will result in an infill strength ratio close to 0.35. In this illustration, the expected strength of the AAC infill is based on the experimental results obtained from the AAC-infilled frame specimen of Chapter 4.

11.8.6 Applicability of proposed design approach to conventional masonry infilled frames

Although the design approach proposed in this dissertation has been demonstrated using AAC as the infill material, it is expected to be equally valid for other infill materials with similar stress-strain characteristics.

For the ATC-63 steel moment frame in particular, using clay masonry of 8-in. thickness and specified compressive strength of 4 ksi as infill, the expected strength of the clay masonry infill resulted in an infill strength ratio of 0.68. Because infill strength is essentially proportional to the product of infill thickness and material compressive strength, a 4-in. thick clay masonry infill will have an infill strength ratio close to 0.35, and will be suitable for the proposed design approach.

Along the same lines, suppose that the ATC-63 steel moment frame is infilled with 8-in. thick solid concrete masonry with a specified compressive strength of 2 ksi. Because this material strength is about half that of clay masonry, the infill has about half the strength of an 8-in. clay masonry infill, or about the strength of a 4-in. clay masonry infill. The 8-in. thick solid concrete masonry infill will therefore have an infill strength ratio close to 0.35, and will be suitable as well for the proposed design approach.

The proposed design approach may be easier to implement for weaker infills such as AAC, than for stronger infills such as clay or concrete masonry, because the stronger the infill, the greater the local shear demand produced in the bounding frame elements by

infill strut forces, and the greater may be the probable necessary modifications in the design of the original bare frame. In addition, the stronger the infill, the greater the increases in column axial forces, and again the greater may be the probable necessary modifications in the design of the original bare frame.

A weak material such as AAC, in contrast, permits the limiting infill strength ratio of about 0.35 to be achieved using a large number of panels, each of which produces relatively small increases in design shears and axial forces for the original bare frame.

11.8.7 Applicability of proposed design approach to infilled reinforced concrete moment frames

The proposed design approach is expected to be applicable to infilled reinforced concrete moment frames, because the fundamental principles involved in behavior, analysis and design of reinforced concrete moment frames are same as those for steel moment frames.

11.8.8 Concluding remarks on proposed design approach

When AAC-infilled steel moment frames are designed using this approach, they reduce the probability of collapse at MCE, and also reduce drift (damage) at MCE and DBE ground motions. The infills begin to crush early in the response history of the infilled frame structure, and hence act as stable energy dissipation devices.

11.9 SUMMARY OF CHAPTER

Results from ATC-63 evaluation of archetypical infilled steel moment frames have been synthesized and discussed. Based on this, seismic design factors for AAC-infilled steel moment frames with uniformly infilled and open ground story configurations are proposed to be same as those prescribed by ASCE7-05 for the bare steel moment frame. Guidelines are outlined for the design of the infills and of the frame members bounding them. The proposed design approach is believed to be applicable in general to steel moment frames with uniformly infilled and open ground story

configurations. In principle, it can be extended to infilled reinforced concrete moment frames as well.

CHAPTER 12
Summary, Conclusions and Recommendations

12.1 SUMMARY OF DISSERTATION

In this dissertation, the seismic behavior and design of AAC-infilled steel moment frames are investigated systematically. The fundamental vehicle for this investigation is the ATC-63 methodology (ATC-63 2008), which is intended for the establishment of seismic design factors for structural systems. The research presented in this dissertation is summarized as follows:

1) The structural behavior of infilled frames is reviewed. The structural action of infills, their effect on the behavior of frames, and the observed seismic performance of infilled frames are summarized. A brief background on AAC is presented, including its possible usefulness as an infill material. Previous investigations on the behavior of infilled frames, their analytical modeling, and assessments of their seismic performance, are reviewed. The need to develop comprehensive design provisions for infilled frames is pointed out.

2) The ATC-63 methodology is briefly reviewed, including the concepts of archetypical structures, design rules and mathematical models simulating the behavior of those archetypes. Steps in the methodology are discussed in more detail, and the criteria outlined by the methodology for acceptance of a structural system and associated design rules, are presented.

3) A limited experimental investigation on the hysteretic behavior of an AAC-infilled steel moment frame is developed, conducted, and discussed. Using the experimental results of that investigation, the draft infill design provisions of the

Masonry Standards Joint Committee (MSJC) are extended to AAC infills, and a mathematical model is developed and calibrated to simulate the behavior of AAC infills under reversed cyclic loads.

4) To demonstrate the ATC-63 methodology and verify understanding of it, the ATC-63 methodology is applied to an example steel moment frame designed using the rules for steel moment frames given in AISC (2005), and evaluated in ATC-63 (2008).

5) The archetypical infilled frames to be evaluated by the ATC-63 methodology are developed, using the following steps.
   a) The archetypical bare steel frame is selected as the same one discussed immediately above and reported in ATC-63 (2008). It is a reasonable reference frame for low to medium-rise structures.
   b) Using a series of pushover analyses, the effects of different infill strengths and configurations on the collapse behavior of the steel frame are investigated. Infill configurations whose total lateral strength in a particular story exceeds about 35% of the lateral strength of the bare frame in that story are observed to provoke story mechanisms in the frame.
   c) Based on that observation, archetypical infilled frames are selected. The archetypes conform to two infill configurations: uniformly infilled frames, and open ground story frames. Each infill configuration includes archetypes whose ratio of infill strength to bare-frame strength at each story is less than 35%, and archetypes whose ratio is greater than 35%. The former archetype is typical of steel moment frames infilled with AAC; the latter archetype is typical of steel moment frames infilled with conventional (clay or concrete) masonry.
6) The ATC-63 methodology, specialized for application to infilled frames, is applied to the archetypical infilled frames developed above. The performance of

those archetypical infilled frames is evaluated, and seismic design factors are proposed for AAC-infilled steel moment frames.

7) The extension of this work to other types of infilled frames is discussed.

12.2 CONCLUSIONS OF DISSERTATION

1) Infills of AAC masonry and of conventional (clay or concrete) masonry can be designed to improve the seismic performance of an original bare frame by reducing the probability of collapse under strong earthquakes, and also by reducing drift (damage) under all levels of earthquakes.

2) In this process, the original seismic design factors used for the bare frame are retained, and hence the design of the frame is generally unchanged. Nevertheless, infilling is advantageous because it improves seismic performance.

3) To achieve this objective, infills should be configured and designed so that in each story, their lateral strength is less than about 35% of the lateral strength of the bare frame in that story. For calculation of this infill strength ratio, the strength of the infill should be computed as the nominal strength given by the draft MSJC provisions, multiplied by 3.5 for AAC and by 2.0 for conventional masonry, to achieve an upper fractile of the expected strength. For the ATC-63 steel moment frame considered here, this limiting infill strength ratio corresponds to an AAC infill with a thickness of about 16 in., a concrete masonry infill with a thickness of about 8 in., or a clay masonry infill with a thickness of about 4 in. If hollow masonry units are used, the above thicknesses refer to effective thicknesses (face shells only).

4) If the infill strength ratio, so computed, is kept below about 35%, then the preliminary design of the frame can be completed without considering the infill, and the same seismic design factors used for the original bare frame can safely be retained for the corresponding infilled frame. This conclusion is independent of infill configuration (uniform versus open ground story) and infill material. After completion of preliminary design of the bare frame, masonry infills should be

modeled as equivalent struts with the dimensions and material properties prescribed by the draft infill provisions of the Masonry Standards Joint Committee (MSJC) Code. Static analysis is performed on the infilled frame using the same lateral loads used for design of the bare frame. From the results of this analysis, shear capacity of frame members is checked for additional shear forces produced by strut reactions. Axial capacity of columns is checked for additional force obtained as the vertical component of the axial force in the equivalent struts. If the infill is weak enough, the preliminary design of the bare frame may be adequate to resist these additional shear and axial forces. Stronger infills will necessitate greater modifications in the preliminary design of the bare frame.

5) When the infill strength ratio is maintained below 35%, ATC-63 evaluation shows that the seismic behavior of the infilled frame is better than that of the original bare frame. The probability of collapse under MCE-level ground motions remains the same or decreases in a consistent manner, and maximum interstory drifts (a measure of damage) decrease under MCE-level and DBE-level ground motions.

6) If the infill strength ratio exceeds the above limit of about 35%, the ATC-63 evaluation shows that the seismic behavior of infilled frames becomes worse than that of the original bare frame. This is consistent with anecdotal experience in earthquakes. With uniformly infilled frames, increasing values of the infill strength ratio lead to an increasing probability of failure due to local shear failures of the frame elements bounding the infills (referred to in the ATC-63 methodology as “non-simulated” collapse modes). With open ground story frames, the same tendency for local shear failures is observed, and is accompanied (for infill strength ratios above about 1) by an increasing tendency for ground-level, weak-story mechanisms.

7) Because the behavior and design of bare reinforced concrete frames follow the same principles as for bare steel moment frames, the work described here is in principle applicable to infilled frames of reinforced concrete as well as steel.

12.3 RECOMMENDATIONS FOR IMPLEMENTATION

1) Table 12.2-1 of ASCE7-05 should be modified for special steel moment frames to permit the use of masonry infills meeting the above requirements, while retaining the currently mandated seismic design factors (R, C_d , Ω_0).
2) Similar modifications may be introduced for other types of frames as additional research results warrant.

12.4 RECOMMENDATIONS FOR FUTURE INVESTIGATION

The following issues are investigated in a limited manner in this dissertation. It is recommended that they be studied in more detail:

1) *Behavior of AAC infills*: Experimental results from a single AAC-infilled frame specimen tested as part of this dissertation are used to extend the draft MSJC infill provisions and calibrate the Ibarra-Krawinkler hysteretic model for AAC infills. As AAC infills have been shown to be structurally useful, more tests should be performed to refine their stiffness, strength and hysteretic properties.
2) *Lateral strength of infills*: It has been shown in this dissertation that lateral strength of infills is an important parameter governing behavior of infilled frames. Draft MSJC provisions for infills are oriented toward the safe design of the infill itself; that is, they produce nominal strengths which are lower fractiles of the expected strength. To meet the design objective that the lateral strength of the infills be less than 35% of the lateral strength of the bare frame, however, it is desirable to have estimates of the nominal strengths which are upper fractiles of the expected strength. This has been done to a limited extent for the AAC infills studied here. If it is desired to apply this approach to infills of other masonry materials, the statistical distribution of reported strengths with respect to the nominal strengths given by the draft MSJC formulas needs to be examined further.
3) *Characterizing hysteretic behavior of infills*: Hysteretic behavior of infills has been modeled in this dissertation using the state-of-the-art, Ibarra-Krawinkler

hysteretic model. In the study described in this dissertation, however, that model was calibrated using experimental data from a single AAC-infilled frame specimen only. Also, because that specimen was not tested to failure, the descending branch of the monotonic strength envelope was chosen by judgment rather than test. Finally, because a monotonic test was not performed, it was impossible to distinguish between envelope deterioration and in-cycle deterioration, so the latter was not explicitly modeled. Despite these shortcomings, the model captures reasonably well the lateral load-deflection behavior of the AAC-infilled frame specimen tested in this dissertation. Therefore, it is suggested this model be refined based on a wider collection of experimental data from different types of infills.

4) *Effect of infills on different types of frames*: The conclusions of this dissertation are based on application of the ATC-63 methodology to a single four-bay, four-story steel moment frame. To refine the conclusions of this dissertation on the behavior of infilled frames in general, it is necessary to study a wider variety of steel and reinforced concrete frames.

5) *Effect of the ratio between moment capacity of columns and beams framing into a beam column joint*: Story mechanisms can form in infilled frames even when the design satisfies the strong-column, weak-beam criterion. Therefore, the effect of different ratios of the required sum of moment capacities of columns to those of beams framing into a beam-column joint needs to be investigated. For the four-story steel moment frame used in this dissertation, this ratio is 2.5 in the bottom stories and 3.1 in the top stories. The effect of this ratio needs to be investigated for a wide range of values, including the typical value of about 1.5.

6) *Infill-panel configurations*: Only two configurations of infill panels are considered in this dissertation: uniform and open ground story. In the first configuration, identical infill panels are located in vertically continuous bays in all stories. The second configuration is the same as the first, except that infills are not

located in the ground story. Other configurations, not yet studied, are outlined below:

a) Infills can be spread across different bay lines in a story, rather than being located in vertically continuous bays at all stories. This may be advantageous for non-structural reasons.

b) Infills at a particular story can be spread across different frame lines rather than being located in the plane of a single frame. This method may be particularly suitable for buildings symmetric in plan. The placement of infills should also be symmetric in plan, to minimize torsional response.

c) It has been shown in this dissertation that if the lateral strength of infills at a story remains less than 35% of that of the bare frame, the native failure mechanism of the bare frame is not affected. This is also true for open ground story frames. It may be true as well for infilled frames in which other stories are left open.

d) In this dissertation, for the sake of simplicity, identical infill panels were placed at all stories. For the four-story steel moment frame used in this dissertation, the column sections were different at the upper and bottom two stories. This resulted in two different values for the ratio of lateral strength of infill to that of bare frame in the upper and lower stories. It may be more beneficial to maintain constant or decrease the ratio between lateral strength of infills and that of the bare frame at each story along the height of the frame. This may facilitate nearly simultaneous crushing of infills at all stories without triggering story mechanisms.

7) *Effect of different infill failure mechanisms on frame behavior*: In this dissertation, hysteretic behavior of infills is modeled using equivalent struts between beam-column joints. Although such struts can adequately simulate the global hysteretic behavior of an infilled frame, they are fundamentally best at capturing the diagonal and corner crushing failure modes of infills. They are not able to address, for example, the column hinging that has been observed as a

consequence of horizontal shear failure of the infill. More complex strut mechanisms are needed for such cases.

APPENDIX A

OpenSees input files

A.1 ANALYTICAL MODEL OF THE AAC UNIFORMLY INFILLED FRAME

```
#First clean the data belonging to the previous model that may still be residing in the RAM
wipe

#Create the model builder
model basic -ndm 2 -ndf 3

#Transformation for the columns
geomTransf PDelta 1

#Transformation for the beams
geomTransf Linear 2

source materials.tcl

set infill "yes"
#set infill "no"

#column line 1
node 101 0 0
node 104 0 0
node 105 0 141.1
node 102 0 141.1
node 103 -12.85 156

node 111 0 170.9
node 114 0 170.9
node 115 0 297.1
node 112 0 297.1
node 113 -12.85 312

node 121 0 326.9
node 124 0 326.9
node 125 0 455.95
node 122 0 455.95
```

node 123 -12.5 468

node 131 0 480.05
node 134 0 480.05
node 135 0 611.95
node 132 0 611.95
node 133 0 636.05
node 136 -12.5 624

#column line 2
node 201 360 0
node 204 360 0
node 205 360 141.1
node 202 360 141.1

node 211 360 170.9
node 214 360 170.9
node 215 360 297.1
node 212 360 297.1

node 221 360 326.9
node 224 360 326.9
node 225 360 455.95
node 222 360 455.95

node 231 360 480.05
node 234 360 480.05
node 235 360 611.95
node 232 360 611.95
node 233 360 636.05

#column line 3
node 301 720 0
node 304 720 0
node 305 720 141.1
node 302 720 141.1

node 311 720 170.9
node 314 720 170.9
node 315 720 297.1
node 312 720 297.1

node 321 720 326.9
node 324 720 326.9
node 325 720 455.95
node 322 720 455.95

node 331 720 480.05
node 334 720 480.05
node 335 720 611.95
node 332 720 611.95
node 333 720 636.05

#column line 4
node 401 1080 0
node 404 1080 0
node 405 1080 141.1
node 402 1080 141.1

node 411 1080 170.9
node 414 1080 170.9
node 415 1080 297.1
node 412 1080 297.1

node 421 1080 326.9
node 424 1080 326.9
node 425 1080 455.95
node 422 1080 455.95

node 431 1080 480.05
node 434 1080 480.05
node 435 1080 611.95
node 432 1080 611.95
node 433 1080 636.05

#column line 5
node 501 1440 0
node 504 1440 0
node 505 1440 141.1
node 502 1440 141.1
node 503 1452.85 156

node 511 1440 170.9
node 514 1440 170.9

node 515 1440 297.1
node 512 1440 297.1
node 513 1452.85 312

node 521 1440 326.9
node 524 1440 326.9
node 525 1440 455.95
node 522 1440 455.95
node 523 1452.5 468

node 531 1440 480.05
node 534 1440 480.05
node 535 1440 611.95
node 532 1440 611.95
node 533 1440 636.05
node 536 1452.5 624

#Nodes on beam lines

#Bay 1
node 1101 12.85 156
node 1103 27.85 156
node 1104 27.85 156
node 1105 332.15 156
node 1106 332.15 156
node 1102 347.15 156

node 1201 12.85 312
node 1203 27.85 312
node 1204 27.85 312
node 1205 332.15 312
node 1206 332.15 312
node 1202 347.15 312

node 1301 12.5 468
node 1303 27.85 468
node 1304 27.85 468
node 1305 332.15 468
node 1306 332.15 468
node 1302 347.5 468

node 1401 12.5 624

node 1403 27.85 624
node 1404 27.85 624
node 1405 332.15 624
node 1406 332.15 624
node 1402 347.5 624

#Bay 2
node 2101 372.85 156
node 2103 387.85 156
node 2104 387.85 156
node 2105 692.15 156
node 2106 692.15 156
node 2102 707.15 156

node 2201 372.85 312
node 2203 387.85 312
node 2204 387.85 312
node 2205 692.15 312
node 2206 692.15 312
node 2202 707.15 312

node 2301 372.5 468
node 2303 387.85 468
node 2304 387.85 468
node 2305 692.15 468
node 2306 692.15 468
node 2302 707.5 468

node 2401 372.5 624
node 2403 387.85 624
node 2404 387.85 624
node 2405 692.15 624
node 2406 692.15 624
node 2402 707.5 624

#Bay 3
node 3101 732.85 156
node 3103 747.85 156
node 3104 747.85 156
node 3105 1052.15 156
node 3106 1052.15 156
node 3102 1067.15 156

node 3201 732.85 312
node 3203 747.85 312
node 3204 747.85 312
node 3205 1052.15 312
node 3206 1052.15 312
node 3202 1067.15 312

node 3301 732.5 468
node 3303 747.85 468
node 3304 747.85 468
node 3305 1052.15 468
node 3306 1052.15 468
node 3302 1067.5 468

node 3401 732.5 624
node 3403 747.85 624
node 3404 747.85 624
node 3405 1052.15 624
node 3406 1052.15 624
node 3402 1067.5 624

#Bay 4
node 4101 1092.85 156
node 4103 1107.85 156
node 4104 1107.85 156
node 4105 1412.15 156
node 4106 1412.15 156
node 4102 1427.15 156

node 4201 1092.85 312
node 4203 1107.85 312
node 4204 1107.85 312
node 4205 1412.15 312
node 4206 1412.15 312
node 4202 1427.15 312

node 4301 1092.5 468
node 4303 1107.85 468
node 4304 1107.85 468
node 4305 1412.15 468
node 4306 1412.15 468
node 4302 1427.5 468

node 4401 1092.5 624
node 4403 1107.85 624
node 4404 1107.85 624
node 4405 1412.15 624
node 4406 1412.15 624
node 4402 1427.5 624

#Make the restraints
fix 101 1 1 1
fix 201 1 1 1
fix 301 1 1 1
fix 401 1 1 1
fix 501 1 1 1

#1st column line
element Joint2D 114 102 1101 111 103 10001 100 100 100 100 12 0
element Joint2D 124 112 1201 121 113 10002 100 100 100 100 12 0
element Joint2D 134 122 1301 131 123 10003 100 100 100 100 11 0
element Joint2D 144 132 1401 133 136 10004 100 100 100 100 11 0

#2nd column line
element Joint2D 214 202 2101 211 1102 10005 100 100 100 100 12 0
element Joint2D 224 212 2201 221 1202 10006 100 100 100 100 12 0
element Joint2D 234 222 2301 231 1302 10007 100 100 100 100 11 0
element Joint2D 244 232 2401 233 1402 10008 100 100 100 100 11 0

#3rd column line
element Joint2D 314 302 3101 311 2102 10009 100 100 100 100 12 0
element Joint2D 324 312 3201 321 2202 10010 100 100 100 100 12 0
element Joint2D 334 322 3301 331 2302 10011 100 100 100 100 11 0
element Joint2D 344 332 3401 333 2402 10012 100 100 100 100 11 0

#4th column line
element Joint2D 414 402 4101 411 3102 10013 100 100 100 100 12 0
element Joint2D 424 412 4201 421 3202 10014 100 100 100 100 12 0
element Joint2D 434 422 4301 431 3302 10015 100 100 100 100 11 0
element Joint2D 444 432 4401 433 3402 10016 100 100 100 100 11 0

#5th column line
element Joint2D 514 502 503 511 4102 10017 100 100 100 100 12 0
element Joint2D 524 512 513 521 4202 10018 100 100 100 100 12 0

```
element Joint2D 534 522 523 531 4302 10019 100 100 100 100 11 0
element Joint2D 544 532 536 533 4402 10020 100 100 100 100 11 0

#ELASTIC BEAM COLUMN ELEMENTS
#*********************************

set inertia24162 [expr 1.1*5170]
set inertia24207 [expr 1.1*6820]
set inertia2484 [expr 1.1*2370]
set inertia30108 [expr 1.1*4470]

set area24162 47.7
set area24207 60.7
set area2484  24.7
set area30108 31.7


#Along Column lines

#1st column line
element elasticBeamColumn 112 104 105 $area24207 29000 $inertia24207 1
element elasticBeamColumn 122 114 115 $area24207 29000 $inertia24207 1
element elasticBeamColumn 132 124 125 $area24162 29000 $inertia24162 1
element elasticBeamColumn 142 134 135 $area24162 29000 $inertia24162 1

#2nd column line
element elasticBeamColumn 212 204 205 $area24207 29000 $inertia24207 1
element elasticBeamColumn 222 214 215 $area24207 29000 $inertia24207 1
element elasticBeamColumn 232 224 225 $area24162 29000 $inertia24162 1
element elasticBeamColumn 242 234 235 $area24162 29000 $inertia24162 1

#3rd column line
element elasticBeamColumn 312 304 305 $area24207 29000 $inertia24207 1
element elasticBeamColumn 322 314 315 $area24207 29000 $inertia24207 1
element elasticBeamColumn 332 324 325 $area24162 29000 $inertia24162 1
element elasticBeamColumn 342 334 335 $area24162 29000 $inertia24162 1

#4th column line
element elasticBeamColumn 412 404 405 $area24207 29000 $inertia24207 1
element elasticBeamColumn 422 414 415 $area24207 29000 $inertia24207 1
element elasticBeamColumn 432 424 425 $area24162 29000 $inertia24162 1
element elasticBeamColumn 442 434 435 $area24162 29000 $inertia24162 1
```

```
#5th column line
element elasticBeamColumn 512 504 505 $area24207 29000 $inertia24207 1
element elasticBeamColumn 522 514 515 $area24207 29000 $inertia24207 1
element elasticBeamColumn 532 524 525 $area24162 29000 $inertia24162 1
element elasticBeamColumn 542 534 535 $area24162 29000 $inertia24162 1

#Along Beam lines

#Bay 1
element elasticBeamColumn 1011 1101 1103 $area30108 29000 $inertia30108 2
element elasticBeamColumn 1013 1104 1105 $area30108 29000 $inertia30108 2
element elasticBeamColumn 1015 1106 1102 $area30108 29000 $inertia30108 2

element elasticBeamColumn 1021 1201 1203 $area30108 29000 $inertia30108 2
element elasticBeamColumn 1023 1204 1205 $area30108 29000 $inertia30108 2
element elasticBeamColumn 1025 1206 1202 $area30108 29000 $inertia30108 2

element elasticBeamColumn 1031 1301 1303 $area2484 29000 $inertia2484 2
element elasticBeamColumn 1033 1304 1305 $area2484 29000 $inertia2484 2
element elasticBeamColumn 1035 1306 1302 $area2484 29000 $inertia2484 2

element elasticBeamColumn 1041 1401 1403 $area2484 29000 $inertia2484 2
element elasticBeamColumn 1043 1404 1405 $area2484 29000 $inertia2484 2
element elasticBeamColumn 1045 1406 1402 $area2484 29000 $inertia2484 2

#Bay 2
element elasticBeamColumn 2011 2101 2103 $area30108 29000 $inertia30108 2
element elasticBeamColumn 2013 2104 2105 $area30108 29000 $inertia30108 2
element elasticBeamColumn 2015 2106 2102 $area30108 29000 $inertia30108 2

element elasticBeamColumn 2021 2201 2203 $area30108 29000 $inertia30108 2
element elasticBeamColumn 2023 2204 2205 $area30108 29000 $inertia30108 2
element elasticBeamColumn 2025 2206 2202 $area30108 29000 $inertia30108 2

element elasticBeamColumn 2031 2301 2303 $area2484 29000 $inertia2484 2
element elasticBeamColumn 2033 2304 2305 $area2484 29000 $inertia2484 2
element elasticBeamColumn 2035 2306 2302 $area2484 29000 $inertia2484 2

element elasticBeamColumn 2041 2401 2403 $area2484 29000 $inertia2484 2
element elasticBeamColumn 2043 2404 2405 $area2484 29000 $inertia2484 2
element elasticBeamColumn 2045 2406 2402 $area2484 29000 $inertia2484 2

#Bay 3
```

```
element elasticBeamColumn 3011 3101 3103 $area30108 29000 $inertia30108 2
element elasticBeamColumn 3013 3104 3105 $area30108 29000 $inertia30108 2
element elasticBeamColumn 3015 3106 3102 $area30108 29000 $inertia30108 2

element elasticBeamColumn 3021 3201 3203 $area30108 29000 $inertia30108 2
element elasticBeamColumn 3023 3204 3205 $area30108 29000 $inertia30108 2
element elasticBeamColumn 3025 3206 3202 $area30108 29000 $inertia30108 2

element elasticBeamColumn 3031 3301 3303 $area2484 29000 $inertia2484 2
element elasticBeamColumn 3033 3304 3305 $area2484 29000 $inertia2484 2
element elasticBeamColumn 3035 3306 3302 $area2484 29000 $inertia2484 2

element elasticBeamColumn 3041 3401 3403 $area2484 29000 $inertia2484 2
element elasticBeamColumn 3043 3404 3405 $area2484 29000 $inertia2484 2
element elasticBeamColumn 3045 3406 3402 $area2484 29000 $inertia2484 2

#Bay 4
element elasticBeamColumn 4011 4101 4103 $area30108 29000 $inertia30108 2
element elasticBeamColumn 4013 4104 4105 $area30108 29000 $inertia30108 2
element elasticBeamColumn 4015 4106 4102 $area30108 29000 $inertia30108 2

element elasticBeamColumn 4021 4201 4203 $area30108 29000 $inertia30108 2
element elasticBeamColumn 4023 4204 4205 $area30108 29000 $inertia30108 2
element elasticBeamColumn 4025 4206 4202 $area30108 29000 $inertia30108 2

element elasticBeamColumn 4031 4301 4303 $area2484 29000 $inertia2484 2
element elasticBeamColumn 4033 4304 4305 $area2484 29000 $inertia2484 2
element elasticBeamColumn 4035 4306 4302 $area2484 29000 $inertia2484 2

element elasticBeamColumn 4041 4401 4403 $area2484 29000 $inertia2484 2
element elasticBeamColumn 4043 4404 4405 $area2484 29000 $inertia2484 2
element elasticBeamColumn 4045 4406 4402 $area2484 29000 $inertia2484 2

#Zero-length elements

#column line 1
element zeroLength 111 101 104 -mat 2 2 24207 -dir 1 2 6 -orient 0 1 0 -1 0 0
element zeroLength 113 105 102 -mat 2 2 24207 -dir 1 2 6 -orient 0 1 0 -1 0 0

element zeroLength 121 111 114 -mat 2 2 24207 -dir 1 2 6 -orient 0 1 0 -1 0 0
element zeroLength 123 115 112 -mat 2 2 24207 -dir 1 2 6 -orient 0 1 0 -1 0 0

element zeroLength 131 121 124 -mat 2 2 24162 -dir 1 2 6 -orient 0 1 0 -1 0 0
```

element zeroLength 133 125 122 -mat 2 2 24162 -dir 1 2 6 -orient 0 1 0 -1 0 0

element zeroLength 141 131 134 -mat 2 2 24162 -dir 1 2 6 -orient 0 1 0 -1 0 0
element zeroLength 143 135 132 -mat 2 2 24162 -dir 1 2 6 -orient 0 1 0 -1 0 0

#column line 2
element zeroLength 211 201 204 -mat 2 2 24207 -dir 1 2 6 -orient 0 1 0 -1 0 0
element zeroLength 213 205 202 -mat 2 2 24207 -dir 1 2 6 -orient 0 1 0 -1 0 0

element zeroLength 221 211 214 -mat 2 2 24207 -dir 1 2 6 -orient 0 1 0 -1 0 0
element zeroLength 223 215 212 -mat 2 2 24207 -dir 1 2 6 -orient 0 1 0 -1 0 0

element zeroLength 231 221 224 -mat 2 2 24162 -dir 1 2 6 -orient 0 1 0 -1 0 0
element zeroLength 233 225 222 -mat 2 2 24162 -dir 1 2 6 -orient 0 1 0 -1 0 0

element zeroLength 241 231 234 -mat 2 2 24162 -dir 1 2 6 -orient 0 1 0 -1 0 0
element zeroLength 243 235 232 -mat 2 2 24162 -dir 1 2 6 -orient 0 1 0 -1 0 0

#column line 3
element zeroLength 311 301 304 -mat 2 2 24207 -dir 1 2 6 -orient 0 1 0 -1 0 0
element zeroLength 313 305 302 -mat 2 2 24207 -dir 1 2 6 -orient 0 1 0 -1 0 0

element zeroLength 321 311 314 -mat 2 2 24207 -dir 1 2 6 -orient 0 1 0 -1 0 0
element zeroLength 323 315 312 -mat 2 2 24207 -dir 1 2 6 -orient 0 1 0 -1 0 0

element zeroLength 331 321 324 -mat 2 2 24162 -dir 1 2 6 -orient 0 1 0 -1 0 0
element zeroLength 333 325 322 -mat 2 2 24162 -dir 1 2 6 -orient 0 1 0 -1 0 0

element zeroLength 341 331 334 -mat 2 2 24162 -dir 1 2 6 -orient 0 1 0 -1 0 0
element zeroLength 343 335 332 -mat 2 2 24162 -dir 1 2 6 -orient 0 1 0 -1 0 0

#column line 4
element zeroLength 411 401 404 -mat 2 2 24207 -dir 1 2 6 -orient 0 1 0 -1 0 0
element zeroLength 413 405 402 -mat 2 2 24207 -dir 1 2 6 -orient 0 1 0 -1 0 0

element zeroLength 421 411 414 -mat 2 2 24207 -dir 1 2 6 -orient 0 1 0 -1 0 0
element zeroLength 423 415 412 -mat 2 2 24207 -dir 1 2 6 -orient 0 1 0 -1 0 0

element zeroLength 431 421 424 -mat 2 2 24162 -dir 1 2 6 -orient 0 1 0 -1 0 0
element zeroLength 433 425 422 -mat 2 2 24162 -dir 1 2 6 -orient 0 1 0 -1 0 0

element zeroLength 441 431 434 -mat 2 2 24162 -dir 1 2 6 -orient 0 1 0 -1 0 0
element zeroLength 443 435 432 -mat 2 2 24162 -dir 1 2 6 -orient 0 1 0 -1 0 0

```
#column line 5
element zeroLength 511 501 504 -mat 2 2 24207 -dir 1 2 6 -orient 0 1 0 -1 0 0
element zeroLength 513 505 502 -mat 2 2 24207 -dir 1 2 6 -orient 0 1 0 -1 0 0

element zeroLength 521 511 514 -mat 2 2 24207 -dir 1 2 6 -orient 0 1 0 -1 0 0
element zeroLength 523 515 512 -mat 2 2 24207 -dir 1 2 6 -orient 0 1 0 -1 0 0

element zeroLength 531 521 524 -mat 2 2 24162 -dir 1 2 6 -orient 0 1 0 -1 0 0
element zeroLength 533 525 522 -mat 2 2 24162 -dir 1 2 6 -orient 0 1 0 -1 0 0

element zeroLength 541 531 534 -mat 2 2 24162 -dir 1 2 6 -orient 0 1 0 -1 0 0
element zeroLength 543 535 532 -mat 2 2 24162 -dir 1 2 6 -orient 0 1 0 -1 0 0

#Bay 1
element zeroLength 1012 1103 1104 -mat 2 2 30108 -dir 1 2 6 -orient 1 0 0 0 1 0
element zeroLength 1014 1105 1106 -mat 2 2 30108 -dir 1 2 6 -orient 1 0 0 0 1 0

element zeroLength 1022 1203 1204 -mat 2 2 30108 -dir 1 2 6 -orient 1 0 0 0 1 0
element zeroLength 1024 1205 1206 -mat 2 2 30108 -dir 1 2 6 -orient 1 0 0 0 1 0

element zeroLength 1032 1303 1304 -mat 2 2 2484 -dir 1 2 6 -orient 1 0 0 0 1 0
element zeroLength 1034 1305 1306 -mat 2 2 2484 -dir 1 2 6 -orient 1 0 0 0 1 0

element zeroLength 1042 1403 1404 -mat 2 2 2484 -dir 1 2 6 -orient 1 0 0 0 1 0
element zeroLength 1044 1405 1406 -mat 2 2 2484 -dir 1 2 6 -orient 1 0 0 0 1 0

#Bay 2
element zeroLength 2012 2103 2104 -mat 2 2 30108 -dir 1 2 6 -orient 1 0 0 0 1 0
element zeroLength 2014 2105 2106 -mat 2 2 30108 -dir 1 2 6 -orient 1 0 0 0 1 0

element zeroLength 2022 2203 2204 -mat 2 2 30108 -dir 1 2 6 -orient 1 0 0 0 1 0
element zeroLength 2024 2205 2206 -mat 2 2 30108 -dir 1 2 6 -orient 1 0 0 0 1 0

element zeroLength 2032 2303 2304 -mat 2 2 2484 -dir 1 2 6 -orient 1 0 0 0 1 0
element zeroLength 2034 2305 2306 -mat 2 2 2484 -dir 1 2 6 -orient 1 0 0 0 1 0

element zeroLength 2042 2403 2404 -mat 2 2 2484 -dir 1 2 6 -orient 1 0 0 0 1 0
element zeroLength 2044 2405 2406 -mat 2 2 2484 -dir 1 2 6 -orient 1 0 0 0 1 0

#Bay 3
element zeroLength 3012 3103 3104 -mat 2 2 30108 -dir 1 2 6 -orient 1 0 0 0 1 0
element zeroLength 3014 3105 3106 -mat 2 2 30108 -dir 1 2 6 -orient 1 0 0 0 1 0
```

```
element zeroLength 3022 3203 3204 -mat 2 2 30108 -dir 1 2 6 -orient 1 0 0 0 1 0
element zeroLength 3024 3205 3206 -mat 2 2 30108 -dir 1 2 6 -orient 1 0 0 0 1 0

element zeroLength 3032 3303 3304 -mat 2 2 2484 -dir 1 2 6 -orient 1 0 0 0 1 0
element zeroLength 3034 3305 3306 -mat 2 2 2484 -dir 1 2 6 -orient 1 0 0 0 1 0

element zeroLength 3042 3403 3404 -mat 2 2 2484 -dir 1 2 6 -orient 1 0 0 0 1 0
element zeroLength 3044 3405 3406 -mat 2 2 2484 -dir 1 2 6 -orient 1 0 0 0 1 0

#Bay 4
element zeroLength 4012 4103 4104 -mat 2 2 30108 -dir 1 2 6 -orient 1 0 0 0 1 0
element zeroLength 4014 4105 4106 -mat 2 2 30108 -dir 1 2 6 -orient 1 0 0 0 1 0

element zeroLength 4022 4203 4204 -mat 2 2 30108 -dir 1 2 6 -orient 1 0 0 0 1 0
element zeroLength 4024 4205 4206 -mat 2 2 30108 -dir 1 2 6 -orient 1 0 0 0 1 0

element zeroLength 4032 4303 4304 -mat 2 2 2484 -dir 1 2 6 -orient 1 0 0 0 1 0
element zeroLength 4034 4305 4306 -mat 2 2 2484 -dir 1 2 6 -orient 1 0 0 0 1 0

element zeroLength 4042 4403 4404 -mat 2 2 2484 -dir 1 2 6 -orient 1 0 0 0 1 0
element zeroLength 4044 4405 4406 -mat 2 2 2484 -dir 1 2 6 -orient 1 0 0 0 1 0

#Masses, 2nd floor to fourth floor 940kips, roof 1045 kips, g=385.83i/s2
mass 1101 0.305          0       0
mass 1102 0.305     0    0
mass 2101 0.305     0    0
mass 2102 0.305     0    0
mass 3101 0.305     0    0
mass 3102 0.305     0    0
mass 4101 0.305     0    0
mass 4102 0.305     0    0

mass 1201 0.305     0    0
mass 1202 0.305     0    0
mass 2201 0.305     0    0
mass 2202 0.305     0    0
mass 3201 0.305     0    0
mass 3202 0.305     0    0
mass 4201 0.305     0    0
mass 4202 0.305     0    0

mass 1301 0.305     0    0
```

```
mass 1302 0.305         0         0
mass 2301 0.305         0         0
mass 2302 0.305         0         0
mass 3301 0.305         0         0
mass 3302 0.305         0         0
mass 4301 0.305         0         0
mass 4302 0.305         0         0

mass 1401 0.33875     0         0
mass 1402 0.33875     0         0
mass 2401 0.33875     0         0
mass 2402 0.33875     0         0
mass 3401 0.33875     0         0
mass 3402 0.33875     0         0
mass 4401 0.33875     0         0
mass 4402 0.33875     0         0

if {$infill == "yes"} {

        ###############################################################
        ###%  Infill   #####
        ###############################################################

        #Nodes at the center of beam-column joints
        #*****************************************

        #Column line 1
        node 107 0 156
        node 117 0 312
        node 127 0 468
        node 137 0 624

        #Column line 2
        node 207 360 156
        node 217 360 312
        node 227 360 468
        node 237 360 624

        #Column line 3
        node 307 720 156
        node 317 720 312
        node 327 720 468
        node 337 720 624
```

#Column line 4
node 407 1080 156
node 417 1080 312
node 427 1080 468
node 437 1080 624

#Column line 5
node 507 1440 156
node 517 1440 312
node 527 1440 468
node 537 1440 624

#Fix the rotational degree of freedom of nodes at center of beam-column joints
#**********
#Column line 1
fix 107 0 0 1
fix 117 0 0 1
fix 127 0 0 1
fix 137 0 0 1

#Column line 2
fix 207 0 0 1
fix 217 0 0 1
fix 227 0 0 1
fix 237 0 0 1

#Column line 3
fix 307 0 0 1
fix 317 0 0 1
fix 327 0 0 1
fix 337 0 0 1

#Column line 4
fix 407 0 0 1
fix 417 0 0 1
fix 427 0 0 1
fix 437 0 0 1

#Column line 5
fix 507 0 0 1
fix 517 0 0 1

```
fix 527 0 0 1
fix 537 0 0 1

#Make the trusses linking the center of beam-column joints to the faces of joints
#*************************************************************
#Column Line 1
element truss 115 107 102      1 3
element truss 116 107 1101 1 3
element truss 117 107 111      1 3
element truss 118 107 103      1 3

element truss 125 117 112      1 3
element truss 126 117 1201 1 3
element truss 127 117 121      1 3
element truss 128 117 113      1 3

element truss 135 127 122      1 3
element truss 136 127 1301 1 3
element truss 137 127 131      1 3
element truss 138 127 123      1 3

element truss 145 137 132      1 3
element truss 146 137 1401 1 3
element truss 147 137 133      1 3
element truss 148 137 136      1 3

#Column Line 2
element truss 215 207 202      1 3
element truss 216 207 2101 1 3
element truss 217 207 211      1 3
element truss 218 207 1102 1 3

element truss 225 217 212      1 3
element truss 226 217 2201 1 3
element truss 227 217 221      1 3
element truss 228 217 1202 1 3

element truss 235 227 222      1 3
element truss 236 227 2301 1 3
element truss 237 227 231      1 3
element truss 238 227 1302 1 3

element truss 245 237 232      1 3
```

```
element truss 246 237 2401 1 3
element truss 247 237 233  1 3
element truss 248 237 1402 1 3

#Column Line 3
element truss 315 307 302  1 3
element truss 316 307 3101 1 3
element truss 317 307 311  1 3
element truss 318 307 2102 1 3

element truss 325 317 312  1 3
element truss 326 317 3201 1 3
element truss 327 317 321  1 3
element truss 328 317 2202 1 3

element truss 335 327 322  1 3
element truss 336 327 3301 1 3
element truss 337 327 331  1 3
element truss 338 327 2302 1 3

element truss 345 337 332  1 3
element truss 346 337 3401 1 3
element truss 347 337 333  1 3
element truss 348 337 2402 1 3

#Column Line 4
element truss 415 407 402  1 3
element truss 416 407 4101 1 3
element truss 417 407 411  1 3
element truss 418 407 3102 1 3

element truss 425 417 412  1 3
element truss 426 417 4201 1 3
element truss 427 417 421  1 3
element truss 428 417 3202 1 3

element truss 435 427 422  1 3
element truss 436 427 4301 1 3
element truss 437 427 431  1 3
element truss 438 427 3302 1 3

element truss 445 437 432  1 3
element truss 446 437 4401 1 3
```

```
element truss 447 437 433      1 3
element truss 448 437 3402 1 3

#Column Line 5
element truss 515 507 502      1 3
element truss 516 507 503      1 3
element truss 517 507 511      1 3
element truss 518 507 4102 1 3

element truss 525 517 512      1 3
element truss 526 517 513      1 3
element truss 527 517 521      1 3
element truss 528 517 4202 1 3

element truss 535 527 522      1 3
element truss 536 527 523      1 3
element truss 537 527 531      1 3
element truss 538 527 4302 1 3

element truss 545 537 532      1 3
element truss 546 537 536      1 3
element truss 547 537 533      1 3
element truss 548 537 4402 1 3

#create the infills
set area_infill_bstorey [expr 227.4*1]
set area_infill_tstorey [expr 214.6*1]
set nbays 4

  if {$nbays == 4} {

        element truss 10001 101 207 $area_infill_bstorey 8
        element truss 10002 107 217 $area_infill_bstorey 8
        element truss 10003 117 227 $area_infill_tstorey 9
        element truss 10004 127 237 $area_infill_tstorey 9

        element truss 10011 201 107 $area_infill_bstorey 8
        element truss 10012 207 117 $area_infill_bstorey 8
        element truss 10013 217 127 $area_infill_tstorey 9
        element truss 10014 227 137 $area_infill_tstorey 9

        element truss 20001 201 307 $area_infill_bstorey 8
        element truss 20002 207 317 $area_infill_bstorey 8
```

```
        element truss 20003 217 327 $area_infill_tstorey 9
        element truss 20004 227 337 $area_infill_tstorey 9

        element truss 20011 301 207 $area_infill_bstorey 8
        element truss 20012 307 217 $area_infill_bstorey 8
        element truss 20013 317 227 $area_infill_tstorey 9
        element truss 20014 327 237 $area_infill_tstorey 9

        element truss 30001 301 407 $area_infill_bstorey 8
        element truss 30002 307 417 $area_infill_bstorey 8
        element truss 30003 317 427 $area_infill_tstorey 9
        element truss 30004 327 437 $area_infill_tstorey 9

        element truss 30011 401 307 $area_infill_bstorey 8
        element truss 30012 407 317 $area_infill_bstorey 8
        element truss 30013 417 327 $area_infill_tstorey 9
        element truss 30014 427 337 $area_infill_tstorey 9

        element truss 40001 401 507 $area_infill_bstorey 8
        element truss 40002 407 517 $area_infill_bstorey 8
        element truss 40003 417 527 $area_infill_tstorey 9
        element truss 40004 427 537 $area_infill_tstorey 9

        element truss 40011 501 407 $area_infill_bstorey 8
        element truss 40012 507 417 $area_infill_bstorey 8
        element truss 40013 517 427 $area_infill_tstorey 9
        element truss 40014 527 437 $area_infill_tstorey 9
    }

}
```

A.2 DEFINITION OF HYSTERETIC MODELS FOR PLASTIC HINGES IN FRAME MEMBERS, BEAM-COLUMN JOINTS AND INFILLS

```
uniaxialMaterial Steel01 1 50 29000 0.001
uniaxialMaterial Elastic 2 1e12
uniaxialMaterial Elastic 6 0.1
uniaxialMaterial Elastic 3 1e12

#Damage models for the W-sections obtained using Lignos formulas
damageModel HystereticEnergy       2484   15140  1
damageModel HystereticEnergy       30108  18439  1
damageModel HystereticEnergy       24162  85239  1
```

```
damageModel HystereticEnergy       24207  186824          1

#moment rotation materials for zero-length elements
#*****************************************

#uniaxialMaterial Bilinear tag Ke Fy+ Fy- alpha-h alpha-cap delta+cap delta-cap
flagCutEnv R DmgS DmgK DmgD

#For the columns
uniaxialMaterial        Bilinear        24162  7.50E+07        25740  -25740 6.84E-04
        -1.99E-03       0.0254 -0.0254          1       0.4     24162  0       24162
uniaxialMaterial        Bilinear        24207  1.03E+08        33330  -33330 5.26E-04
        -1.68E-03       0.0310 -0.0310          1       0.4     24207  0       24207

#For the beams
uniaxialMaterial        Bilinear        2484   1.49E+07        8310   -8310  2.54E-03
        -3.51E-03       0.0170 -0.0170          1       0.4     2484   0       2484
uniaxialMaterial        Bilinear        30108  2.81E+07        13294  -13294 2.31E-03
        -3.17E-03       0.0158 -0.0158          1       0.5     30108  0       30108

#*************************************************
#Hysteretic models for the joints
#*************************************************

#material for hinges on the face of joints
uniaxialMaterial Elastic 100 1e12

#Material tag for the shear panel of W24x162
uniaxialMaterial Bilinear 11  4737800  14017        -14017 0.045   -1e-6   0.0118 -
0.0118          1       0.4     0       0       0

#Material tag for the shear panel of W24x207
uniaxialMaterial Bilinear 12  7431787  21988        -21988 0.048   -1e-6   0.0118 -
0.0118          1       0.4     0       0       0

# Hysteretic models for the equivalent strut
#***********************************
#bottom stories
uniaxialMaterial        PinchingDamage        8        592     0.0008 -0.233 0.079   0.3
        -0.073  1.8E-05                 -0.0054         0.15    0.15    0.5     0       0
        0       0

#top stories
```

```
uniaxialMaterial PinchingDamage 9 592 0.0008 -0.247 0.084 0.3
    -0.077 1.8E-05 -0.0054 0.15 0.15 0.5 0 0
    0 0
```

A.3 ANALYSIS PARAMETERS

```
#set Tol1 0.00001
set Tol1 0.0001
set Tol2 0.0002
set Tol3 0.0005
set Tol4 0.001
set Tol5 0.0015
set Tol6 0.002
set Tol7 0.0025
set Tol8 0.005
set Tol9 0.01
set Tol10 0.1

set numIterations 35
set returnCode 1

set largest_dt 0.01

set Dt1 $largest_dt
set Dt2 [expr $largest_dt/2]
set Dt3 [expr $largest_dt/4]
set Dt4 [expr $largest_dt/8]

set NewmarkGamma 0.5
set NewmarkBeta 0.25

constraints Penalty 1e12 1e12
numberer Plain
system BandGeneral
test NormDispIncr $Tol1 $numIterations $returnCode
algorithm Newton
integrator Newmark $NewmarkGamma $NewmarkBeta
analysis Transient
```

A.4 SOLUTION ALGORITHM FOR INCREMENTAL DYNAMIC ANALYSIS

```
set analysis_status "pass"
set i 1
while {$i < $Nsteps} {
        set ok [analyze 1 $Dt1]
        if {$ok != 0} {
                #create a log in the file as to what happened
                puts $fileid "Analysis failed at time [getTime] Dt $Dt1 tolerance $Tol1"

                #halve the time step and see if it will work
                puts $fileid "Decreasing the time step to $Dt2"

                #Have to analyze twice at this time step now
                set j 1
                while {$j < 3} {

                   set ok [analyze 1 $Dt2]

                        if {$ok != 0} {

                                        #create a log in the file as to what happened
                                        puts $fileid "Analysis failed at time [getTime] Dt $Dt2 tolerance $Tol1"

                                        #halve the time step and see if it will work
                                        puts $fileid "Decreasing the time step to $Dt3"

                                        #Have to analyze twice at this time step now
                                        set k 1
```

```
while {$k < 3} {

        set ok [analyze 1 $Dt3]

        if {$ok != 0} {

                #create a log in the file as to what happened
                puts $fileid "Analysis failed at time [getTime] Dt $Dt3 t
                olerance $Tol1"

                #halve the time step and see if it will work
                puts $fileid "Decreasing the time step to $Dt4"

                #Have to analyze twice at this time step now
                set m 1

                while {$m < 3} {

                        set ok [analyze 1 $Dt4]

                        if {$ok != 0} {

                        #create a log in the file as to what happened
                        puts $fileid "Analysis failed at time [getTime] Dt
                        $Dt4 tolerance $Tol1"

                        puts $fileid "Decreasing the tolerance to $Tol2 and
                        trying"
```

```
test NormDispIncr $Tol2 $numIterations $returnCode

set ok [analyze 1 $Dt4]
}

if {$ok != 0} {

#create a log in the file as to what happened
puts $fileid "Analysis failed at time [getTime] Dt $Dt4 tolerance $Tol2"

puts $fileid "Decreasing the tolerance to $Tol3 and trying"

test NormDispIncr $Tol3 $numIterations $returnCode

set ok [analyze 1 $Dt4]
}

if {$ok != 0} {

#create a log in the file as to what happened
puts $fileid "Analysis failed at time [getTime] Dt $Dt4 tolerance $Tol3"

puts $fileid "Decreasing the tolerance to $Tol4 and trying"
```

```
test NormDispIncr $Tol4 $numIterations $returnCode
set ok [analyze 1 $Dt4]
}

if {$ok != 0} {

#create a log in the file as to what happened
puts $fileid "Analysis failed at time [getTime] Dt $Dt4 tolerance $Tol4"

puts $fileid "Decreasing the tolerance to $Tol5 and trying"

 test NormDispIncr $Tol5 $numIterations $returnCode

set ok [analyze 1 $Dt4]
}

if {$ok != 0} {

#create a log in the file as to what happened
puts $fileid "Analysis failed at time [getTime] Dt $Dt4 tolerance $Tol5"

puts $fileid "Decreasing the tolerance to $Tol6 and trying"
```

```
test NormDispIncr $Tol6 $numIterations $returnCode

set ok [analyze 1 $Dt4]

}

if {$ok != 0} {

#create a log in the file as to what happened
puts $fileid "Analysis failed at time [getTime] Dt $Dt4 tolerance $Tol6"

puts $fileid "Decreasing the tolerance to $Tol7 and trying"

test NormDispIncr $Tol7 $numIterations $returnCode

set ok [analyze 1 $Dt4]

}


if {$ok != 0} {

#create a log in the file as to what happened
puts $fileid "Analysis failed at time [getTime] Dt $Dt4 tolerance $Tol7"
```

```
puts $fileid "Decreasing the tolerance to $Tol8 and trying"

test NormDispIncr $Tol8 $numIterations $returnCode

set ok [analyze 1 $Dt4]
}

 if {$ok != 0} {

#create a log in the file as to what happened
puts $fileid "Analysis failed at time [getTime] Dt $Dt4 tolerance $Tol8"

puts $fileid "Decreasing the tolerance to $Tol9 and trying"

test NormDispIncr $Tol9 $numIterations $returnCode

set ok [analyze 1 $Dt4]
}

if {$ok != 0} {

#create a log in the file as to what happened
puts $fileid "Analysis failed at time [getTime] Dt $Dt4 tolerance $Tol9"
```

```
puts $fileid "Decreasing the tolerance to $Tol10 and trying, converged results may not be accurate"

test NormDispIncr $Tol10 $numIterations $returnCode

set ok [analyze 1 $Dt4]
}

if {$ok != 0} {

#create a log in the file as to what happened
puts $fileid "Analysis failed at time [getTime] Dt $Dt4 tolerance $Tol8"

puts $fileid "Changing algorithm to LineSearch 0.5 and trying one last time before quitting"

algorithm NewtonLineSearch 0.5
set ok [analyze 1 $Dt4]
}

if {$ok != 0} {

#create a log in the file as to what happened
puts $fileid "Not able to find a soultion at time [getTime] Dt $Dt4 -- quitting analysis for this scale factor \n"

puts $fileid "\n"
```

```
                                                    flush $fileid

                                                    #close $fileid
                                                    set analysis_status "fail"

                                                    # exit
                                                    }

            #revert back to the ideal tolerance and algorithm
            algorithm Newton
            test NormDispIncr $Tol1 $numIterations $returnCode

            if {$analysis_status == "fail"} {
               break;
            }

            incr m

            }
            #end of while m<3

            #get the time step back to previous one
            set currentDt $Dt3

            }
#end if ok!=0

if {$analysis_status == "fail"} {
  break;
}
```

```
                incr k
                }
            #end of while k<3

        #get the time step back to previous one
        set currentDt $Dt2

        }
        #end of ok!=0

   if {$analysis_status == "fail"} {
   break;
   }

    incr j

    }
    #end of while {$j < 3}

    #get the time step back to previous one
    set currentDt $Dt1

     }
     ##end if ok!=0

flush $fileid

if {$analysis_status == "fail"} {
        break;
```

```
    }
    incr i

}
#end of while {$i < $Nsteps}
```

A.5 BATCH PROCESS TO RUN IDA

```
set fileid [open "analysis_log_bf_1.tcl" a]

source constants.tcl

# Ground motion 120111
#********************
puts $fileid "\n \n"
puts $fileid "starting 120111 \n"

for {set scaling_factor 0.2} { $scaling_factor<=5.0} {set scaling_factor [expr $scaling_factor+0.20]} {

puts $fileid "starting scaling factor $scaling_factor \n"

source pp_model_with_bcjoint.tcl
source gravity_loads.tcl

set file "dyn_op_bf/120111/$scaling_factor"
file mkdir $file

source dyn_recorders.tcl

set GMfile "normalized_gms/120111.txt"
set dt 0.01

source uni_exc_parameters_bf.tcl

set Nsteps 4000
#Now call the solution algorithm for incremental dynamic analysis
source solution_algo.tcl

if {$analysis_status == "fail"} {
        wipe
        break;
}

wipe

}
```

APPENDIX B

Calculations for backbone curve of Ibarra-Krawinkler hysteretic model for infills

The following table illustrates calculation of the backbone parameters of the Ibarra-Krawinkler hysteretic model for infills. The table uses properties of the 8-in clay masonry infill, as presented in Chapter 8. It computes the backbone curve of the Ibarra-Krawinkler hysteretic model that represents the hysteretic force-deformation behavior of the infill, when the clay masonry infill panel is located in the bottom story of the ATC-63 steel moment frame.

Table B-1: Calculation of backbone curve of Ibarra-Krawinkler hysteretic model for 8-in clay masonry infill located in bottom story of ATC-63 steel moment frame

Em	4200
fm	6
t	8
h-infill	130.3
E-col	29000
I-col	6820
d-col	25.7
cos-theta	0.917556
theta (deg)	23.42869
sin(2-theta)	0.729654
Equivalent strut parameter	0.022083
Width of equivalent strut	14.80545
Horizontal strength	361.7568
Axial strength of equivalent strut	394.2614
Strain at crushing of equivalent strut	0.002345
Backbone curve for Ibarra-Krawinkler hysteretic model	
Strain	**Stress**
0.00200	0.00
0.00000	0.00
-0.00020	-1.66

-0.00235	-3.33
-0.00352	-2.50
-0.00563	-1.00
-0.00800	-1.00
Elastic stiffness	8400
Slope of strain hardening branch	0.092
Slope of descending branch	-0.084

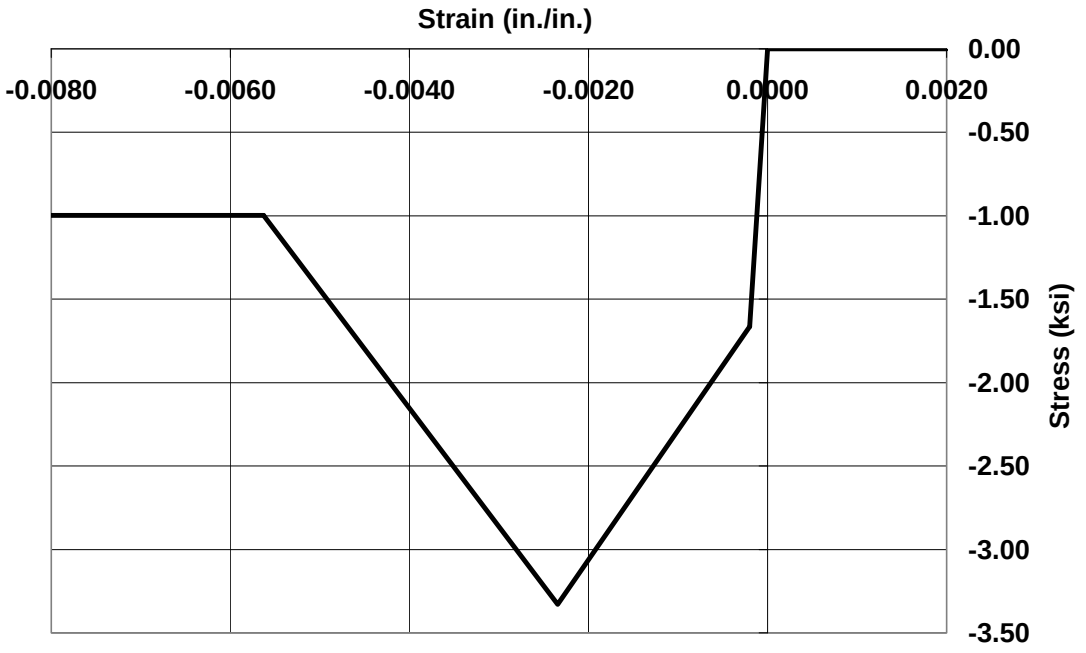

Figure B.1: Backbone curve of Ibarra-Krawinkler hysteretic model for equivalent strut of 8-in clay masonry infill located in bottom story of ATC-63 steel moment frame

REFERENCES

AISC 2005: Manual of Steel Construction, 13th edition, 2005, printed by American Institute of Steel Construction

Altoontash (2004): Altoontash, A., "Simulation and damage models for performance assessment of reinforced concrete beam-column joints", PhD Dissertation, August 2004, Stanford University, USA.

ASCE7-05 (2005): Minimum Design Loads for Buildings and Other Structures, American Society of Civil Engineers and Structural Engineering Institute; ASCE Standard No. 7-05

ATC-63 (2007): Applied Technology Council, "Recommended Methodology for Quantification of Building System Performance and Response Parameters" - 75% Draft, 2007, Prepared by Applied Technology Council for the Federal Emergency Management Agency, Washington, D.C.

ATC-63 (2008): Applied Technology Council, Quantification of Building Seismic Performance Factors - 90% Draft, *Report No. ATC-63*, 2008, prepared by the Applied Technology Council, Redwood City, California for the Federal Emergency Management Agency, Washington, D.C.

Baber (1981): Baber, T. T. and Wen, Y. K., "Random vibration of hysteretic degrading systems", *Journal of Engineering Mechanics*, ASCE, 107(6), 1069-1087.

Bouc (1967): Bouc, R., "Forced vibration of mechanical systems with hysteresis", Proceedings of the 4th Conference on Non-linear Oscillation, place, date.

Chiou (1999): Chiou, Y. J., J. C. Tzeng, and Y. W. Liou, "Experimental and analytical study of masonry infilled frames", *Journal of Structural Engineering*, ASCE, October 1999, 1109-1117.

Combescure (2000a): Didier Combescure and Pierre Pegon, "Application of the local-to-global approach to the study of infilled frame structures under seismic loading", *Nuclear Engineering and Design*, Volume 196, 2000, 17–40

Combescure (2000b): Combescure, D., and Pegon, P., "Application of the local to global approach to the study of infilled frame structures under seismic loading,"

Proceedings of the 12th World Conference on Earthquake Engineering, CD-ROM, Paper No. 505, Auckland: New Zealand, 2000

Crisafulli (2000): Crisafulli, F., J., Carr, A., J., and Park, R., "Analytical modeling of infilled frames structures - a general review", *Bulletin of the New Zealand Society for Earthquake Engineering*, 2000, Vol. 33, 30–47

Chiou (1999): Chiou, Y. J., J. C. Tzeng, and Y. W. Liou, "Experimental and analytical study of masonry infilled frames," *Journal of Structural Engineering*, ASCE, October 1999, 1109-1117.

Dawe (1989): Dawe, J. L., and C. K. Seah, "Behavior of masonry infilled steel frames," *Canadian Journal of Civil Engineering*, Ottawa, 16, 865-876.

Dhanasekhar (1986): Dhanasekhar, M., A. W. Page, "The influence of brick masonry infill properties on behavior of infilled frames," *Proceedings*, Institution of Civil Engineers (London), Part 2, Vol. 73, 473-478

Dolsek (2001): Dolsek, M., and Fajfar, P., "Soft storey effects in uniformly infilled reinforced concrete frames", Journal of Earthquake Engineering, 2001, Vol. 5, No. 1, 1-12

Dolsek (2002): Dolsek, M., and Fajfar, P., "Mathematical modelling of an infilled RC frame structure based on the results of pseudo-dynamic tests", *Earthquake Engineering and Structural Dynamics*, 2002, Vol. 31, 1215–1230

Dolsek (2004): Dolsek, M., and Fajfar, P., "Inelastic spectra for infilled reinforced concrete frames," *Earthquake Engineering and Structural Dynamics*, Volume 33, 2004, 1395–1416.

Dolsek (2004): Dolsek, M., and Fajfar, P., "IN2—A simple alternative for IDA", *Proceedings of the 13th world conference on earthquake engineering*, 2004, page:3353.

Dolsek (2005): Dolsek, M., and Fajfar, P., "Simplified non-linear seismic analysis of infilled reinforced concrete frames," *Earthquake Engineering and Structural Dynamics*, 2005; Vol. 34, 49–66

Dolsek (2007): Dolsek, M., and Fajfar, P., "Simplified probabilistic seismic performance assessment of plan-asymmetric buildings", *Earthquake Engineering and Structural Dynamics*, 2007; Volume 36, pages 2021–41.

Dolsek (2008a): Dolsek, M., and Fajfar, P., "The effect of masonry infills on the seismic response of a four-storey reinforced concrete frame—a probabilistic assessment", *Engineering Structures*, 2008, Vol. 30, 1991–2001

Dolsek (2008b): Dolsek, M., and Fajfar, P., "The effect of masonry infills on the seismic response of a four-storey reinforced concrete frame—a deterministic assessment", *Engineering Structures*, 2008, Vol. 30, 1991–2001

Engelhardt (1998): Engelhardt, M., Winneberger, T., Zekany, A. J., Potyraj, T. J., "Experimental investigation of dogbone moment connections", *Engineering Journal of Steel Construction*, Vol. 4, 1998, 128-139.

Fajfar (2000): Fajfar P., "A nonlinear analysis method for performance-based seismic design," *Earthquake Spectra,* 2000, Volume 16, 573–92.

Flanagan (1999): Flanagan, R., D., and Bennett, R., M. (1999). "In-plane behavior of structural clay tile infilled frames." *Journal of Structural Engineering*, Vol. 125, No. 6, 590-599.

Flanagan (2001): Flanagan, R. D., and Bennett, R. M., "In-plane analysis of masonry infill materials", *Practice periodical on Structural Design and Construction, 2001,* Vol.6 No.4, 176-182

Gatto (2002): Gatto, K.S., and Uang, C., M., "Effects of loading protocol and rate of loading on woodframe shearwall response", *Seventh U.S. National Conference on Earthquake Engineering*, EERI, Oakland, California, 2002.

FEMA 307 (1998): FEMA, "Evaluation of earthquake damaged concrete and masonry wall buildings," 1998, Applied Technology Council, Redwood City, California.

Hamburger (2006): Hamburger, R.O., and Meyer, J. D., "The performance of steel-frame buildings with infill masonry walls in the 1906 San Francisco earthquake," *Earthquake Spectra*, Volume 22, No. S2, April 2006, S43-S67.

Haselton (2006): Haselton., C., B., "Assessing seismic collapse safety of modern reinforced concrete moment frame buildings", PhD Dissertation, December 2006, Stanford University.

Holmes (1961): Holmes, M., "Steel frames with brickwork and concrete infilling," *Proceedings, Institution of Civil Engineers (London)*, Vol. 19, Part 2, 473-478.

Humar (2001): Jag Mohan Humar, David Lau, and Jean-Robert Pierre, "Performance of buildings during the 2001 Bhuj earthquake," Canadian Journal of Civil Engineering, 2001, Vol. 28, 979–991

Ibarra (2005): Ibarra, L. F., Medina, R. A., and Krawinkler, H. (2005). "Hysteretic models that incorporate strength and stiffness deterioration," *Earthquake Engineering and Structural Dynamics*, Vol. 34, 1489–1511.

Kaushik (2006): Kaushik. H. B., Rai, D. C., and Jain. S. K., "Code Approaches to Seismic Design of Masonry-Infilled Reinforced Concrete Frames: A State-of-the-Art Review," *Earthquake Spectra*, Volume 22 No. 4, November 2006, 961–983

Klingner (1976): Klingner, R.E. and V. V. Bertero, "Infilled frames in earthquake resistant construction", 1976, SESM Report 76–32, University of California, Berkeley, CA.

Klingner (1978): Klingner, R. E. and V. Bertero, "Earthquake resistance of infilled frames," *Journal of Structural Engineering*, ASCE, Vol. 104, No. 6, 973-989.

Kodur (1995): V.K.R. Kodur, M.A. Erki, and J.H.P. Quenneville, "Seismic design and analysis of masonry-infilled frames," *Canadian Journal of Civil Engineering*, 1995, Vol. 22, 576-587

Krawinkler (1978): Krawinkler, H., 1978, "Shear design of steel frame joints," *Engineering Journal*, AISC, Vol. 15, No. 3.

Krawinkler (2007): Krawinkler, H., and Lignos, D. G., "How to Predict and Reduce the Probability of Collapse of Non-Ductile Building Structures", *Proceedings*, International Workshop On Measures for the Prevention of Total Collapse of Existing Low-Rise Structures, November 19-20, Istanbul Technical University, Istanbul, Turkey

Liauw (1983): Liauw, T. C. and K. H. Kwan, "Plastic theory on non-integral infilled frames," *Proceedings, Institution of Civil Engineers (London)*, Vol. 75, Part 2, 379 – 396.

Lignos (2007): Lignos, D.G., and Krawinkler, H., 2007, "A Database in Support of Modeling of Component Deterioration for Collapse Prediction of Steel Frame Structures", *Proceedings*, ASCE Structures Congress, Long Beach, California, May 18-20, 2007.

Liu (2005): Liu, Y., and G. Li, "Experimental and theoretical research on lateral load resistance of steel frames with infilled walls," *Jianzhu Jiegou Xuebao (Journal of Building Structures)*, Vol. 26, No. 3, June, 2005, 78-84, ISSN 0529-1399, China Academic Journal Electronic Publishing House, Beijing.

Lowes (2003): Lowes, L. N. and Altoontash, A., "Modeling of Reinforced-Concrete Beam-Column Joints Subjected to Cyclic Loading," *Journal of Structural Engineering*, ASCE, 2003, v. 129 (12).

Madan (1997): Madan, A., A. M. Reinhorn, and J. B. Mander, "Modelling of masonry infill panels for structural analysis," *Journal of Structural Engineering*, ASCE, October 1997, 1295-1302.

Mehrabi (1997): Mehrabi, A. B. and P. B. Shing, "Finite element modeling of masonry infilled RC frames," *Journal of Structural Engineering*, ASCE, May 1997, 604-613.

Memari (1999): A.M. Memari, A.A. Aghakouchak, M. Ghafory Ashtiany, M. Tiv, "Full-scale dynamic testing of a steel frame building during construction", *Engineering Structures*, 1999, Vol. 21, 1115–1127

MSJC (2008a): Masonry Standards Joint Committee, *Building Code Requirements for Masonry Structures*, The Masonry Society, Boulder, Colorada, USA

MSJC (2008b): Masonry Standards Joint Committee, *Specification for Masonry Structures*, The Masonry Society, Boulder, Colorada, USA

OpenSees (2006): Open System for Earthquake Engineering Simulation (http://opensees.berkeley.edu/), developed by University of California Berkeley and Pacific Earthquake Engineering Research Center (http://peer.berkeley.edu).

Panagiotakos (1993): Panagiotakos T. B. and Fardis, M. N., "Seismic response of infilled RC framed structures", *Proceedings*, 11th World Conference on Earthquake Engineering, Acapulco, Mexico, 1996.

PEER (2006): PEER NGA Database, Pacific Earthquake Engineering Research Center, University of California, Berkeley, California, http://peer.berkeley.edu/nga/

Riddington (1984): Riddington, J.R., "The influence of initial gaps on infilled frame behavior," *Proceedings*, Institution of Civil Engineers, 77, 295-310.

Saneinejad (1995): Saneinejad, A. and B. Hobbs, "Inelastic design of infilled frames," *Journal of Structural Engineering*, ASCE, April 1995, 634-650.

Saatcioglu (2001): Murat Saatcioglu, Denis Mitchell, René Tinawi, N. John Gardner, Anthony G. Gillies, Ahmed Ghobarah, Donald L. Anderson, and David Lau, "The

August 17, 1999, Kocaeli (Turkey) earthquake — damage to structures," *Canadian Journal of Civil Engineering*, Vol. 28, 2001, 715-737

Scawthorn (2000): C. Scawthorn and G.S. Johnson , "Preliminary report Kocaeli (Izmit) earthquake of 17 August 1999," *Engineering Structures*, 2000, Vol. 22, 727–745

Stafford Smith (1969): Stafford Smith, B., and C. Carter, "A method of analysis for infilled frames," *Proceedings, Institution of Civil Engineers*, Vol. 44, 31-48.

Schneider (2002): Schneider, S.P. and Teeraparbwong, I., "Inelastic behavior of bolted flange plate connections," *Journal of Structural Engineering*, ASCE, Vol.128 No.4, April 2002, 492-500

Tanner (2003): Tanner, J. (2003). "Design provisions for Autoclaved Aerated Concrete (AAC) structural systems," PhD Dissertation, University of Texas at Austin, USA.

Tanner (2005a): Tanner, J.E., Varela, J.L., Klingner, R.E., "Design and Seismic Testing of a Two-story Full-scale Autoclaved Aerated Concrete (AAC) Assemblage Specimen," Structures Journal, American Concrete Institute, Farmington Hills, Michigan, vol. 102, no. 1, January - February 2005, pp. 114-119.

Tanner (2005b): Tanner, J.E., Varela, J.L., Klingner, R.E., Brightman M. J. and Cancino, U., "Seismic Testing of Autoclaved Aerated Concrete (AAC) Shear Walls: A Comprehensive Review," Structures Journal, American Concrete Institute, Farmington Hills, Michigan, vol. 102, no. 3, May - June 2005, pp. 374-382.

Tonga (2005): Xiangdong Tonga, Jerome F. Hajjar, Arturo E. Schultz, Carol K. Shield, "Cyclic behavior of steel frame structures with composite reinforced concrete infill walls and partially-restrained connections," *Journal of Constructional Steel Research*, 2005, Vol. 61, 531–552

Vamvatsikos (2002): Vamvatsikos, D. and Cornell, C. A., "Incremental Dynamic Analysis," *Earthquake Engineering and Structural Dynamics*, 2002, Vol. 31 No.3, 491-514.

Vamvatsikos (2004): Vamvatsikos, D. and Cornell, C. A., "Applied Incremental Dynamic Analysis," *Earthquake Spectra*, May 2004, Volume 20 No. 2, 523–553.

Varela (2003): Varela, J. L., "Proposed Values of R and C_d for AAC Structural Systems," Ph.D. dissertation, Department of Civil Engineering, The University of Texas at Austin, May 2003.

Varela (2006): Varela, J. L., Tanner, J. E. and Klingner, R. E., “Development of Seismic Force-Reduction and Displacement Amplification Factors for AAC Structures,” EERI Spectra, Earthquake Engineering Research Institute, Oakland, California, vol. 22, no. 1, February 2006, pp. 267-286.

Zarnic (1997): Zarnic, R., Gostic, S., “Masonry infilled frames as an effective structural sub-assemblage”, *Seismic Design Methodologies for the Next Generation of Codes*, Fajfar P, Krawinkler H (eds), Balkema: Rotterdam, 1997, 335–346.

VITA

Shiv Shanker was born on 8 October 1979 in Chennai, India. He spent most of his childhood in Chennai, which is also known as Madras. He received his Bachelor of Technology in Civil Engineering in 2001 from Indian Institute of Technology Madras. He received his Masters degree in Civil Engineering from University of Illinois at Urbana Champaign in 2003. He worked as a Project Associate in Indian Institute of Technology Madras from 2003 to 2005 assessing seismic vulnerability of reinforced concrete buildings in India. He entered the PhD program at The University of Texas at Austin in August 2005.

Permanent address: 382, West street
Panneer Nagar
Mogappair
Chennai – 600037
India

This dissertation was typed by the author.